# Feeder Voltage Regulation with High-Penetration PV Using Advanced Inverters and a Distribution Management System

## A Duke Energy Case Study

Bryan Palmintier, Julieta Giraldez, Kenny Gruchalla, Peter Gotseff, Adarsh Nagarajan, Tom Harris, Bruce Bugbee, and Murali Baggu
*National Renewable Energy Laboratory*

Jesse Gantz and Ethan Boardman
*GE Grid Solutions*

**NREL is a national laboratory of the U.S. Department of Energy**
**Office of Energy Efficiency & Renewable Energy**
**Operated by the Alliance for Sustainable Energy, LLC**

This report is available at no cost from the National Renewable Energy Laboratory (NREL) at www.nrel.gov/publications.

**Technical Report**
NREL/TP-5D00-65551
November 2016

Contract No. DE-AC36-08GO28308

NREL
NATIONAL RENEWABLE ENERGY LABORATORY

# Feeder Voltage Regulation with High-Penetration PV Using Advanced Inverters and a Distribution Management System

## A Duke Energy Case Study

Bryan Palmintier, Julieta Giraldez, Kenny Gruchalla, Peter Gotseff, Adarsh Nagarajan, Tom Harris, Bruce Bugbee, and Murali Baggu
*National Renewable Energy Laboratory*

Jesse Gantz and Ethan Boardman
*GE Grid Solutions*

Prepared under Task Numbers: WRGJ1000, ST13IN15, and OE10.4520

**NREL is a national laboratory of the U.S. Department of Energy**
**Office of Energy Efficiency & Renewable Energy**
**Operated by the Alliance for Sustainable Energy, LLC**

This report is available at no cost from the National Renewable Energy Laboratory (NREL) at www.nrel.gov/publications.

National Renewable Energy Laboratory
15013 Denver West Parkway
Golden, CO 80401
303-275-3000 • www.nrel.gov

**Technical Report**
NREL/TP-5D00-65551
November 2016

Contract No. DE-AC36-08GO28308

**NOTICE**



This report is available at no cost from the National Renewable Energy Laboratory (NREL) at www.nrel.gov/publications.

Available electronically at SciTech Connect http:/www.osti.gov/scitech

Available for a processing fee to U.S. Department of Energy and its contractors, in paper, from:

U.S. Department of Energy
Office of Scientific and Technical Information
P.O. Box 62
Oak Ridge, TN 37831-0062
OSTI http://www.osti.gov
Phone: 865.576.8401
Fax: 865.576.5728
Email: reports@osti.gov

Available for sale to the public, in paper, from:

U.S. Department of Commerce
National Technical Information Service
5301 Shawnee Road
Alexandria, VA 22312
NTIS http://www.ntis.gov
Phone: 800.553.6847 or 703.605.6000
Fax: 703.605.6900
Email: orders@ntis.gov

*Cover Photos by Dennis Schroeder: (left to right) NREL 26173, NREL 18302, NREL 19758, NREL 29642, NREL 19795.*

NREL prints on paper that contains recycled content.

# Acknowledgments

The authors thank Duke Energy and the U.S. Department of Energy (DOE), Solar Energy Technologies Office, for their support of this research through the Integrate Project. Thanks to the superb engagement, technical expertise, guidance, data support, feedback, and more from Leslie Ponder, Mark Howard, Ted Thomas, Jonathan Ryne, and Ron Belvin of Duke Energy. Thanks to Ethan Boardman and David Sun of Alstom Grid (now GE Grid Solutions) for their support of the project and to Doug Bradley (GE/Alstom) for his assistance with configuring the e-terra*control* supervisory control and data acquisition (SCADA) system for the power hardware-in-the-loop tests. The NREL team extends a special thank-you to Jesse Gantz of GE/Alstom for his amazing technical support, quick feature additions, and invaluable help configuring and maintaining the e-terra*distribution* system, models, and py4etd at NREL. The authors also appreciate the knowledgeable input and helpful feedback from our NREL reviewers: Annabelle Pratt and Barry Mather. We are grateful to the Energy Systems Integration Laboratory (ESIF) lab operations team: Mike Simpson, Ishmael Mendoza, Greg Marten, Mari Shirazi, Blake Lundstrom, Rick Ferre, and Adam Bailey; the ESIF Internet technology team: Tony Magri, Susan Bond, and James Shelby; and the Power Systems Engineering Center project support team: Amy Osten and Becky Schell. Without their invaluable help, expertise, and support, this project would not have been possible.

This work was funded by the DOE, Office of Energy Efficiency and Renewable Energy, Solar Energy Technologies Office, under Contract No. DE-AC36-08GO28308.

# List of Acronyms

| | |
|---|---|
| 2D | two-dimensional |
| 3D | three-dimensional |
| ANSI | American National Standards Institute |
| BLA | bus load allocation |
| CBAAT | Cost-Benefit Alternatives Analysis Tool |
| CVR | conservation voltage reduction |
| DCF | discounted cash flow |
| DGPV | distributed-generation solar photovoltaic |
| DMS | distribution management system |
| DOTS | Distribution Operator Training Simulator |
| ESIF | Energy Systems Integration Facility |
| IVVC | integrated volt/VAR control |
| LTC | load tap changer |
| LVM | load and volt/VAR management |
| NPV | net present value |
| NREL | National Renewable Energy Laboratory |
| PF | power factor (An absorbing power factor is produced by an inductive load and can also be referred to as lagging.) |
| PHIL | power hardware-in-the-loop |
| PV | photovoltaic |
| QSTS | quasi-steady-state time series (analysis) |
| RT | real time (mode) |
| RTS | Real-Time digital Simulator |
| SCADA | supervisory control and data acquisition system |
| SIM | simulator (mode) |
| ST | study (mode) |
| VAR | volt-ampere reactive (unit of reactive power) |
| VI | variability index |

# Executive Summary

Duke Energy, Alstom Grid (now GE Grid Solutions), and the National Renewable Energy Laboratory (NREL) collaborated to better understand advanced inverter and distribution management system (DMS) control options for large (1–5 MW) distributed solar photovoltaics (PV) and their impacts on distribution system operations. The specific goal of the project was to compare the operational—specifically, voltage regulation—impacts of three methods of managing voltage variations resulting from such PV systems:

1. Active power only (baseline)
2. Local autonomous inverter control: power factor (PF) ≠1 and volt/volt-ampere reactive (VAR)[1] (Q(V))
3. Integrated volt/VAR control (IVVC) coordinated through the DMS to both manage voltage and reduce demand through conservation voltage reduction (CVR). IVVC was run with and without the PV system(s) included in the control scheme.

The project found that all tested configurations of DMS-controlled IVVC provided improved performance and provided operational cost savings compared to the baseline and local control modes. Specifically, IVVC combined with PV at a 0.95 PF proved the technically most effective voltage management scheme for the system studied. This configuration substantially reduced both utility regulation equipment operations and observed voltage challenges.[2] On a cost basis, central IVVC (excluding direct PV control and only commanding existing/legacy utility equipment) performed slightly better than IVVC with PV at a 0.95 PF due to the latter's need to purchase more traditionally generated electricity to cover slightly higher system losses from increased reactive power flows. Among all IVVC scenarios, this preliminary cost-benefit analysis showed operational cost savings for the IVVC scenarios that were partially driven by reduced wear and tear on utility regulation equipment but dominated by the use of CVR to reduce the need to purchase energy from traditional generation. IVVC with central, DMS control of PV reactive power also provided substantial operational improvement beyond baseline and local control modes; however, in these experiments the variability of solar generation between nominal 10-minute IVVC solution intervals resulted in somewhat higher equipment operations, slightly increased voltage challenges, and small increases in operating costs compared to the other IVVC scenarios. Such integration of distributed generation from PV (DGPV) represents an exciting area for further development as the algorithms and solution intervals are further refined and solar forecasts are increasingly incorporated into utility operations.

In addition, the project produced a number of other key insights and developed a wide range of new analytic approaches that will provide a solid foundation and accelerated results for future research projects among Duke Energy, NREL, and GE Grid Solutions. The research used multiple approaches to analyze the results of these comparisons, each of which represents an important research-and-development effort on its own:

[1] VAR is a unit of reactive power. The official IEEE/SI unit abbreviation is "var," but "VAR" is used in this report to match power industry practice.

[2] Here, voltage challenges are measured as customer minutes outside of desired voltage levels and reported as a percentage of total customer minutes. In most cases, although these voltage challenges are outside of the Ameircan National Standards Institute (ANSI) thresholds, they are not outside of it long enough to count as a violation.

- Quasi-steady-state time-series (QSTS) simulations of system operations at a 1-minute time resolution using Alstom Grid's e-terra*distribution* (Distribution Operator Training Simulator, or DOTS) DMS system as a simulation engine, augmented by Python scripting for faster-than-real-time simulation and modeling of the PV inverter(s)
- Statistics-based methods to reduce simulation times by conducting detailed time-series analysis for only 40 days and then using these to estimate full-year results
- Advanced visualization to provide improved insights into time-series results and other PV operational impacts
- Power hardware-in-the-loop (PHIL) testing with a 500-kVA advanced inverter linked through cosimulation to full-scale feeder simulations using DOTS in real time
- Cost-benefit analysis to compare financial impacts of each control approach.

The study focused on PV integration in North Carolina, which ranks third in the United States in terms of total installed solar capacity (GTM Research and SEIA 2016); however, unlike many other high-solar states that have seen rapid growth in both smaller residential systems and larger, utility-scale distributed solar power plants, 98% of PV capacity in North Carolina is at the utility scale, which is in the range of 500 kW–5 MW (Palmintier et al. 2016), due to favorable incentive structures for such larger systems. Duke has been using the Alstom/GE DMS system for a number of years in its Carolinas West and Midwest Distribution Control Centers (DCCs) and has piloted and rolled out IVVC in a number of service territories.

Specifically, this project explored one of these distribution-connected utility-scale systems on a rural feeder in Duke's North Carolina service territory.[3] The existing 5-MW solar power plant is located approximately 2 miles from the substation, and feeder peak demand is approximately 5 MW, such that the PV system back-feeds the substation during most clear daylight hours.

A comparison of the summary results of the six simulated scenarios is shown in Table ES-1, which includes both the total number of voltage regulation equipment operations and voltage challenges at load locations. Comparisons among scenarios are also presented in Figure ES-1 and Figure ES-2, which show the total number of voltage regulation equipment operations and voltage challenges at load locations, respectively. Note that only the numbers of operations of Phase B line regulators are shown in Figure ES-1, but, as detailed in the report, results were very similar for Phase A and Phase C.

[3] Detailed identifying information, cost assumptions, and other nonpublic information is included in Appendix D for this report, which is available only with permission from project team members.

**Table ES-1. Summary Comparison of Six Annualized Scenarios for Advanced PV Inverters**

| | | IVVC Control | | | | Annualized Equipment Operations | | | | Voltage Challenges | |
|---|---|---|---|---|---|---|---|---|---|---|---|
| Scenario | PV Mode | LTC | Regulators | Capacitors | PV | LTC (Total for 1) | Regulators (Total for 6) | Capacitors (Total for 2) | Total (All devices) | Over | Under |
| **Baseline** | Default | - | - | - | - | 5,043 | 19,160 | 125 | 24,328 | 1.47% | 0.00% |
| **Local PV Control (PF = 0.95)** | PF=0.95 | - | - | - | - | 5,063 | 19,943 | 505 | 25,511 | 1.48% | 0.00% |
| **Local PV Control (Volt/VAR)** | Q(V) | - | - | - | - | 5,087 | 19,857 | 541 | 25,485 | 1.44% | 0.00% |
| **Legacy IVVC (Exclude PV)** | Default | Y | Y | Y | - | 2,869 | 2,943 | 1,863 | 7,675 | 0.02% | 0.00% |
| **IVVC with PV (PF = 0.95)** | PF=0.95 | Y | Y | Y | - | 2,498 | 1,888 | 1,409 | 5,795 | 0.01% | 0.00% |
| **IVVC (Central PV Control)** | IVVC for reactive power | Y | Y | Y | Y | 2,312 | 2,698 | 1,151 | 6,161 | 0.05% | 0.02% |

Today (in the baseline), the study feeder generally manages the large power injection by the solar power plant well. The operating cycle of the substation three-phase load tap changer (LTC), three sets of line regulators, and VAR-controlled capacitor are tolerable,[4] and the number of voltage challenges is quite small, especially for a feeder with such a large PV system. Further, these voltage challenges are typically minor, short-lived, over-/undervoltage conditions that are still within the ANSI C.84.1 Range B that is acceptable for short durations.

Still, there is room for advanced PV inverter and DMS technologies to provide operational improvements by reducing the number of equipment operations to save equipment wear and tear; by improving customer power quality by reducing voltage excursions; and to help reduce system energy demand through CVR. As explored in a sensitivity analysis, these concerns become particularly relevant as additional solar comes online, especially when PV systems are located toward the end of the line, farther from the substation.

Interestingly, most of the few baseline voltage challenges at load locations are not directly caused by the PV system because they occur during nonproduction hours. The low number of baseline voltage challenges is partially due to well-designed, existing control settings at the substation LTC that provide line-drop compensation only during forward power flow and automatically convert to different settings during periods of reverse power flow using "cogen" mode. These control settings are sufficient in this case to limit overvoltages due to the PV.

[4] Thousands of annual operations may seem high, but it still provides multiple decades of service life because such equipment is typically rated for multiple tens of thousands of operations.

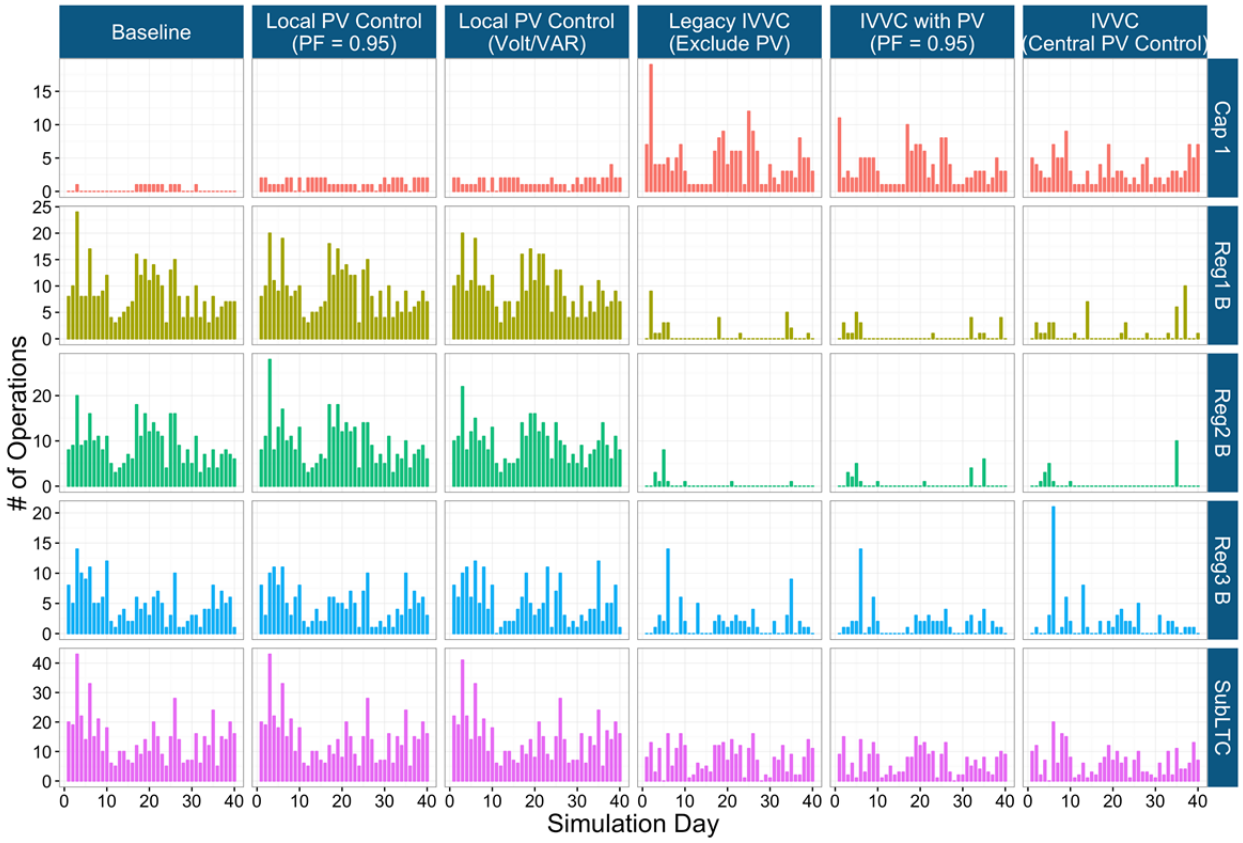


**Figure ES-1. Feeder 40-day results of number of operations of voltage regulation equipment**

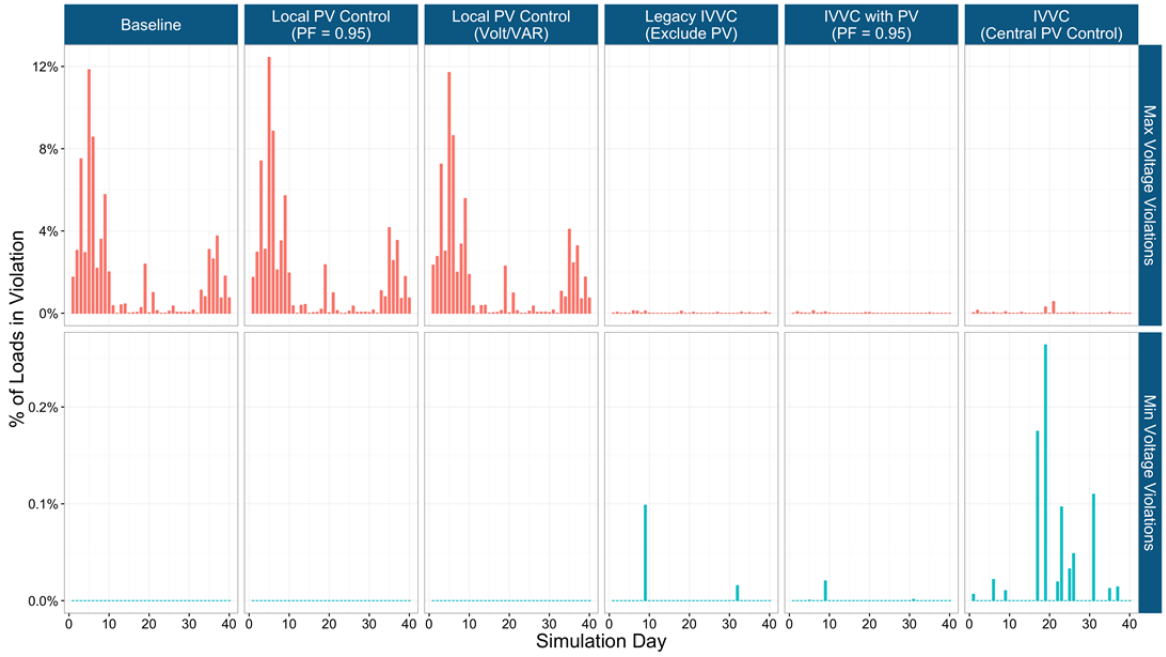


**Figure ES-2. Feeder 40-day results of number of load-voltage violations. Each violation count represents a customer minute of violation out of approximately 1 million possible customer minutes per simulation day.**

Key results from the simulated scenarios with alternate advanced PV inverter and DMS control modes for the existing 5-MW solar power plant are the following:

- In all three DMS-coordinated IVVC scenarios, the simulated existing load voltage violations were significantly reduced compared to the baseline.
- The central IVVC optimization algorithm also reduced the daily number of operations of the substation LTC by more than half, and it drastically reduced the operation of the line regulators. In fact, for most days the line regulators were not used at all in the voltage regulation of the feeder, suggesting the possibility of removing some or all of this equipment to save costs.
- Running IVVC for existing utility regulation equipment while the inverter also provided local voltage support at a constant 0.95 PF absorbing (inductive) showed the best performance of all of the simulated control strategies because the local control mode was able to compensate for the variability effects that the 10-minute IVVC solves are not able to address. In future research, IVVC could also be configured to run faster or to trigger additional solutions on observed voltage violations or other events, both of which could help further improve IVVC results, especially those where PV is centrally controlled.
- Simulated results of using local control modes—0.95 PF absorbing (inductive) and volt/VAR with reactive power as a function of voltage—at the existing PV plant showed minimal changes in the operation of the voltage regulation equipment. Likewise, these modes had minimal effect on the number of voltage challenges at load locations on the feeder. This is likely because the PV plant was located close to the substation, and as such it was not likely to impact the load voltage challenges occurring downstream and during hours of low or no PV production.
- The voltage management strategy in the study feeder dramatically changed when using the DMS-controlled IVVC optimization algorithm[5] with the objective of minimizing feeder net demand while reducing voltage violations.
- With the tested IVVC settings, the voltage regulation was largely performed by the capacitors. The few remaining load voltage challenges in the IVVC scenarios occurred during highly variable PV days, and as such they were largely because the IVVC algorithm was configured to solve every 10 minutes and the voltage management plan was locked between discrete solution instances, making it difficult to compensate for large PV ramping events. This could potentially be mitigated by increasing the frequency of the IVVC solves or by configuring inverters for local ramp rate limiting.
- In many tested control modes, reactive power—either from the capacitors or the PV inverter—was used to manage voltage. This tended to somewhat increase distribution system losses. It also slightly increased reactive power demands from the substation/transmission system during sunny periods while slightly decreasing reactive

[5] Note that IVVC control schemes are user-configured to weigh the relative "penalties" for different classes of equipment operations and for constraint violations such as voltage and reactive power. The results described here correspond to the IVVC configuration currently used by Duke in other service territories, but results corresponding the relative operations of different equipment could be changed, if desired, through this configuration.

power demands during lower solar periods. This increased reactive power demand could potentially act like absorbing power factors for PV and thereby help subtransmission and transmission manage voltage rise for substations with large reverse power flow from PV; however, the additional reactive demand must be provided somewhere, potentially demanding more from central generators or other transmission-connected reactive power devices. Further research is needed to explore these interactions and could also explore the possibility of adding additional IVVC parameters to minimize losses or optimize feeder head reactive power flows to further improve performance.

- The changes in feeder head net reactive power were generally relatively small for all scenarios, except IVVC with PV control; however, despite the small reactive power changes, feeder head power factor changed dramatically because back-feed from PV production can cause very low real power exchange. This suggests future research to look beyond power factors for specifying transmission-distribution interfaces.
- Allowing the IVVC system to control the large PV inverter reactive power target[6] was able to further reduce capacitor operations by one-third because the central optimization algorithm chose to dispatch the inverter as a capacitor for most hours of PV production; however, the increased reliance on the inverter to manage the voltage caused increased voltage challenges when PV output—and hence reactive power capability—varied from one IVVC solve to another.

Two-day sensitivity analyses explored how these results change with alternate fixed power factors and (separately) when a second large PV plant (also 5 MW) was added near the end of the feeder. None of the tested power factors had a significant impact on voltage for the existing PV power plant, and 0.95 PF absorbing (inductive) provided the lowest number of equipment operations. For the additional PV sensitivity, a second 5-MW PV plant was added at the end of the three-phase portion of the feeder, which was approximately 5.7 miles from the substation. With this addition and without any control adjustments, the feeder had much larger challenges with voltage and increased regulation equipment operations compared to the scenarios using a single, closer PV plant. With the additional 5-MW PV plant, the local control modes—with a 0.95 PF and volt/VAR—were both effective at mitigating the adverse impacts to voltages, and IVVC notably reduced equipment operations while still managing voltage. This suggested another key result:

[6] The IVVC system controlled the reactive power (kVAR) set point up to and including an assumed 0.8 PF PV limit. Between IVVC runs, actual PV reactive power could be lower if real power production drops enough that reactive power must also drop to stay within a 0.8 PF.

- Sensitivity analysis with the addition of a second, 5-MW solar PV plant near the end of the feeder's three-phase trunk showed considerable improvement using local PV control modes: both volt/VAR and 0.95 PF absorbing (inductive) power factor. Volt/VAR had the best performance because it not only reduced the total number of substation LTC and line regulator operations but also locally managed the voltage fluctuations caused by the large PV plant at the end of the feeder.
- With the additional 5-MW solar plant, the IVVC (for existing utility equipment only) continued to perform well, managing voltage while notably decreasing LTC and regulator operations with a modest increase in capacitor switching

In summary, these results point to the effectiveness of the IVVC for managing voltage with high-penetration, MW-scale, distributed PV. In all scenarios tested, coordinating voltage regulation using the central DMS IVVC algorithm drastically reduced regulator operations while only modestly increasing capacitor switches and nearly eliminating load voltage challenges observed in the baseline; however, solving and implementing the IVVC algorithm every 10 minutes (or longer) may not be able to effectively regulate voltage effects caused by highly variable PV. More frequent IVVC solutions and/or including PV forecasting in IVVC are enhancements that could be further explored to address such issues. Sensitivity analysis highlighted the strong impact location has on the effectiveness of local PV controls and suggests increased value of local inverter control modes—particularly volt/VAR—with even higher penetrations of solar PV or when PV is located farther from the substation.

These results also suggest a number of hypotheses that could be confirmed with future research. For instance, under tested IVVC settings, the line regulators are seldom used, suggesting that for this system—at least in nominal operations—results similar to those of the IVVC might be achievable with careful settings of local controllers; however, the IVVC streamlines and centralizes such adjustments, suggesting that a single (or small number of) IVVC configuration(s) may be able effectively manage an entire service territory under high-penetration PV. In addition, the IVVC's feeder-wide perspective could also provide added value for places where end-of-line customers might otherwise experience voltage challenges with high-penetration PV that are not directly observable by traditional local-sensing regulating devices, particularly with tighter voltage tolerances under CVR. Finally, the IVVC's online optimization approaches could provide effective voltage management, with little to no manual adjustment, during reconfiguration of feeders, even with substantial PV deployments.

# Table of Contents


**1 Utility Background ..... 1**
1.1 North Carolina Solar Adoption ..... 1
1.2 DMS Deployment Status at Duke Energy ..... 1
**2 Advanced Inverter Background ..... 2**
2.1 Voltage Impacts of Distributed Solar ..... 2
2.2 Opportunities for Advanced Inverters ..... 2
2.3 Advanced Inverter Standards and Communications Architectures ..... 4
2.4 Advanced Inverters and DMS ..... 5
**3 Test Scenarios ..... 6**
3.1 Study System ..... 6
3.1.1 Feeder and PV Plant ..... 6
3.1.2 Existing Utility Equipment ..... 7
3.2 Inverter Control Modes Under Study ..... 9
3.2.1 Local Control Modes ..... 9
3.2.2 IVVC and Advanced Inverters ..... 11
3.3 Alternative PV and Load Scenarios for Sensitivity ..... 12
**4 Analysis Approach ..... 13**
4.1 Simulation with DMS ..... 13
4.1.1 e-terradistribution/DOTS ..... 13
4.1.2 py4etd ..... 14
4.1.3 NREL Simulation Code ..... 14
4.2 Data and Statistical Processing ..... 17
4.2.1 Preprocessing of SCADA Time-Series Data ..... 17
4.2.2 Daily Statistics ..... 18
4.2.3 Representative Day Selection ..... 21
4.2.4 Extrapolating Representative Simulations to Annual Results ..... 25
4.3 Cost-Benefit Alternatives Analysis ..... 26
4.3.1 Tool Description ..... 26
4.3.2 High-Level Approach ..... 27
4.3.3 Alternatives Analysis ..... 28
4.3.4 Cost-Benefit Assumptions ..... 28
**5 Advanced Time-Series Visualizations ..... 32**
5.1 3D Immersive Visualization ..... 32
5.1.1 Time-Series View ..... 35
5.1.2 2D Topology View ..... 36
5.1.3 3D Topology View ..... 37
5.1.4 3D Distance View ..... 38
5.1.5 Discussion ..... 39
5.2 R-Based Visualization ..... 40
**6 Simulation Results ..... 41**
6.1 40-Day Results Summary ..... 41
6.1.1 Scenario List ..... 41
6.1.2 Regulation equipment Impacts ..... 41
6.1.3 Voltage Impacts ..... 42
6.2 Validation of Feeder DOTS Model ..... 44
6.2.1 Time-Series Simulation Methodology ..... 45
6.2.2 Evolution of Baseline Validation Methodology ..... 45
6.2.3 Comparison of Measured Data to DOTS Simulation ..... 47
6.3 Baseline Results ..... 51

6.3.1 Baseline Detail Results for Two Days ..... 51
6.4 Autonomous Local Control ..... 60
6.4.1 Constant Power Factor (0.95 Absorbing) ..... 60
6.4.2 Local Volt/VAR Control ..... 63
6.5 Integrated Volt/VAR Control through DMS ..... 66
6.5.1 IVVC with Traditional Inverter ..... 66
6.5.2 IVVC with the PV Inverter in Autonomous Local Control (PF=0.95) ..... 69
6.5.3 Integrating Advanced Inverters into IVVC ..... 72
6.6 Additional Sensitivity Analysis ..... 75
6.6.1 Local Constant Power Factor Control Sensitivity Analysis ..... 75
6.6.2 Additional Central Solar ..... 78
6.7 Cost-Benefit Alternative Analysis Results ..... 88
6.7.1 Results Summary: Scenario NPVs at Decade Planning Horizons ..... 88
6.7.2 Scenario Value Analysis ..... 89
6.7.3 Cost Benefit Discussion ..... 93
6.7.4 Simulated Voltage Regulation Equipment Replacement Schedules ..... 94
6.7.5 Cost-Benefit Analysis Assumptions ..... 94
6.8 Substation-Level Impacts ..... 95
6.8.1 Feeder Head Real-Reactive Power Relations ..... 95
6.8.2 Thinking Beyond Power Factors ..... 96
6.8.3 Real-Reactive Relationships with Additional 5 MW of PV ..... 96
**7 Power Hardware-In-the-Loop Verification ..... 99**
7.1 Hardware Setup ..... 99
7.2 PHIL Cosimulation ..... 101
7.2.1 Cosimulation Sequence ..... 101
7.2.2 Cosimulation Software Description ..... 101
7.3 PHIL Results ..... 102
7.3.1 Baseline ..... 102
7.3.2 Local Advanced Inverter Control (Constant Power Factor, Volt/VAR) ..... 103
7.3.3 Toward PHIL with IVVC ..... 104
**8 Discussion and Conclusions ..... 105**
**References ..... 107**
**Appendix A Additional Description of the Cost-Benefit Analysis Tool ..... A-1**
**Appendix B Detailed PHIL Block Diagrams ..... B-1**
**Appendix C Additional Simulation Results ..... C-1**
C.1 40-Day Summaries ..... C-1
C.2 Voltage-Distance Plots for Sensitivity Analysis ..... C-5
C.3 Complete 40-Day Results ..... C-38

# List of Figures

Figure ES-1. Feeder 40-day results of number of operations of voltage regulation equipment ..... viii
Figure ES-2. Feeder 40-day results of number of load-voltage violations. Each violation count represents a customer minute of violation out of approximately 1 million possible customer minutes per simulation day. ..... viii
Figure 1. Simplified voltage impacts of DGPV and mitigation using a voltage regulator. *Images by Michael Coddington, NREL, as published in Palmintier et al. (2016)* ..... 2
Figure 2. Simplified depiction of the ability of advanced inverters to absorb reactive power and help mitigate challenges to voltage rise on the feeder. *Image by Michael Coddington, NREL, as published in Palmintier et al. (2016)* ..... 3
Figure 3. Locations of feeder voltage regulating and protection equipment. Asterisks indicate SCADA measurement points. Rcl1 and Rcl2 are reclosers. ..... 9
Figure 4. Operation region of a PV inverter showing power factor limit. Two prototypical operating points are shown: One where the PV apparent power limit is binding such that reactive power provision at full sun requires curtailing active power (assumed for local control modes), and a second where certain components are oversized for higher current flows to allow the inverter to provide reactive power at the full rated real power (assumed for IVVC modes). ..... 10
Figure 5. Q(V) curve simulated in volt/VAR mode for calculating reactive power based on the PCC voltage. When the voltage is too high, the inverter acts like an inductor and absorbs reactive power ..... 11
Figure 6. Real and reactive power capability curve of the inverter at the PV plant modeled for the IVVC algorithm ..... 12
Figure 7. DOTS server and client architecture setup at NREL ..... 13
Figure 8. Example of smoothing to create native load ..... 18
Figure 9. Histogram of PV variability index and relationship to measured data ..... 20
Figure 10. Seasonal loading type assigned by daily MWh ..... 20
Figure 11. Historic operations per day for Cap1 on the study feeder ..... 21
Figure 12. Histogram of bootstrap errors for the ability of the sampled 40 days to predict annual capacitor switching behavior. For reference, the capacitor bank switched more than 2,100 times during the year. ..... 25
Figure 13. High-level data flow diagram of cost-benefit analysis used in this report ..... 27
Figure 14. Data flow diagram for commodity value streams calculations ..... 29
Figure 15. Assigning maintenance and replacement unit costs for switching equipment ..... 30
Figure 16. The immersive virtual environment in the ESIF's Insight Center. Six stereoscopic projectors (four rear-projecting on the wall, and two front-projecting on the floor) create a 3,540 × 2,790 pixel display. Six optical cameras track the space, allowing a user's actions to directly manipulate the 3D objects and perspective. ..... 33
Figure 17. Three-dimensional analysis of the feeder simulation results on a zSpace immersive desktop .. 34
Figure 18. NREL power systems engineers evaluate the results of a DOTS simulation in the immersive virtual environment in the ESIF's Insight Center. Multiple views are shown simultaneously. A 2D temporal graph depicting the day's PV generation and line voltages can be interactively pinned anywhere in the space. The "current" time can then be selected on this graph. The 2D topography of the feeder is projected on the floor, while a 3D representation of each line's phased voltage, real power, and reactive power float in 3D space. ..... 35
Figure 19. Time-series view. This view provides the global temporal context for a single day (single simulation) of the feeder. The PV generation is shown in yellow. The individual line voltages for every line in the study feeder are shown in desaturated red, green, and blue (representing Phase A, Phase B, and Phase C voltages). ..... 36

Figure 20. Two-dimensional topology view. This provides a typical geographically mapped view of the feeder lines with width and color mapped to voltage, real power, or reactive power. ..... 37
Figure 21. Three-dimensional rendering of the study feeder. Voltage is displayed on the z-axis. Reactive and active power are represented by line (tube) height/width and color saturation. Individual phases are shown in red, green, and blue. ..... 38
Figure 22. Three-dimensional distance view. Distance from the feeder head is along the x-axis, time is along the y-axis, and voltage is along the z-axis. Individual phases are colored red, green, and blue (A, B, and C). Reactive and active power are represented by line width and color saturation. ..... 39
Figure 23. Feeder 40-day results of number of operations of voltage regulation equipment ..... 43
Figure 24. Feeder 40-day results of number of load-voltage violations. Each violation count represents a customer minute of violation, so although the numbers may seem high, they generally represent a small fraction of the approximately 1 million possible customer minutes per simulation. ..... 44
Figure 25. PV generation on a clear day and cloudy day ..... 45
Figure 26. Initial validation of recloser Rcl2 currents using BLA only at the feeder head and PV system, showing large differences on Phase B ..... 46
Figure 27. Greatly improved validation currents at recloser Rcl2 when BLA also uses historic Rcl2 data 47
Figure 28. Comparison of measured feeder-head loads to DOTS power-flow simulation results ..... 48
Figure 29. Comparison of measured feeder-head voltages to DOTS power-flow simulation results ..... 49
Figure 30. Comparison of measured feeder-head currents to DOTS power-flow simulation results. These results do not include corrections made later to properly account for capacitor operations in the baseline load data. ..... 50
Figure 31. Comparison of measured recloser currents to DOTS power-flow simulation ..... 51
Figure 32. April 5 baseline time series ..... 53
Figure 33. April 5 baseline voltage profiles from 7 a.m.–7:30 a.m. (nonreverse power flow). Dashed lines indicate +/-5% limits from ANSI C84.1. ..... 54
Figure 34. April 5 baseline voltage profiles from 1:30 p.m.–2 p.m. (reverse power flow). Dashed lines indicate +/-5% limits from ANSI C84.1. ..... 55
Figure 35. August 15 baseline time series ..... 57
Figure 36. August 15 baseline voltage profiles from 7 a.m.–7:30 a.m. (nonreverse power flow). Dashed lines indicate +/-5% limits from ANSI C84.1. ..... 58
Figure 37. August 15 baseline voltage profiles from 13:30 p.m.–14 p.m. (reverse power flow). Dashed lines indicate +/-5% limits from ANSI C84.1. ..... 59
Figure 38. April 5 time-series comparison to baseline with a constant power factor of 0.95 absorbing (inductive) ..... 61
Figure 39. August 15 time-series comparison to baseline with a constant power factor of 0.95 absorbing (inductive) ..... 62
Figure 40. Volt/VAR curve used in simulations ..... 63
Figure 41. April 5 time-series comparison to baseline of autonomous volt/VAR ..... 64
Figure 42. August 15 time-series comparison to baseline of autonomous volt/VAR ..... 65
Figure 43. April 5 IVVC time-series comparison to baseline with PV not eligible for control ..... 67
Figure 44. August 15 IVVC time-series comparison to baseline with PV not eligible for control ..... 68
Figure 47. April 5 IVVC time-series comparison to baseline for IVVC (Central PV Control) ..... 73
Figure 48. August 15 IVVC time-series comparison to baseline IVVC (Central PV Control) ..... 74
Figure 49. April 5 and August 15 time-series comparison to baseline with a constant power factor of 0.9 absorbing (inductive) ..... 76
Figure 50. April 5 and August 15 time-series comparison to baseline with a constant power factor of 0.8 absorbing (inductive) ..... 77
Figure 51. Feeder layout showing the location of the two central PV plants ..... 78

Figure 52. April 5 time-series comparison of the new baseline with two 5-MW PV plants to the baseline with only the existing PV plant ..... 80
Figure 53. August 15 time-series comparison of the new baseline with two 5-MW PV plants to the baseline with only the existing PV plant ..... 81
Figure 54. April 5 time-series comparison of the new baseline with two PV plants operating at a power factor of 0.95 absorbing (inductive), to the baseline with only the existing PV plant ..... 82
Figure 55. August 15 time-series comparison of the new baseline with two PV plants operating at a power factor of 0.95 absorbing (inductive), to the baseline with only the existing PV plant ..... 83
Figure 56. April 5 time-series comparison of the new baseline with two 5-MW PV plants operating in local volt/VAR to the baseline with only the existing PV plant ..... 84
Figure 57. August 15 time-series comparison of the new baseline with two 5-MW PV plants operating in local volt/VAR to the baseline with only the existing PV plant ..... 85
Figure 58. April 5 time-series comparison of the new baseline with IVVC algorithm not controlling the two PV plants to the baseline with only the existing PV plant ..... 86
Figure 59. August 15 time-series comparison of the new baseline with IVVC not controlling the two PV plants to the baseline with only the existing PV plant ..... 87
Figure 60. Cumulative NPVs (without DMS, communication, or PV costs) comparing planning horizons in 5yr increments across all scenarios ..... 88
Figure 62. Categorical cost and savings differences from those of Baseline ..... 91
Figure 63. Categorically aggregated cumulative discounted cash flows for costs of feeder losses and equipment replacement ..... 92
Figure 64. Aggregated cumulative discounted cash flows for equipment replacement broken down by type of equipment ..... 93
Figure 65. Simulated feeder-head P/Q plots showing the impacts of advanced inverter mode on the real (horizontal axis) and reactive (vertical axis) power flows at the substation with the existing 5-MW solar power plant ..... 97
Figure 66. Simulated substation-level P/Q plots with a second 5-MW PV system located near the end of the three-phase feeder trunk for different scenarios ..... 98
Figure 67. Power hardware installed at NREL (500TX and capacitor bank) ..... 100
Figure 68. Simplified diagram of PHIL cosimulation power and data flow ..... 100
Figure 69. Baseline PHIL DOY19 1-hour simulation with measured PV power factor of 0.99 ..... 103
Figure 70. PHIL DOY19 1-hour simulation (power factor of 0.95) ..... 103
Figure 71. PHIL DOY19 1-hour simulation (volt/VAR) showing the oscillations induced by the large time delays from one set point to another ..... 104
Figure 72. Feeder-head summary for baseline ..... C-2
Figure 73. Feeder-head summary for Local PV Control (PF=0.95) ..... C-3
Figure 74. Feeder-head summary for Local PV Control (Volt/VAR) ..... C-4

# List of Tables

Table ES-1. Summary Comparison of Six Annualized Scenarios for Advanced PV Inverters ..... vii
Table 1. Study System Characteristics ..... 7
Table 2. Substation Regulator Settings for Forward and Reverse Power Flow ..... 8
Table 3. Feeder Measurements ..... 17
Table 4. Daily Statistics ..... 19
Table 5. PV Variability Day Classification ..... 22
Table 6. Day Selection Groupings ..... 23
Table 7. Example of Day Classification ..... 26
Table 8. Rates Used to Calculate Value and Cost of Energy ..... 31
Table 9. CBA analysis years in which equipment replacements occur ..... 94
Table 10. Cumulative NPVs at 5-, 10-, 20-, 40-, and 50-Year Planning Horizons ..... A-2

# 1 Utility Background

## 1.1 North Carolina Solar Adoption

North Carolina has seen rapid increases in installed solar photovoltaic (PV) systems, making it the second state for installations in 2014–2015 (GTM Research and SEIA 2016) and the third state overall (as of March 2016) for total installed PV capacity.(SEIA 2016) Unlike other parts of the United States—where smaller rooftop solar plays an important role—the vast majority of solar adoption in North Carolina has been utility scale (> 500 kW), with a majority in the range of 1–5 MW and connected to the distribution system (GTM Research and SEIA 2016; Palmintier et al. 2016). These large distributed-generation solar photovoltaic (DGPV) systems can introduce local voltage challenges because power flows bidirectionally on distribution-line segments, and their associated variability can impact cycling of existing regulation equipment. Advanced inverters can support voltage management both by locally controlling their reactive power output and by changing their reactive power output in response to control commands received via communications.

Duke Energy serves the vast majority of North Carolina and has engaged with the National Renewable Energy Laboratory (NREL) and Alstom Grid (now GE Grid Solutions) to better understand PV-distribution interactions and to examine the potential opportunities enabled by advanced inverters.

## 1.2 DMS Deployment Status at Duke Energy

Duke Energy has deployed a DMS system in its Midwest and Carolinas service territories, and is in the process of deploying DMS in their Florida service territory.

# 2 Advanced Inverter Background

## 2.1 Voltage Impacts of Distributed Solar

As described further in Palmintier et al. (2016), distributed generation of any kind—including DGPV—can raise local distribution system voltage, potentially resulting in overvoltage violations, as shown in Figure 1(a). Utility voltage regulation equipment (e.g., a tap-changing voltage regulator), originally installed to manage voltage drop on a long feeder, can also manage this voltage rise—but only if properly configured to handle bidirectional power flows (Figure 1(b)); however, this can result in increased operations of utility regulation equipment and may not be sufficient for very high DGPV penetrations.

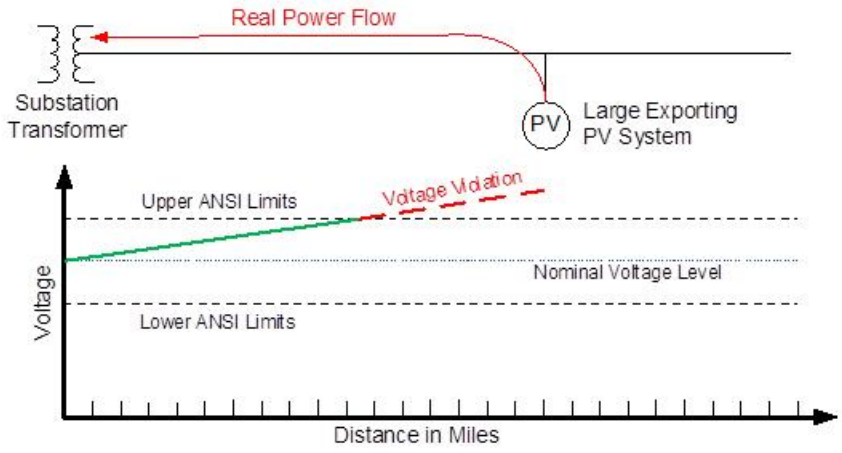


**(a) Voltage rise resulting from reverse power flow from DGPV**

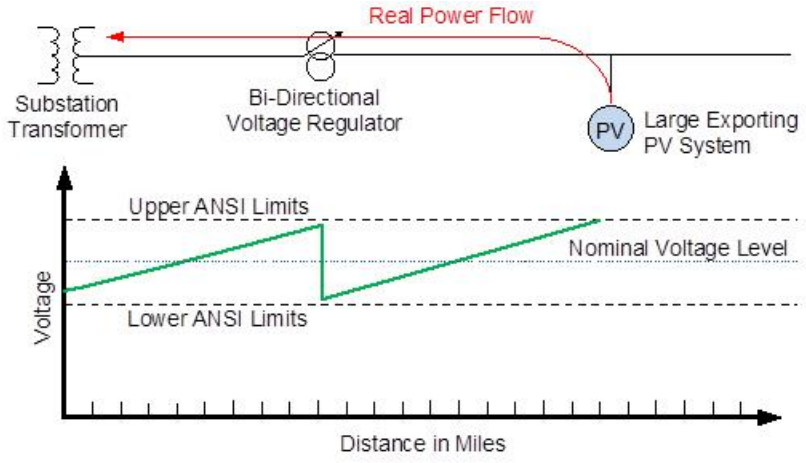


**(b) DGPV overvoltage corrected using a voltage regulator**

**Figure 1. Simplified voltage impacts of DGPV and mitigation using a voltage regulator. *Images by Michael Coddington, NREL, as published in Palmintier et al. (2016)***

## 2.2 Opportunities for Advanced Inverters

Advanced (or "smart") inverters can provide utility-support features such as voltage support, enhanced frequency and voltage ride-through, and a host of autonomous and externally

controllable functions. Many of these advanced inverter capabilities are described in more detail in the Electric Power Research Institute's report on *Common Functions for Smart Inverters, Version 3* (2014). In particular, the power electronics inside modern PV inverters can be used to correct voltage challenges from distributed generation by shifting the phase angle of their sinusoidal current output to absorb (or inject) reactive power (Figure 2). However, as described below, prior to 2014, U. S. interconnection standards required DGPV to act as passive grid participants by not actively managing voltage[7] and by tripping off-line during grid disturbances.

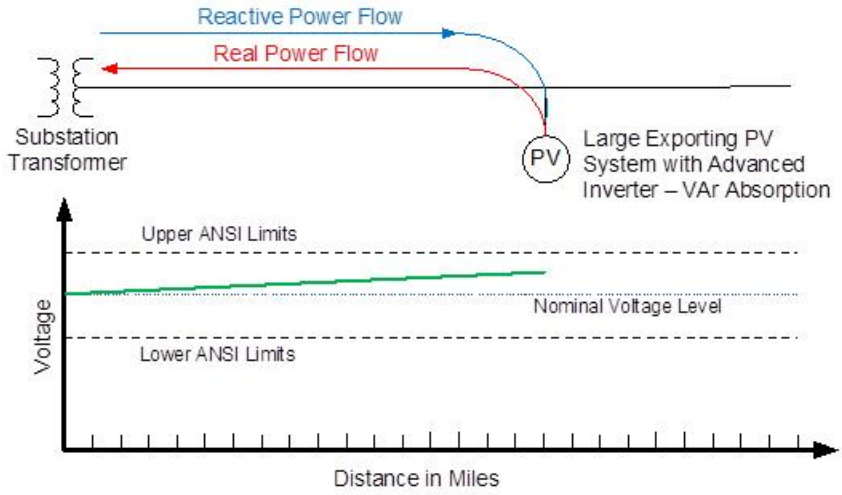


**Figure 2. Simplified depiction of the ability of advanced inverters to absorb reactive power and help mitigate challenges to voltage rise on the feeder.** ***Image by Michael Coddington, NREL, as published in Palmintier et al. (2016)***

Despite these restrictions, since 2010, there has been a dramatic upswing in the availability of "advanced" features in PV inverters, largely in response to international requirements (Braun et al. 2011). Today (2016), inverters purchased off the shelf in the United States likely have many advanced functions built in, even though these features may be disabled or hidden in U.S. markets. Previous studies have shown that advanced inverters can mitigate voltage-related issues and that 25%–100+% more PV can be accommodated using advanced reactive power controls such as volt/volt-ampere reactive (VAR) and constant power factor (PF) ( Braun et al. 2011; Coddington et al. 2012; Seuss et al. 2015).

Another key feature typically found in advanced inverters is support for external communications. Such interfaces allow remote control systems to interact with and manage inverter settings. This potentially opens up considerable opportunity for utilities to integrate DGPV into operational schemes either through traditional communications channels or via new pathways such as through aggregators, broadcast data, or the emerging Internet of Things.

[7] Some reactive power injection/absorption has long been allowed, but prior to 2014 it was allowed only at a constant power factor.

## 2.3 Advanced Inverter Standards and Communications Architectures

As described further in Palmintier et al. (2016), DGPV installations are subject to a wide range of standards and requirements, including both traditional electrical safety and performance standards (e.g., National Electrical Safety Code, National Electrical Code, and ANSI C84.1) and DER-specific codes (e.g., IEEE 1547 and UL 1741).

Of these, the IEEE 1547 Standard for Interconnecting Distributed Resources with Electric Power Systems deserves special mention. It provides requirements for interconnecting all types of distributed generation, including DGPV. Released in 2003, it standardized previously diverse interconnection requirements. The original version explicitly required DERs to disconnect during over-/underfrequency and voltage events and forbid DERs from actively regulating voltage (IEEE 2003). In 2014, the standard was amended to make it possible—but not required—for utilities to work with DER providers to enable grid support through voltage regulation and/or grid disturbance ride-through (IEEE 2014). A full revision of the standard is underway and is expected to require DGPV to support large-scale grid operations through frequency and voltage ride-through requirements and explicitly require configurable advanced functions including voltage control. IEEE 1547 also includes complementary standards and guidelines—1547.1–1547.8—for testing, larger systems, microgrids, and other applications.

The closely related Underwriters Laboratories (UL) Standard 1741—Standard for Inverters, Converters, Controllers and Interconnection System Equipment for Use with Distributed Energy Resources—provides a compliance testable safety standard for PV inverters and other equipment (2010). In most jurisdictions, customer-owned—but not utility-owned—inverters must be UL 1741 qualified to interconnect. The standard is generally harmonized with IEEE 1547 and hence also undergoing a full revision; however, UL 1741 currently lags behind IEEE1547a-2014 such that UL 1741 Supplemental A is currently available only as a draft and is not expected to be published until later in 2016.

In addition, a number of efforts target specific communications-related aspects for smart inverters, including IEC 61850-90-7, which provides a description of advanced inverters for use in the Common Information Model (CIM); SunSpec, which provides a standardized field map for lower-level (e.g., modbus) communications for PV inverters; Smart Energy Profile version 2 (SEP2), also known as IEEE P2030.5, which provides an Internet-protocol-based smart-grid control protocol designed to run via many communications layers (e.g., WiFi, ZigBee, and HomePlug); and the open field message bus (OpenFMB), which provides an industrial/utility-class architecture for peer-to-peer and data-driven hub/exchange interoperability. OpenFMB grew out of the Duke Energy-led Distributed Intelligence Platform and targets integrating existing and emerging utility devices in addition to (typically larger) DERs.

A number of other efforts are looking more broadly at future power system architectures. The Smart Grid Interoperability Panel (SGIP) began at the National Institute of Standards (NIST) and has since become an industry consortium. SGIP uses a consensus approach to "accelerate standards harmonization and advance the interoperability of smart grid devices and systems." (NIST 2016) In California, CA Rule 21 and the closely related Smart Inverter Working Group (SIWG) are taking a leading-edge look at DGPV interconnection and communications requirements.

## 2.4 Advanced Inverters and DMS

High-penetration DGPV in general and advanced inverters in particular provide challenges and opportunities for distribution management systems (DMS). DGPV, particularly smaller systems, represent critical but typically hidden changes to (net) customer demand. With the integration of communications, DGPV represents a new, high-performance resource that might be controlled by utilities when regulations and contracts allow (Nagarajan, Palmintier, and Baggu 2016).

On its own, increased DGPV represents a weather-dependent source of distributed generation that looks like negative load yet no longer follows standard load patterns. This complicates the load allocation step in power flow simulations and suggests a need to use emerging support for DERs as a unique asset class within DMS systems and utility operational practice. Advanced inverter features—particularly reactive power support and voltage regulation—require additional attention for accurate distributed VAR injection/absorption, to obtain accurate estimates of feeder-wide voltage state, and to manage possible interactions with existing regulation equipment. In addition, it is important to recognize that DGPV behaves very differently from both load and traditional generation during anomalies. In particular, inverter-based technologies have much shorter duration and lower intensity fault current (Keller and Kroposki 2010), which can impact protection and potentially fault location schemes.

With communications and supportive regulations/contracts, advanced inverters represent a new controllable resource that can support utility operations through the DMS. Advanced inverters can provide an additional DMS-managed source of voltage control, either through direct power factor control, through reactive power set points (less flexibly), or most powerfully by dynamically volt/VAR and related response curves. Communications also enable selective curtailment of DGPV to manage voltage, overloading, and system-wide needs, at least in favorable policy environments. In addition, DGPV inverters can monitor not only their own power production but also can measure other operator relevant data such as local voltage.

# 3 Test Scenarios

We conducted a detailed study of one distribution feeder in Duke Energy's North Carolina service territory. This feeder already has a 5-MW solar PV plant installed approximately 2 miles from the substation. The PV plant is sufficiently large to provide the entire feeder load and back-feed the substation during most sunny periods. We explored a number of scenarios using this feeder, including the following:

- Baseline validation of the simulation environment using recorded data for 2014. In addition to providing a reference comparison for the other scenarios, this analysis revealed that the solar farm currently operates at a power factor (PF) of about 0.99 absorbing (inductive).
- Impacts of two autonomous voltage-control modes:
    - Power factor of 0.95 absorbing (inductive)
    - Volt/VAR control where the amount of reactive power absorbed/injected into the system is varied in response to voltage changes at the point of common coupling (PCC).
- Impacts of DGPV interactions with DMS-integrated volt/VAR control (IVVC) for three scenarios:
    - DMS control of utility regulation equipment (regulators, load tap changers [LTCs], and capacitors) optimized through IVVC to minimize feeder head net demand (i.e., to use conservation voltage reduction [CVR]) while avoiding voltage violations. In this scenario solar operates as it does in the baseline.
    - IVVC control to minimize feeder head net demand while avoiding voltage violations where the solar farm operates at a power factor of 0.95 absorbing (inductive)
    - IVVC control where the DMS also sends set points for the PV system reactive power output—in addition to utility equipment—to minimize feeder head net demand while avoiding voltage violations.

In addition, 2-day sensitivity analyses were conducted for:

- Alternative power factors
- The addition of a second 5-MW utility-scale PV system installed near the end of the feeder.

## 3.1 Study System

### *3.1.1 Feeder and PV Plant*

The Duke Energy-owned substation is served by a 44-kV line and includes one 10-MVA 44/13.5-kV fixed tap transformer serving three nominally12.47-kV circuits, each controlled by their own feeder head regulators. One of these circuits was analyzed in this project, and it has an estimated native (i.e., without PV) winter peaking load of 5.26 MW. What would otherwise be an unremarkable, sprawling, rural feeder also happens to have a 5-MW solar PV plant, configured with 10 500-kW inverters, located approximately 2 miles from the substation. The

feeder has a relatively low native load and high PV penetration, and thus it back-feeds significant power to the substation almost daily, making it an excellent candidate for studying advanced inverter control opportunities for utility-scale DGPV. Key circuit and PV plant characteristics are summarized in Table 1..

**Table 1. Study System Characteristics**

| | |
|---|---|
| **Feeder Characteristics** | |
| Substation primary/secondary voltage (kV LL) | 44/13.5 |
| Substation transformer (MVA/%X) | 10/6.84 |
| Feeder head gang-operated regulators, set of three (kVA/%X) | 250/6.25 (each) |
| Feeder head X/R | 4.25 |
| P(Est. Native)$_{annual\ avg}$ (MW) | 1.71 |
| P(Est. Native)$_{peak}$ (MW and date) | 5.26 (Jan. 30, 2014) |
| P(Measured)$_{annual\ avg}$ (MW) | 0.678 |
| P(Measured)$_{min}$ (MW) | -3.72 |
| Capacitor Banks (number/total kVAR) | 2/900 |
| Line Regulator groups | 1x3-phase, 2x2-phase |
| **PV Plant Characteristics** | |
| Commission date | March 2013 |
| Plant rating ($MW_{DC}/MW_{AC}$) | 6.4/4.8 |
| PV recloser X/R | 1.82 |
| Distance to substation (overhead line miles) | 1.75 |

### *3.1.2 Existing Utility Equipment*

The feeder has a range of existing voltage regulation equipment, including a set of gang-operated substation voltage regulators,[8] a VAR controlled capacitor, a fixed capacitor, and three sets of single-phase voltage regulators: One group with a regulator on each of three phases and two other groups with only B- and C-phase regulators.

[8] These regulators act as the LTC for the feeder

This substation is operated such that the main 10-MVA transformer steps down a 44-kV line to a medium-voltage bus operated at 13.5 kV (1.08 p.u. on a 12.47-kV base). From this substation bus, a set of three gang-operated regulators act as a load tap changer (LTC) to regulate the feeder head voltage. These regulators have +/-16 taps and operated in "cogen" mode, which supports separate settings for forward and reverse power flow. In cogen mode, the "reference winding" for the voltage target is always the secondary side, regardless of forward/reverse flow.[9] This ensures the regulator is always managing voltage on the "non-stiff" side.

The corresponding line-drop compensation values for each power flow direction are shown in Table 2. Because of the relatively high substation bus voltages, the LTC-like regulators nearly always operate in the negative tap positions to maintain the 123-V set point. Note that these regulator settings reflect the most recent change in set points, which were last made by Duke Energy in July 2015.

**Table 2. Substation Regulator Settings for Forward and Reverse Power Flow**

| Equipment Name | Forward | Reverse |
|---|---|---|
| R (Ω) | 7 | 0 |
| X (Ω) | 0 | 0 |
| Voltage base (V) | 123 | 123 |
| Bandwidth (V) | 3 | 3 |

Downstream of the substation regulator, the feeder has two capacitor banks, three sets of voltage regulators, and three reclosers as shown in Figure 3. Specifically:

1. **Cap1:** A 450-kVAR (150 kVAR per phase) VAR-controlled capacitor with temperature override. The capacitor switches in at 600 kVAR (three-phase) and switches off at 10 kVAR (three-phase). The high-temperature override settings for switching in and out are 95°F and 85°F, respectively, and the low-temperature override settings are 35°F and 25°F, respectively.
2. **Cap2:** A three-phase 450-kVAR capacitor (always disconnected unless controlled otherwise by IVVC)
3. **Reg1:** A set of three single-phase 167-kVA regulators with a voltage target of 123 V; R and X line-drop compensation values of 4 and 0, respectively; and 3 V of voltage bandwidth.
4. **Reg2:** A set of two single-phase 114-kVA regulators on phase B and phase C with a voltage target of 123 V; R and X line-drop compensation values of 4 and 0, respectively; and 3 V of voltage bandwidth.

[9] This is the key distinguishing point between cogen mode and "bidirectional mode" (used for switching), which also uses alternate settings for reverse flow. In bidirectional mode (not used here) the voltage target reference winding flips to the primary side with reverse power flow. This is appropriate when a feeder might be reconfigured to have an alternate utility source that results in reverse power flow and the voltage still needs to be managed downstream. Bidirectional mode is less effective when the reverse power flow results from distributed generation since it is impractical to try to regulate voltage from the stiff grid source.

5. **Reg3:** A second set of two single-phase 76.2-kVA regulators on phase B and phase C with a voltage target of 124 V; no R and X line-drop compensation; and 3 V of voltage bandwidth.

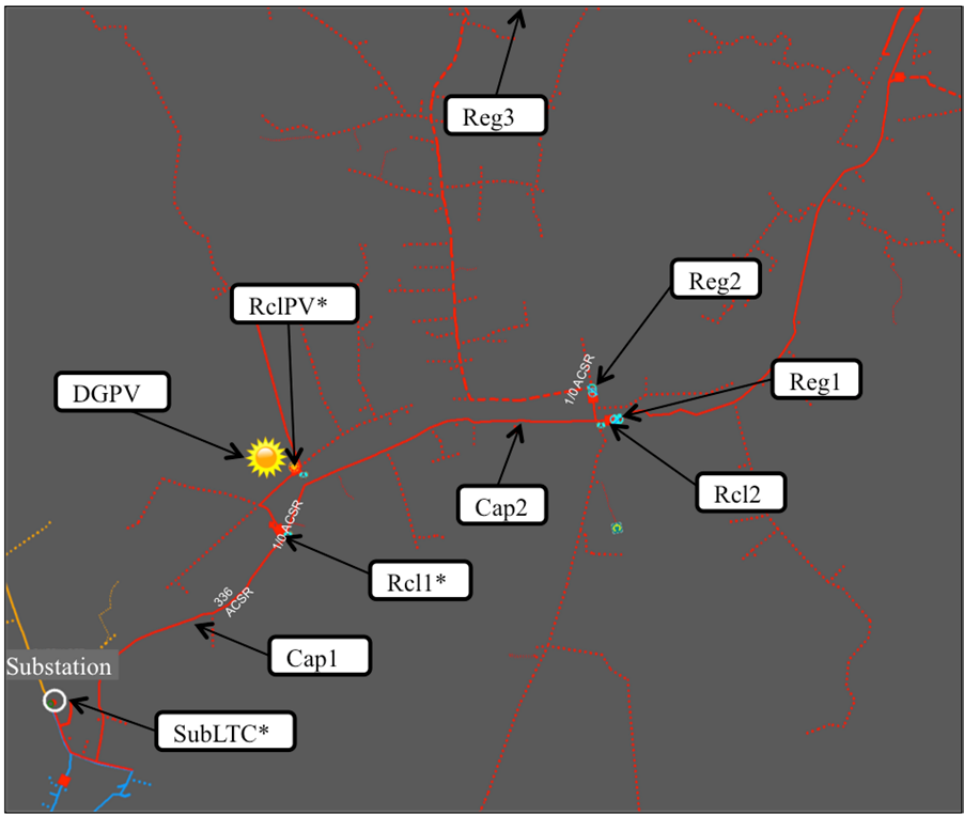


**Figure 3. Locations of feeder voltage regulating and protection equipment. Asterisks indicate SCADA measurement points. Rcl1 and Rcl2 are reclosers.**

## 3.2 Inverter Control Modes Under Study

A range of feeder equipment and PV inverter control modes—both local autonomous modes and centrally coordinated by the DMS—were integrated into the Alstom Distribution Operator Training Simulator (DOTS) using NREL-developed inverter models that cosimulate with DOTS through the Alstom Grid provided py4etd Python interface.

### *3.2.1 Local Control Modes*

This section describes the details of the local control modes implemented in Python and connected into DOTS using the py4etd interface. The local control modes implemented are constant power factor and volt/VAR.

Figure 4 presents a classic circle diagram that depicts the operation region of the inverters. Because PV generators cannot absorb active power, only the right half of the circle diagram is plotted. Typically, inverters have a minimum allowable power factor, which is user-configurable in the simulation. Additionally, some emerging inverters support night mode, which allows the inverter to provide pure reactive power for voltage support (PF=0) when active power drops below a user-configurable threshold near zero. Finally, there are multiple ways of handling total

apparent power (kVA) limits when the vector sum of the active-power generation (kW) and the reactive power (kVAR) exceeds the nameplate (kVA). In these simulations, we assume VAR priority where rating the active power will be curtailed, if needed, to provide the required reactive power.

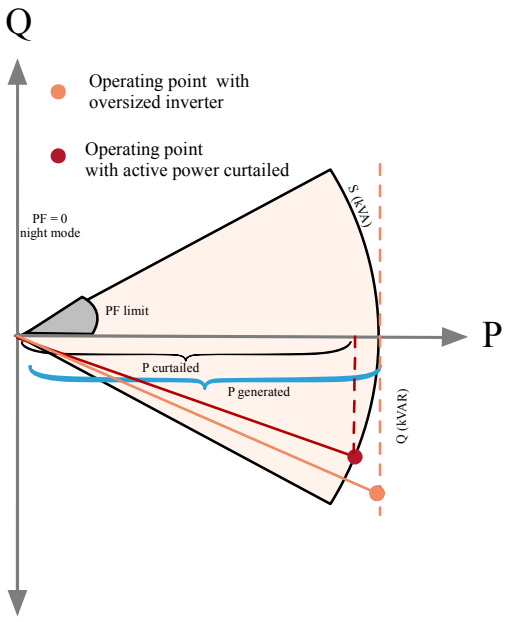


**Figure 4. Operation region of a PV inverter showing power factor limit. Two prototypical operating points are shown: One where the PV apparent power limit is binding such that reactive power provision at full sun requires curtailing active power (assumed for local control modes), and a second where certain components are oversized for higher current flows to allow the inverter to provide reactive power at the full rated real power (assumed for IVVC modes).**

#### *3.2.1.1 Constant Power Factor*

In this local control mode, a user specifies the power factor (typically absorbing/inductive/lagging) in which the PV generator is expected to operate. For example, if the user-specified power factor results in an apparent output power that exceeds the kVA rating of the PV inverter, then the active power will be curtailed to accommodate the set point.

#### *3.2.1.2 Volt/VAR*

This control mode is an automated process that requires the user to specify a curve, as shown in Figure 5. The curve used in this analysis was modeled after the volt/VAR set points proposed in (Smith et al. 2011). This control mode uses the voltage at the PCC to calculate the reactive power. For example, if the voltage at the PCC is higher than 1.03 p.u. and less than 1.05 p.u., then the required reactive power will be calculated based on linear interpolation. The resulting apparent power was then compared to the inverter's kVA and power factor limits, as shown in Figure 4. If the vector sum of active power (P) and reactive power (Q) exceeds the inverter's kVA limit, then the active power will be curtailed to accommodate the calculated reactive power.

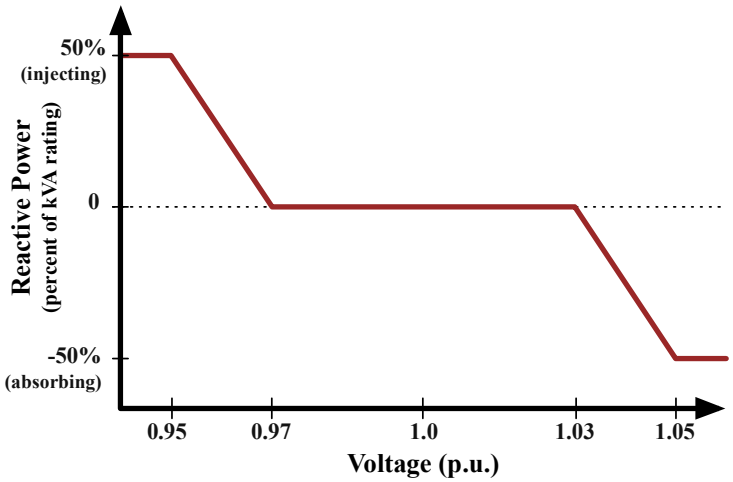


**Figure 5. Q(V) curve simulated in volt/VAR mode for calculating reactive power based on the PCC voltage. When the voltage is too high, the inverter acts like an inductor and absorbs reactive power.**

### 3.2.2 IVVC and Advanced Inverters

Integrated volt/VAR control (IVVC) is an advanced DMS function that determines an optimal set of control actions for all voltage regulating devices and VAR control devices to achieve one or more specified operating objectives while attempting to avoid violating any of the fundamental operating constraints (high/low voltage limits, load limits, etc.). In the Alstom/GE system, these constraints are implemented as penalty functions that strongly encourage compliance, but may allow for some small violations. Additional user-defined penalties are used for controller operations. The IVVC function in the DMS can also have different objectives, such as minimizing real-power demand, losses, voltage violations or a combination. The large number of configurable parameters can require some one-time system-wide setup to achieve reasonable control plans. In this project Alstom Grid provided these configuration parameters based on those used in Duke Energy's Midwest operating region.

In this project, the IVVC algorithm is configured to minimize demand and reduce voltage violations. The control actions to achieve these objectives are implemented by the LTC, capacitor banks, and feeder-line voltage regulators. This project also explores including the inverter at the PV plant as a resource for IVVC. The IVVC algorithm is typically solved every 10 minutes,[10] and the control settings are locked to the IVVC plan settings during the time between one IVVC solve and the next.

In the scenario in which the inverter at the PV plant is eligible to receive reactive power commands from the centralized IVVC optimization algorithm, the inverter is modeled following the real and reactive power capability curve shown in Figure 6. In this case, for simplicity, we assume that the inverter is oversized, and as such there is no curtailing of real power (as opposed

[10] IVVC triggering period is user configurable. There also a number of advanced triggering features to allow IVVC to trigger faster, on event such as a low/high SCADA voltage, SCADA loading rate of change, etc. These were not used in these simulations.

to the local control modes in which active power is curtailed to accommodate the reactive power set point when the kVA limit of the PV inverter is exceeded). The reactive power capability curve is modeled to a power factor ± 0.8 within the kVAR limits of the inverter (± 2,500 kVAR).

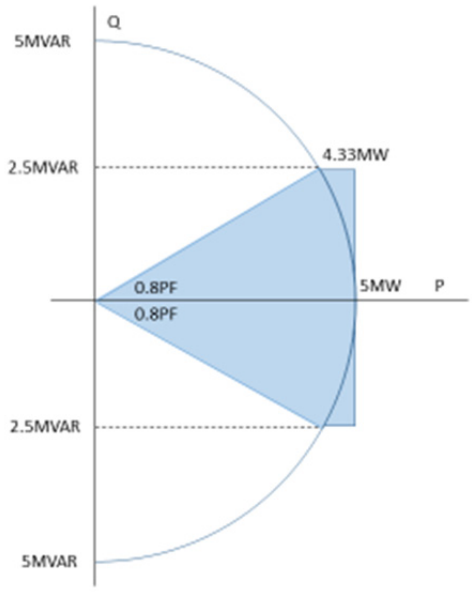


**Figure 6. Real and reactive power capability curve of the inverter at the PV plant modeled for the IVVC algorithm**

## 3.3 Alternative PV and Load Scenarios for Sensitivity

For the sensitivity analyses, we also considered two alternate load/generator cases:

1. Adding an additional 5-MW DGPV site at the end of the three-phase feeder trunk while maintaining the existing PV plant to bring the feeder total to 10MW of DGPV.
2. The use of other power factors for Local Control with fixed power factors.

# 4 Analysis Approach

We conducted a series of quasi-steady-state time-series (QSTS) simulations of the potential for advanced inverters to help mitigate feeder voltage challenges with high-penetration DGPV as found on the study feeder. This section describes our use of Alstom Grid's e-terra*distribution* DMS real-time operations package, and its Distribution Operator Training System (DOTS) to conduct high-fidelity off-line studies at rates faster than real time. This approach afforded a number of key advantages beyond the modeling approaches normally used for this type of analysis:

1. Direct use of the established feeder models and simulation engine in the DMS, avoiding the often time-consuming conversion processes required to use alternative simulation engines
2. A rich, existing library of validated and trusted controller models
3. Native support for integrating historic supervisory control and data acquisition system (SCADA) data into the results. This helps scale load to match actual observations.
4. Easy access to the DMS-coordinated IVVC control features using the exact algorithms used in operations.

## 4.1 Simulation with DMS

### *4.1.1 e-terra*distribution/DOTS

The DOTS development environment at NREL was deployed using a group of virtual machines at NREL's Energy Systems Integration Facility (ESIF) as shown in Figure 7 below.

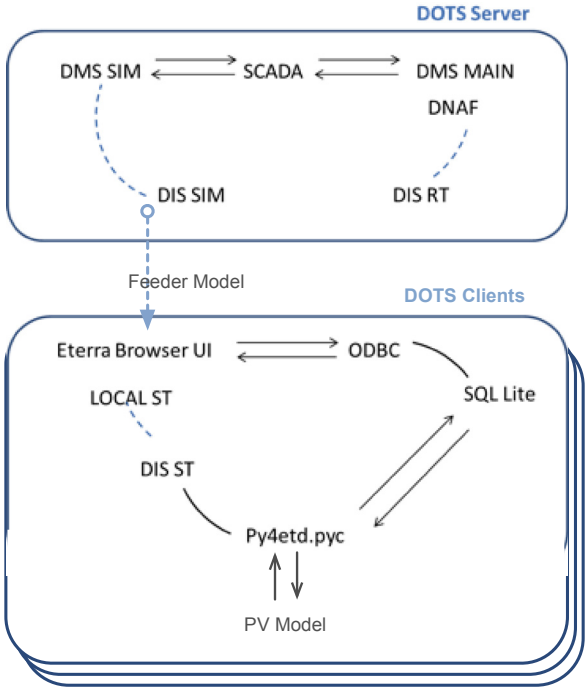


**Figure 7. DOTS server and client architecture setup at NREL**

The DOTS server virtual machine houses the following software components:

- The Distribution Management System Simulation server, which simulates the power system and drives simulated SCADA measurements
- The Real Time server (DMS Main) which uses SCADA measurements to provide simulated control-room operator interaction. This also provides access to the Distribution Network Analysis Function (DNAF) server.

The Distribution Management System Simulation and DMS Main servers connect to the DMS Interface server, which drives the three DOTS modes of operation: (1) real-time (RT) mode, (2) simulator (SIM) mode, and (3) study (ST) mode.

The server and seven client training stations were set up for NREL researchers to use on a single powerful workstation using virtualization. This configuration is highly scalable and was used for both time-series and power hardware-in-the-loop (PHIL) testing needs throughout the project.

The client virtual machines connect to the DOTS server through the e-terra browser user interface. The local client machines connect to the Local ST Server to run in study mode, which is private to the individual client workstation and uses a copy of the real-time distribution model imported from the DOTS server. The py4etd Python scripting package is also set up in the client workstations, and it allows users to access DOTS functionality (e.g., query data, modify the network, and run the DNAF application) and provides tools to perform time-series simulations and store results in a database. An Open Database Connectivity (ODBC) interface can be accessed by the e-terra browser using standard SQL queries through the Python SQL interface module.

### 4.1.2 py4etd

The Python library, py4etd, contains functions and data structures that allow users to control the e-terra*distribution* environment using the Python scripting language. This library provides the critical link between NREL-developed PV inverter models and the feeder power flow and simulation in DOTS.

In study mode, py4etd runs directly on a client workstation and connects to a local DMS study server (Local ST), as shown in Figure 7. Py4etd functions are grouped into user tools, data query, dynamics control, and application requests. The most important functions used in this project were:

- Accessing the study feeder model
- Modifying the PV plant P and Q outputs
- Running the power flow solution
- Extracting data from the results.

### 4.1.3 NREL Simulation Code

An extensive code base was developed to manage and automate the simulation process and model the behavior of the PV inverter. The code was developed in Python and used a partial object oriented structure, particularly for PV simulation. As described below, the components of this code provide support for the following features:

- QSTS simulation
- PV modeling
- IVVC-based simulation
- Management and automation of large numbers of simulations.

#### 4.1.3.1 QSTS Simulation

Although there is some support for time-series analysis through the py4etd interface to the DMS study server simulation environment, the level of interaction required to model the PV system prompted developing code to manage time-series simulation. In general, this code effectively manages two interleaved time-series simulations: one in which historic measurements were used to compute the baseline native load levels across the feeder and a second wherein these loadings were incorporated into a scenario-specific simulation with PV. This interleaved approach was used because it was difficult to precompute and apply time series for all loads on the feeder. Specifically the steps followed for all simulation scenarios (including baseline) were as follows:

1. Cache the current scenario simulation configuration for utility equipment, including regulator tap positions and capacitor status. This allows the load allocation step to change these settings to historic values.
2. Read historic measurements from data file. These historic measurements include sufficient data to accurately estimate the real and reactive levels for all loads: known voltages, feeder head native load,[11] and the state of Cap1.
3. Run Bus Load Allocation (BLA) to allocate loads. This built-in e-terra*distribution* algorithm interpolates between the coarse time steps of generic customer-class load profiles and then adjusts the simulated loading up or down for each region with measurements to closely match the historic values.
4. Restore simulation configuration for utility equipment so that the simulation-specific power flow case appears to be a continuous series of simulations including proper capturing of any hysteresis or other sequence-dependent control settings.
5. Simulate the PV system and control modes to compute PV real and reactive power (see further details in Section 4.1.3.2)
6. Rerun power flow using the load allocation computed in Step 3 and the PV production computed in Step 5.
7. Query and store desired simulation output data for post-processing. Typically this included all regulator and capacitor statuses, feeder head and PV complex power, line flows, and voltage at all nodes.
8. Increment time step and repeat steps 1–8 until end of simulation.

[11] The native loads were computed in preprocessing by subtracting the measured PV production from the measured feeder head net load.

#### 4.1.3.2 PV model

Because historic power production from the existing solar plant was available, the PV model did not need to include sophisticated PV cell or inverter efficiency models. Instead it focused on reactive power output for the simulated advanced inverter modes, and corresponding adjustments to real power output needed to stay within inverter limits. This simplified the PV model to the following steps:

1. Read historic measured PV real and reactive production from data file.
2. Compute updated reactive power production based on the selected advanced inverter mode and set points.
3. Check inverter constraints and adjust simulated real (or reactive) power as needed.

For baseline, constant power, and IVVC control these steps could proceed linearly as described above, but the local volt/VAR control mode required iterating with power flow during steps 2 and 3 to capture the equilibrium PCC voltage resulting from the inverter reactive power output. This was required because the production of reactive power in response to high/low PCC voltage can itself strongly influence the secondary PCC voltage for such a large PV plant. Initially, we observed slow convergence of this volt/VAR iteration because of these large PCC voltage impacts. In response, we implemented a damping factor to slow the iteration-by-iteration changes in reactive power injections. This approach greatly decreased the number of iterations required for convergence in most situations allowing for faster overall simulations.

#### 4.1.3.3 Adjustments for IVVC

With IVVC there are two types of solutions: those where a new IVVC plan is computed and those that simulate power flow between IVVC solutions. Here we adopted the 10-minute IVVC interval used in Duke Energy's DMS deployment in the Midwest, because DMS has not yet been fully deployed in North Carolina. As a result, every 10 minutes, the QSTS steps described in Section 4.1.3.1 are modified to compute IVVC. In general the simulation approach matches that for QSTS except that Step 6 is replaced with the following:

6a. Solve load and volt/VAR management (LVM) power flow using the load allocation computed in Step 3 and the PV production computed in Step 5 using the following steps:

   A. Compute an LVM solution (involves a series of power flow solutions).
   B. Implement the LVM plan. This includes configuring utility equipment and for scenarios where IVVC controls PV, resimulating the PV using the commanded set points.
   C. Rerun power flow using the loads from Step 3, PV from Step 5, and LVM equipment set points from Step 6A–B.

#### 4.1.3.4 Run automation

The final capability of the NREL simulation code is to standardize and automate the large number of simulations. This was done by abstracting out the setup and run sequence such that the user only needs to specify the simulation parameters as listed below:

1. Day of simulation
2. Simulation Start and End times
3. PV model—baseline from historic measurements, constant power factor, or volt/VAR
4. Run mode—QSTS or IVVC[12]
5. (Optional) Alternative PV location scenario for sensitivity analysis.

Multiple sets of these scenario parameters can be passed to the simulation engine in a simple csv file to allow automated simulation of multiple scenarios. At the beginning of each simulated day, the study server is restarted, the required DMS model file is loaded, and the DMS dynamics file—which logs all configuration changes relative to the base model, including the large number of cached and restored equipment states used with QSTS and IVVC simulations—is cleared for faster performance.

## 4.2 Data and Statistical Processing

### *4.2.1 Preprocessing of SCADA Time-Series Data*

Duke Energy made a significant amount of SCADA data available to NREL for this project. Table 3 summarizes data associated with the study feeder that was used for this project. The location of these measurements and their associated equipment is shown in Figure 3.

**Table 3. Feeder Measurements**

| Equipment Name | Type | Measurement (All Three-Phase) | Interval: Range | Additional Interval: Range |
|---|---|---|---|---|
| Feeder | Feeder breaker | P, Q, I, V | 1 min: 6 a.m.–9 p.m. | 1 h: 24 h |
| RclPV (at PV Plant) | Recloser | P, Q, I, V | 1 min: 6 a.m.–9 p.m. | 1 h: 24 h |
| Rcl1 | Recloser | P, Q, I, V | 1 min: 6 a.m.–9 p.m. | 1 h: 24 h |
| Rcl2 | Recloser | P, Q, I, V | 1 min: 6 a.m.–9 p.m. | 1 h: 24 h |
| Cap1 | Capacitor bank | State (tripped/close) | 5 min: 24 h | |

To capture the high ramp rates associated with the PV plant variability on the feeder and to generate accurate feeder statistics, a complete 1-minute data set (i.e., 525,600 measurements) for 2014 was used. Specifically, the 1-minute 6 a.m.–9 p.m. SCADA data were merged with the 24-hour hourly data, which was linearly interpolated to 1 minute. All missing or out-of-range

[12] The corresponding py4etd simulation modes are named “dpf_solve” and “lvm_solve”, respectively.

SCADA values were replaced with a 30-minute running average value before and after the missing data sample or group of samples.

To create "native" feeder-head load (i.e., the original load not masked by PV power production), the positive 1-minute feeder-head real and reactive power were added to the negation of the real and reactive measurements at the PV plant recloser for each time stamp. There was not perfect synchronism in the time stamping of the PV plant recloser and feeder-head measurements, which thus created large, unrealistic step changes in the native-load calculation. To manage this, a 30-minute running average filter was found to adequately smooth the native load. A sample day demonstrating this smoothing method is shown in Figure 8 for real power. The green line is the directly calculated native value, and the black line is the filtered value.

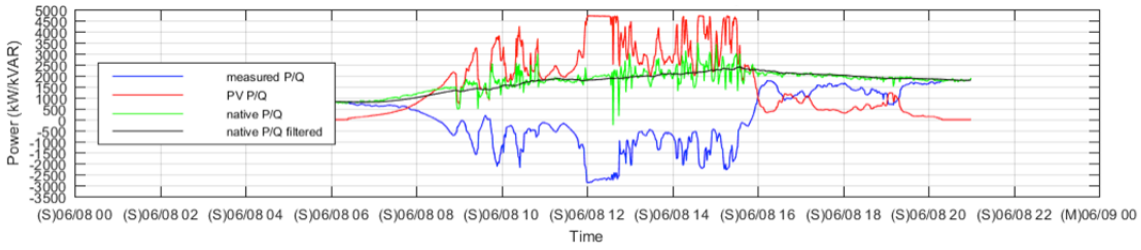


**Figure 8. Example of smoothing to create native load**

This data filling, interpolation, and smoothing process created a complete 1-minute data set of the 2014 feeder-head, PV, and recloser data that were then queried to create daily statistics and subsampled to generate time-series input data files for the e-terra*distribution* modeling.

### 4.2.2 Daily Statistics

Daily statistics were created for a host of parameters to understand the behavior of the feeder and to guide the selection of representative sample days that can accurately represent one year, as discussed in Section 4.2.3. The parameters selected are summarized in Table 4. Most of these metrics are simply daily summaries of the measured or calculated value of interest; however, the variability index, season, and capacitor bank operations described in detail below.

**Table 4. Daily Statistics**

| |
|---|
| Day of year |
| Day of week |
| Season |
| Native MWh |
| Native MW_avg |
| PV MWh |
| PV MW_avg |
| PV variability index (VI) |
| Daily PV penetration on energy basis ($E_{PV}/E_{FDR}$) |
| Daily load factor ($F_{ld}=P_{avg}/P_{max}$) |
| Capacitor bank operations |

The daily variability index (VI) is defined as:

$$\boldsymbol{VI}_{n=1\ldots365} = {\sum_{\boldsymbol{n,P>0}}|\boldsymbol{\Delta P}|}\Big/{max(VI)}$$

where |ΔP| is the absolute difference in real-power output from the PV plant from one sample minute to the next for the times during the day that the plant was producing power; max(VI) is the annual maximum of the daily sum of |ΔP|, which normalizes the variability index such that 1.0 represents the highest variable day during the year. The variability index is divided into five regions: clear, cloudy, moderately variable, highly variable, and extremely variable. Figure 9 shows the histogram of variability index for each day in 2014 with a time series (inset) of the PV and feeder-head power for a sample day with that index.

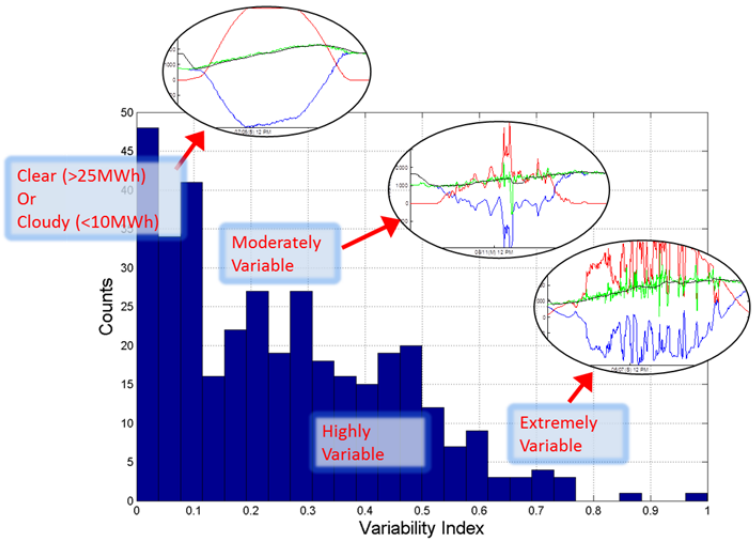


**Figure 9. Histogram of PV variability index and relationship to measured data**

The seasonal selection for this circuit was based on daily native energy use in for 2014 on the study feeder. Daily energy consumption was divided into five distinct seasons for this feeder: winter, extreme winter, spring, summer, and fall. Here, *extreme winter* was defined as days when total daily energy exceeded 65 MWh, which represents large excursions beyond normal winter loadings. The remaining season boundaries were manually selected based on the readily apparent delineation shown in Figure 10 and not on calendar dates.

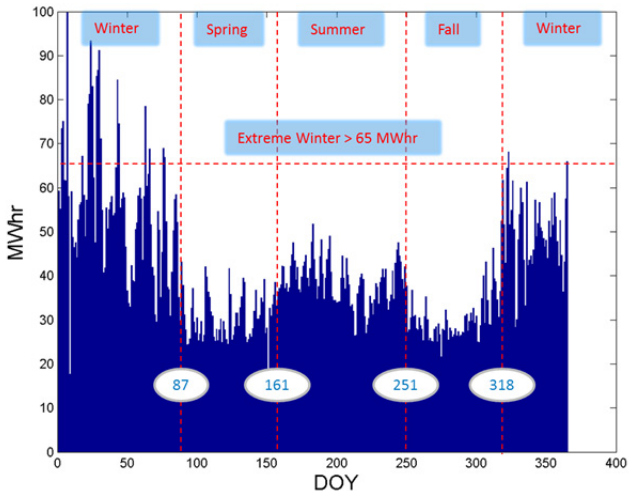


**Figure 10. Seasonal loading type assigned by daily MWh**

SCADA capacitor switching states were available for Cap1, located approximately 1 mile from the PV plant. The 2014 cumulative daily switching data are shown in Figure 11. Note that Cap1 had 2,100 recorded operations in 2014 and consistently more than 15 operations per day until July 21, when total daily operations appeared to have been limited to 8. Retrieval of this

capacitor bank's settings in May 2015 indicates that the daily limit is now restricted to 4 and the control set points were also updated.[13]

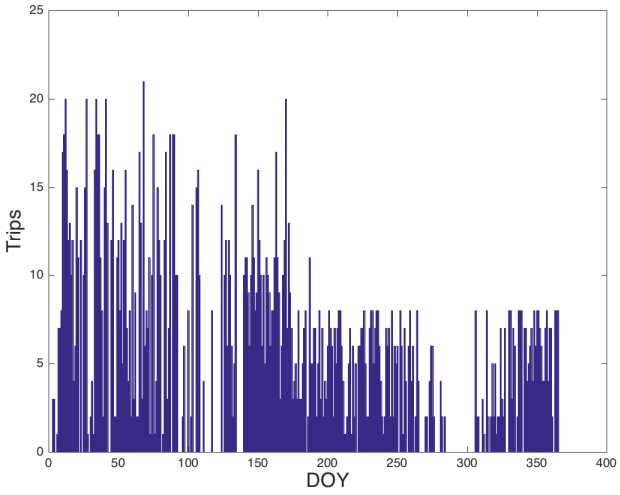


**Figure 11. Historic operations per day for Cap1 on the study feeder**

### 4.2.3 Representative Day Selection

#### 4.2.3.1 Motivated by Computational Demands

Given the extensive simulation time required for the QSTS simulation using e-terra*distribution*, it would be computationally prohibitive to simulate an entire year at a 1-minute time step.[14] As a result, two simplifications were used for the annual analysis:

1. Model 1-minute time steps during daylight hours only (6 a.m.–9 p.m.).
2. Simulate a representative sample of 40 days rather than all 365 days.

This section describes the process of selecting the 40 days.

#### 4.2.3.2 Selection Overview

*Goal:* identify a selection of 40 representative days that capture the diversity of day types throughout the year and that can accurately estimate the entire year operations.

[13] This new, maximum operations setting of 4 is used during simulation runs for the switched capacitor (Cap1). This means that simulation results for the feeder that are presented later do not directly match the 2014 operations. Instead they approximate how the feeder equipment would have behaved had the current settings been in place during 2014.

[14] e-terra*distrbution* was principally designed for distribution system operations, not for QSTS power flow analysis; as a result, it contains a lot of other infrastructure that slows down QSTS simulations. To partially mitigate computational time, the scenarios were run simultaneously across five different virtual machines.

*Approach:*

1. Expand day classification from the data analysis effort to identify a set of day categories that capture load and PV variability throughout the year.
2. Visually verify and refine these selections.
3. Combine similar day types with small numbers of days to bring the number of day types down to 40 or fewer.
4. Identify candidate multivariate regression model formulations for annual estimates based on historic capacitor-bank switch counts.
5. Randomly sample from these day types (stratified sampling).
6. Parameterize the regression model based on the stratified sample of 40 days.
7. Use bootstrapping to validate the ability of the parameterized regression model to accurately estimate the annual capacitor bank switches.
8. Repeat steps 5–7 hundreds of times.
9. Select the stratified sample that provides the best annual estimate with tight confidence intervals.

All of this processing was conducted in the open-source statistics language R (v3.1.3) using NREL-developed scripts in the open-source R-studio development and analysis environment.

#### 4.2.3.3 Day Classification

The day classification was built on the data analysis efforts above to classify all days in the year. The final classification considered four dimensions:

1. **Season:** five seasons—spring, summer, fall, winter, and extreme winter heating—based on the actual load seasons, described above, rather than calendar seasons
2. **PV variability:** five variability patterns based on a combination of PV variability index and daily total PV energy production as summarized in Table 5

**Table 5. PV Variability Day Classification**

| | Variability Index | PV Daily Energy Production[15] |
|---|---|---|
| **Clear** | < 0.2 | > 25 MWh |
| **Cloudy** | < 0.2 | < 10 MWh |
| **Moderate** | < 0.3 | Not clear or cloudy |
| **High** | 0.3–0.65 | All |
| **Extreme** | > 0.65 | All |

[15] The PV plant has a maximum power output of 5 $MW_{ac}$.

3. **Day type:** two load categories to distinguish weekend from weekend days. In addition, 10 major holidays were included in the weekend (and holiday) bin, specifically: New Year's Day, Martin Luther King Day, Presidents' Day, Memorial Day, Independence Day, Labor Day, Thanksgiving, day after Thanksgiving, Christmas Day, day after Christmas (Friday).
4. **Capacitor control setting:** to account for the changing capacitor-controller settings on July 21, the seasons were further subdivided into "old" and "new" capacitor-settings bins. This subdivision affected only the winter and summer seasons because the capacitor settings were constant for the entire spring (old) and fall (new).
5. The full factorial combination of these attributes resulted in:

$$(4 + 2\ seasons) \times 5\ PVvariability \times 2\ day\ types = 60$$

or too many days. As a result, similar bins with small populations were manually combined to give a set of 40 day types. The resulting bins are shown in Table 6.

**Table 6. Day Selection Groupings**

<table>
<tr><th></th><th>Spring</th><th>Summer (Old)</th><th>Summer (New)</th><th>Fall</th><th>Winter (Old)</th><th>Winter (New)</th><th>Extreme Heating</th></tr>
<tr><td>Clear weekday</td><td>14</td><td colspan="2" rowspan="2">9</td><td>11</td><td>11</td><td>6</td><td rowspan="2">6</td></tr>
<tr><td>Clear weekend</td><td>5</td><td>5</td><td>7</td><td>9</td></tr>
<tr><td>Cloudy weekday</td><td rowspan="2">5</td><td colspan="2" rowspan="2">4</td><td rowspan="2">7</td><td>7</td><td>12</td><td rowspan="2">8</td></tr>
<tr><td>Cloudy weekend</td><td colspan="2">8</td></tr>
<tr><td>Moderate weekday</td><td>13</td><td rowspan="2">6</td><td rowspan="2">14</td><td>17</td><td>17</td><td>6</td><td rowspan="6">5</td></tr>
<tr><td>Moderate weekend</td><td>4</td><td>5</td><td colspan="3" rowspan="3">16</td></tr>
<tr><td>High weekday</td><td>16</td><td>19</td><td>15</td><td>15</td><td>9</td></tr>
<tr><td>High weekend</td><td>13</td><td>8</td><td>9</td><td>6</td><td>6</td></tr>
<tr><td>Extreme weekday</td><td rowspan="2">5 for all shoulder seasons</td><td colspan="2" rowspan="2">6</td><td rowspan="2">(Combine with spring)</td><td colspan="3" rowspan="2"></td></tr>
<tr><td>Extreme weekend</td></tr>
</table>

#### *4.2.3.4 Sampling Methodology*

Rather than randomly sampling from among the entire year's set of days, we used the variance-reduction technique of stratified sampling, wherein we force selected randomly from each of these identified bins separately—in this case, with only one sample per bin.

In addition, we wanted to ensure that we included days with the peak native demand (January 30) and minimum net demand (April 19).[16] The peak demand was added to a separate "peak" stratum, whereas the minimum demand was forced to be used as the representative for its day type.

Finally, before sampling, approximately 8 days with extensive bad or missing data were removed.

#### 4.2.3.5 Annual Validation with Multivariate Regression

To test the ability of our 40-day selections to roll up to a full-year analysis, we tested the abilities of hundreds of candidate samples to estimate a full year's results. The only data available for this comparison were the number of capacitor switches on Cap1, which also provided an indirect proxy for the voltage conditions on the feeder.

We then used a multivariate linear regression built from the sampled subset of days as a training set. The most (predictively) powerful terms for this regression were identified by comparing the accuracy of the predictions from multiple-regression models using the entire year's data. The selected model struck a balance between predictive power and the ability to capture the dynamics of interest including PV variability and load diversity. The selected model:

$$CapSw \sim DayType + Season + CapBankControl + PVvariability + PVproduction + LoadFactor$$

captures a number of dimensions beyond those used for data binning. Specifically, it builds a linear regression for the number of capacitor switches, *CapSw*, as a weighted function of day type, season, cap bank operation limit, PV variability, PV energy production, and the load factor.

The statistical "F-test" was used to confirm that this set of parameters actually has predictive capability. For the selected value, the F-statistic value was 13.71 on 9 and 347 degrees of freedom. This corresponds to a p-value: $< 2.2\times10^{-16}$. For this test, any p-value below 0.05 is significant and indicates that the predictive power of the selected parameters is much better than random noise.

#### 4.2.3.6 Validation and Final Selection via Bootstrap

The remaining steps after identifying a model and sampling approach were to:

1. Conduct the sampling.
2. Use the sampled data as training data to compute regression coefficients.
3. Validate the resulting predictive capability of the sampled days throughout the full annual data set (validation data).

Ideally, the sampled days and resulting regression model would not be overtrained to a single year but, rather, would work for multiple years; however, in this case, we only had a single year

[16] We might normally have also included the peak variability day, but this day (July 28) had a considerable number of bad data points so it was discarded.

of input data so we employed the statistical technique known as bootstrapping. With bootstrapping, multiple samples of the validation data (remainder of the days in the year) were drawn. For each, the predictive capabilities of the model were evaluated to estimate not only how well the selected days—and corresponding regression coefficients—did at predicting the single available year, but also how much variability there might be in this predictive power for different validation data. By treating each of the bootstrap samples as a different annual data set, it was possible to estimate the confidence intervals for the sampled scenarios.

Bootstrapping also provides a way of comparing the quality of alternate 40-day samples. In this analysis, we sampled from our 40-day types hundreds of times and then compared the expected predictive error and confidence interval using bootstrapping. Because both low mean error and low confidence intervals were of interest, a weighted error was computed as:

$$WeightedError = \frac{\sqrt{MeanBSerror^2 + max(+/-95\%BSconfidence\ Intervals^2)}}{AnnualCapSwitchCount}$$

and the sampled day set with the lowest weighted error was selected as the representative days. In this case, the ability of the sampled days to predict the annual number of capacitor bank switches had the following:

- A mean error of only 0.31%
- 95% confidence intervals of -7.94% and + 8.18%.

A histogram of these errors is shown in Figure 12.

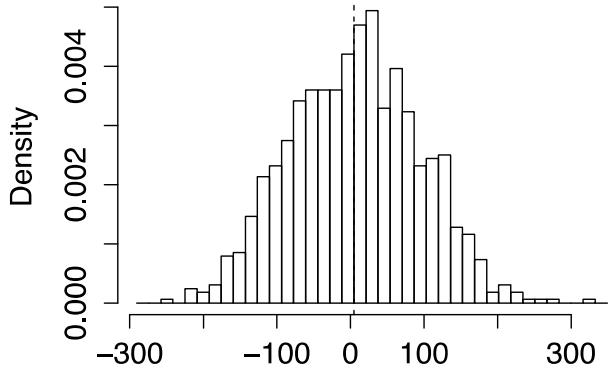


**Figure 12. Histogram of bootstrap errors for the ability of the sampled 40 days to predict annual capacitor switching behavior. For reference, the capacitor bank switched more than 2,100 times during the year.**

The complete set of days and corresponding PV and native-load results are shown in Figure 12.

### 4.2.4 Extrapolating Representative Simulations to Annual Results

The QSTS simulation was run for each scenario for each of the final 40 representative days described above. The resulting data consist of high-resolution time series taken at 1-minute intervals from 6 a.m.–9 p.m. Although the 40-day simulation runs are highly informative on their

own, further cost-benefit analyses and characterizations required data for the entire year. Being able to generate an estimate of the annual data based on 40-day simulations is very important given the previously discussed computational costs associated with the QSTS simulation via e-terra*distribution*. This is a challenging statistical problem given the complex structure of the data (multiple high-resolution time series) and complex correlations (e.g., temporal, climate).

The simplest approach to this annual roll-up problem was to leverage the unique classification of each of the 40 days and extrapolate the corresponding members of each class. For example, daily time series for each of the 4 days in the "Cloudy, Summer" class were assumed to match exactly to the "Cloudy, Summer" day result from the 40-day simulations (see Table 7). The simplicity of this approach made it very appealing. The main downside is that extrapolating does not allow any within-class variability to be present.

**Table 7. Example of Day Classification**

| "Cloudy, Summer" Day Included in Simulation | All Days Classified as "Cloudy, Summer" |
|---|---|
| August 2 | August 1 |
| | August 2 |
| | August 9 |
| | August 10 |

Preliminary work on using more advanced statistical models to annualize daily summary characteristics was therefore also carried out. The focus was on modeling the underlying processes associated with aggregated regulator operations as a function of daily metadata (e.g., weather, day type, PV visibility) during the course of a year. To account for the physical structure of the measure of interest (positive count data), a Bayesian-Poisson generalized linear mixed model was used. These efforts mainly highlighted the complex correlation structure within the data, resulting in wide prediction intervals for the unsimulated days of interest.

As a result of these challenges when using more "advanced" statistical techniques to annualize the data, it was decided to simply use the classification as the primary method of annualizing 40-day simulation results used in this project. The rigorous combination of statistical validation and domain expertise used to select the 40-day classification minimized the impact of within-class variability and enabled better results.

A future path of research is to study the impact of modeling the daily time series as functional objects and then estimating the missing days under this framework. This could prove to provide a better predictive capacity of additional days as well as provide uncertainty estimates that can be used to test scientific and engineering hypotheses in a more rigorous fashion.

## 4.3 Cost-Benefit Alternatives Analysis

### *4.3.1 Tool Description*

The NREL-developed Cost-Benefit Alternatives Analysis Tool (CBAAT) was used to compare net cost-benefit of various PV control mode alternatives. CBAAT was originally developed for

Arizona Public Service, upgraded with additional features for San Diego Gas & Electric, and further enhanced for this work. CBAAT is a cash-flow analysis engine that dynamically generates per alternative pro forma cash flow matrices from time series of unit cost, financial parameter, and feeder performance data that are loaded into the tool databases and combined with user configurations and evaluates them into aggregate metrics.

The tool is built around a Microsoft Access database to structure and manage the substantial amount of simulation data and configuration parameters. It uses Access' forms and reports with Visual Basic for Applications (VBA), Access Structured Query Language (SQL), and R code. Additional details on CBAAT can be found in Appendix A.

### 4.3.2 High-Level Approach

The cost-benefit analyses performed for this study calculated dollar value streams associated with energy consumption, energy production, and operational characteristics in each scenario of the simulated feeder and its components. Specifically, value streams were associated with PV energy production, feeder losses, loads, and the frequency of operation of switching equipment on the feeder with the expected resulting requisite maintenance and replacement expenditures. The tool tabulated the results of the cost-benefit analysis for each alternative scenario for comparison. Figure 13 shows the high-level processes and data flows through the cost-benefit alternatives analysis that was performed on the Duke Energy feeder simulation results.

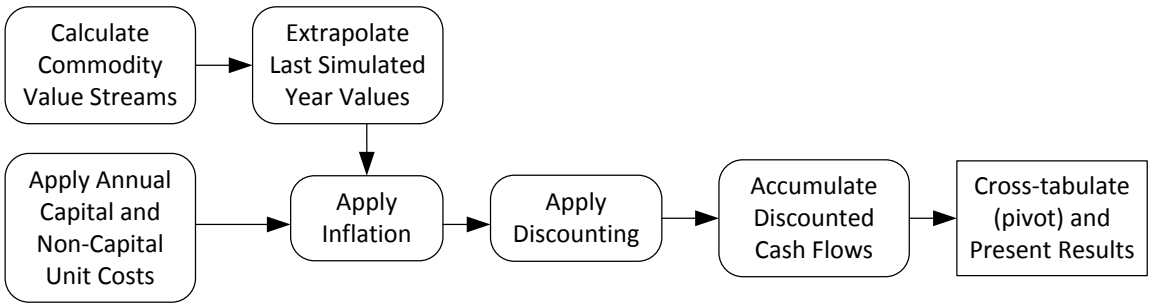


**Figure 13. High-level data flow diagram of cost-benefit analysis used in this report**

As shown in the interface box (rightmost) in Figure 13, the tool used for the cost-benefit analysis generated a report of results for each alternative scenario. The report breaks each scenario down by value stream and shows annual aggregates for each. It categorizes cash flows as those associated with loads, losses, PV production, and others, if present, such as storage dispatch and charging, provision of ancillary services, etc. It presents the results as the annually and categorically aggregated cash flows for three computations: inflation (not yet discounted), discounted cash flow (DCF), and annual accumulation of discounted cash flows. The cumulative discounted cash flows were aggregated within each category, totaled across categories, and accumulated among all prior analysis years. This effectively produced the net present values (NPV) at successive annual planning horizons.[17]

[17] The tool automatically generates cash flows out 50 years on the assumption that most cash flow analyses will use planning horizons of less than 50 years.

### 4.3.3 Alternatives Analysis

A standard approach to alternatives analysis is to omit factors that are common to all scenarios to avoid cluttering the analysis with elements that are equivalent among scenarios and do not affect the ordering or ranking of results, which is the key output sought from alternatives analysis. For this reason, *the cumulative DCF (NPV) metrics computed by CBAAT should not be taken as absolute expected costs or values of a scenario.* These results omit costs and benefits common to all alternatives, e.g., there were costs associated with initial construction of the feeder and with ongoing operation of the feeder independent of the scenarios.[18]

The alternatives analysis is illustrated in Figure 13 and proceeded as follows:

1. "Unadjusted" (i.e., without inflation or discounting applied) cash flows were calculated and assigned to the year of analysis for which either simulations were conducted or other expenditures or revenues were predicted.
    A. Commodity energy cash flows: one year of cash flows was calculated from the 328,865 minutes (based on a subset of each day) of real power data per circuit element (losses, loads, PV) per scenario. The year's cash flows were taken as representative and extrapolated as the expected set of cash flows for all following years.
    B. Equipment replacement cash flows: cash flows required for equipment replacement were assigned to each year in which an equipment replacement was expected to be needed based on the number of switching operations the simulations showed for each switching line component in the simulated year.
2. The cash flows were adjusted with escalation rates for expected inflation. A simple 3% annual inflation rate was applied to the extrapolated energy related cash flows. An electric utility construction distribution plant inflation rate schedule was applied to equipment replacement cash flows.
3. The inflation-adjusted cash flows were discounted back to year zero of the analysis period at a discount rate corresponding to Duke Energy's after-tax cost of money.
4. Annual cash flows were aggregated by category (value or cost stream), and discounted cash flows of all prior years were accumulated for each analysis year to yield cumulative discounted cash flows (cumulative NPV).

### 4.3.4 Cost-Benefit Assumptions

No costs were "capitalized" or normalized, nor were property or income tax effects accounted for. The second capacitor bank was not included in cost benefit analysis.

[18] One example of an element that was provided by Duke Energy that was omitted was the cost of annual inspections and minor maintenance of regulators, such as servicing control panels, estimated at $70 annually per phase. This cost does not vary by scenario because all scenarios have the same number of regulators in operation and hence can be omitted without changing the relative ranking of alternatives.

#### 4.3.4.1 Commodity Value and Cost Streams: PV Energy Production, Losses, and Loads

The costs and benefits associated with PV energy production, feeder losses, and loads were calculated according to rates in the North Carolina Purchased Power Tariff ("Tariff"). Cash flows associated with PV production were rendered positive (i.e., positive cash flows indicate cash inflows to the utility), and cash flows associated with feeder losses and loads were rendered negative (i.e., negative cash flows indicate cash outflows from the utility).

From the annual results generated from the extrapolated representative simulated days (discussed in Section 4.2.4) and Tariff rates, one representative year of cash flows related to each of PV energy production, loads, and losses were generated for each scenario. Figure 14 illustrates the data stores, flows, and process of calculating cash flows from commodity rates and commodity profiles—in this case, energy rates and production, load, and loss profiles.

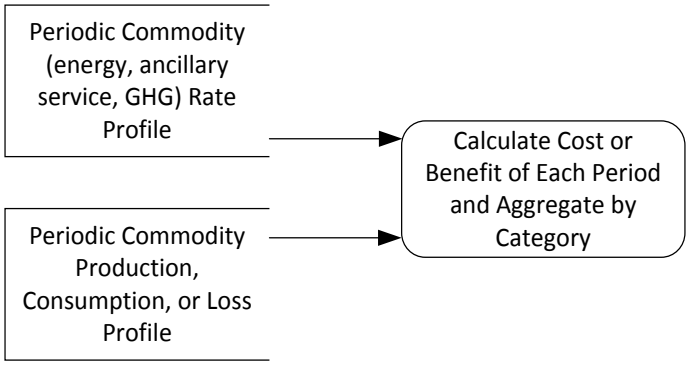


**Figure 14. Data flow diagram for commodity value streams calculations**

After calculation, the commodity cash flows were extrapolated to years beyond the simulated year. They were inflated using 3% per year and discounted to present value using Duke Energy's after-tax weighted average cost of capital.

#### 4.3.4.2 Replacement Costs Associated with Switching Equipment

Costs (cash flows) associated with expected expenditures for replacement of switching equipment resulting from wear and tear were modeled as being triggered by the cumulative number of equipment switching operations since the beginning of the analysis and since the last prior replacement.

Duke Energy provided NREL with its policy for replacing regulators after a number of operations and the costs associated with replacing each type of regulator, single phase and three phase. For this study, replacement costs were modeled as simple unadjusted cash outflows (assumed to be fully-loaded costs), without "capitalization" (property tax treatment or depreciation) or normalization. The cash flows were adjusted for expected inflation and discounted at Duke Energy's after-tax weighted average cost of capital. Figure 15 illustrates the data stores, flows, and processes associated with generating unit cost cash flows associated with maintaining and replacing switching equipment based on the number of switching operations per piece of switching equipment per scenario. Assigning unit costs to years beyond the last

simulated year was based on extrapolation to subsequent years of number of switching operations in the last simulated year.

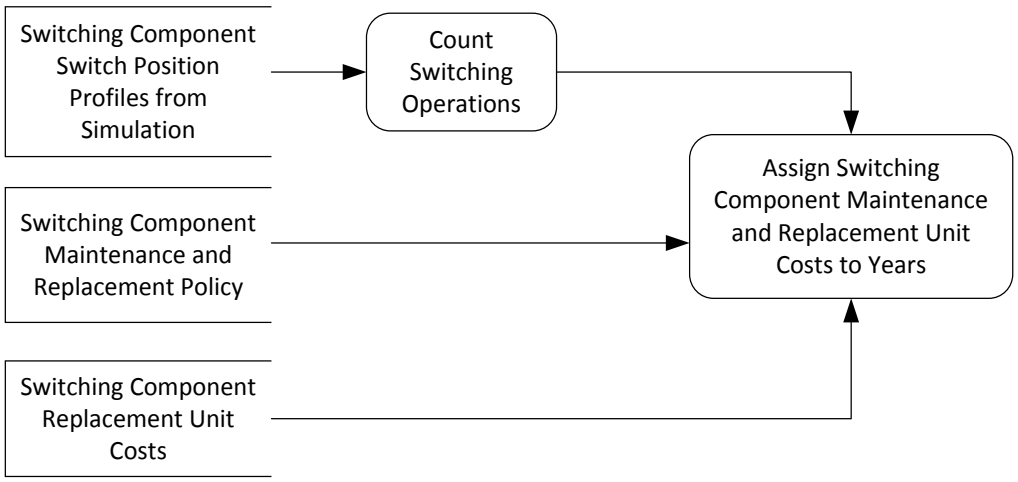


**Figure 15. Assigning maintenance and replacement unit costs for switching equipment**

Figure 15 illustrates one of the subprocesses in the "Apply Annual Capital and Non-Capital Unit Costs" block shown in Figure 13.

#### *4.3.4.3 Energy Prices*

Energy and related prices for the cost-benefit analysis were taken from the actual North Carolina Tariff Option B, for distribution-connected generation, covering "all other hydroelectric and all non-hydroelectric facilities." This tariff includes time-of-use values for both energy and capacity. The variable rate was taken as the best estimate of avoided present-day energy cost without the influence of inflation "priced in," as is thought to be the case with the 5-, 10-, and 15-year fixed long-term rates also in the tariff. Table 8 summarizes the rates from the tariff used to calculate the value and cost of energy.

**Table 8. Rates Used to Calculate Value and Cost of Energy**

| Dates | Days of Week | Times | Value of Energy (¢ per kWh) | |
|---|---|---|---|---|
| | | | Capacity Credit | Energy Credit |
| **June 1–Sept. 30** | M–F | Summer on-peak: 1 p.m.–9 p.m. | 6.00 | 3.87 |
| | | Summer off-peak: 9 p.m.–1 p.m. | | 3.33 |
| | Sun. & Sat. | Summer off-peak: All | | 3.33 |
| **Oct. 1–May 31** | M–F | Winter on-peak: 6 a.m.–1 p.m. | 2.19 | 3.87 |
| | | Winter off-peak: 1 p.m.–6 a.m. | | 3.33 |
| | Sun. & Sat. | Winter off-peak: All | | 3.33 |

Tax benefit (burden) associated with increases (decreases) in energy expenditures were not explicitly calculated because they were assumed to be accounted for in the tariff rates.

#### *4.3.4.4 Equipment Replacement Costs*

Cash flows associated with replacing voltage regulators were applied in analysis years on the basis of the policy that both station and line regulators are replaced after 100,000 operations. These cash flows were imposed at a rate of $7,500 per single-phase regulator replacement and $22,500 per three-phase regulator (e.g., LTC) replacement.

Cash flows associated with replacing capacitor switches were applied in analysis years on the basis of policy that vacuum/oil capacitor switches are replaced after 30,000 operations. These cash flows were imposed at a cost of $3,900 per three-phase capacitor switch replacement.

# 5 Advanced Time-Series Visualizations

Electrical distribution feeder data represent a dense collection of multivariate time series (e.g., voltage, current, power, capacitor state) attached to a network topology. In general, effective visualization of time-series data on graphs is a difficult problem and an open area of research in the visualization community. Historically, representations (and analyses) of the distribution system have been for single or few time periods. Now, with increasing time-varying distributed energy resources including solar, we need new techniques. In addition, the presence of distributed generation including PV can impact local voltage, making the voltage profiles across the feeder increasingly important to understand with reverse power flows and reactive power.

One visualization best practice is known as the Information Visualization Mantra, "overview first, zoom and filter, details-on-demand," which speaks to the ability to interactively select parts of the data to be visualized in detail while proving a global context for understanding the data set. Providing a good global overview of the time evolution of a distribution feeder is difficult due to the highly multivariate nature of the data. There are complicated geographical, topological, and temporal relationships among these variables. A standard two-dimensional (2D) geographical information system has inherent limitations because the two primary degrees of freedom (i.e., the two dimensions of the plane) are dedicated to the geographical layout, making it difficult to display multiple variables simultaneously—not to mention displaying time series of multiple variables.

Our strategy has been to employ *multiple coordinated views*, which is a specific exploratory visualization technique that enables users to explore their data wherein interactions in one view are automatically reflected in the other views. The premise of the technique is that users understand their data better if they interact with the presented information and see the effects of those interactions across different representations. This is best suited to large high-resolution displays that provide sufficient visual real estate to arrange these views.

Further, for some of these views, we leveraged immersive three-dimensional (3D) visualization technology. We found that the extra degrees of freedom afforded by an immersive environment provide novel visibility into the multivariate relationships in these data.

## 5.1 3D Immersive Visualization

An immersive virtual environment is a combination of hardware and software that provides a psychophysical experience of being surrounded by a computer-generated scene, physically immersing users in a virtual world wherein they can explore complex spatial systems by looking through them, walking around them, and viewing them from different perspectives. This is usually accomplished using both a stereo parallax (i.e., each eye has a slightly different viewpoint, providing stereo depth perception) and a motion parallax (i.e., a monocular depth cue based on motion). NREL's Insight Center houses a custom state-of-the-art immersive virtual environment composed of six stereoscopic projectors that illuminate two surfaces: a wall and a floor (see Figure 16). The projected space is used in conjunction with an optical tracker that tracks the position and orientation of the user, allowing the visualizations to respond in relation to the movement of the user.

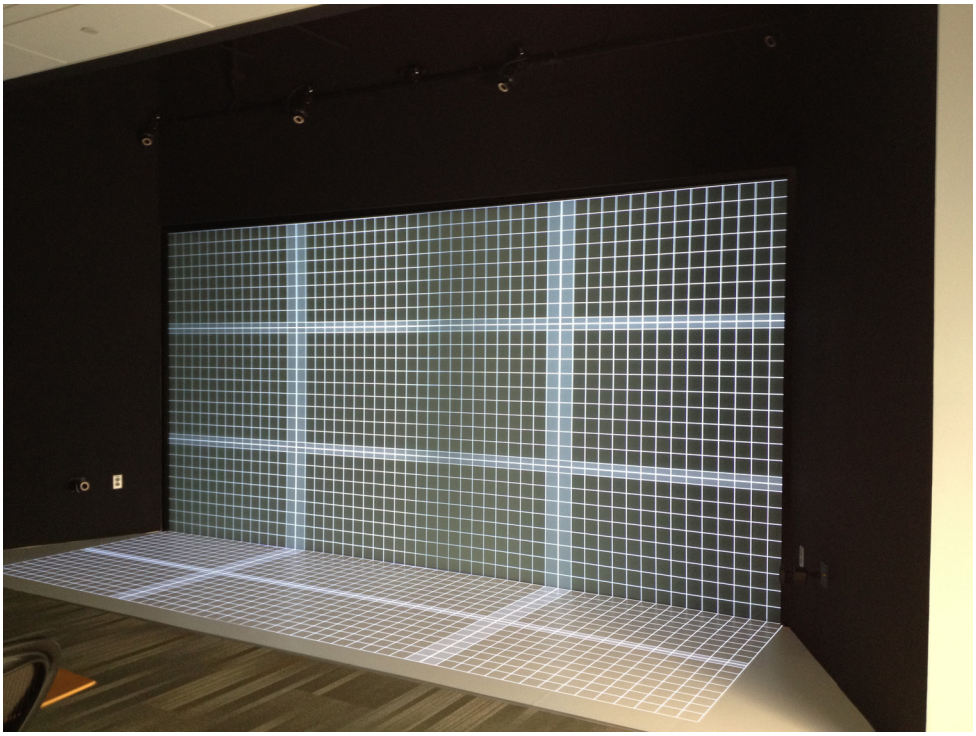

**Figure 16. The immersive virtual environment in the ESIF's Insight Center. Six stereoscopic projectors (four rear-projecting on the wall, and two front-projecting on the floor) create a 3,540 × 2,790 pixel display. Six optical cameras track the space, allowing a user's actions to directly manipulate the 3D objects and perspective.**

In addition to the large-scale custom immersive environment, we also employed the use of a commercial-off-the-shelf immersive *zSpace* desktop immersive environment (see Figure 17). The zSpace provides a 1080p passive stereographic display with integrated optical head tracking.

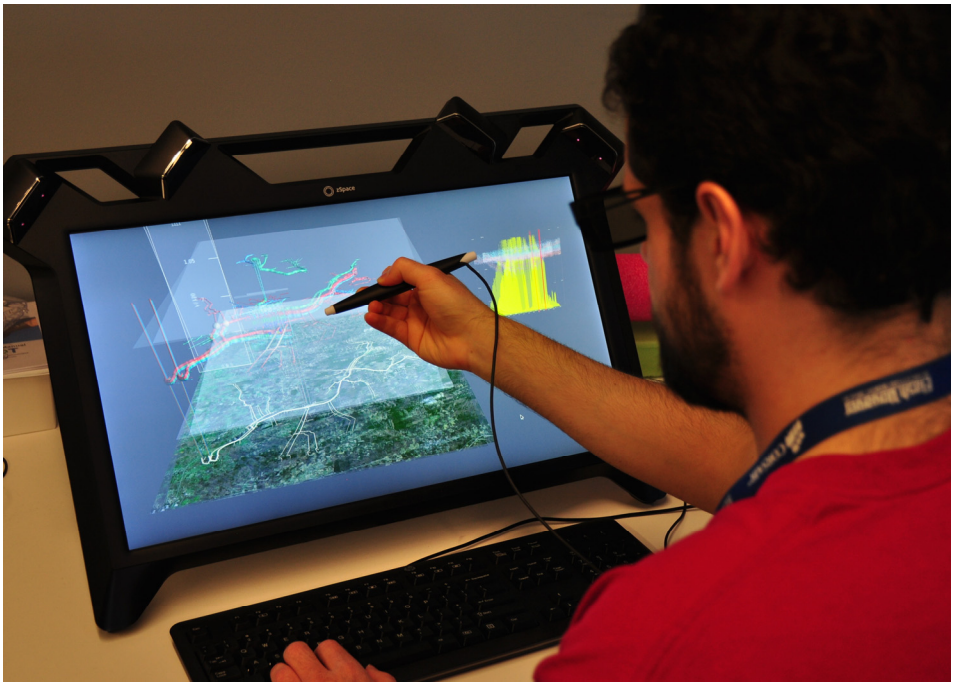

**Figure 17. Three-dimensional analysis of the feeder simulation results on a zSpace immersive desktop**

Generally, introducing 3D visualization to data that does not have an inherent 3D spatial mapping can introduce occlusion problems. When projecting a 3D scene onto a 2D desktop, objects in the foreground may occlude objects in the background. This combined with the 2D projection of these 3D objects can often obfuscate rather than illuminate the global context of the data; however, immersive visualization vastly improves the spatial reasoning of 3D scenes. Natural body movements and well-practiced automatic brain function facilitate reasoning in the virtual world—e.g., users do not have to stop and think about how to move their heads or their bodies to get a better view of something.

Four separate views have been developed for the analysis of the DOTS simulations: a time-series view, 2D topology view, 3D topology view, and 3D distance view. The 3D views are principally designed to be viewed in an immersive environment coupled with the 2D views (see Figure 18); however, it is possible to view all four views simultaneously on a 2D high-resolution display.

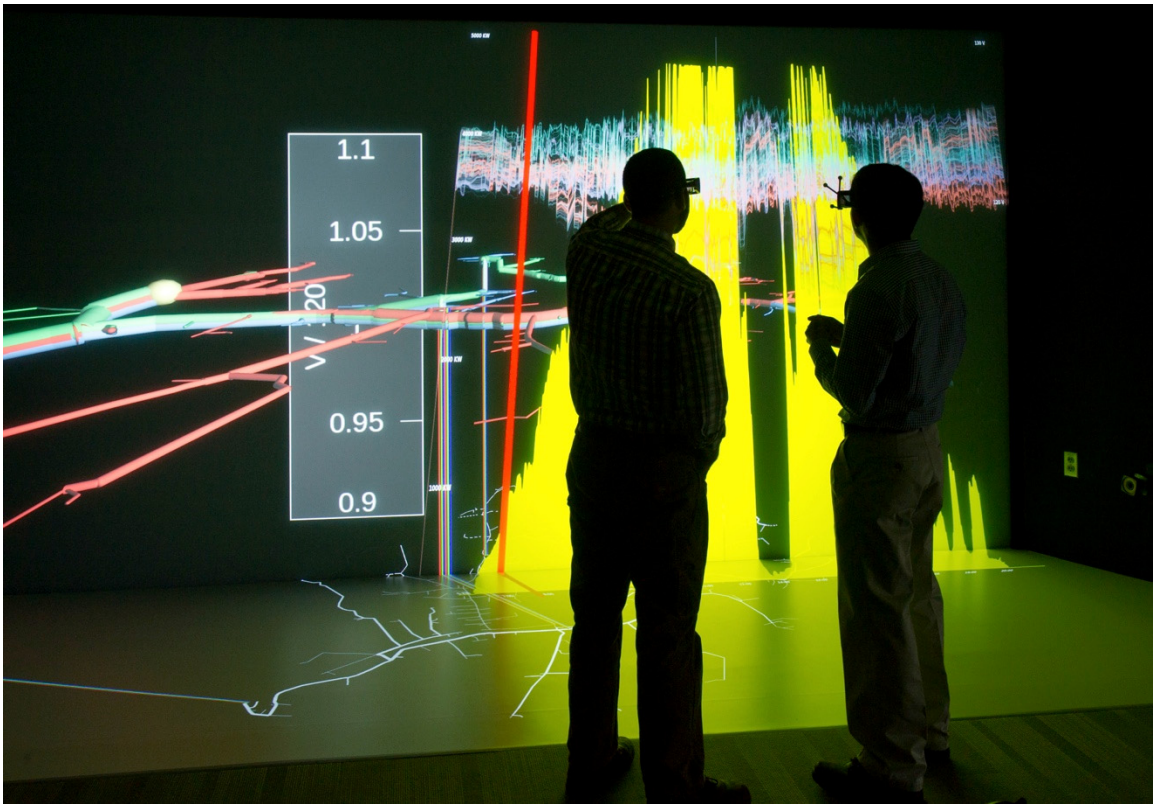


**Figure 18. NREL power systems engineers evaluate the results of a DOTS simulation in the immersive virtual environment in the ESIF's Insight Center. Multiple views are shown simultaneously. A 2D temporal graph depicting the day's PV generation and line voltages can be interactively pinned anywhere in the space. The "current" time can then be selected on this graph. The 2D topography of the feeder is projected on the floor, while a 3D representation of each line's phased voltage, real power, and reactive power float in 3D space.**

### *5.1.1 Time-Series View*

The time-series view provides an overview of the study feeder's line loads and PV generation during a single day (see Figure 19). This provides the primary temporal interface for the other views, allowing the user to set the time across the views. This 2D display acts as a virtual billboard in the immersive space that the user can grab and relocate (see Figure 18).

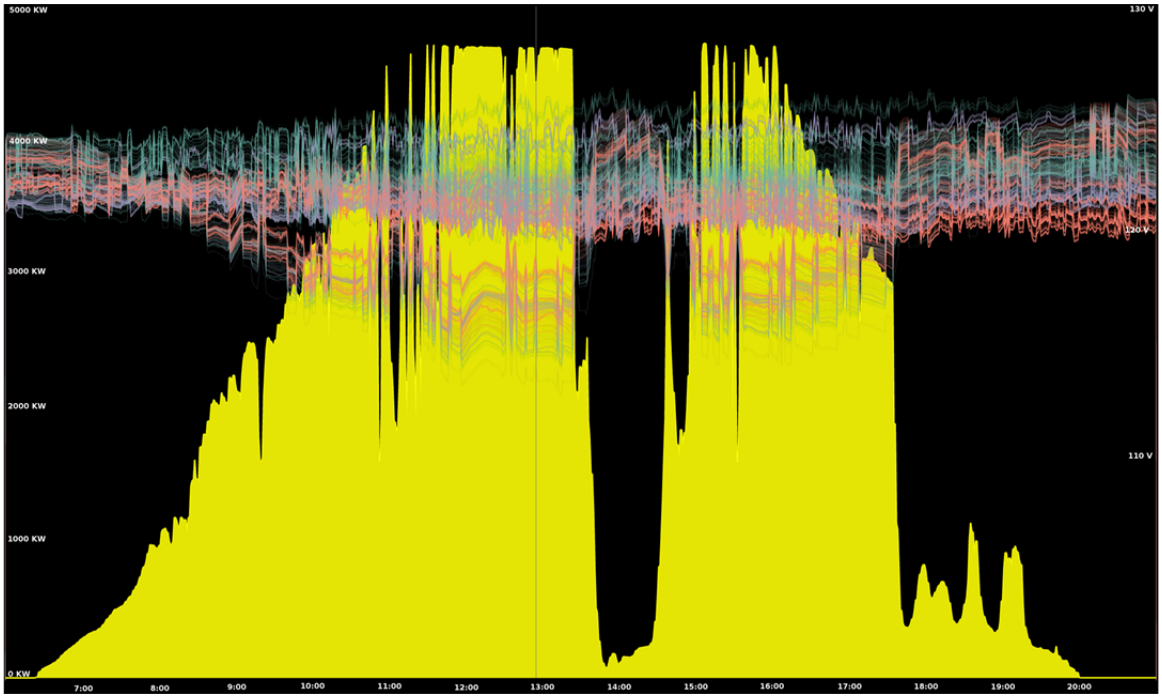


**Figure 19. Time-series view. This view provides the global temporal context for a single day (single simulation) of the feeder. The PV generation is shown in yellow. The individual line voltages for every line in the study feeder are shown in desaturated red, green, and blue (representing Phase A, Phase B, and Phase C voltages).**

### *5.1.2 2D Topology View*

The 2D topology view provides canonical visualization of the distribution feeder (see Figure 20). We recreated and adapted the display to augment more immersive visualizations. Our representation is very similar to the existing DOTS display with feeder lines laid out geographically. The line color and line width can be interactively mapped to voltage, real power, or reactive power. The PV generation and the capacitor and regulator states are represented as icons on the topography. This view can be used independently on a 2D display or as a geographical reference projection in an immersive environment (see Figure 18 and Figure 20).

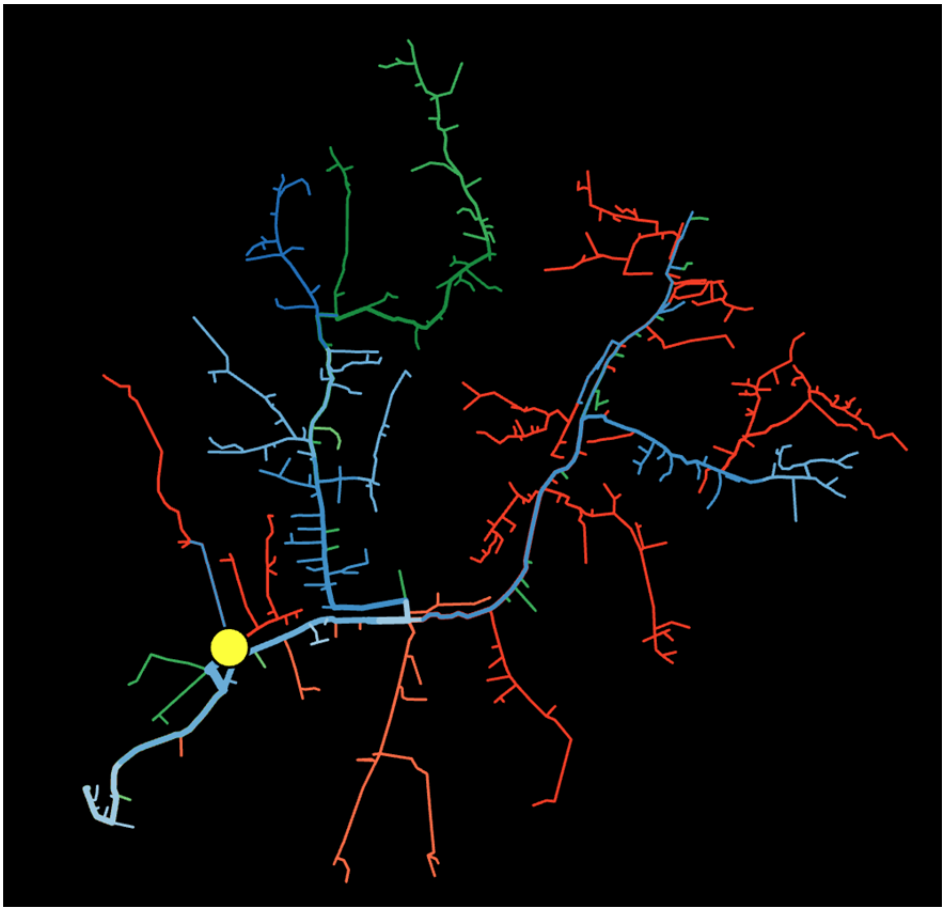

**Figure 20. Two-dimensional topology view. This provides a typical geographically mapped view of the feeder lines with width and color mapped to voltage, real power, or reactive power.**

### *5.1.3 3D Topology View*

The 3D topology view is the 3D analog to the 2D topology view, laying out the feeder lines geographically on the x- and y-axes with voltage on the third axis. Real and reactive power are mapped to line (tube) width/height and color saturation. By adding the additional degree of freedom, significantly more information can be simultaneously represented. Line voltages, real power, and reactive power are all shown together in one visualization; but also all three phases are displayed, with phase separation clearly visible (see Figure 21). This figure has since become a favorite among both the analysis team and Insight Center visitors given its ability to clearly articulate the complexities of feeder operations.

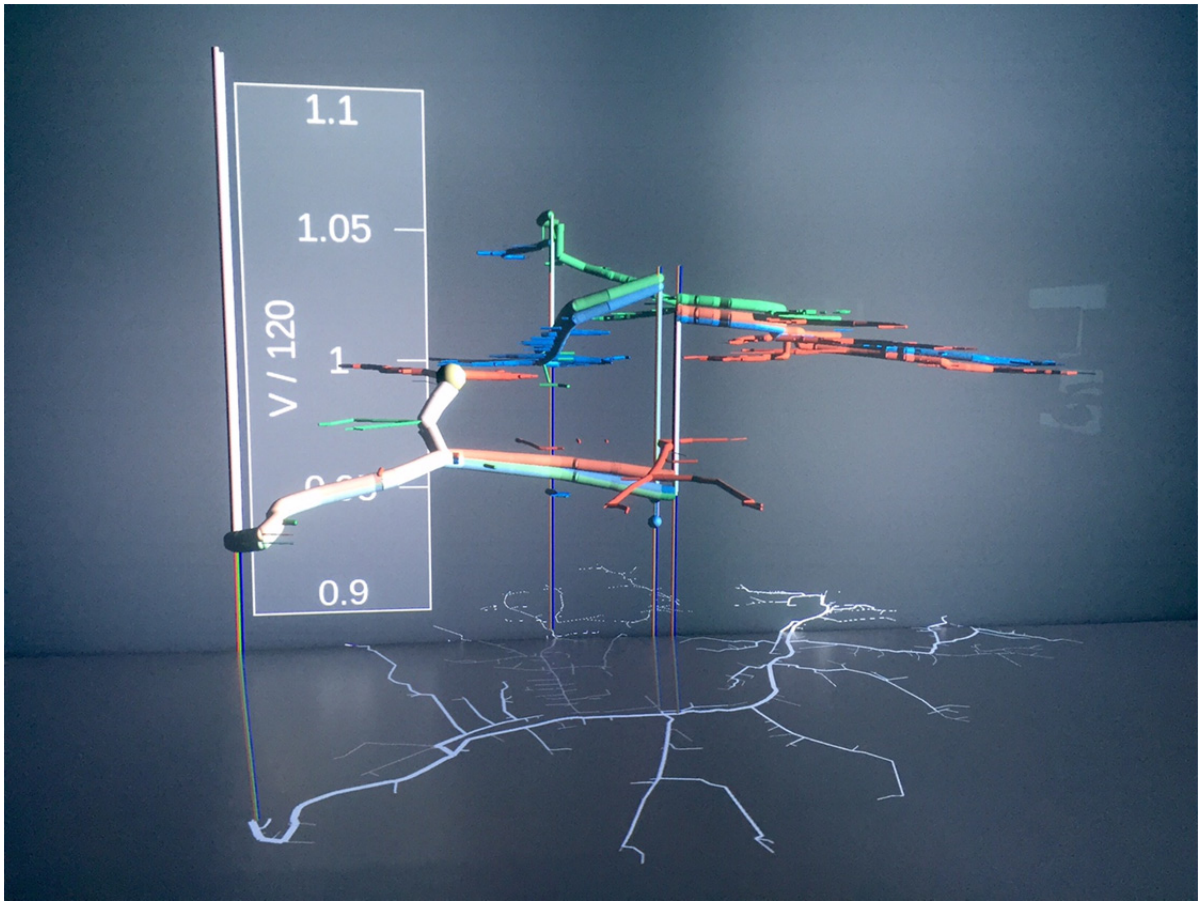


**Figure 21. Three-dimensional rendering of the study feeder. Voltage is displayed on the z-axis. Reactive and active power are represented by line (tube) height/width and color saturation. Individual phases are shown in red, green, and blue.**

### *5.1.4 3D Distance View*

The 3D distance view (Figure 22) depicts the voltage as a function of distance from the feeder head with time evolving on the y-axis. Analogous to the 3D topology view, active and reactive power are mapped to height/width and color saturation, with the three phases represented by red, green, and blue.

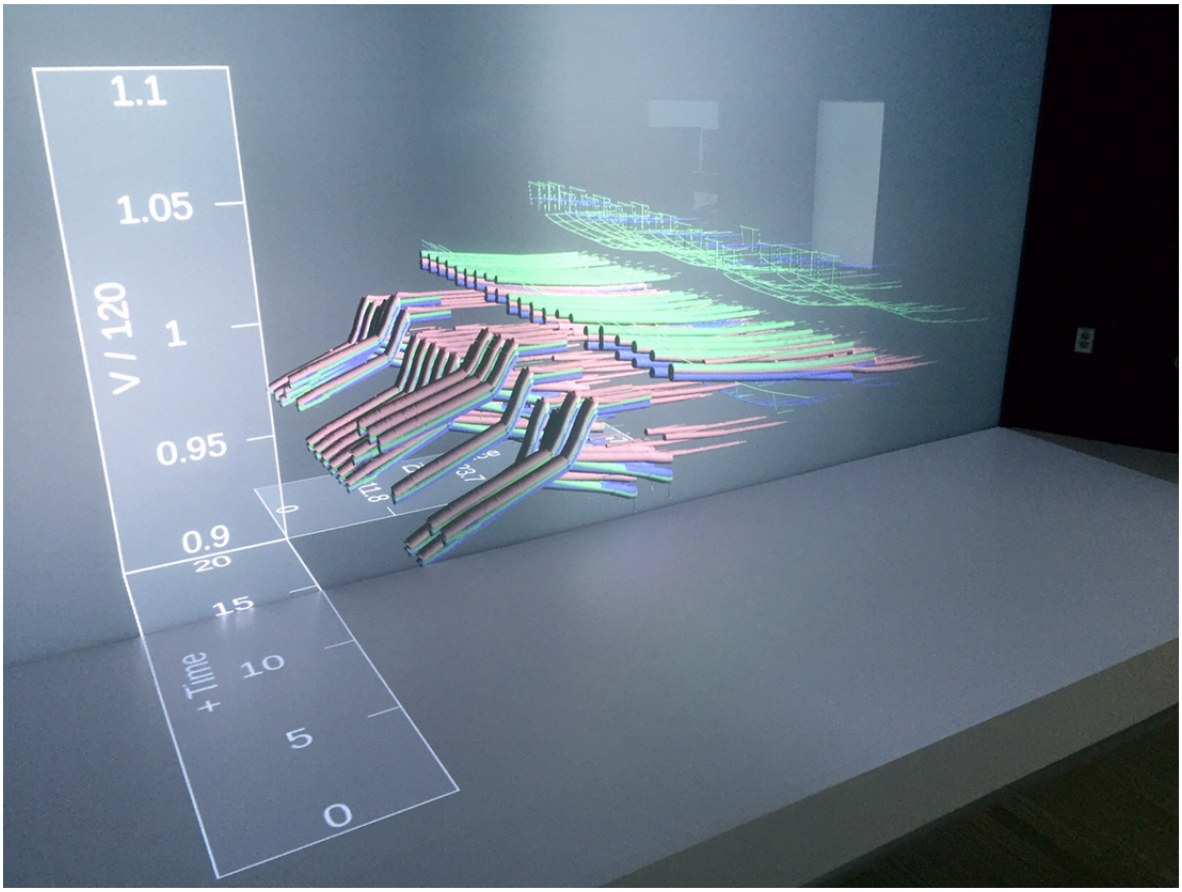


**Figure 22. Three-dimensional distance view. Distance from the feeder head is along the x-axis, time is along the y-axis, and voltage is along the z-axis. Individual phases are colored red, green, and blue (A, B, and C). Reactive and active power are represented by line width and color saturation.**

### 5.1.5 Discussion

Through informal experimentation, NREL power systems engineers have found the 3D topology view coupled with the 2D topology and time-series view inside the immersive environment to be highly useful. Operators have stated that it is much easier to comprehend the dynamics and multivariate correlations of the system when multiple variables are represented simultaneously. The immersive capabilities were instrumental in easily isolating and qualifying voltage violations. For example, various analyses of the data suggested that one control strategy might have more violations than another, but it was difficult to determine the temporal behavior of these violations relative to neighboring lines and where these violations were on feeders relative to the solar site and the voltage regulators. In the immersive space, however, these relationships were immediately apparent.

The 3D distance view has been less successful, which may be because the temporal patterns effectively produce "sheets" of voltage that are not easily separated or distinguished visually (see Figure 22).

## 5.2 R-Based Visualization

In addition to the visualizations designed for the state-of-the-art resources afforded by the ESIF's Insight Center, a set of lightweight R-based visualization scripts were developed. These scripts were used to ingest SQLite databases as they are produced from the DOTS simulations and pushed to NREL's ESIF data store. These scripts serve two purposes: (1) providing more in-depth statistical visualization and analysis of the simulation results and (2) supporting the generation of "publication-quality" images such as those found elsewhere in this report.

# 6 Simulation Results

Extensive simulations were a core focus of the project. This section presents a detailed review of these results beginning with a summary of the 40-day results, then a careful examination of the validation runs, two representative days from each of the 40-day runs, additional sensitivity analyses, annualized results including cost-benefit analyses, and finally a discussion of substation real and reactive power implications.

Complete results for all simulated days from all scenarios are included in Appendix C.

## 6.1 40-Day Results Summary

### 6.1.1 Scenario List

A total of six scenarios were chosen for full annualized analysis and run as 40 days using 2014 data:

1. **Baseline**: feeder voltage regulation equipment control settings provided by Duke Energy and the PV plant modeled using 2014 real and reactive power measured data.
2. **Local PV Control (PF=0.95)**: feeder voltage regulation equipment control settings provided by Duke Energy and the PV plant modeled using 2014 measurement data for real power but with a constant power factor of 0.95 absorbing (inductive).
3. **Local PV Control (Volt/VAR)**: feeder voltage regulation equipment control settings provided by Duke Energy and the PV plant modeled using 2014 measurement data for real power but following the volt/VAR curve previously described in Section 3.2.1.2.
4. **Legacy IVVC (Exclude PV)**: feeder voltage regulation equipment controlled by the centralized IVVC algorithm in the DMS and the PV plant modeled using 2014 real and reactive power measured data.
5. **IVVC with PV @ PF 0.95**: feeder voltage regulation equipment controlled by the centralized IVVC algorithm in the DMS and the PV plant modeled using 2014 measurement data for real power but with the PV simulated to run at a constant power factor of 0.95 absorbing (inductive).
6. **IVVC (Central PV Control)**: feeder voltage regulation equipment controlled by the centralized IVVC algorithm in the DMS with the PV plant's reactive power also eligible to be controlled by IVVC algorithm subject to historic 2014 real power production and the inverter's real and reactive power capability curve (described in Section 3.2.2). When the centralized IVVC algorithm did not choose to send control signals to the PV plant, the PV was modeled using 2014 real and reactive power measured data.

### 6.1.2 Regulation equipment Impacts

Figure 23 shows the summary of the 40-day runs for the voltage regulation equipment in the feeder of study (note that Cap 2 is not included because it is currently a fixed capacitor). Having the inverters at the PV plant operate in local control modes, such as constant power factor of 0.95 absorbing (inductive), and volt/VAR modes, did not greatly affect the operation of the line regulators Reg1, Reg2 and Reg3, or substation LTC. The switched capacitor Cap1 operations increased to switch one or two times daily when the inverter provided local voltage support,

compared to the baseline scenario where the capacitor operated only once per day for 9 of the 40 days simulated.[19]

The voltage regulating strategy for the feeder drastically changed when the central IVVC/LVM algorithm managed the voltage regulation equipment. With the simulated set of penalties used in the IVVC optimization, IVVC reduced the daily number of operations of the substation LTC by more than half and drastically reduced the operation of the line regulators. (In fact, for most of the days the line regulator was not used in the voltage regulation of the feeder). Instead, the voltage regulation was largely performed by the capacitor. Under LVM, the number of switching events for the capacitor increased to more than 4 per day for more than half of the 40 days that were run.

The effects of having the IVVC algorithm control the large PV inverter for reactive power support were that the capacitor was slightly less used because the central optimization algorithm chose to dispatch the inverter as a capacitor for most of the hours of PV production, as will be shown in a later section. Finally, running IVVC for traditional utility equipment while the PV inverter provides local voltage support in the form of constant 0.95 absorbing (inductive) power factor resulted in slightly less frequent use of the capacitor and line regulators compared to the Legacy IVVC simulation.

### 6.1.3 Voltage Impacts

The simulated system currently has very few voltage violations outside of +/-5% of nominal at load locations. These mostly cannot be attributed to PV plant because they typically occur in the early morning hours and evenings when the PV system is not running. The few existing and all observed violations are minor (less than 0.5 V) and short-lived (less than 1h), and hence they seem to be largely in line with the American National Standards Institute (ANSI) C84.1 standards. Instead of indicating problems, tracking the number of overvoltage and undervoltage violations provided a metric for comparing the effectiveness of various voltage control schemes.

Figure 24 summarizes the number of voltage violations seen in the simulations. It shows that the autonomous inverter controls had minimal effect on the number of voltage violations at the load locations on the feeder. This is mainly because the PV plant is located close to the substation, and as such it has relatively small impact the load voltage violations occurring downstream. The use of IVVC sharply reduced the overvoltage violations compared to baseline; however, a few undervoltage violations that were not present in the baseline were observed. Further refinements to the IVVC configuration would likely show better performance, specifically addressing the undervoltage violations when IVVC is controlling the PV plant.

The increased load voltage violations observed when the IVVC algorithm controlled the advanced inverter are mainly due to the effect of PV variability. The centralized IVVC algorithm used in this project solves every 10 minutes, and controls are locked during that interval, and as such the centralized algorithm is not able to adjust settings due to large variations in PV production affecting the voltage within that interval. Potentially including PV forecast data into

[19] The simulations used the most recent (May 2015) capacitor settings that were different than those actually in place in 2014, resulting in different numbers of baseline simulated operations compared to 2014 field data.

the IVVC algorithms could be a way to address some of the integration issues of advanced inverters in centralized voltage management methods. Alternatively faster IVVC solve intervals or the use of IVVC triggering on voltage challenges could also improve this performance.

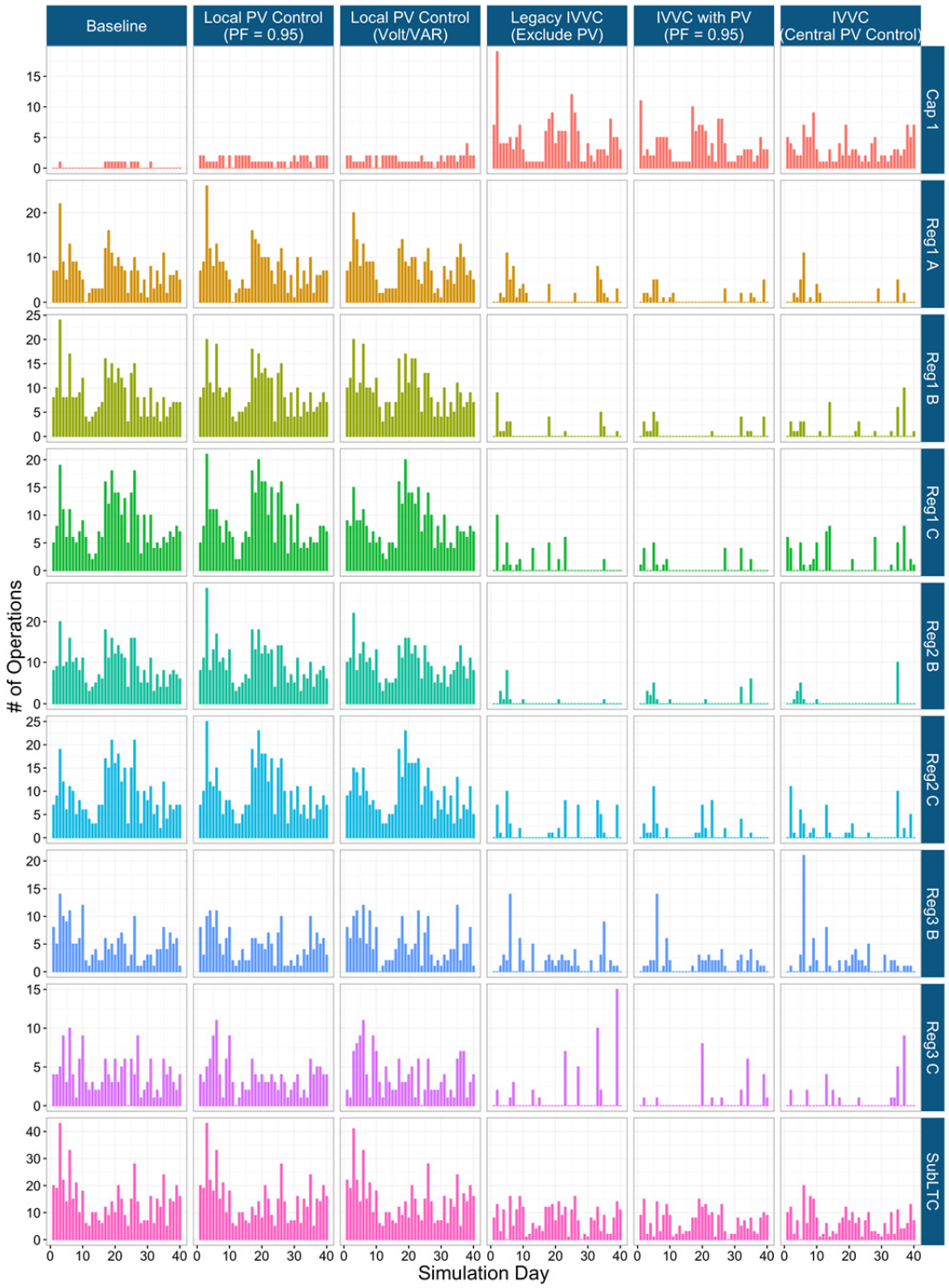


**Figure 23. Feeder 40-day results of number of operations of voltage regulation equipment**

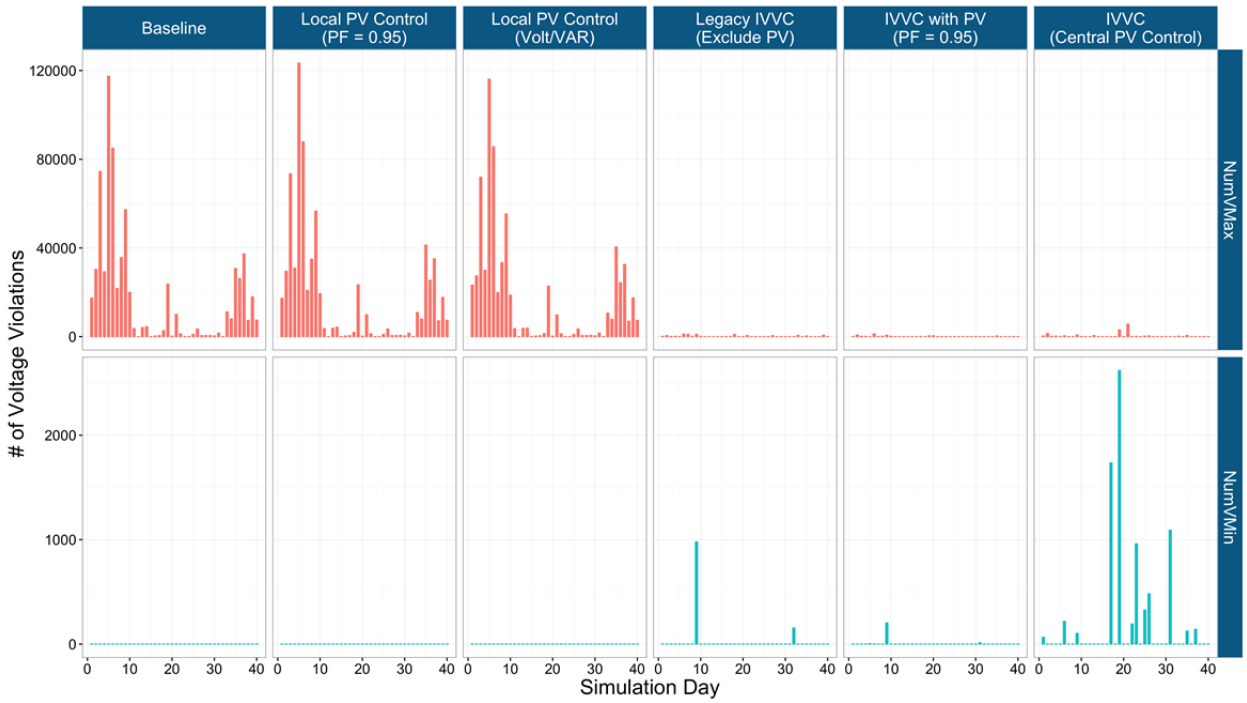


**Figure 24. Feeder 40-day results of number of load-voltage violations. Each violation count represents a customer minute of violation, so although the numbers may seem high, they generally represent a small fraction of the approximately 1 million possible customer minutes per simulation.**

The 40-day substation power flow, PV plant generation, and three-phase feeder-head voltages are included in Appendix C for all scenarios.

## 6.2 Validation of Feeder DOTS Model

All scenarios were based on the same static feeder model used with Duke Energy's production DMS. This base static model is built directly from GIS data using an automated extract process. The ability for load allocation to converge (i.e., true-up model with SCADA) and the IVVC performance can depend greatly on the quality of this static model data.

The simulation environment for the PV system and its interactions with this distribution feeder model in the DOTS tool was validated using historic data from 2014. For the purpose of validation, 2 days—one clear and one cloudy—were chosen for simulation. The PV generation profiles for the chosen days are shown in Figure 25.

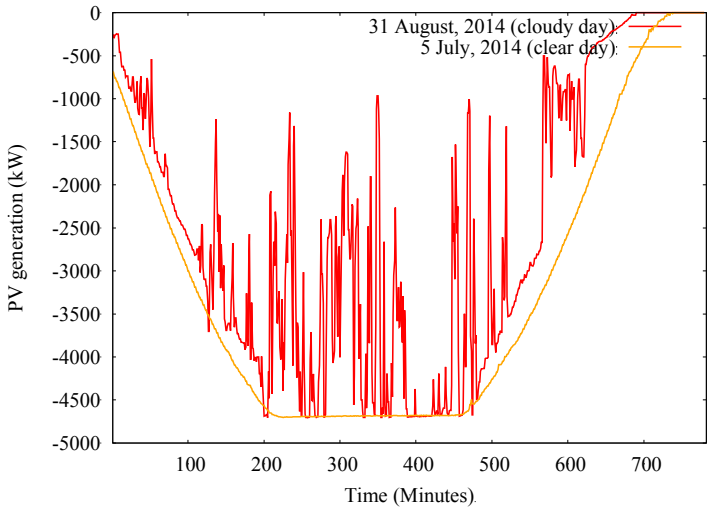


**Figure 25. PV generation on a clear day and cloudy day**

### 6.2.1 Time-Series Simulation Methodology

To run a time-series power-flow simulation, load and PV generation profiles have to be provided along with the voltage profile at the substation. The following section describes how these inputs were incorporated into DOTS to run/drive the time-series simulation.

The DOTS simulation interface has two ways to use the measured feeder data: (1) by using load allocation and (2) by setting the target values at specified locations. The built-in load allocation method in DOTS is called base load allocation (BLA), and it allocates the aggregate load applied at the feeder head among the customer loads available downstream. BLA takes into account losses and load to voltage dependency and can allocate a wide a range of flow measurements.

In validating the baseline case in DOTS, the convergence of the BLA algorithm is a key indicator. A time-series simulation in which the BLA fails to converge for a majority of the simulations cannot be considered for comparison or analysis; hence, it is important to monitor the BLA convergence rate. Thankfully all of the simulations presented here had near perfect rates of BLA convergence.

### 6.2.2 Evolution of Baseline Validation Methodology

To validate the baseline model, the only additional source of measurement data available that was not already used to drive the time-series simulation is the currents at recloser Rcl2, and these data were initially used to compare to the currents from the DOTS simulation power-flow solution. Figure 26 provides a comparison of the calculated currents to the measured currents at the recloser. For this simulation, BLA was used only at the feeder head and PV generator locations, and the voltages at the feeder head were set manually to measured values. As shown in Figure 26, Phase A and Phase C currents matched relatively well; however, the Phase B calculated power-flow currents were far from the measurements at the recloser.[20] To fix this mismatch, historic currents from the recloser were added to the BLA solution to produce a much

[20] This could be due to missing Phase B loads in the DOTS model.

better match, as shown in Figure 27. This improved approach was used for all subsequent simulations.

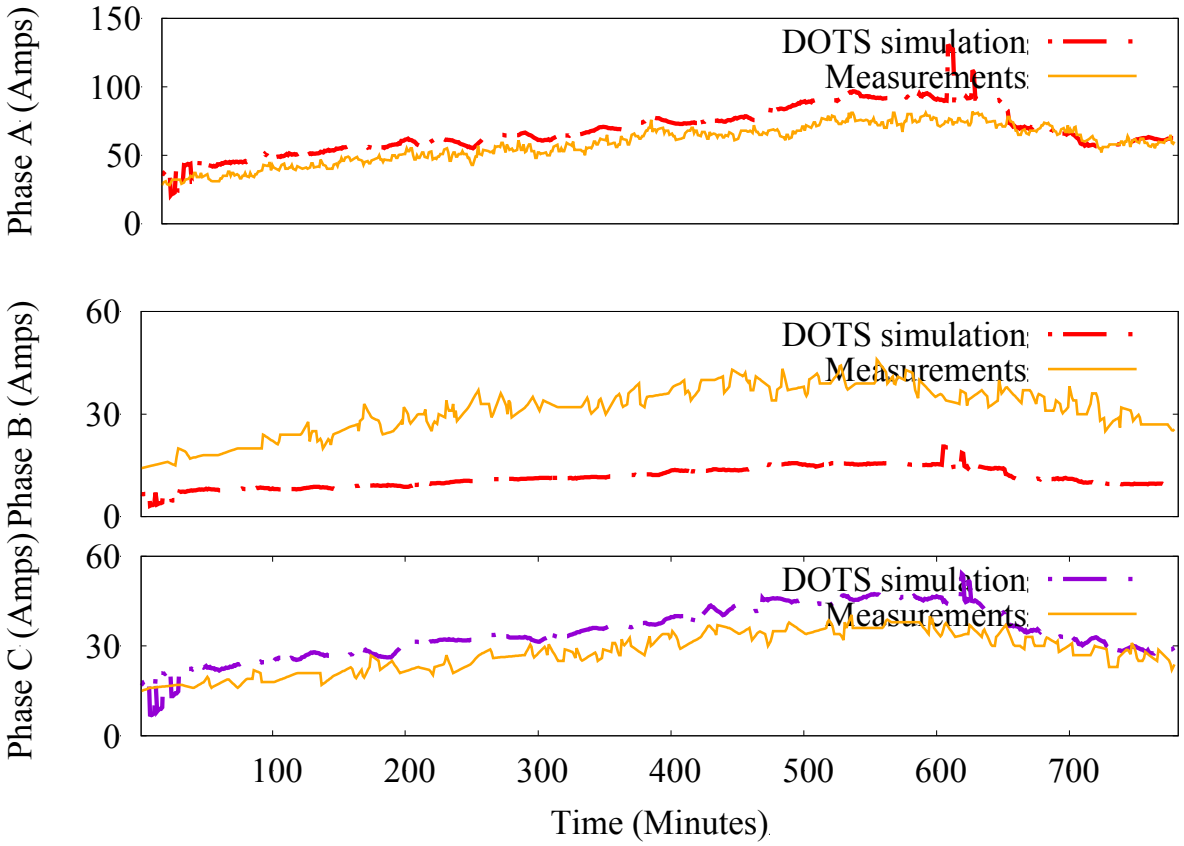


**Figure 26. Initial validation of recloser Rcl2 currents using BLA only at the feeder head and PV system, showing large differences on Phase B**

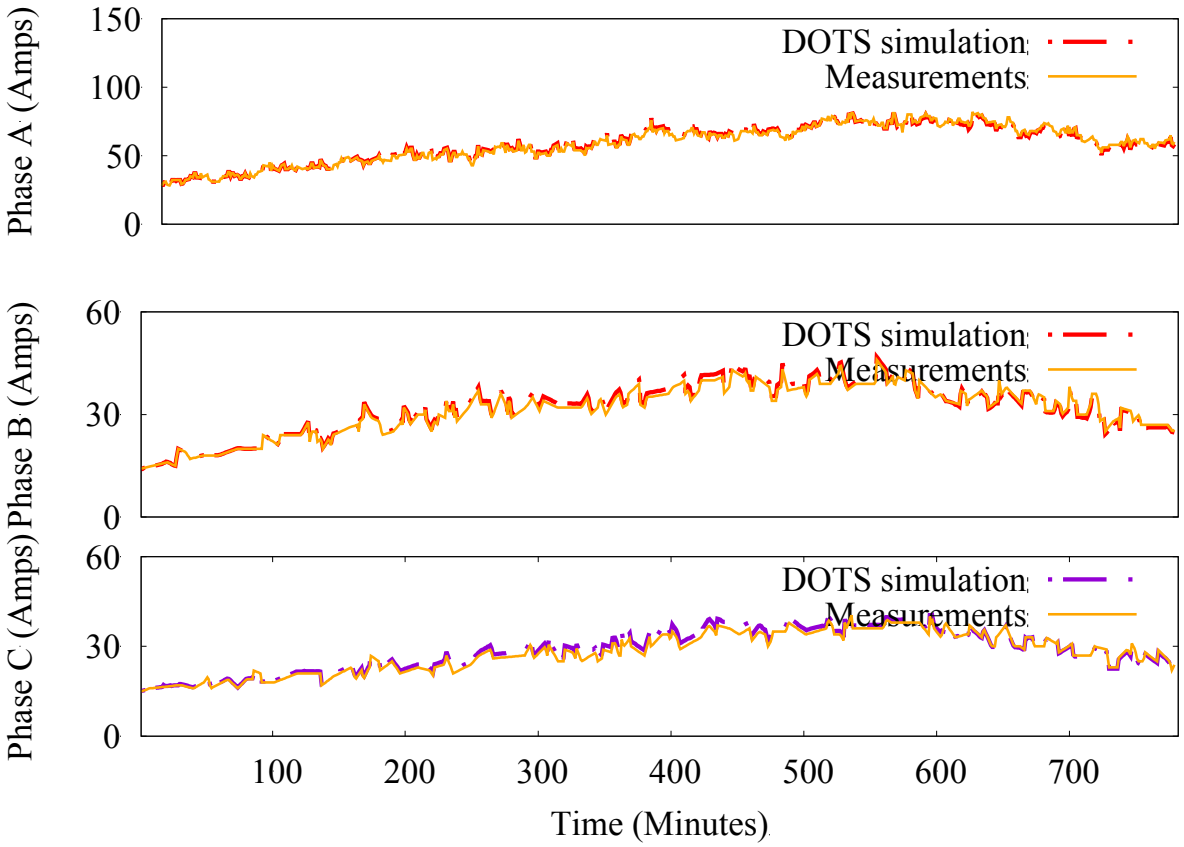


**Figure 27. Greatly improved validation currents at recloser Rcl2 when BLA also uses historic Rcl2 data**

### *6.2.3 Comparison of Measured Data to DOTS Simulation*

To further validate the load allocation approach and corresponding simulation, the historic measured data was compared to DOTS simulation results for a number of other data points on the feeder, specifically: the feeder-head load, feeder-head voltages, feeder-head currents, and recloser (Rcl2) currents. The comparison plots are presented as four figures: Figure 28 through Figure 31. The results show close matches with feeder-head load and recloser Rcl2 currents within 5% and voltages within 1% deviation from measured values. The only larger discrepancies were found with feeder head currents. Later analysis revealed that the reactive power flows from the capacitor were initially not properly captured in the simulation resulting in important differences in the allocated reactive power demands from load. This error explains the discrepancies in feeder-head current shown in Figure 30 and has since been corrected. The corrected approach was used in all subsequent simulations.

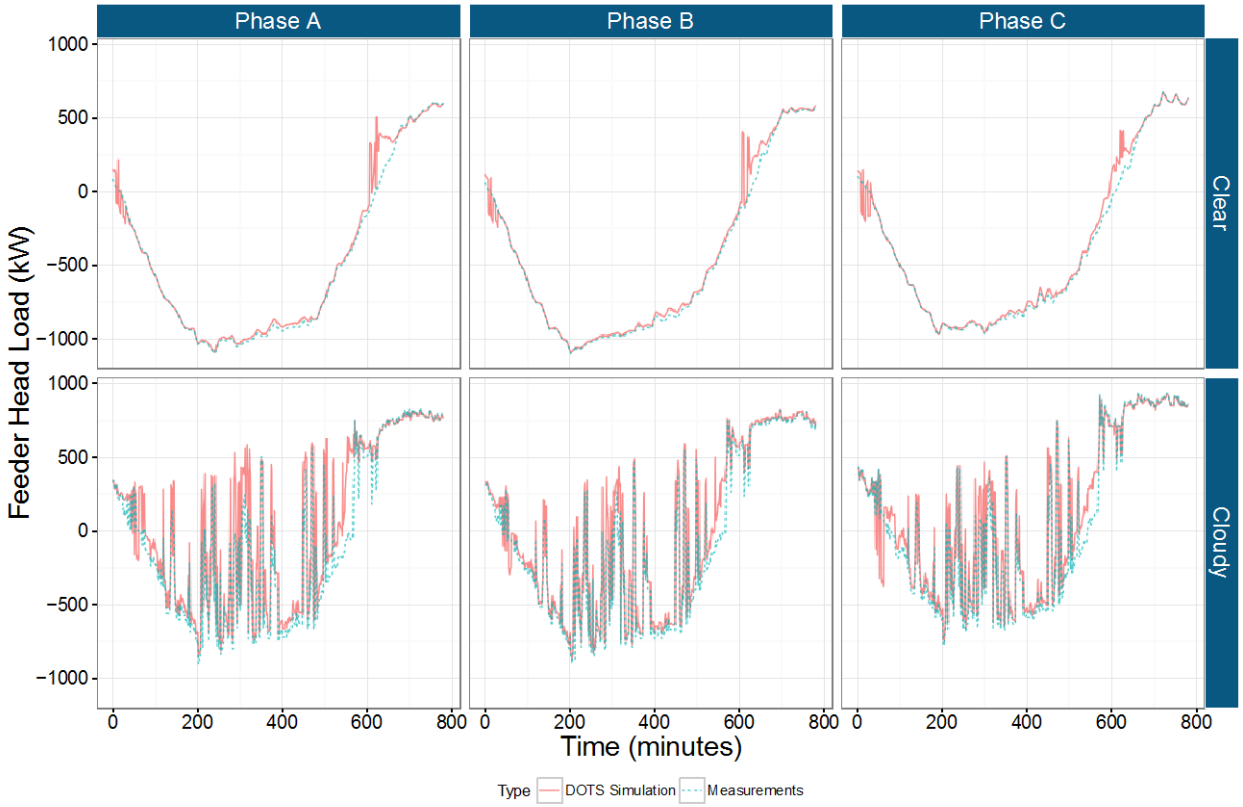


**Figure 28. Comparison of measured feeder-head loads to DOTS power-flow simulation results**

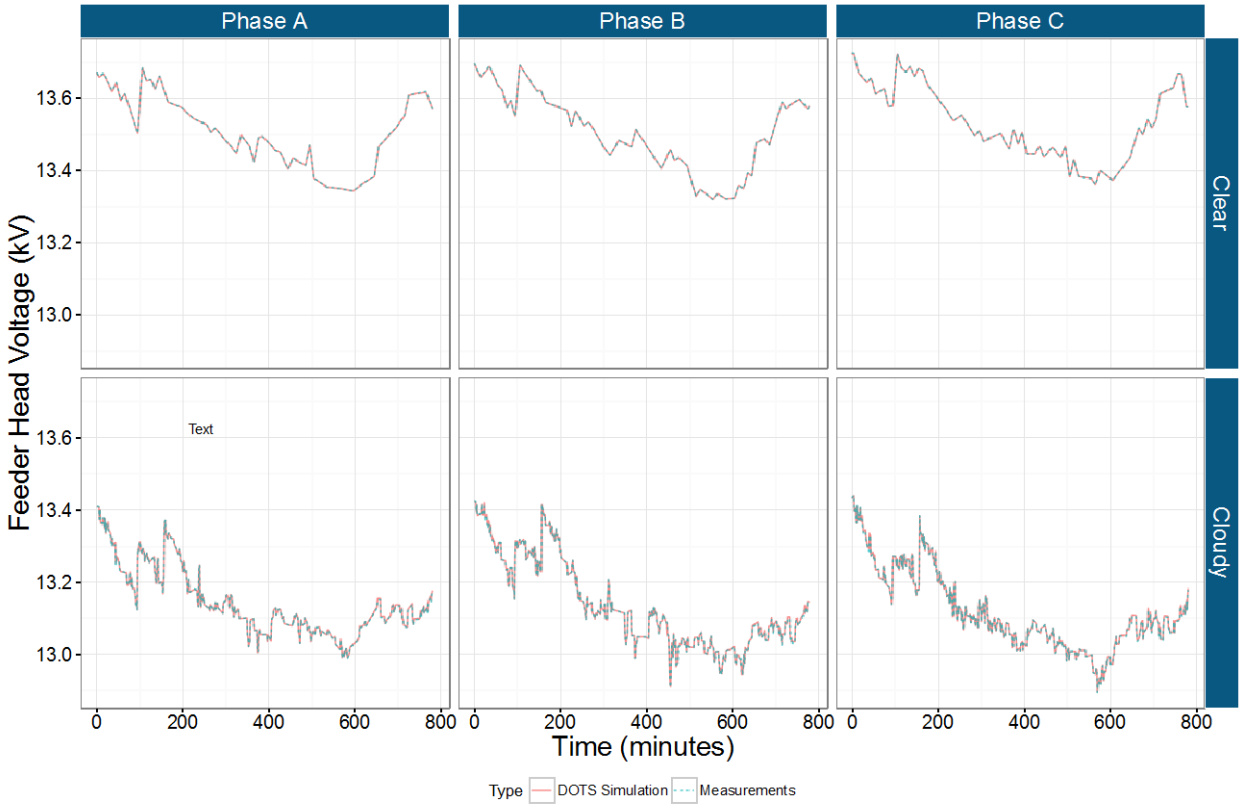


**Figure 29. Comparison of measured feeder-head voltages to DOTS power-flow simulation results**

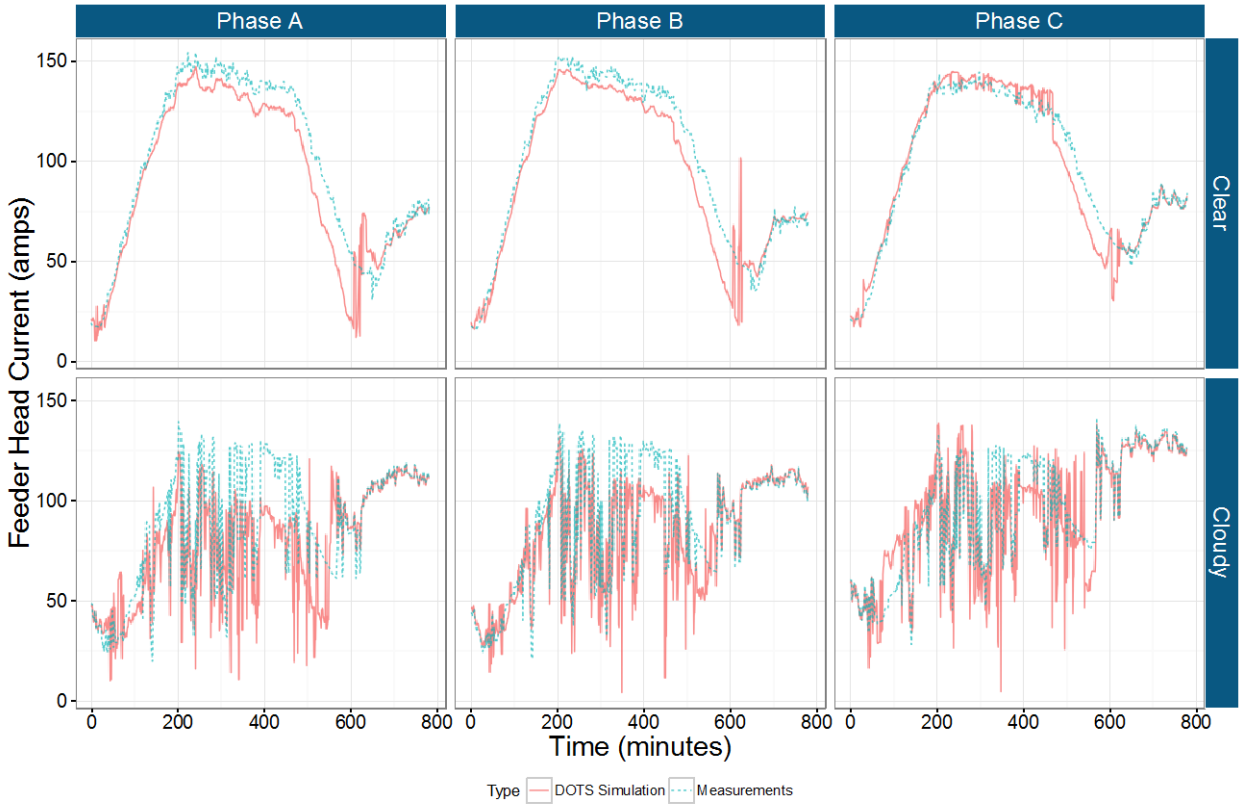


**Figure 30. Comparison of measured feeder-head currents to DOTS power-flow simulation results. These results do not include corrections made later to properly account for capacitor operations in the baseline load data.**

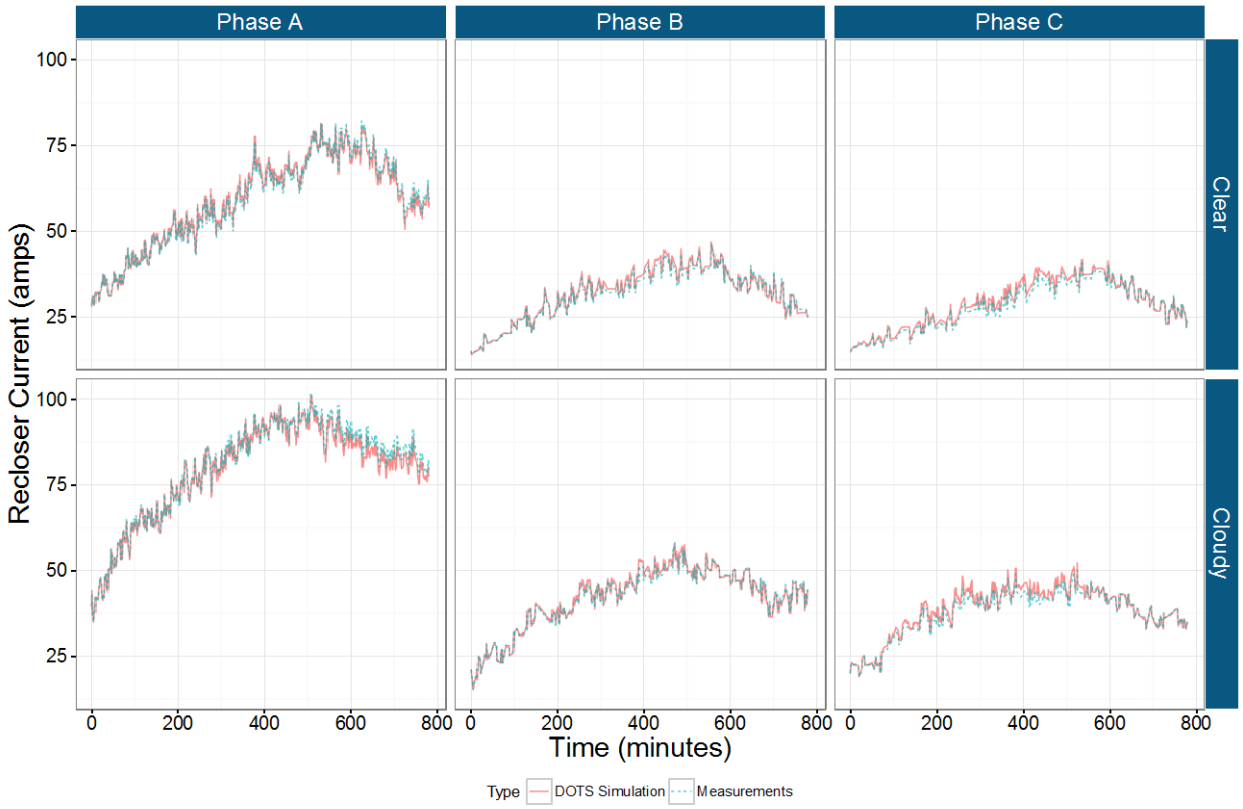


**Figure 31. Comparison of measured recloser currents to DOTS power-flow simulation**

## 6.3 Baseline Results

Detailed results for the baseline scenario are presented in this section for two days: a clear-sky PV irradiance and a variable PV generation day. The two days were selected based on the 40-day results of the advanced inverter control modes as representative of the impacts of such control modes in the feeder voltage management schemes. These same two days were used for other scenarios and the sensitivity analysis to facilitate comparisons.

Complete 40-day results for all scenarios can be found in Appendix C.

### *6.3.1 Baseline Detail Results for Two Days*

The real and reactive power at the feeder head of the feeder and at the PV generator are shown on the top two graphs in Figure 32 and Figure 35. The operation of the voltage regulation equipment—including the switched capacitor (Cap1), fixed capacitor (Cap2, always off in this scenario), substation LTC, and line regulators—is also included in the figures. The bottom graphs show the number of voltage violations at load locations.

Saturday, April 5, is representative of a shoulder month day in April when the PV plant was operating at full capacity on a clear-sky day. These types of lighter-loaded and sunny days tend to be the most worrisome for utilities in terms of adverse impacts of PV, but no voltage violations were observed. The plant is located relatively close to the substation, which is why it

did not impact the voltage. There was reverse power flow at the substation when the PV plant produced more than approximately 2.5 MW. When reverse power flow occurs, the substation LTC changed to cogen mode and does not compensate for voltage drop. The substation regulator was typically in the negative tap positions; it slightly reduced taps to decrease the voltage as PV production ramped up, staying constant during full output of the PV plant, and it slightly increased the taps when PV ramped down, changing from cogen mode to normal line-drop compensation mode. The three line regulators Reg1 stayed fairly constant throughout the day at negative tap positions (around -2), increasing to zero in the afternoon when PV production decreased.

Figure 33 shows a detailed feeder voltage profile as a function of the distance to the substation for each of the 30 minutes from 7 a.m.–7:30 a.m. This time period illustrates voltage regulation equipment operation during nonreverse power-flow periods. The substation LTC operated at negative tap positions (-7) in the morning and kept the substation voltage high, close to the allowable limit. The three line regulators Reg1 stepped down the voltage at every phase. Finally, the two (phases B and C) regulators Reg2 (located by the three line regulators Reg1) did not change the voltage; however, the second two (phases B and C) line regulators from Reg3 stepped up the voltage of the two-phase lateral farthest from the substation.

Figure 34 shows the voltage profiles between 1:30 p.m.– 2 p.m. when there was reverse power flow at the substation. In this plot, the PV location is visible by the noticeably elevated voltage due to the PV real power generation and corresponding reverse power flow. The profiles also show how the substation LTC did not compensate for the line voltage drop in cogen mode to accommodate for the voltage rise due to the PV plant. The three line regulators Reg1 still reduced the voltage; however both two-phase line regulators (Reg2 and Reg3) in this case stepped up the voltage of the Phase B and Phase C laterals.

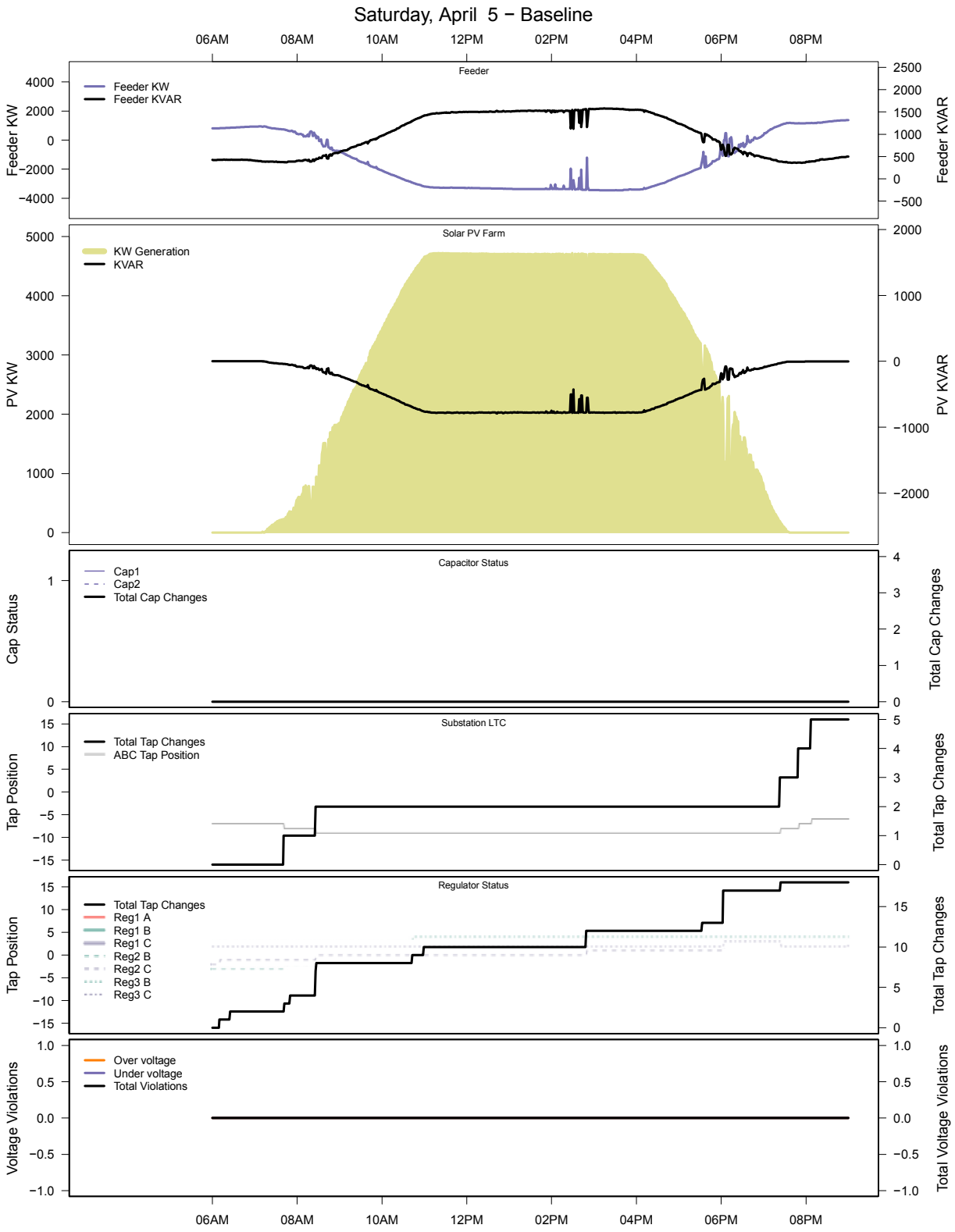


**Figure 32. April 5 baseline time series**

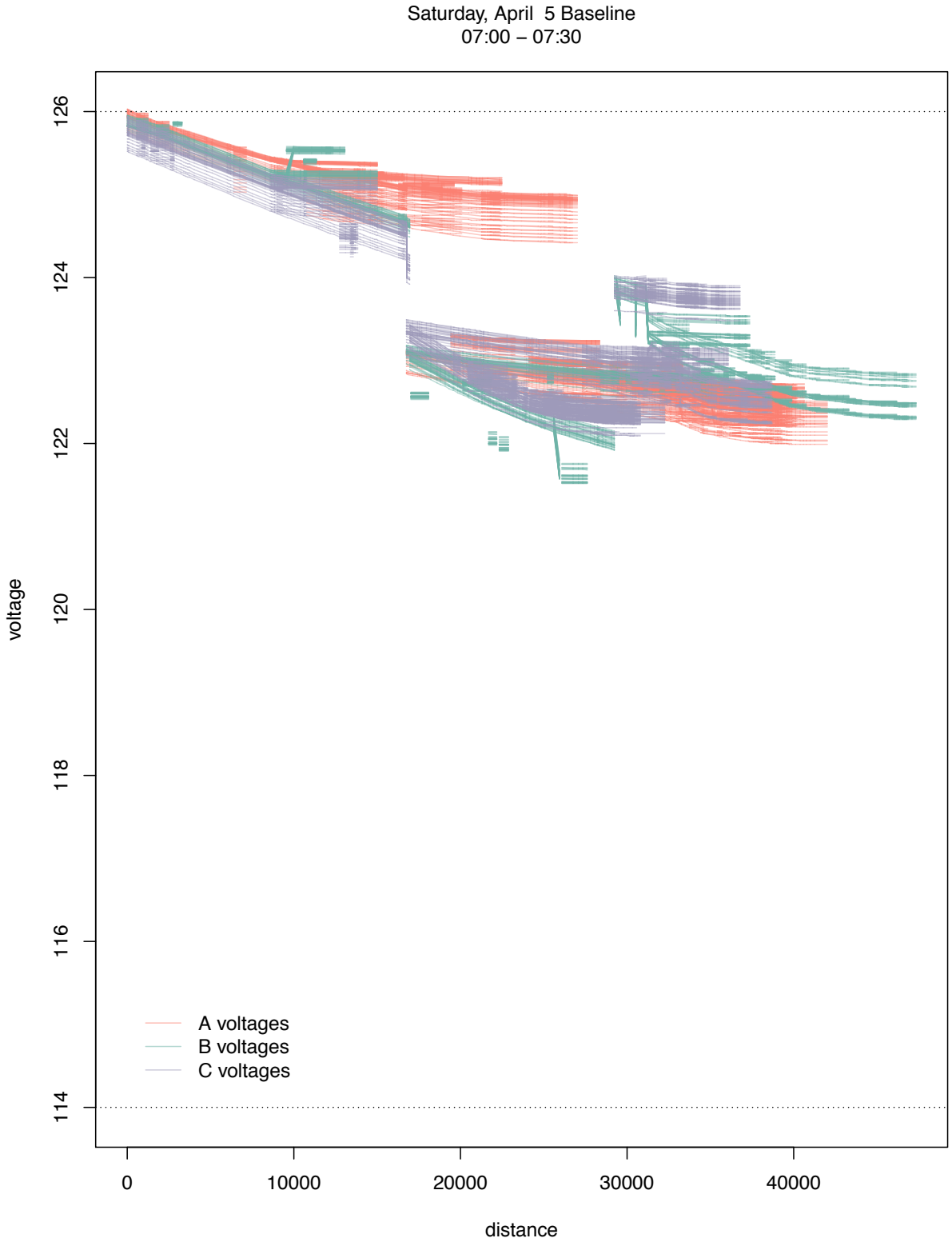


**Figure 33. April 5 baseline voltage profiles from 7 a.m.–7:30 a.m. (nonreverse power flow). Dashed lines indicate +/-5% limits from ANSI C84.1.**

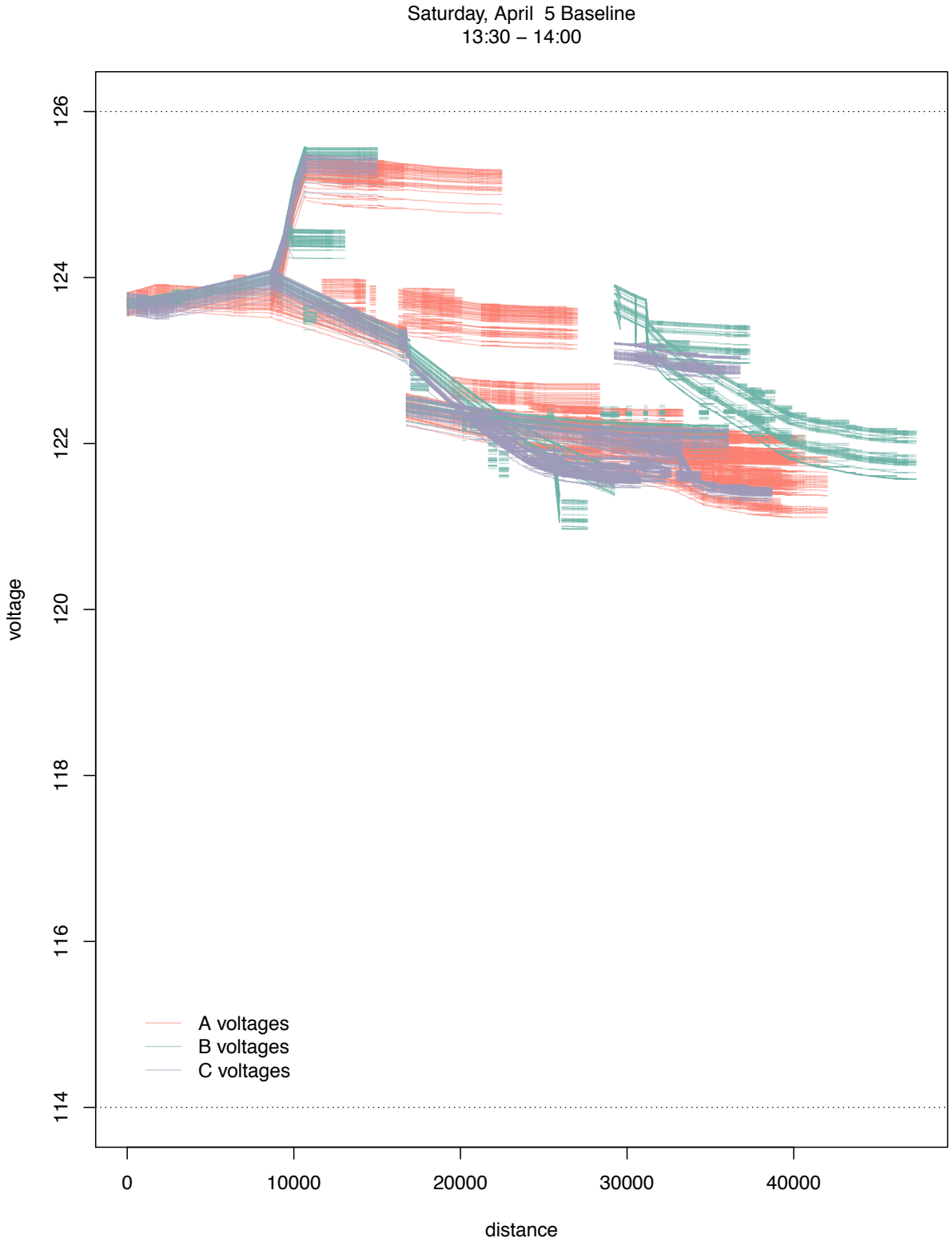


**Figure 34. April 5 baseline voltage profiles from 1:30 p.m.–2 p.m. (reverse power flow). Dashed lines indicate +/-5% limits from ANSI C84.1.**

The second day chosen for detailed analysis was August 15, and it presents a similar general pattern in terms of feeder voltage management strategy as shown in Figure 35. This day is representative of a sunny summer day with high variability due to cloud passage. A few voltage violations (measured in customer minutes) occurred early in the morning and late in the evening that were unrelated to the PV plant. The substation LTC boosted up the voltage in the early morning hours prior to the PV coming online and reduced taps during the day when the PV plant was online, adjusting when needed to compensate for the variability of the PV. The three line regulators Reg1 decreased taps, also adjusting for PV drops when needed, as can be observed between 4 p.m.–5 p.m. Both the substation LTC and line regulators had a higher total number of operations due to the PV variability when compared to the clear-sky day previously described.

Figure 36 shows the feeder voltage profile as a function of the distance to the substation between 7 a.m.–7:30 a.m., and it shows the operation of the voltage regulators when there is no reverse power flow. Figure 37 shows the feeder voltage profile from 1:30 p.m.– 2 p.m. when there was reverse power flow at the substation and the substation LTC operated in cogen mode (when PV was higher than approximately 1 MW).

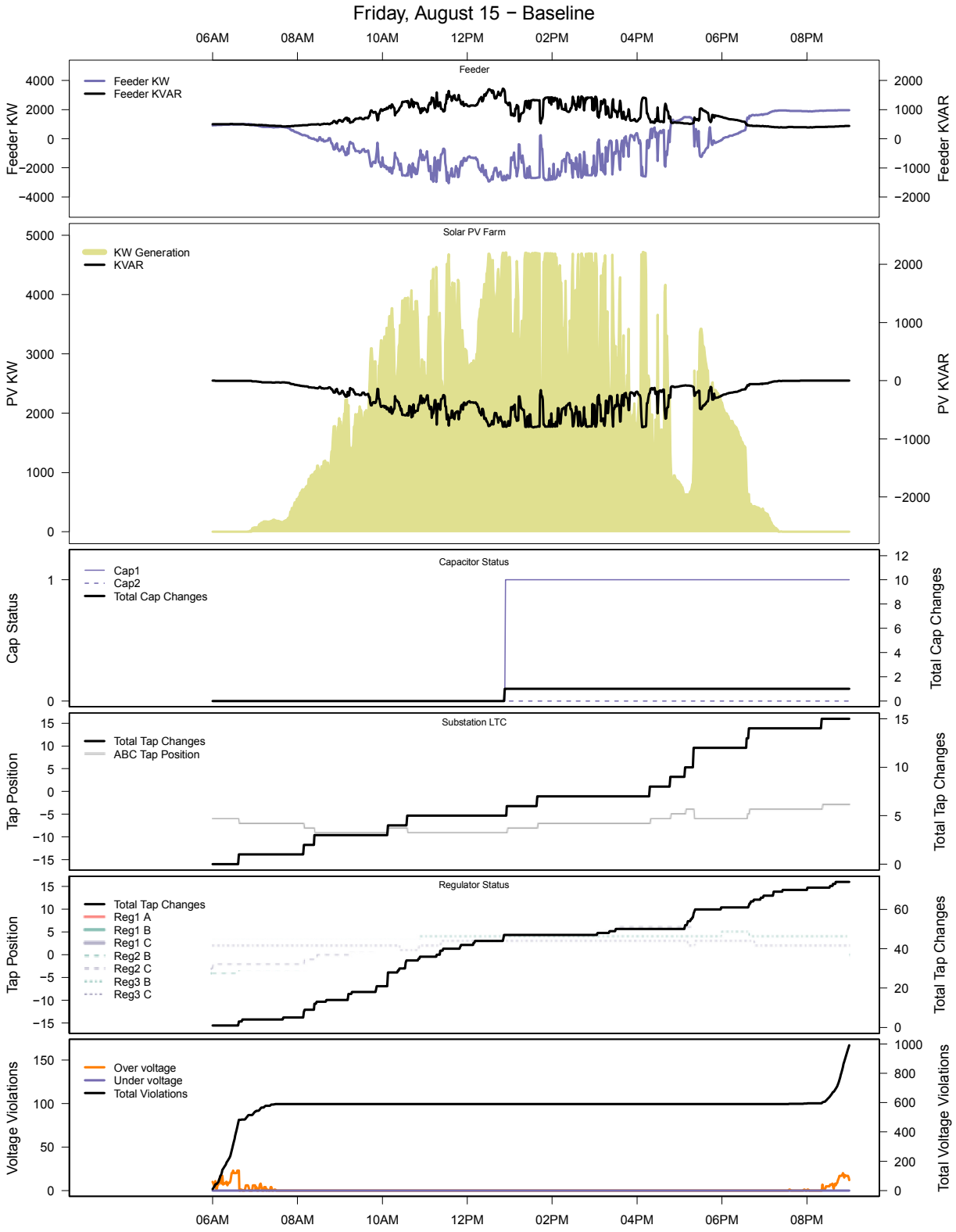


**Figure 35. August 15 baseline time series**

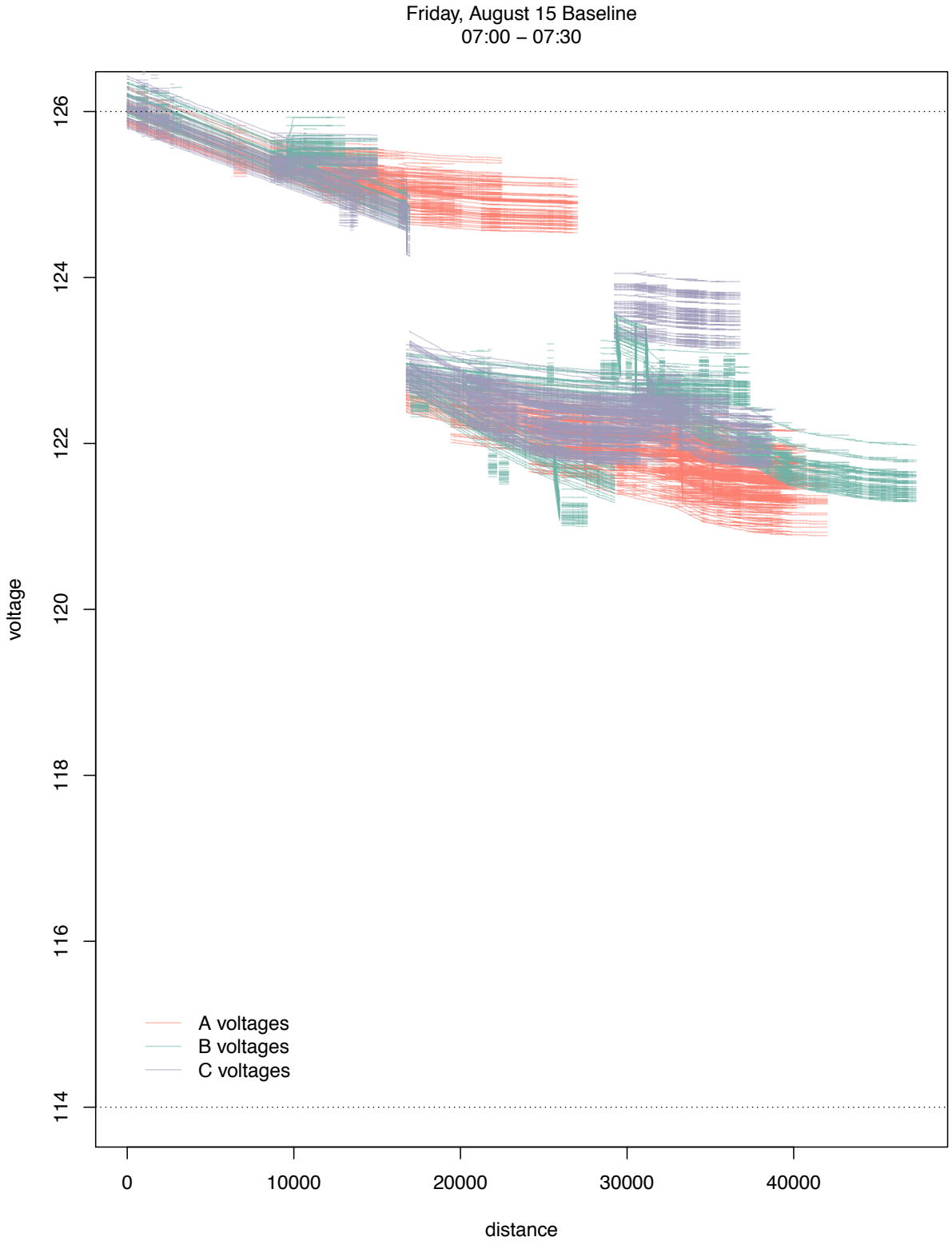


**Figure 36. August 15 baseline voltage profiles from 7 a.m.–7:30 a.m. (nonreverse power flow). Dashed lines indicate +/-5% limits from ANSI C84.1.**

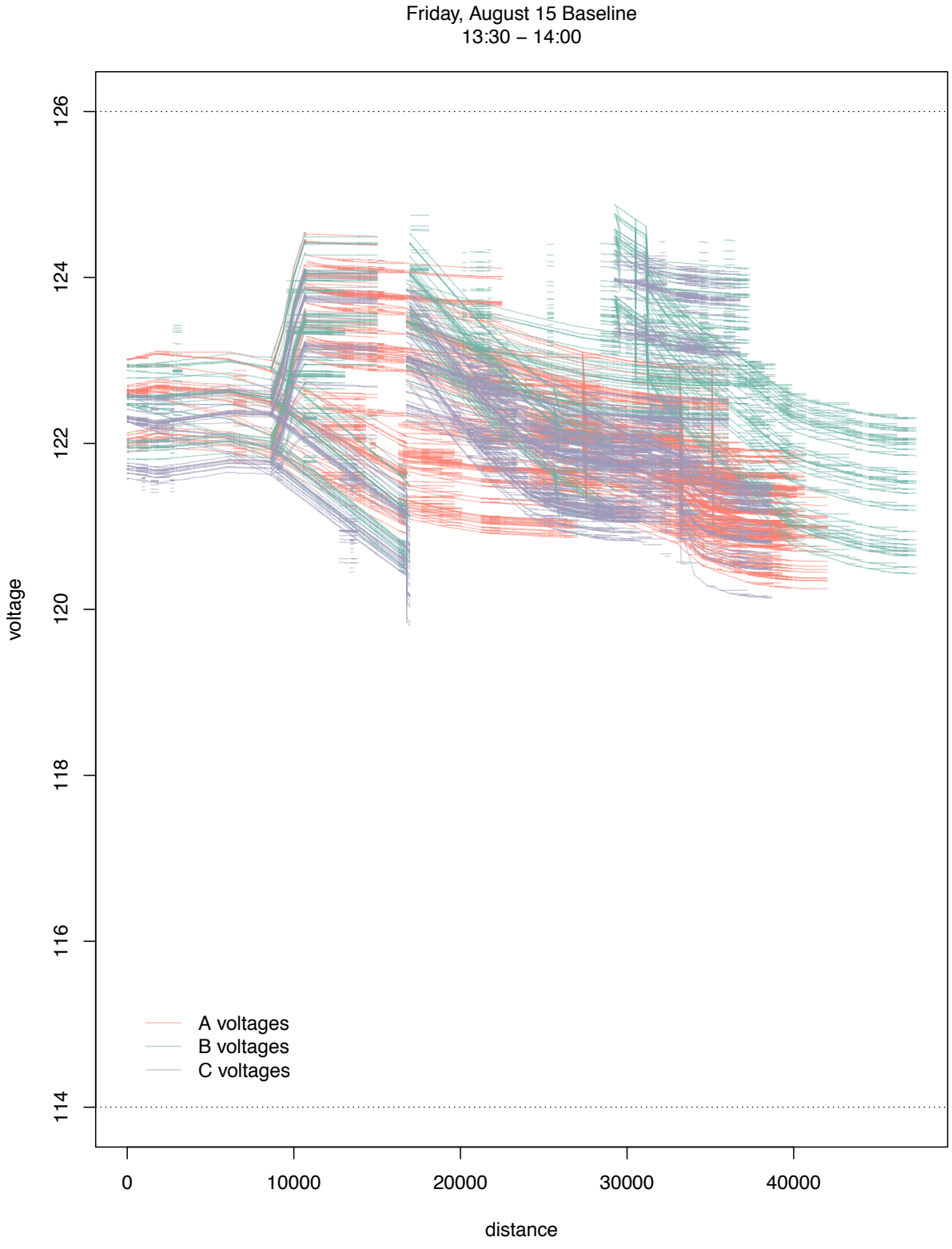


**Figure 37. August 15 baseline voltage profiles from 13:30 p.m.–14 p.m. (reverse power flow). Dashed lines indicate +/-5% limits from ANSI C84.1.**

## 6.4 Autonomous Local Control

In this section, we present results for the same two variable PV generation days discussed in the previous section with autonomous local control functions, and we compare the results to the baseline scenario. Complete 40-day results for these scenarios can also be found in Appendix C.

### *6.4.1 Constant Power Factor (0.95 Absorbing)*

The inverter at the PV plant was modeled to provide constant reactive power support during PV production at a power factor of 0.95 absorbing (inductive), as explained in Section 3.2.1.1.

Figure 38 shows the results of the constant power factor local mode for April 5, 2014. Shading in this and related graphics highlight differences compared to the baseline. The top graph reflects the shift up in total reactive power during PV power generation hours due to the increase in reactive power support provided by the PV plant as well as the step in reactive power due to the capacitor switching during PV production hours when compared to the baseline. The capacitor was turned on to produce reactive power, which suggests that the absorbing reactive power voltage support provided by the PV plant was not required. The number of operations at the substation LTC was unchanged, and the number of line-regulator operations slightly decreased.

Corresponding results for a power factor of 0.95 absorbing (inductive), for August 15, 2014, are shown in Figure 39. The top graph shows the difference in reactive power at the substation when compared to the baseline scenario due to the reactive power support provided by the power plant. The number of operations at the substation LTC and line regulators were also unchanged. Finally, the capacitor switched on 2 hours earlier than it did in the baseline scenario when it was activated by the increase in reactive power demand due to the PV support.

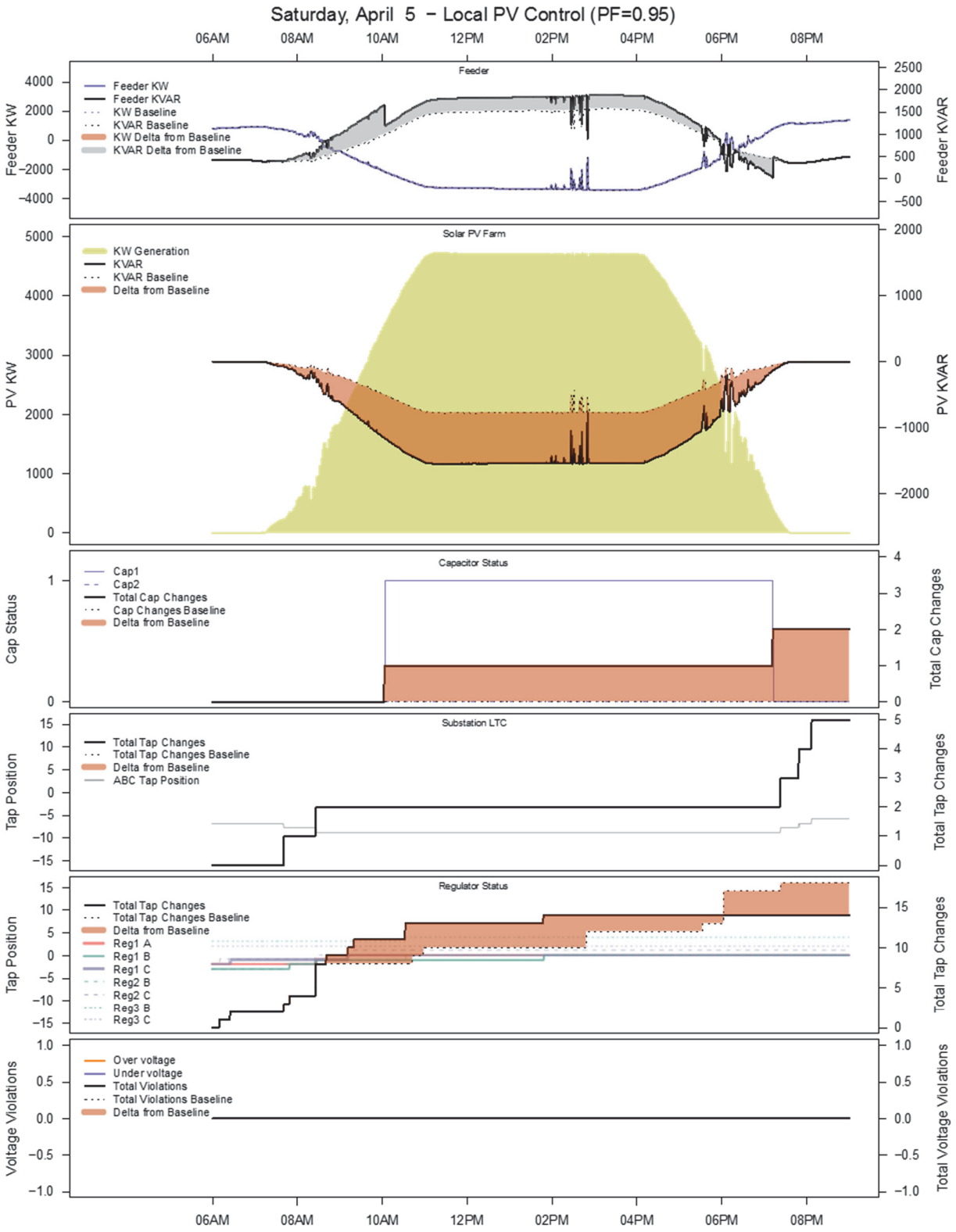


**Figure 38. April 5 time-series comparison to baseline with a constant power factor of 0.95 absorbing (inductive)**

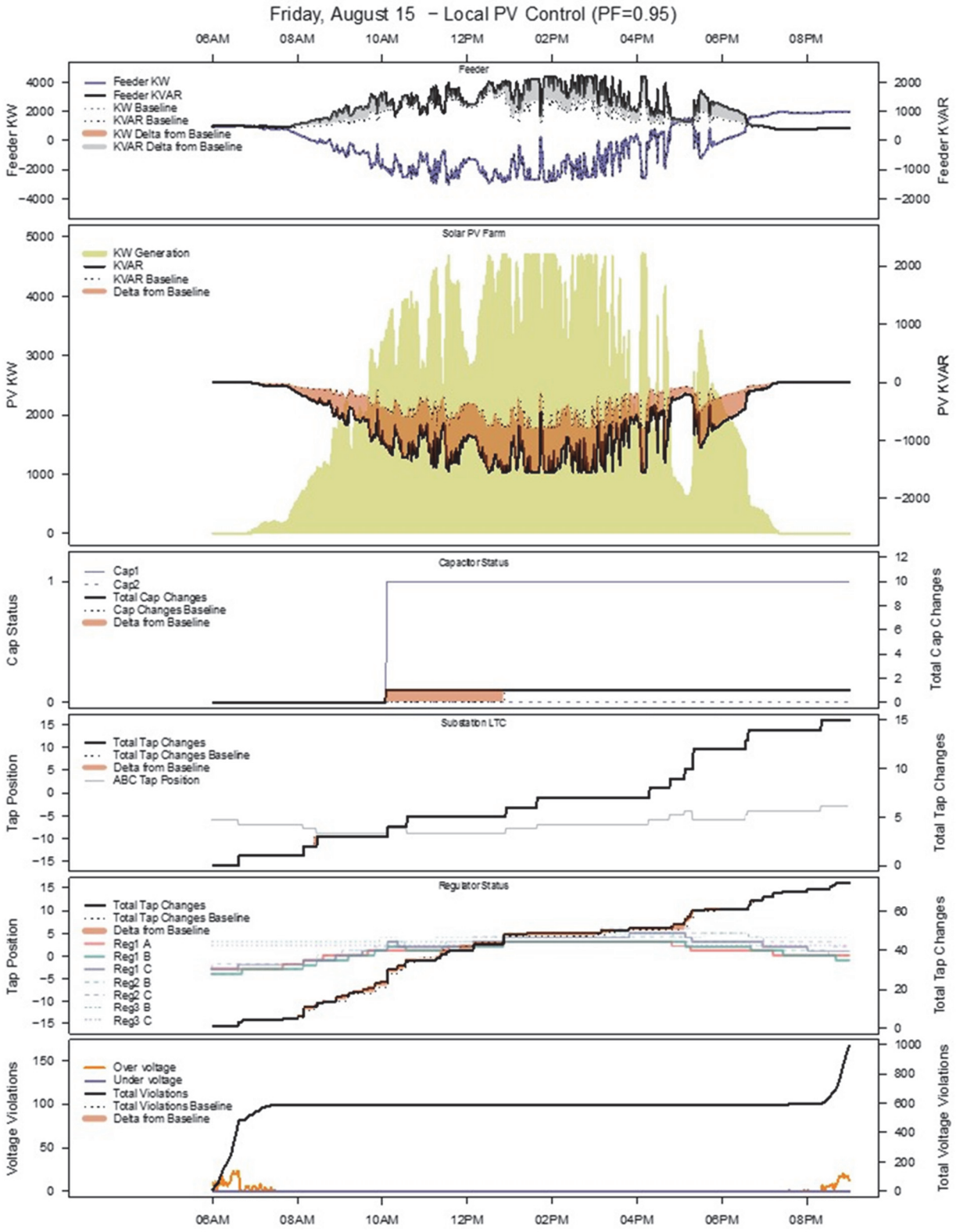


**Figure 39. August 15 time-series comparison to baseline with a constant power factor of 0.95 absorbing (inductive)**

### 6.4.2 Local Volt/VAR Control

For the autonomous volt/VAR scenario, the inverter at the PV plant was modeled to provide reactive power support following the volt/VAR curve shown in Figure 40, as explained in Section 3.2.1.2. These set points were modeled after Smith, et al. (2011) but with the kVAR limits set to 50% of the inverter kW rating, largely because the simulation power flow failed to reliably converge using 100% of the kW rating.

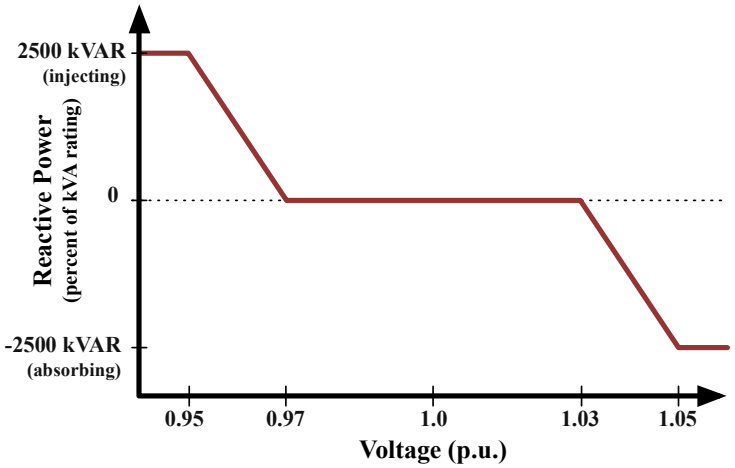


**Figure 40. Volt/VAR curve used in simulations**

Figure 41 shows the results of the volt/VAR mode for April 5, 2014, which are very similar to those of the constant power factor mode discussed in the previous section. The top graph shows the difference in reactive power at the substation when compared to the baseline scenario, and it can be observed that the power plant mostly produced reactive power throughout the PV production hours because it was a clear-sky day. The number of operations at the substation LTC was unchanged and the line regulator operations slightly reduced. The capacitor turned on to produce reactive power during PV production hours.

The results for volt/VAR mode for August 15, 2014, are shown in Figure 42, and they are also very similar to those of the constant power factor scenario. The top graph shows the difference in reactive power at the substation when compared to the baseline scenario, and it can be observed that the power plant mostly produced reactive power when there were no intermittent clouds and then it absorbed and produced reactive power when the PV production was more intermittent in the afternoon. In this case, the number of operations at the substation LTC and the total number of switching operations for the capacitor were unchanged, and at the locations of the line regulators the total number of operations was reduced.

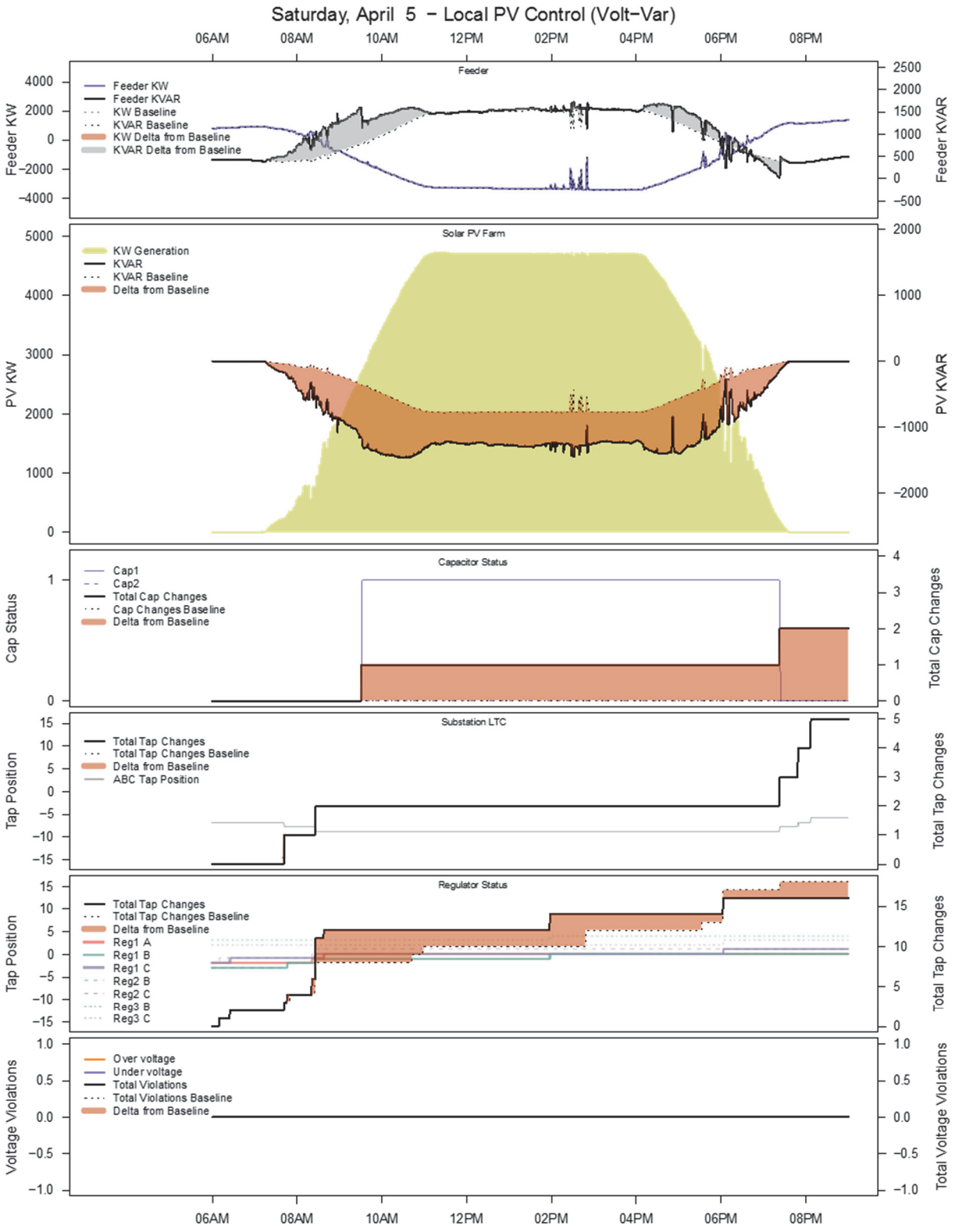


**Figure 41. April 5 time-series comparison to baseline of autonomous volt/VAR**

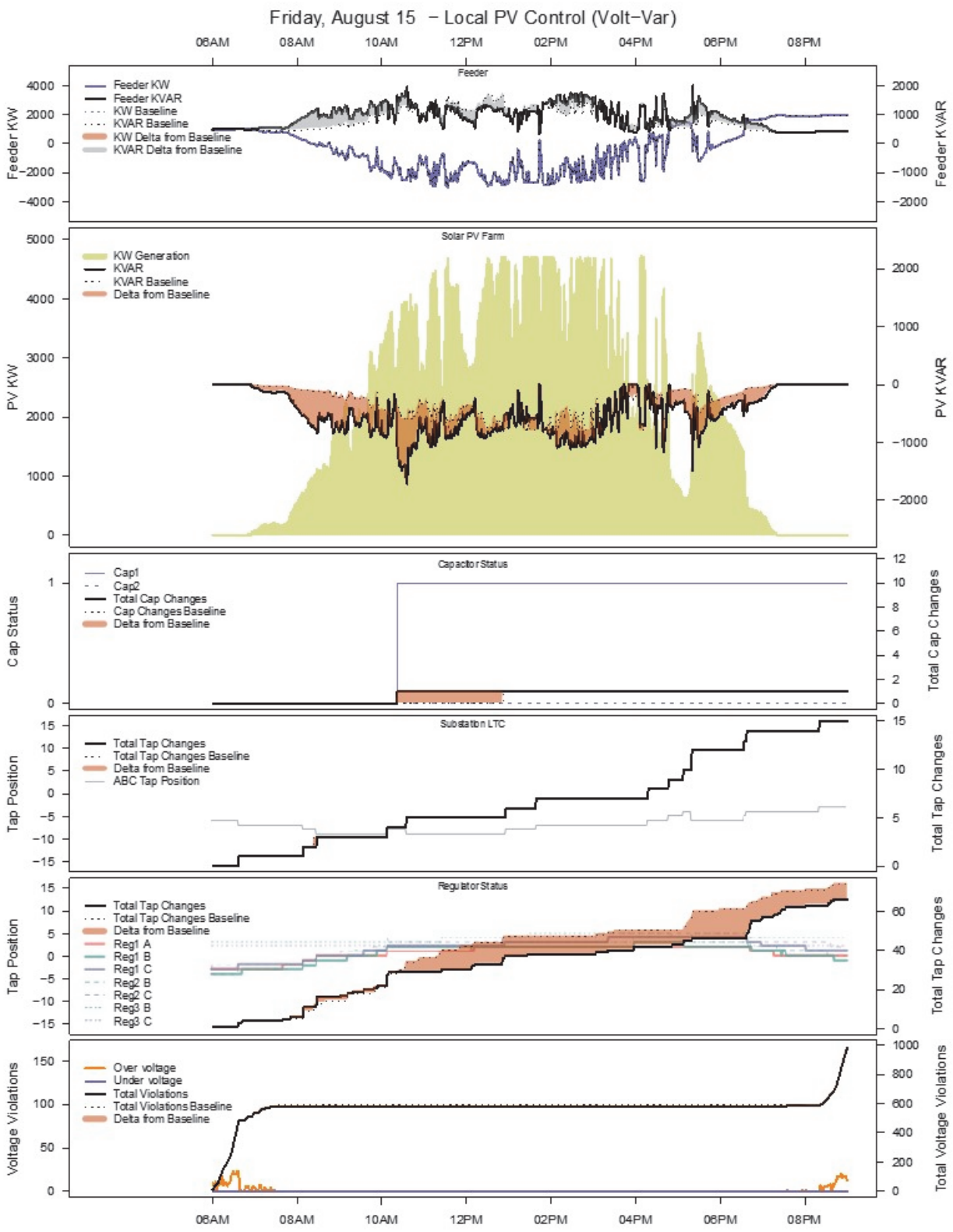


**Figure 42. August 15 time-series comparison to baseline of autonomous volt/VAR**

## 6.5 Integrated Volt/VAR Control through DMS

The IVVC function can have different objectives, such as minimizing real-power demand, losses, and voltage violations or a combination of them. In this section, we present the results of running Alstom Grid's IVVC algorithm with the objective of minimizing demand and reducing voltage violations. The control elements used to achieve these objectives were: the substation LTC, capacitor banks, and feeder line voltage regulators. This section also explores including the inverter at the PV plant as a resource for IVVC.

The summary of these results is presented in this section by comparing the same two days as in previous sections. Complete 40-day results are included in Appendix C.

### *6.5.1 IVVC with Traditional Inverter*

Figure 43 shows the results for April 5 of running the IVVC algorithm to minimize demand and reduce load voltage violations compared to the baseline scenario. It can be observed that the substation LTC was set at a constant negative tap step of -12 for almost the entire day to compensate for the voltage drop across the feeder, and as such the total number of daily operations when compared to the baseline scenario was considerably reduced from 5 to 2. The three line regulators were set to a constant value per phase between -2 and -4, and as such the number of operations was reduced to 0 (compared to 8 in the baseline scenario). The IVVC algorithm chose to regulate with the capacitors, which were switched on for the entire day. Note that the substation reactive power shows the operation of the second capacitor that was modeled as a fixed disconnected capacitor in the baseline scenario and made an eligible resource for voltage control in the IVVC algorithm.

For August 15, the IVVC algorithm chose to regulate voltage with the LTC regulator at the substation and the three-phase capacitor instead of the line regulators without the IVVC optimization as was used in the baseline scenario (Figure 44). As such, the three line regulators Reg1 were set to constant negative values throughout the day. This strategy eliminated all of the baseline overvoltages, and sharply reduced the number of regulator operations; however, with the tested IVVC settings, it considerably increased the number of capacitor switches for Cap 1 from 1 to 12 for the day.[21]

[21]The trade-off between capacitor and regulator operations can be tuned through the IVVC configuration by adjusting weights for operations and/or enforcing substation power factor constraints.

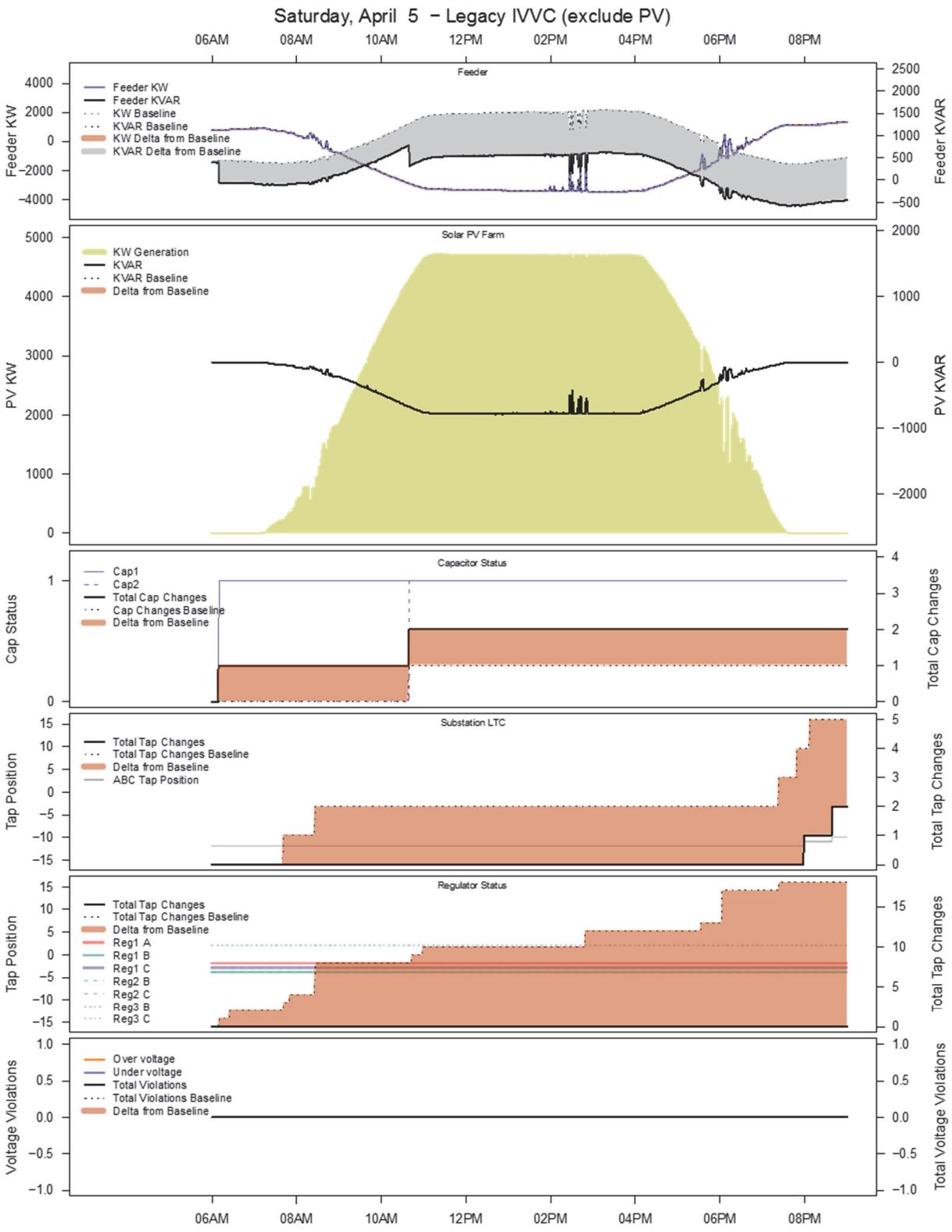


**Figure 43. April 5 IVVC time-series comparison to baseline with PV not eligible for control**

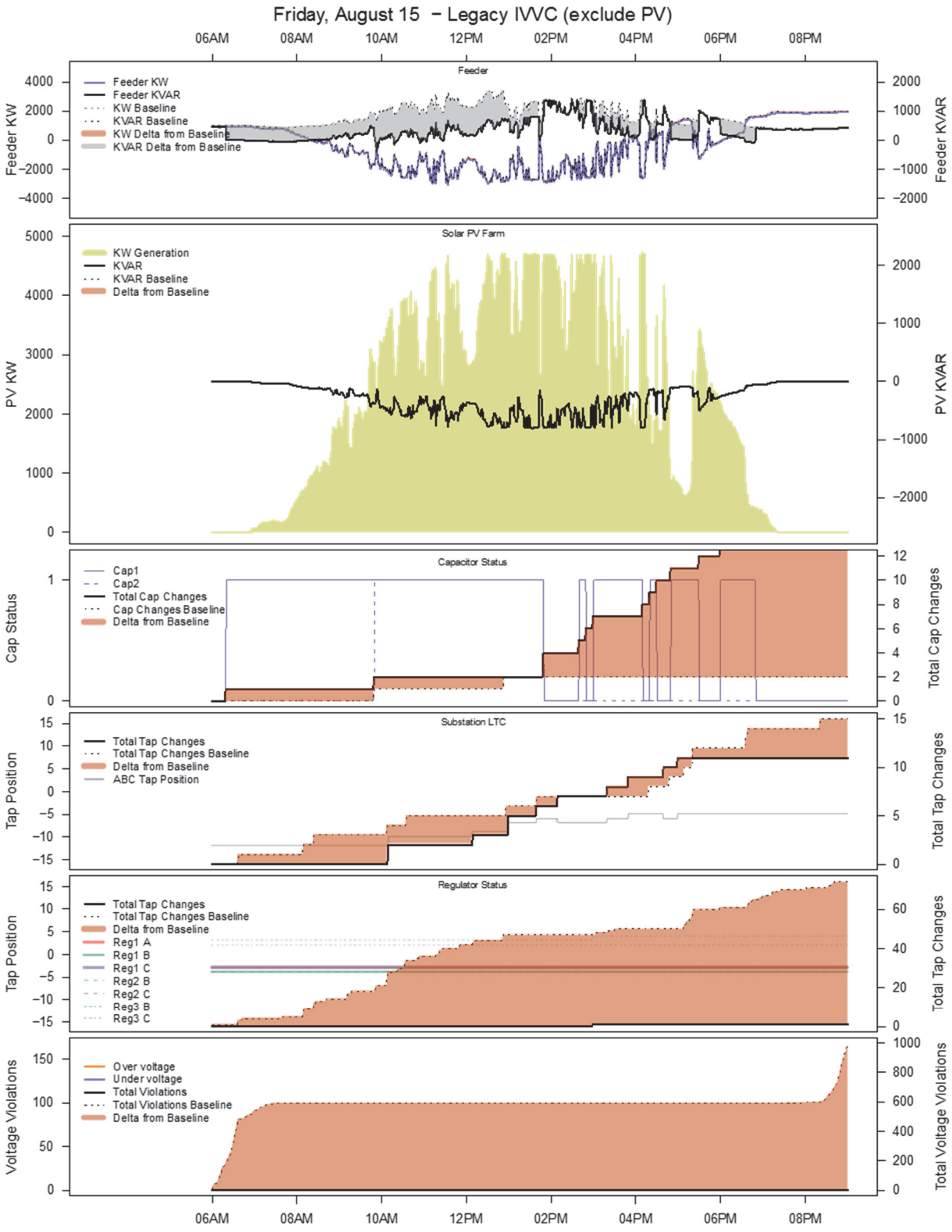


**Figure 44. August 15 IVVC time-series comparison to baseline with PV not eligible for control**

### 6.5.2 IVVC with the PV Inverter in Autonomous Local Control (PF=0.95)

In this case, the same IVVC algorithm as in the previous section was run with PV not eligible as a control resource by the central optimization algorithm but with the PV inverter operating at a constant power factor of 0.95 absorbing (inductive). This scenario is likely to occur in the near future when IVVC and advanced inverters are both deployed but not fully integrated. In this configuration, the central IVVC algorithm controls the devices owned by the utility while advanced PV inverters are operating in autonomous local control. (In this case, constant power factor was chosen as the local control mode.) In this case the combination of DMS controlled IVVC for utility equipment and autonomous PV control performed very well, despite this lack of coordination.

The results for April 5 are shown in Figure 45, and they are very similar to those of the IVVC scenario with legacy inverter operation for this clear-sky PV day. For August 15, as shown in Figure 46, slight improvements were observed compared to the results of the legacy IVVC scenario in terms of total number of capacitor switching events and substation LTC operations. The inverter was operating in local control mode and was able to mitigate some of the negative voltage impacts of the high variability of PV during the 10-minute time interval from one IVVC algorithm solve to the next. As before, the voltage violations were eliminated and the regulator operations sharply reduced.

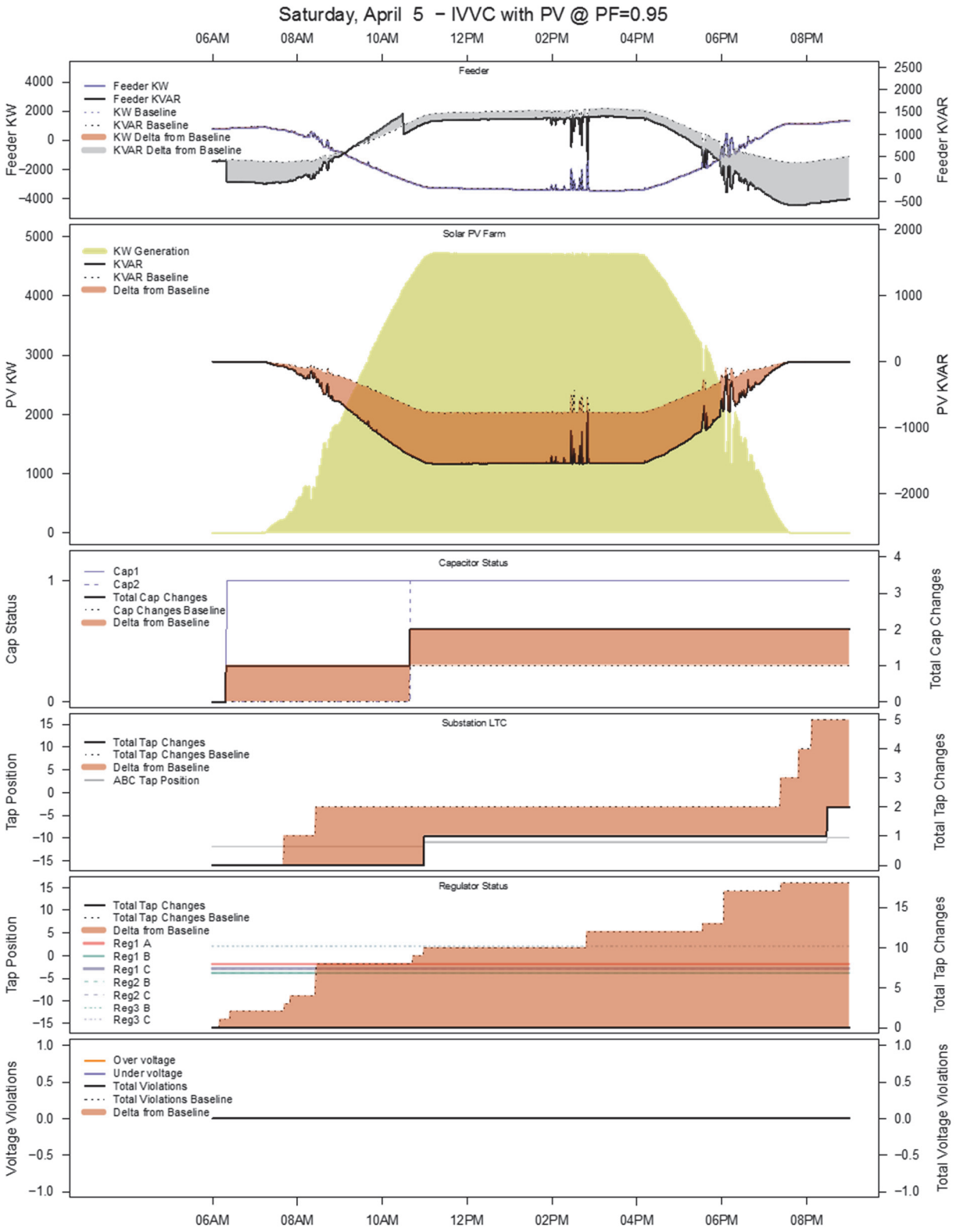


**Figure 45. April 5 IVVC time-series comparison to baseline for Local PV Control (PF=0.95)**

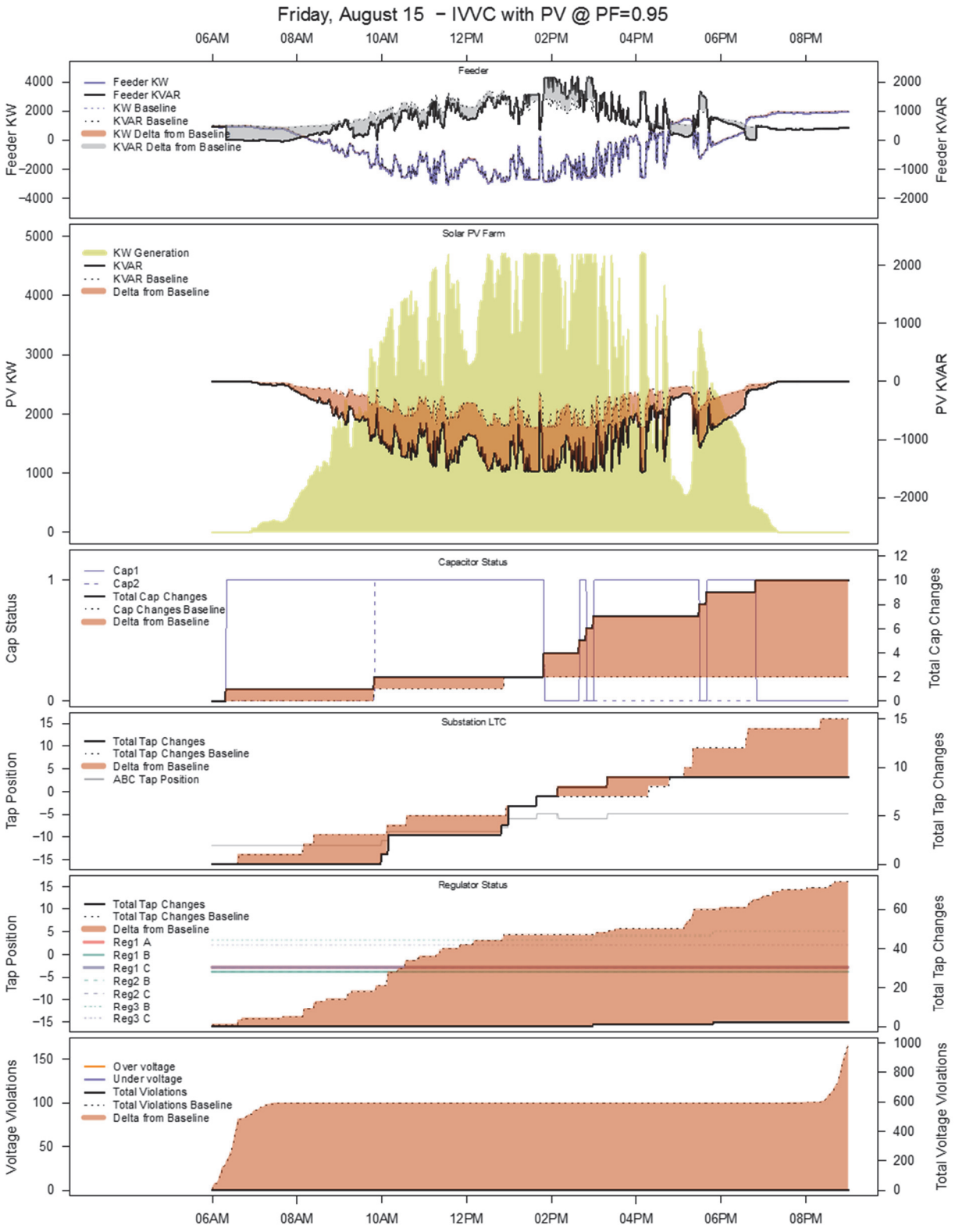


**Figure 46. August 15 IVVC time-series comparison to baseline for Local PV Control (PF=0.95)**

### 6.5.3 Integrating Advanced Inverters into IVVC

The last full 40-day scenario included a PV plant as an eligible resource providing reactive power, to manage voltage by the central IVVC algorithm. Because the PV plant is located close to the substation, the IVVC algorithm chose to regulate mainly with the PV inverter as a capacitive resource (injecting VARs) most of the day.

For April 5, there was no impact on the number of operations of other voltage regulation equipment on the feeder. Figure 47 shows the same improvement in terms of the number of reductions of operations of the substation LTC and line regulators.

For August 15, several undervoltage and overvoltage load violations were observed in the afternoon when PV rapidly dropped and rose, respectively; see Figure 48. As configured, the IVVC algorithm solved every 10 minutes and mainly relied on the PV inverter to regulate voltage, and as such it was not able to compensate for the high variability of the PV in between IVVC solves. Special attention will have to be placed in the future when integrating advanced inverters into central IVVC control strategies. The extreme reliance on advanced inverters versus legacy voltage regulation equipment on high variable PV irradiance days could cause voltage violations. Including the PV forecast in the IVVC algorithm, configuring the DMS to trigger an IVVC resolve as PV changes, and/or solving the centralized strategy faster than the 10 minutes modeled in this case represents promising directions for further work to address these voltage violations.

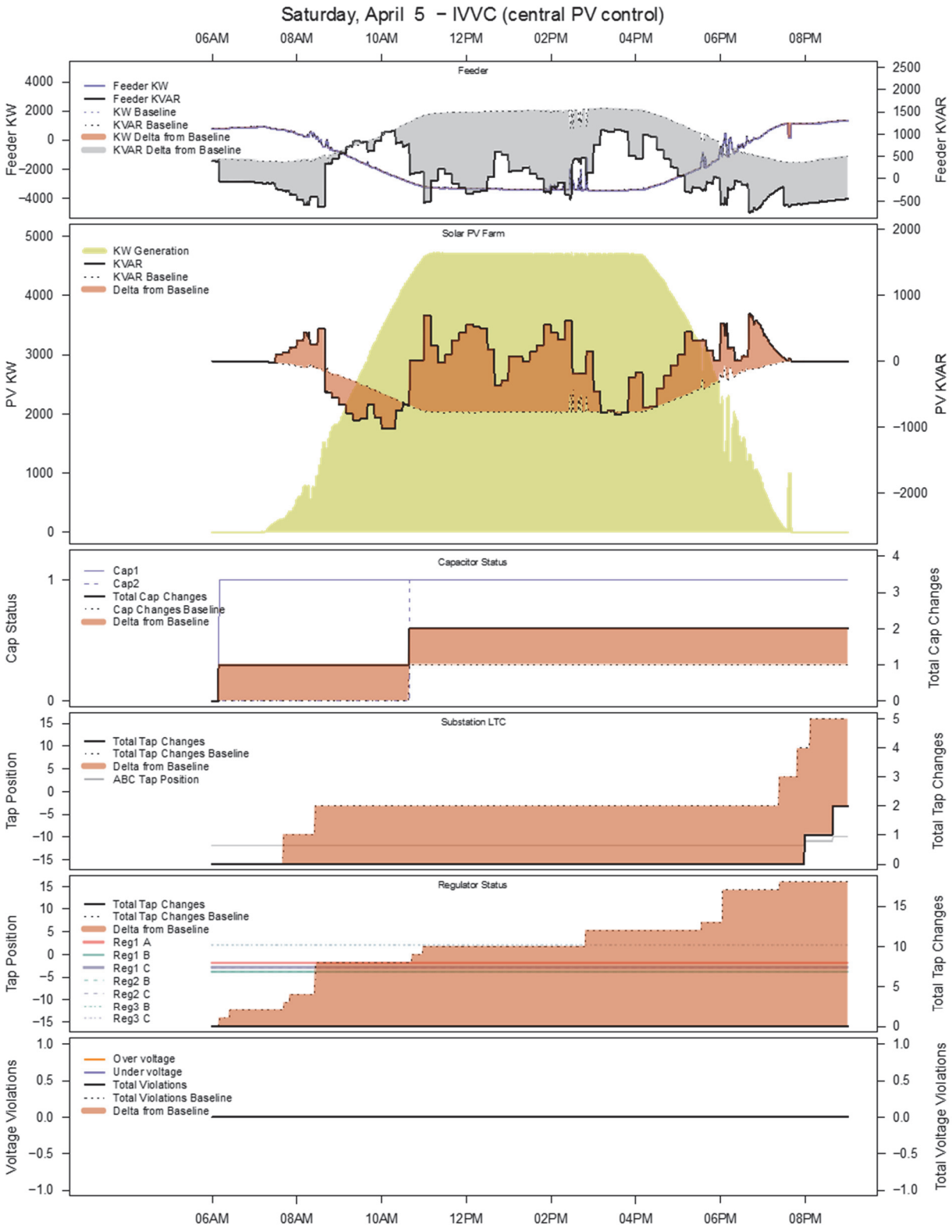


**Figure 47. April 5 IVVC time-series comparison to baseline for IVVC (Central PV Control)**

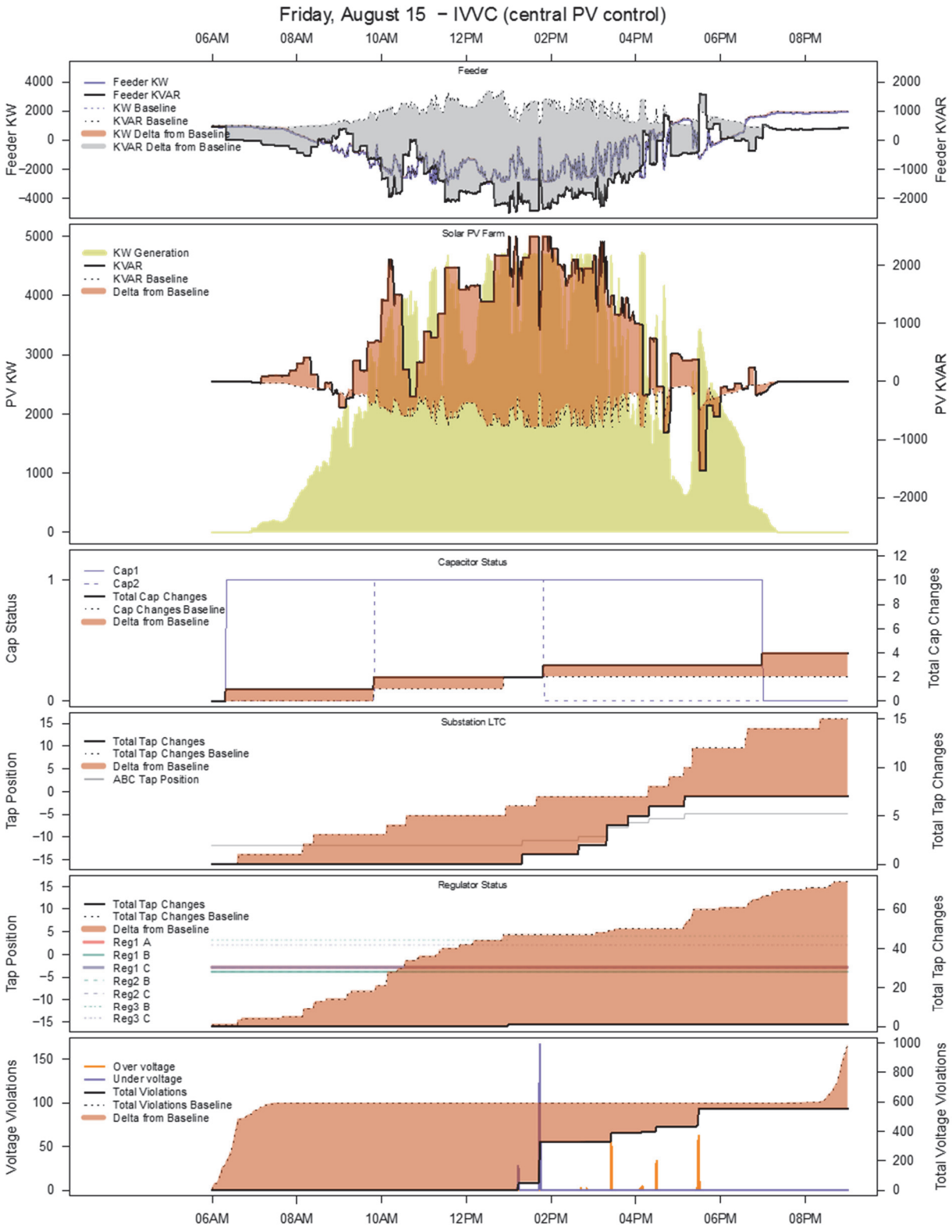


**Figure 48. August 15 IVVC time-series comparison to baseline IVVC (Central PV Control)**

## 6.6 Additional Sensitivity Analysis

For the sensitivity analyses, we considered two alternate cases:

1. Other power factors for Local PV Control modes
2. Additional utility-scale DGPV by adding an additional 5-MW DGPV site at the end of the three-phase feeder trunk

The alternate power factors are compared to the same baseline results used for the 40-day analysis. For the additional utility-scale DGPV sensitivity, a new baseline was first established using the same control settings for voltage regulation equipment. The additional DGPV was then simulated with the two local PV control modes used with the single plant—constant 0.95 absorbing (inductive) power factor and Volt/VAR—and using the Legacy IVVC (exclude PV) strategy.

### *6.6.1 Local Constant Power Factor Control Sensitivity Analysis*

In this section, the two days that were discussed in detail in the previous section were run with different power factor settings at the PV plant inverter. Simulations were run with a power factor of 0.9 and 0.8 absorbing (inductive), at the PV plant inverter to see the effect of increasing the reactive power support at that point. Note that real power from the PV inverter is curtailed to provide the reactive power support as explained in subsection 3.2.1.1. This curtailment was minimal in the 0.95 power factor cases, but becomes more apparent with these more aggressive power factors.

As shown in Figure 49, the additional reactive power absorbed at a power factor of 0.9 did not substantially affect the substation LTC operations on April 5 and August 15. However, on both days the total number of line regulator operations slightly increased. Figure 50 shows how the same trend is observed when the reactive power support from the PV plant was increased even further, to a power factor of 0.8 absorbing (inductive). Here the substation LTC total number of operations was reduced in the variable PV day (August 15$^{th}$), with the drawback of increased line regulator operations. In general, these alternate power factors performed worse than the Local PV Control (PF=0.95) case.

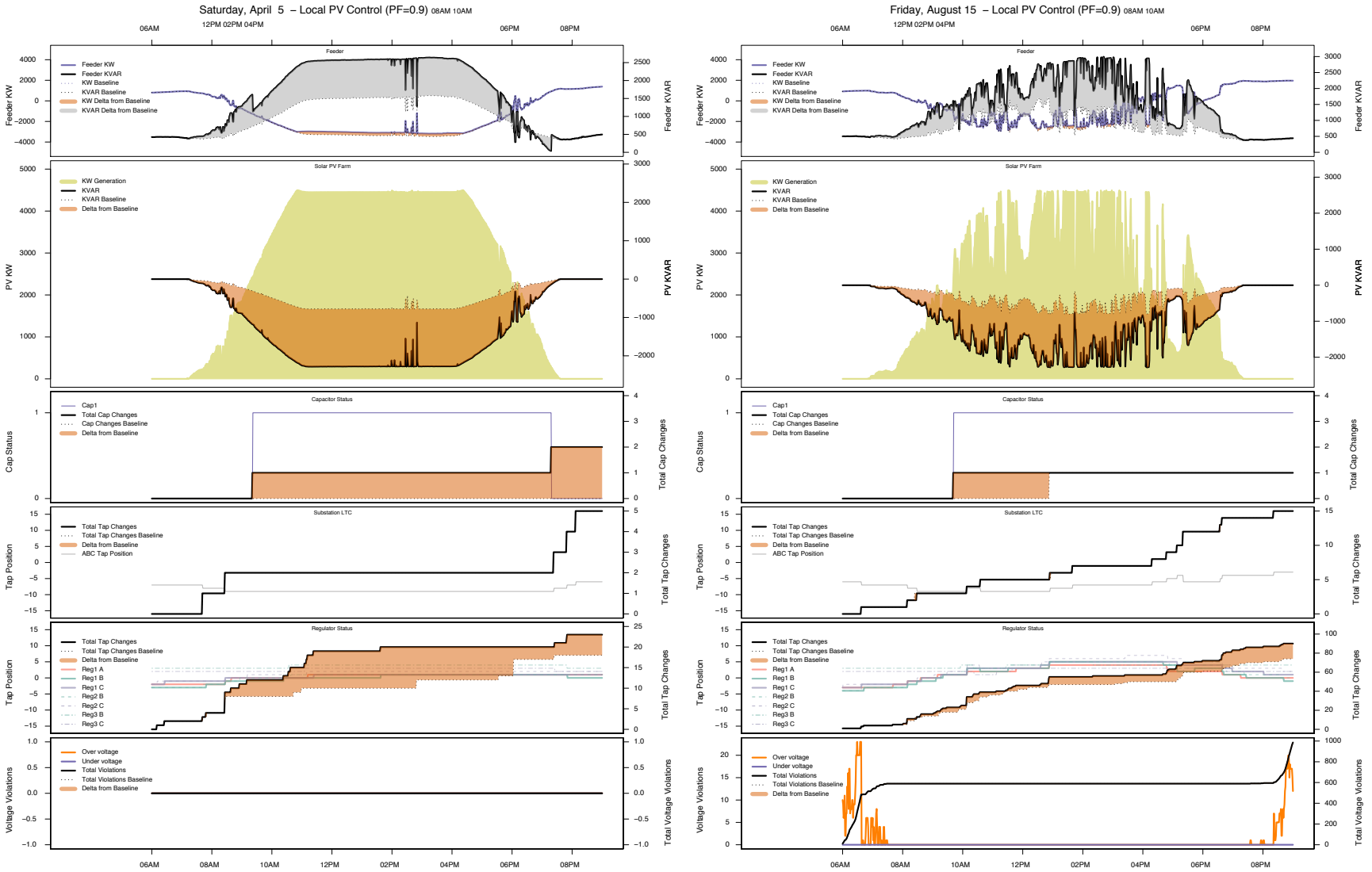


**Figure 49. April 5 and August 15 time-series comparison to baseline with a constant power factor of 0.9 absorbing (inductive)**

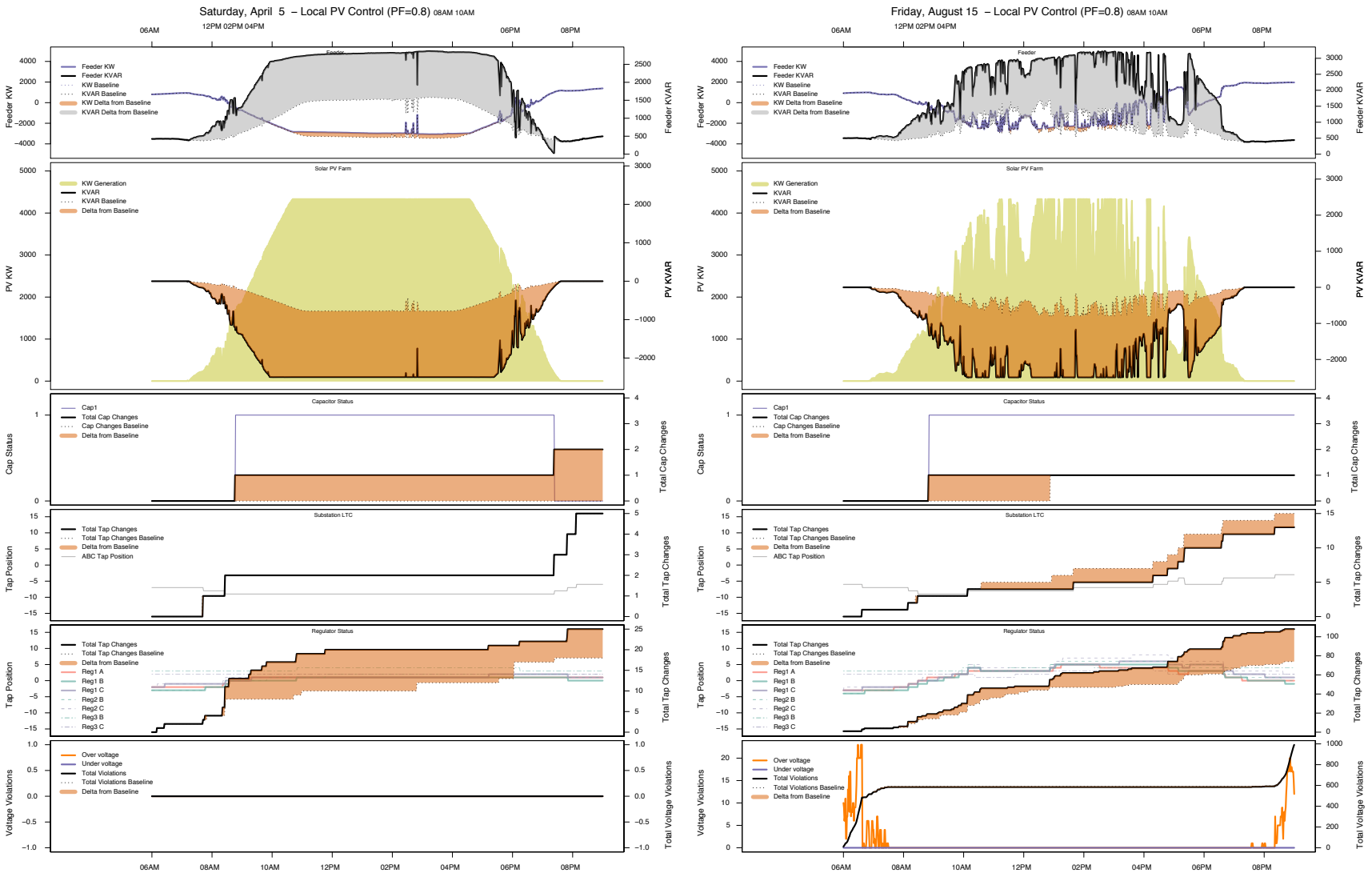


**Figure 50. April 5 and August 15 time-series comparison to baseline with a constant power factor of 0.8 absorbing (inductive)**

### 6.6.2 Additional Central Solar

For this sensitivity scenario, the same measured PV data for 2014 from the existing 5-MW PV plant was used to model a second large PV plant approximately 5.7 miles away from the substation near the end of the three-phase portion of the feeder (dark blue), as shown in Figure 51.

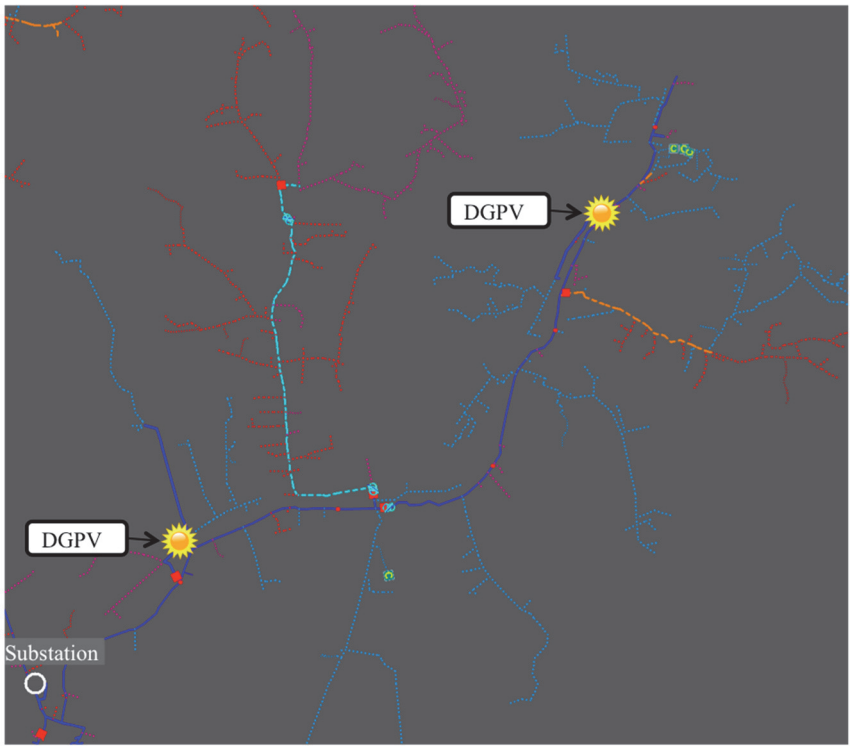


**Figure 51. Feeder layout showing the location of the two central PV plants**

#### 6.6.2.1 New Baseline Scenario with Additional 5MW Solar Farm

In the new baseline, the second PV plant caused overvoltage load violations, and increased the operations of the substation LTC and line regulators. Both PV plants were operating at close to unity power factor (matched to historic measured data), and as such they were not providing any form of voltage support.

The results for April 5 (clear-sky day) are shown in Figure 52. The total number of regulator operations slightly increased compared to the original single PV baseline, and load overvoltage violations remain after 11 a.m. throughout the PV production hours.

For August 15, the two PV plants more dramatically affected the total number of operations of the substation LTC and line regulators, and they also caused a few overvoltages throughout the day; see Figure 53.

#### 6.6.2.2 Local Control Modes with Additional 5MW Solar Farm

The results for the local control with constant power factor of 0.95 absorbing (inductive) used on both PV systems for April 5 and August 15 are shown in Figure 54 and Figure 55, respectively. Here, unlike in the single PV close to the substation baseline, the lower power factor provides

considerable operations improvements. The load overvoltage violations that were caused by the second PV plant were mitigated, and the total number of voltage regulation equipment operations was almost unaffected when compared to that of the new baseline. These results show that the second PV plant in Local PV control (PF=0.95) mode was able to mitigate the overvoltages that it caused in the baseline.

The results for local volt/VAR modes for April 5 and August 15 are shown in Figure 56 and Figure 57, respectively. The results showed a small further improvement over the new baseline compared to those with the fixed absorbing (inductive) power factor mode. On the highly variable PV on August 15, the total number of operations of the substation LTC and line regulators was improved when compared to that of both the constant power factor and new baseline scenarios. By providing Volt/VAR control, the two large PV plants largely mitigated the load overvoltage violations observed in the new baseline scenario.

#### *6.6.2.3 IVVC with Additional 5MW Solar Farm and Legacy Inverter Controls*

Finally, the new baseline with two 5-MW PV plants and existing controls on voltage regulation equipment was compared to having the voltage management strategy controlled by the central IVVC algorithm.

As in the previous results deploying the centralized control methods, IVVC eliminated the voltage violations of the new baseline scenario and dramatically reduced the total number of operations of the LTC and line regulators. The results for April 5 are shown in Figure 58, wherein there were no load voltage violations and very few tap changes for the regulators and the capacitor switching on during non-PV production hours. For August 15, the IVVC regulated voltage mainly with the substation LTC and the capacitor that responded to the highly variable PV resource in the afternoon, as shown in Figure 59. Again, the three line regulators Reg1 were fixed to small negative taps by IVVC.

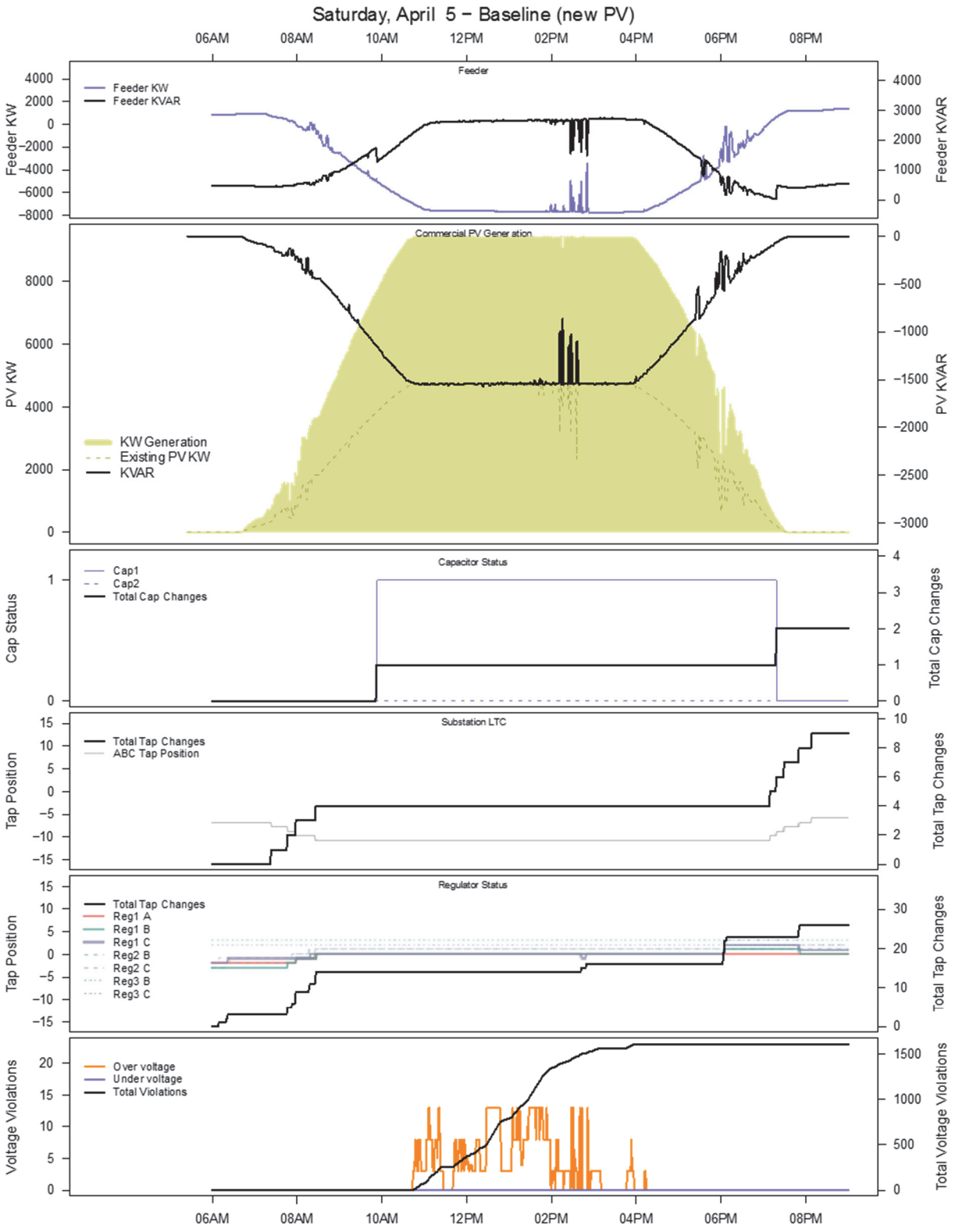


**Figure 52. April 5 time-series comparison of the new baseline with two 5-MW PV plants to the baseline with only the existing PV plant**

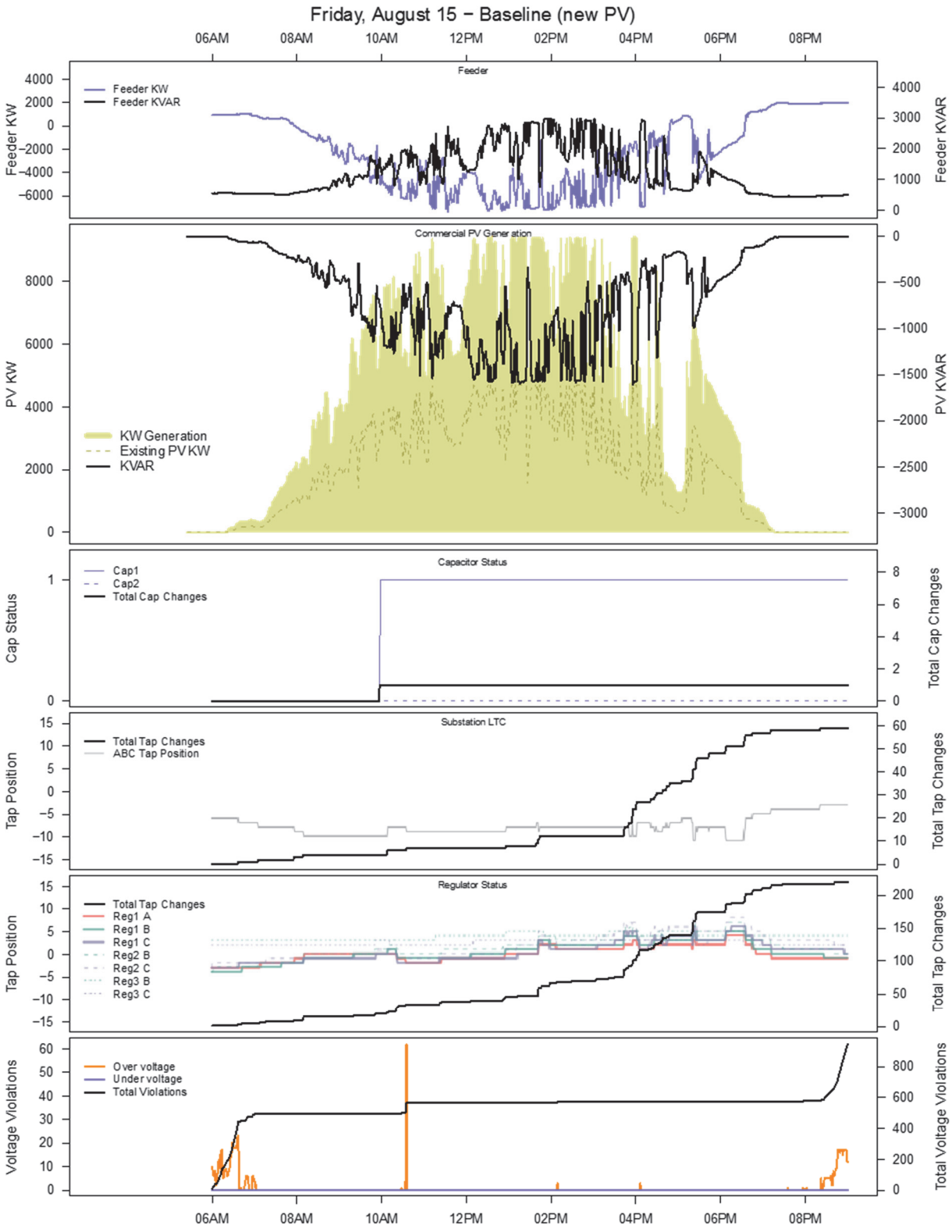


**Figure 53. August 15 time-series comparison of the new baseline with two 5-MW PV plants to the baseline with only the existing PV plant**

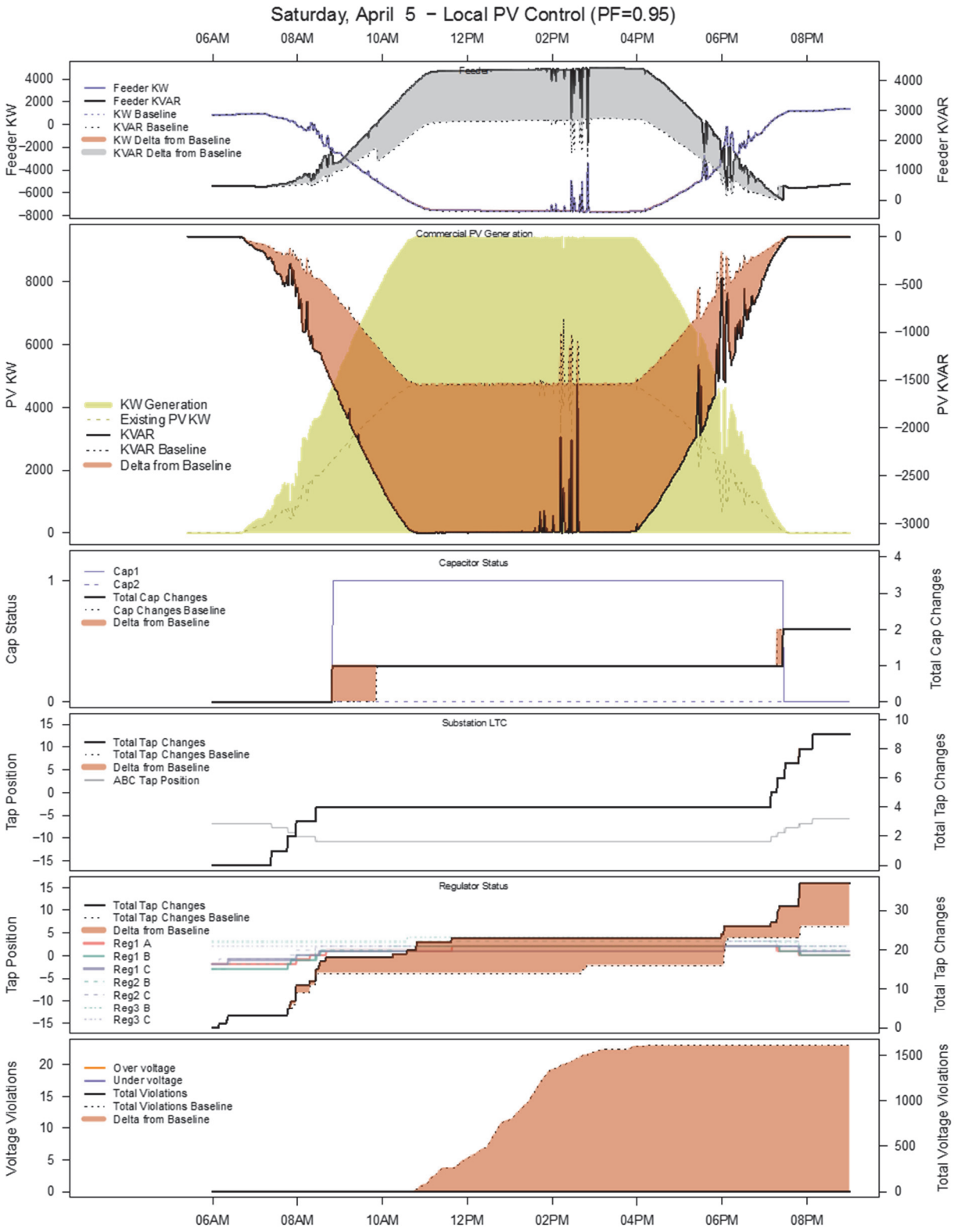


**Figure 54. April 5 time-series comparison of the new baseline with two PV plants operating at a power factor of 0.95 absorbing (inductive), to the baseline with only the existing PV plant**

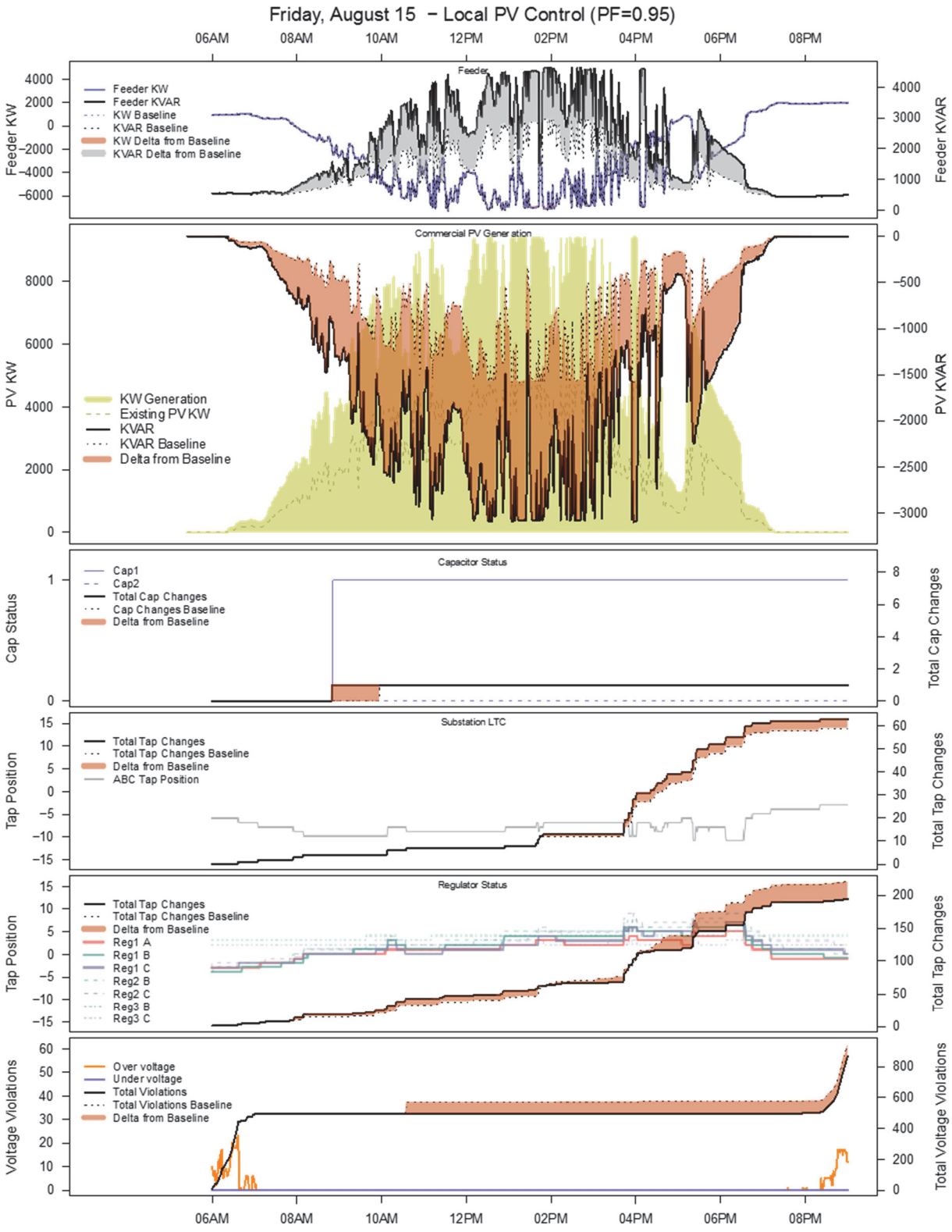


**Figure 55. August 15 time-series comparison of the new baseline with two PV plants operating at a power factor of 0.95 absorbing (inductive), to the baseline with only the existing PV plant**

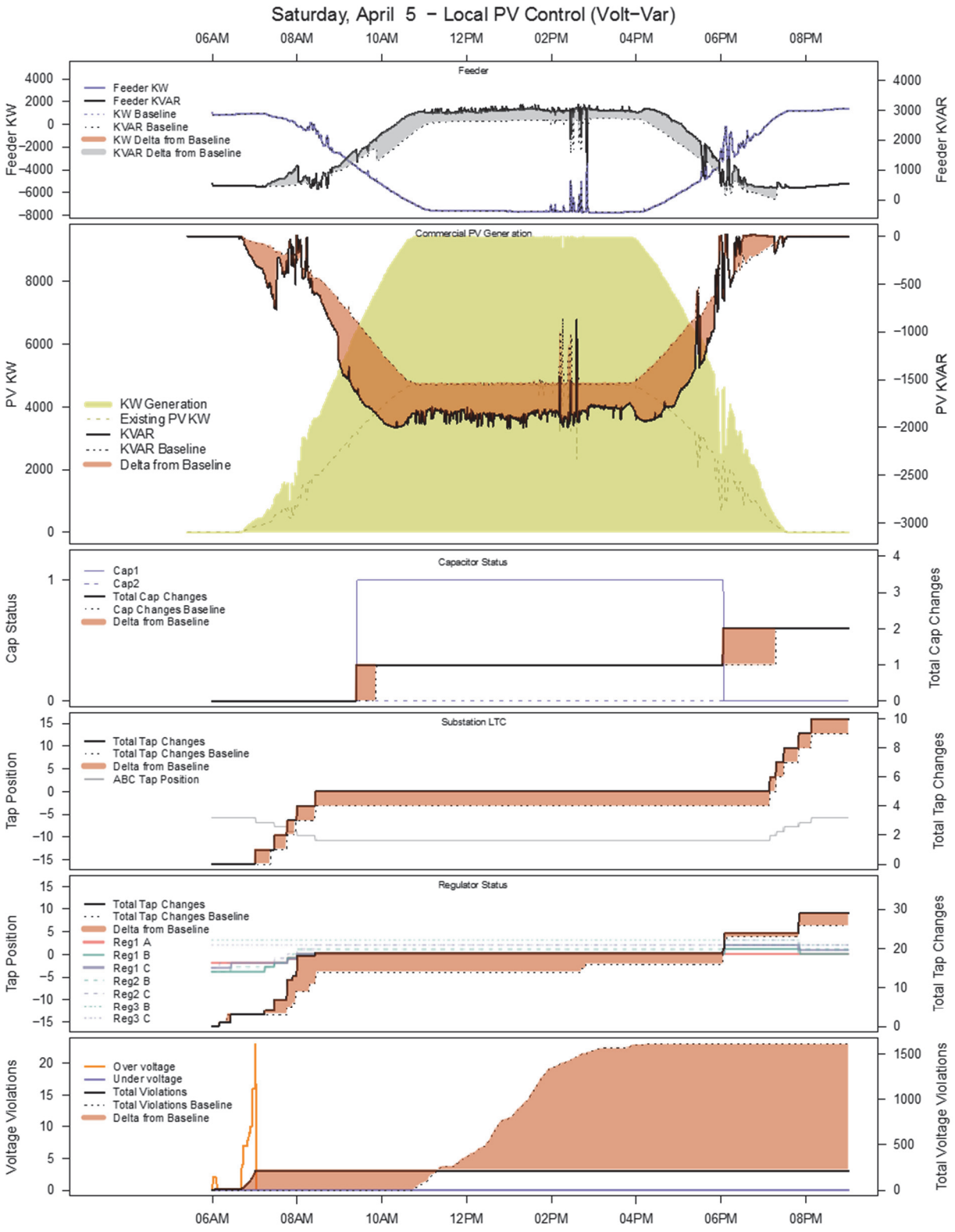


**Figure 56. April 5 time-series comparison of the new baseline with two 5-MW PV plants operating in local volt/VAR to the baseline with only the existing PV plant**

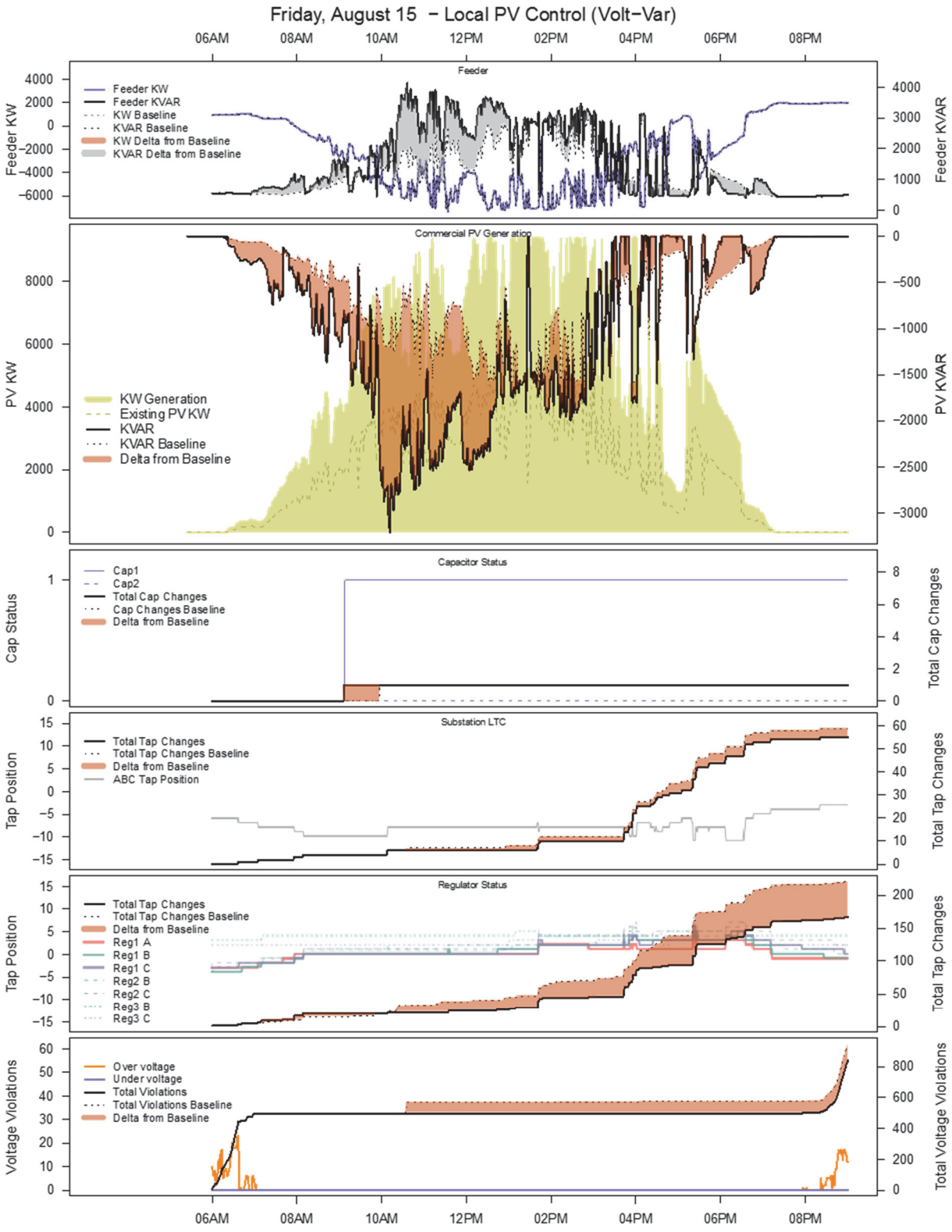


**Figure 57. August 15 time-series comparison of the new baseline with two 5-MW PV plants operating in local volt/VAR to the baseline with only the existing PV plant**

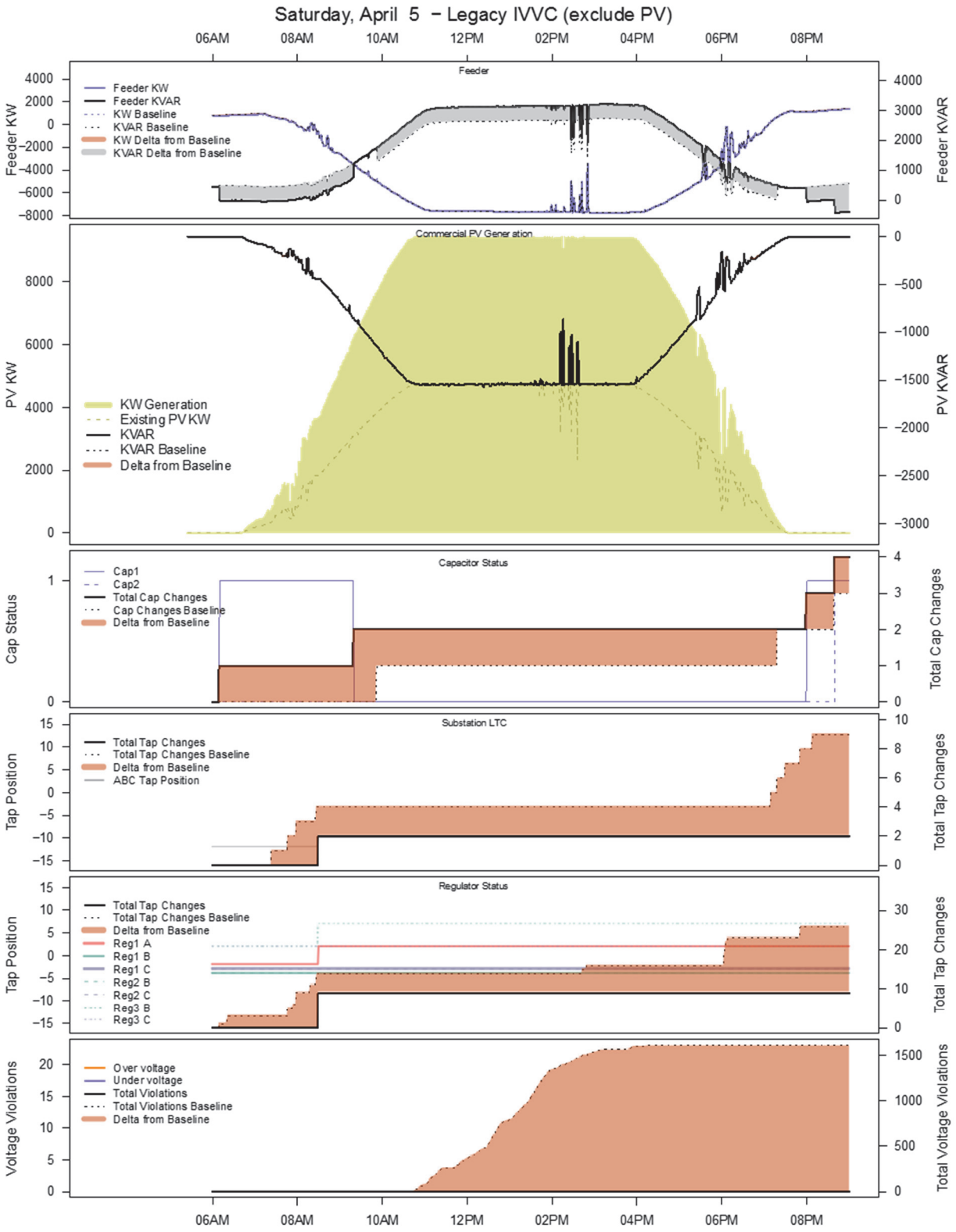


**Figure 58. April 5 time-series comparison of the new baseline with IVVC algorithm not controlling the two PV plants to the baseline with only the existing PV plant**

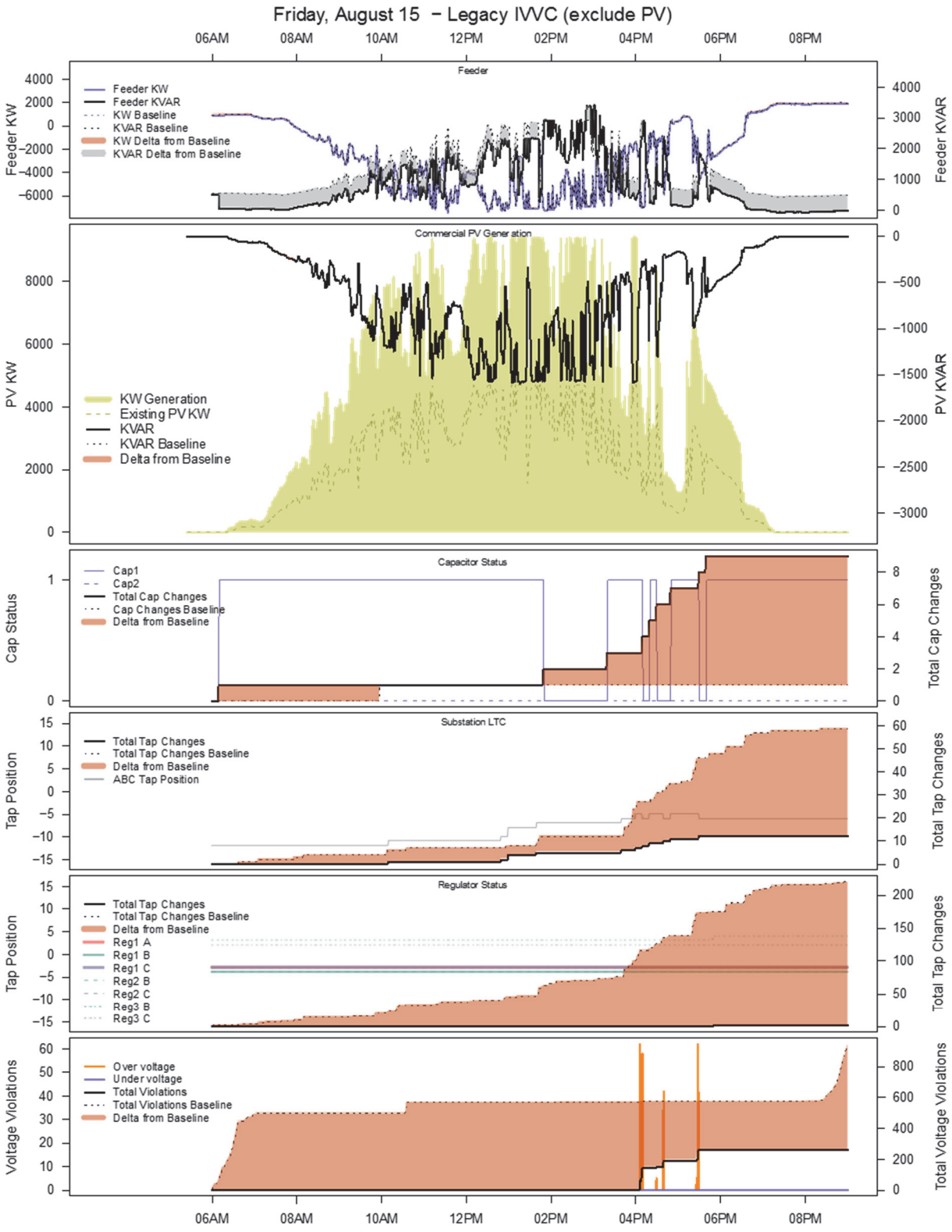


**Figure 59. August 15 time-series comparison of the new baseline with IVVC not controlling the two PV plants to the baseline with only the existing PV plant**

## 6.7 Cost-Benefit Alternative Analysis Results

### 6.7.1 Results Summary: Scenario NPVs at Decade Planning Horizons

Figure 60 summarizes the cumulative NPVs for the scenarios.

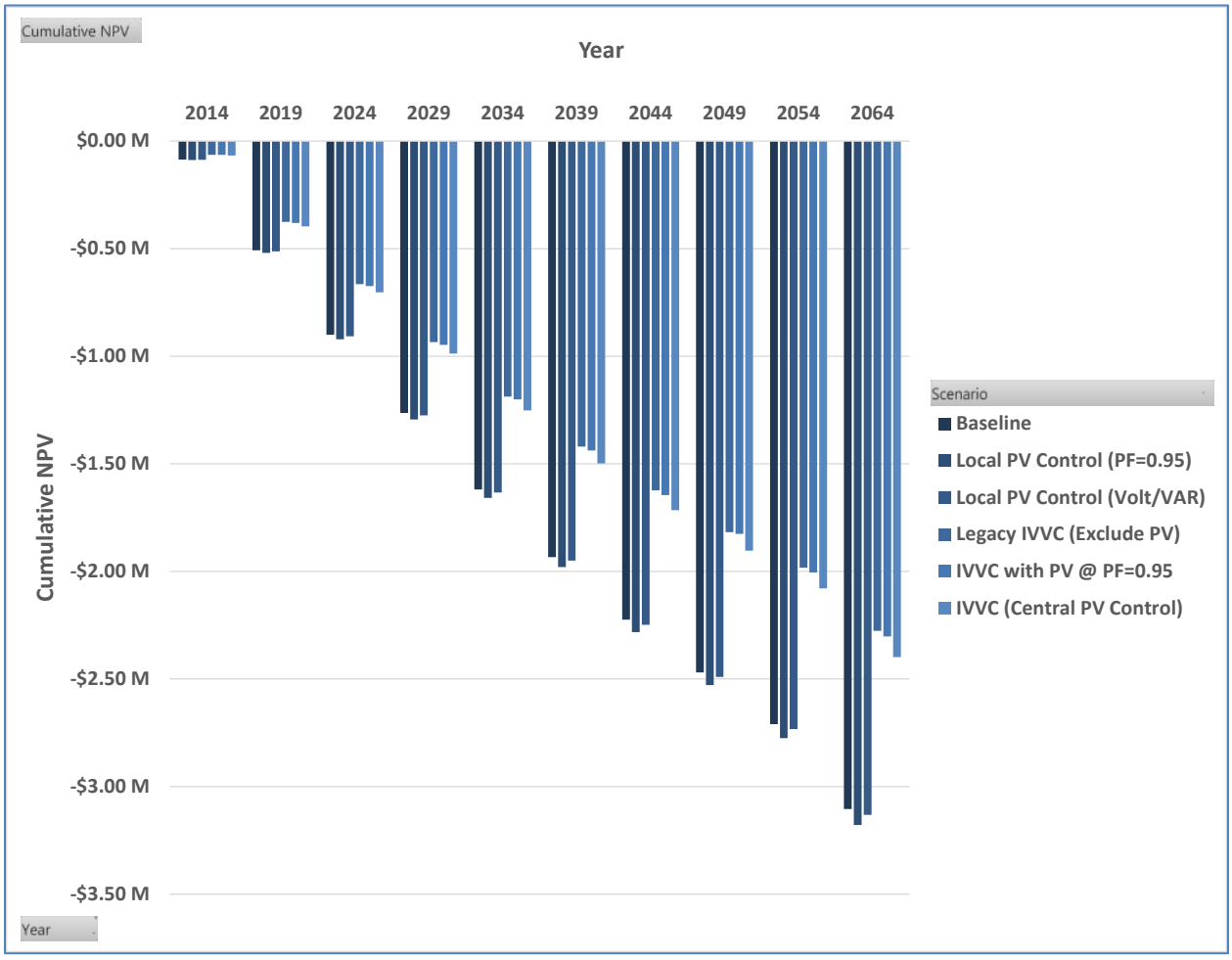


**Figure 60. Cumulative NPVs (without DMS, communication, or PV costs) comparing planning horizons in 5yr increments across all scenarios**

The IVVC scenarios consistently had the lowest total costs/highest NPVs. Legacy IVVC (Exclude PV) was the lowest cost/highest savings, with a higher NPV than the other IVVC scenarios. The Baseline, Local PV Control (PF=0.95), and Local PV Control (Volt/VAR) scenarios were consistently the most costly/lowest NPV scenarios. As described above, the specific technical performance for the IVVC optimization can be tuned by varying the "weights" for different classes of equipment operation. Such changes could impact the relative costs within the IVVC group of scenarios.

Note that this analysis does not include costs associated with DMS investments, additional communications to controllable resources, PV costs, or revenues from customer loads.

### 6.7.2 Scenario Value Analysis

Figure 61 shows the breakdown of categorical costs and benefits of each scenario's NPV.

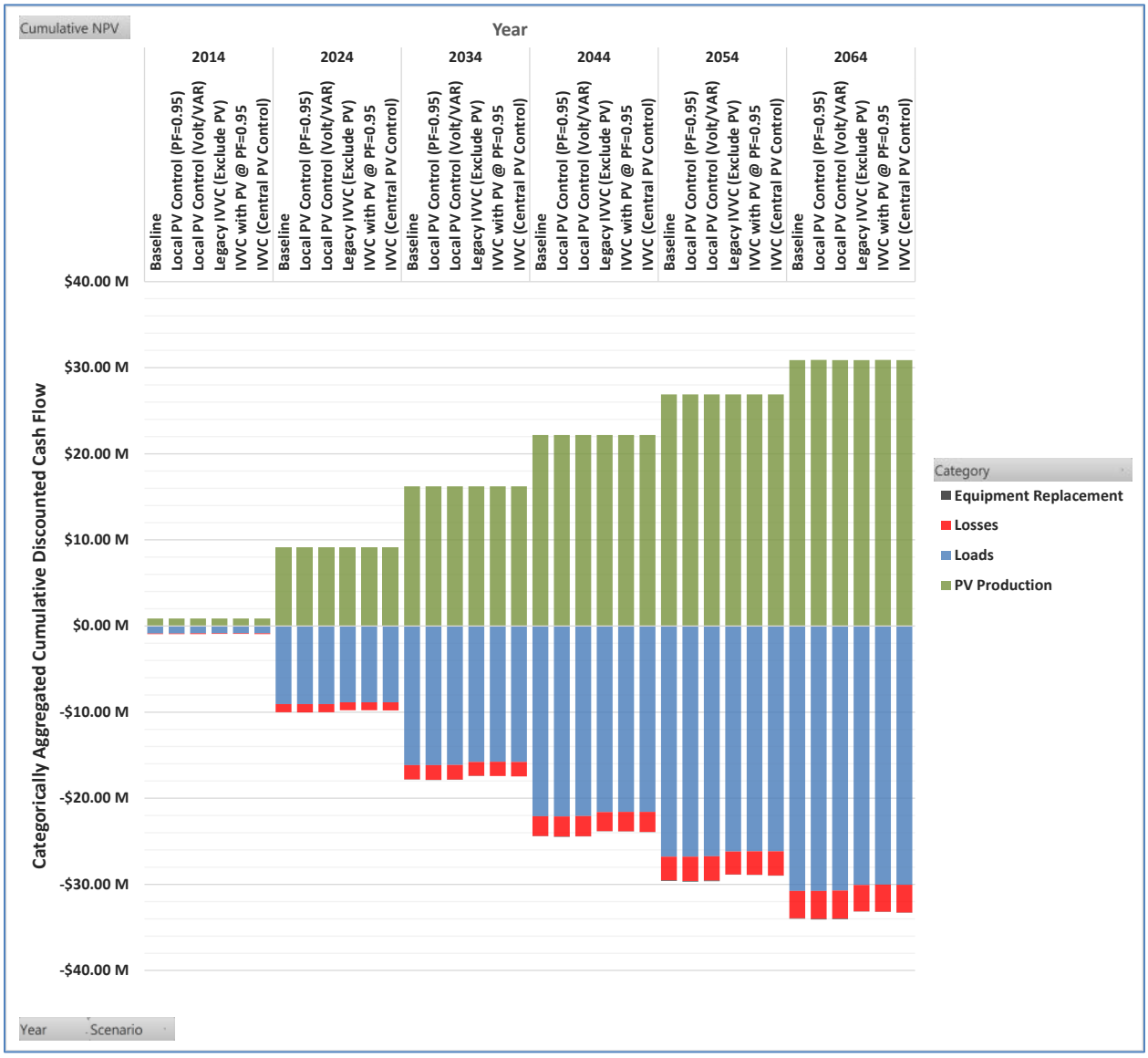


**Figure 61. Categorical cumulative discounted cash flows**

The green bars show the cumulative discounted values of PV production, which represent a cost savings to Duke Energy due to the need to purchase less electricity from traditional generation. Contracted payments for the third-party-owned PV energy are not included in this analysis.

Because the impact of the various control modes on real power production is minimal, these costs are effectively the same across all scenarios.[22]

The blue bars show the cumulative discounted costs of load, corresponding to the energy Duke Energy's distribution operations has to procure from the bulk system to serve load. These values were consistently lower in the scenarios that use IVVC, because IVVC was configured to minimize demand through CVR.

Costs of losses and of equipment replacement are represented in red and dark gray, respectively, but the equipment replacement costs are comparatively small and are difficult to discern (this is addressed in Figure 63).

It is useful to see not only the comparative values of components of scenario costs and savings, but also to see an indication of the differences in their values across scenarios. Figure 62 shows the differences between each alternative scenario components' costs and savings values and those of the Baseline scenario.

Figure 62 shows that the Legacy IVVC (Exclude PV) scenario is the most different from Baseline in terms of cumulative DCFs through all planning horizons Legacy IVVC consistently has the highest NPV because it results in the greatest reduction in feeder losses while maintaining the considerable CVR load reduction found in all IVVC scenarios.

Costs of losses (red bars) and of equipment replacement (gray bars) were both much smaller than the energy-based costs and savings, so they are extracted and enlarged for easier comparison in Figure 63. This figure shows how IVVC, as configured, also slightly reduces the feeder-wide losses relative to the local control modes, and how the use of inverter reactive power to help manage voltage—in the two Local PV control modes, IVVC with PV @ PF=0.95, and IVVC (Central PV Control)—slightly increases losses.

Figure 63 shows that the costs of equipment replacement (gray bars) are significantly smaller still than the costs of feeder losses. Figure 64 further enlarges the equipment replacement costs, and breaks them down by specific device. Here, inter-scenario cost differences largely result from reductions in equipment operations in the group of IVVC scenarios.

[22] As seen in the sensitivity analysis, more aggressive (lower) fixed power factors could result in more noticeable impacts if real power production must be more deeply curtailed to provide required reactive power while remaining within the apparent power (kVA) limit of the inverter.

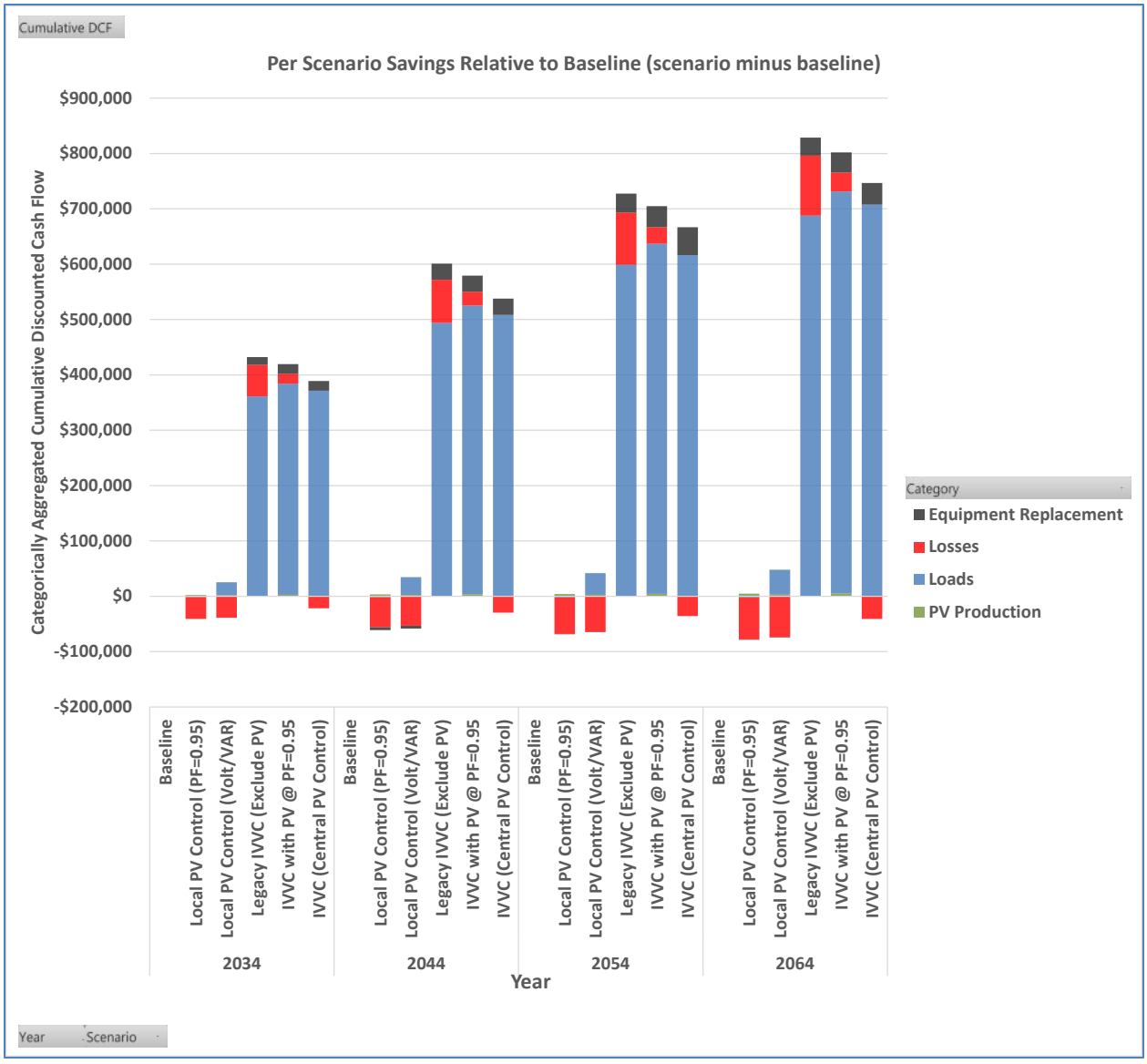


**Figure 62. Categorical cost and savings differences from those of Baseline**

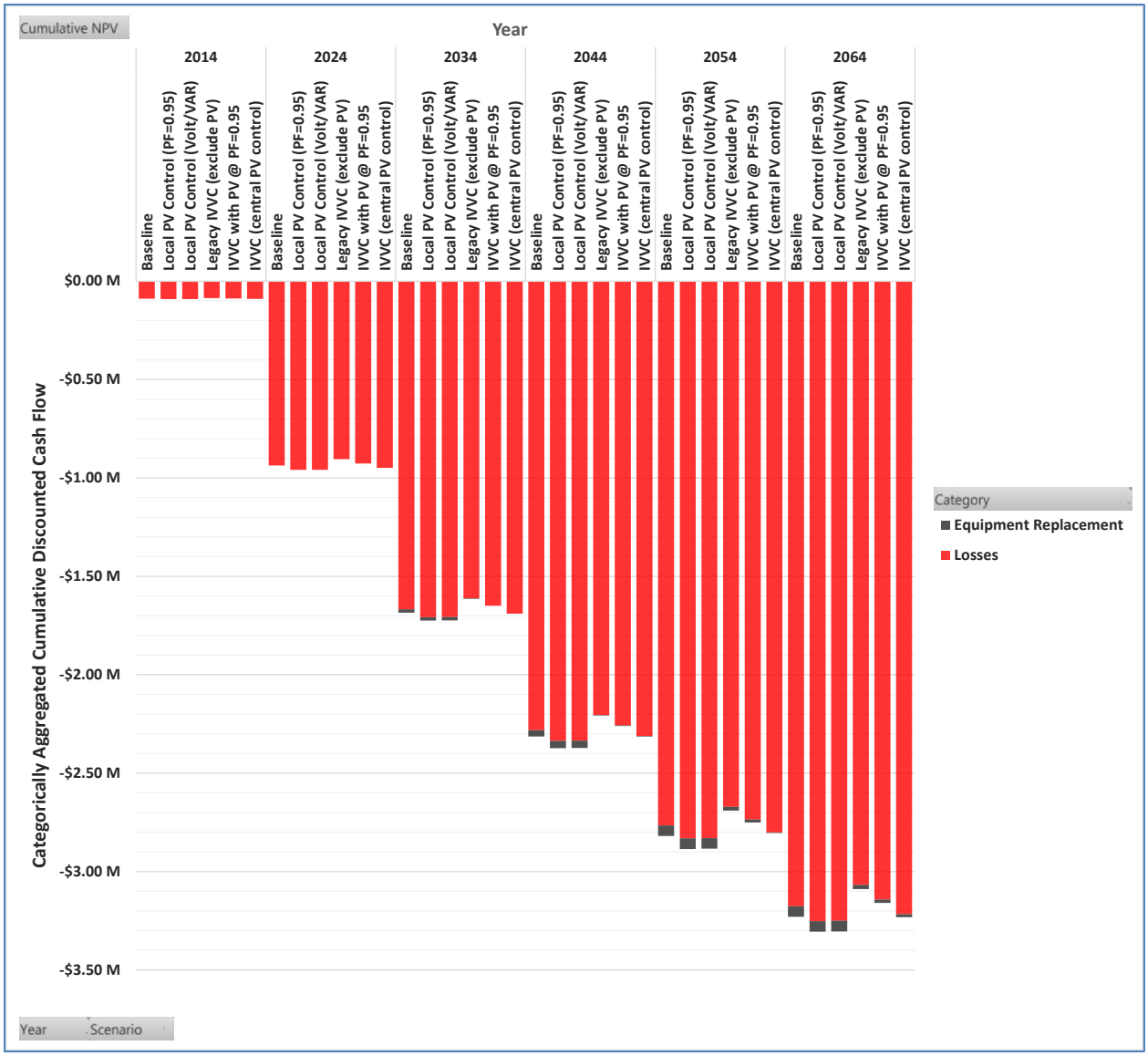


**Figure 63. Categorically aggregated cumulative discounted cash flows for costs of feeder losses and equipment replacement**

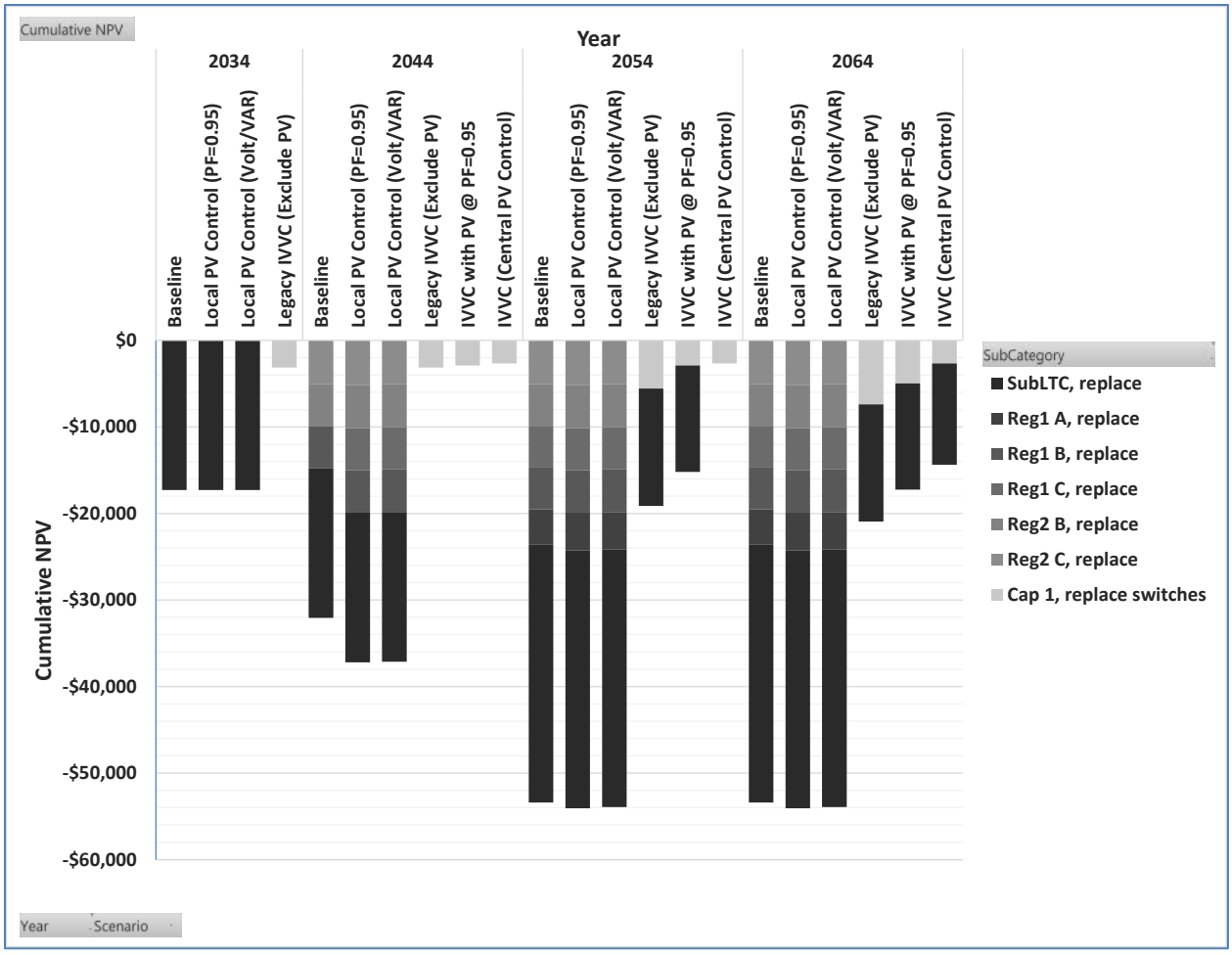


**Figure 64. Aggregated cumulative discounted cash flows for equipment replacement broken down by type of equipment**

Regulator replacements are the most significant equipment replacement cost, even though regulator replacements are not required in any scenario until just prior to analysis year 20. In the IVVC (Central PV Control) scenario, regulator replacements were altogether avoided through the full 50-year planning horizon. The trade-off was that capacitor switching frequency and resulting capacitor switch replacement increased considerably in all the IVVC scenarios. Still, the cumulative discounted costs of capacitor switch replacements were an order of magnitude lower than those of regulator replacements in the other scenarios. The lower cumulative costs of capacitor switch replacements was due to a combination of lower capital costs for capacitor switches (than for regulators) and the fact that the IVVC managed use of capacitors largely replaced the use of four groups of regulators.

### *6.7.3 Cost Benefit Discussion*

The differences in NPV as shown among scenarios in Figure 60 are driven predominantly by differences in load energy, less significantly by differences in losses, and least, but still significantly, by differences in equipment replacement frequency and type. Even though equipment replacement cost differences are small by comparison to energy cost differences, they

still amount to thousands of dollars per year for a single feeder (see Figure 64), which would scale to millions of dollars per year across thousands of feeders throughout a service territory.

### 6.7.4 Simulated Voltage Regulation Equipment Replacement Schedules

Table 9 shows the ordinal planning years in which, as a result of the number of switching operations determined for each simulated equipment item, each equipment item is expected to require replacement in each scenario. Reg3 B and Reg3 C are not shown because, due to their small number of simulated operations, they were not expected to need replacement in any of the 50 planning years in any of the scenarios.

**Table 9. CBA analysis years in which equipment replacements occur**

| Scenario | SubLT C | Reg1 A | Reg1 B | Reg1 C | Reg2 B | Reg2 C | Cap 1 |
|---|---|---|---|---|---|---|---|
| Baseline | 19, 39 | 40 | 30 | 31 | 29 | 27 | |
| Local PV Control (PF=0.95) | 19, 39 | 36 | 29 | 29 | 28 | 26 | |
| Local PV Control (Volt/VAR) | 19, 39 | 37 | 28 | 30 | 28 | 27 | |
| Legacy IVVC (Exclude PV) | 34 | | | | | | 16, 32, 48 |
| IVVC with PV (PF=0.95) | 40 | | | | | | 21, 42 |
| IVVC (Central PV Control) | 43 | | | | | | 25 |

### 6.7.5 Cost-Benefit Analysis Assumptions

A number of simplifying assumptions were made in this study. The contracted cost for the third-party-owned PV was not included, nor was PV degradation. The results do, however, include inflation in cost of energy. Also note that the apparently large increases in magnitudes of metrics from one decade to another are due to the cumulative nature of the DCFs. For example, the 2024 cumulative DCFs are summations of all prior year DCFs.

Further study would be needed to validate these findings with models that account for the utility's financing and accounting practices and additional costs that may vary among scenarios, including:

- Capitalization (with depreciation and normalization) of asset replacements accounting for income tax rates and any tax incentives

- Property tax and depreciation for property tax purposes
- Tax treatment of expenses
- More realistic energy cost inflation assumptions
- Incorporation of the capital cost or cost of power from (third-party ownership of) the PV, PV production degradation, inverter replacement, and more realistic life-of-asset estimation for the PV (probably around 30 years)
- Incorporation of differing costs of control approaches among scenarios (volt/VAR compared to the IVVC approaches, etc.).

CBAAT has the capabilities to account for these factors with configuration changes or minor modifications.

## 6.8 Substation-Level Impacts

Advanced inverter modes often use reactive power to help manage voltage. This can cause changes to the overall feeder's reactive-power demand—potentially requiring sourcing more reactive power from the transmission system if reactive power sources (typically capacitors) from the substation or neighboring feeders are insufficient to meet the increased demand.

### *6.8.1 Feeder Head Real-Reactive Power Relations*

Figure 65 compares the feeder head P/Q plots for our six core 40-day scenarios. These figures plot the relationship between real power (P, on the horizontal axis) and reactive power (Q, on the vertical axis). Each colored point corresponds to a single 1-minute period from the simulation. The color gradient encodes the level of PV real power output. This coloring reveals how, not surprisingly, negative net real power demand corresponds to higher PV production. It also shows a trend—for all but the IVVC (Central PV Control) scenario—toward higher reactive power demand during sunnier periods due to both increased reactive power draw by the solar power plant and, likely, also to increased inductive demands (motors) during the daylight.

The shape and position of the colored areas reveals patterns of P-Q interactions such as the strongly diagonal patterns with constant power factor compared to a more diverse pattern with volt/VAR. The most dramatic pattern comes from the IVVC control with PV as an eligible device. In this case, LVM opts to actively manage the PV reactive power including sometimes injecting —rather than more commonly absorbing to manage voltage rise—high levels of reactive power, causing many periods of net reactive power injection at the feeder head.

These 40-day plots have so many points that it is challenging to determine operating areas of high density compared to moderate density. For this reason, thick black contour lines were overlaid to highlight the most common P-Q operating regions. In many scenarios (e.g., constant power factor, IVVC, IVVC with PV at a power factor of 0.95), the contours helped reveal two separate operating regions—shown as closed circles—during high PV production (and hence strongly negative net real power). These correspond to high-output PV operations with and without the switched capacitor enabled. For the three IVVC modes, there are groups of three common operating regions; these correspond to using zero, one, or two capacitors.

Overall these figures reveal an increase in reactive-power demand (more positive Q); however, this increase was often less so than the additional reactive power absorbed by the PV plant for voltage management because the switched capacitor was enabled more often than it was in the baseline to help provide additional locally sourced reactive power.

### 6.8.2 Thinking Beyond Power Factors

In addition, these figures show radial lines of constant power factor. The highly nonlinear nature of power factor is demonstrated by the nearly equal angles among the power factors of 0.99, 0.95, 0.9, and 0.7. These plots show how at the feeder head there were many periods of low power factors that may be outside the range of generally accepted demand power factor at the transmission bus. However, these power factor guidelines were designed assuming one-way power flow and correspondingly higher net demands. As shown in the figures, the very low power factors, including periods of pure reactive demand (PF=0), did not actually require any more (and may require less) reactive power from the transmission system than other periods with much higher power factors. This suggests a possible need to think beyond traditional power factor standards for transmission-distribution boundaries with high penetrations of distributed generation. It could be that specifying limits on reactive power may be more appropriate

### 6.8.3 Real-Reactive Relationships with Additional 5 MW of PV

Figure 67 shows similar 2-day plots for the set of sensitivity scenarios with an additional 5-MW solar power plant located at the end of the three-phase trunk of the feeder. Not surprisingly, these reveal an increase in reactive power demand for all scenarios because even in the baseline each PV plant absorbed considerable VARs at its average power factor of 0.99. It further shows how operating both PV plants with a power factor of 0.95 requires a substantial increase in feeder head reactive power demand, whereas volt/VAR and IVVC had reactive power demands similar to the baseline despite their improved feeder voltage management. This suggests that volt/VAR and IVVC may be preferable from the perspective of the bulk system operator for this case due to less dramatic reactive power requirements.

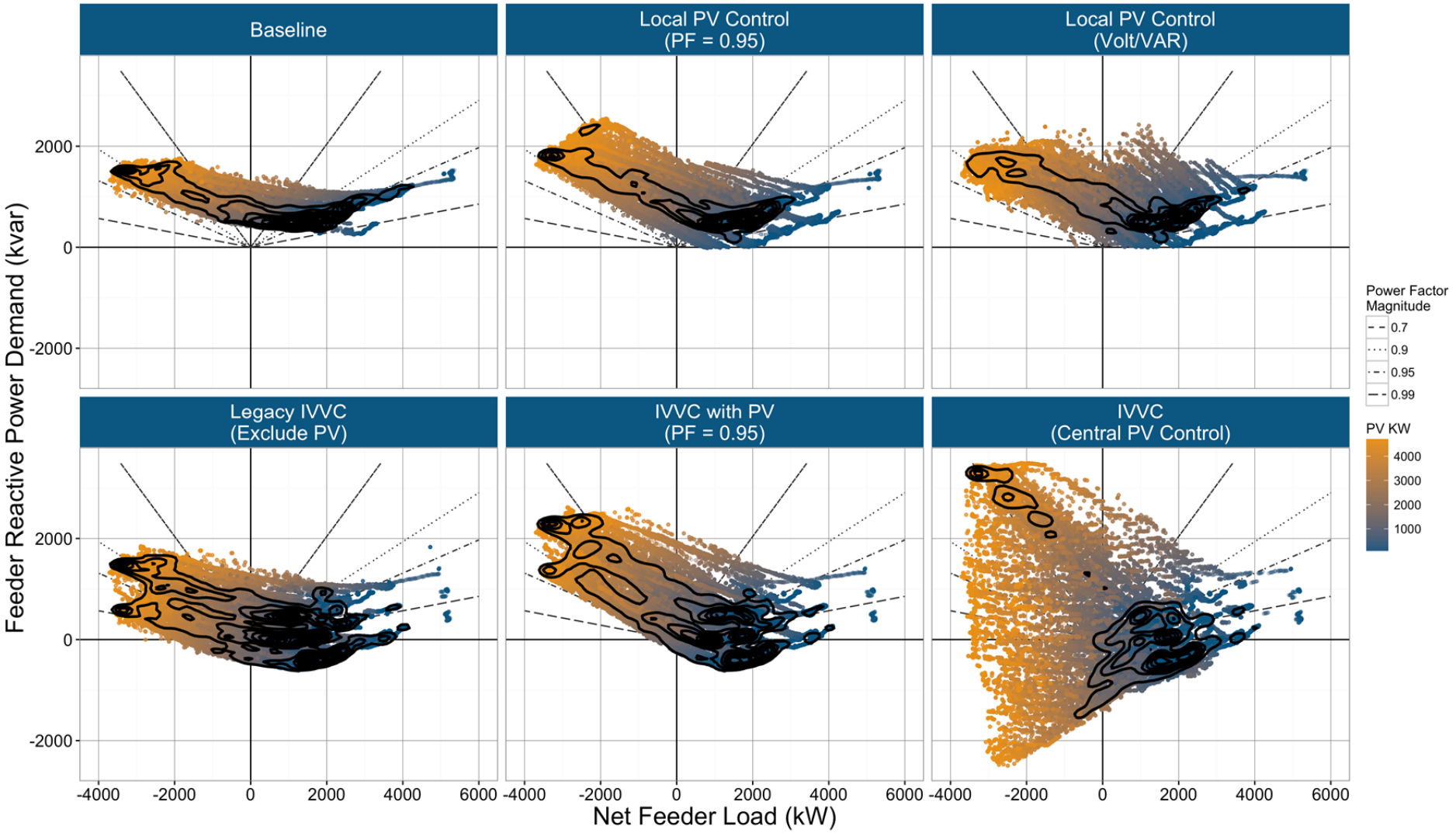


**Figure 65. Simulated feeder-head P/Q plots showing the impacts of advanced inverter mode on the real (horizontal axis) and reactive (vertical axis) power flows at the substation with the existing 5-MW solar power plant**

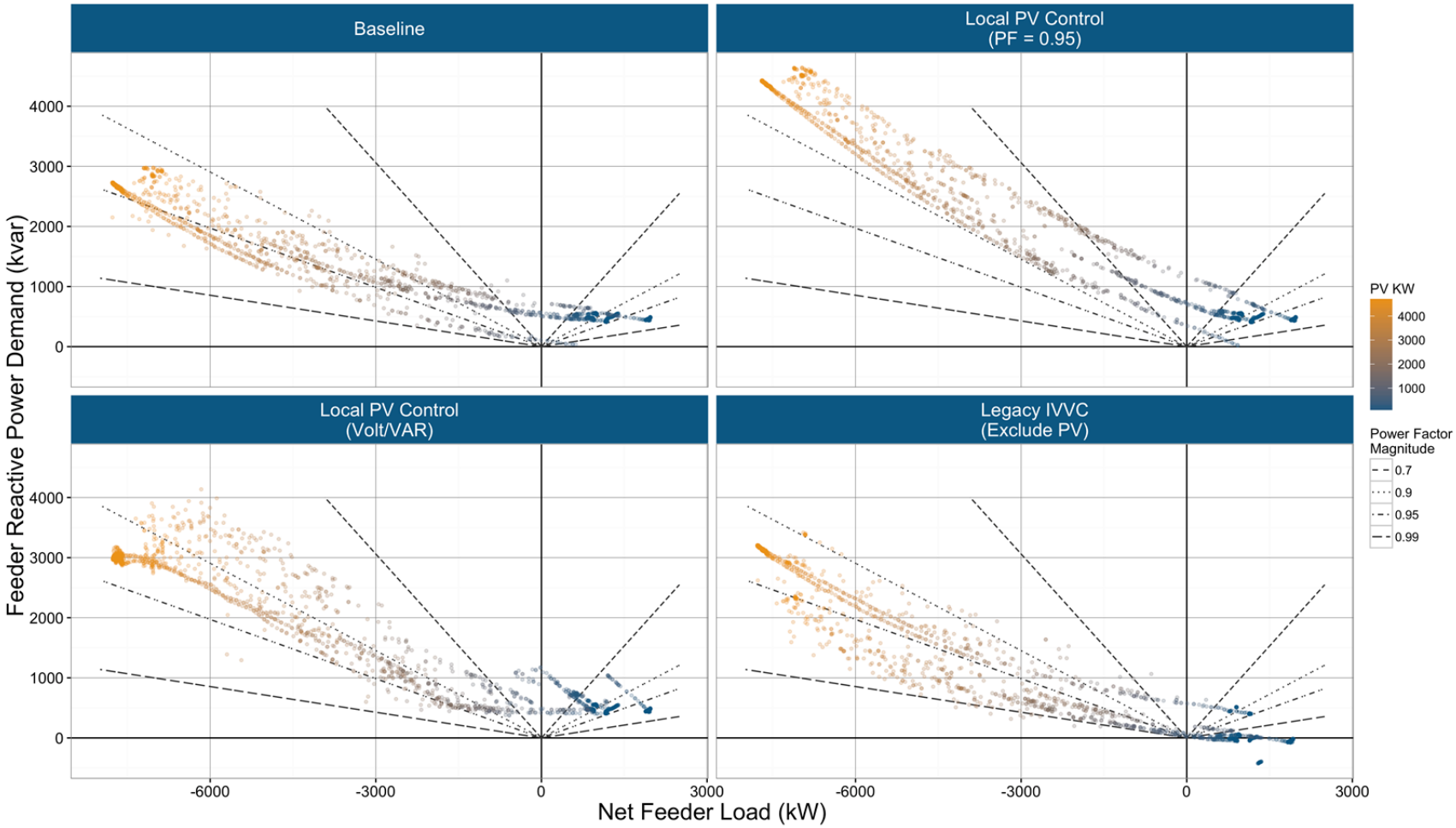


**Figure 66. Simulated substation-level P/Q plots with a second 5-MW PV system located near the end of the three-phase feeder trunk for different scenarios**

# 7 Power Hardware-In-the-Loop Verification

## 7.1 Hardware Setup

The PHIL hardware testing effort was divided into two phases: (1) the first phase using only an advanced PV inverter and (2) a second phase using both an advanced PV inverter and a medium-voltage capacitor bank. Within the scope of this project and at the time of this report, the first phase is complete, and the second has been set up and the components tested individually, but an integrated second-phase project will wait to be conducted as part of a separate, follow-on U.S. Department of Energy Grid Modernization Initiative project.

For both testing phases, the balance of the feeder circuit, equipment, and loads were cosimulated using the same DOTS Python environment as that used for the pure software simulation. Specifically, during Phase 1, all devices on the feeder were simulated except for an advanced PV inverter. The physical PCC for this inverter was generated using PHIL cosimulation, with the DOTS environment providing phasor-domain PCC voltage from QSTS simulation that is converted to fast, time-domain voltage waveforms by an Opal-RT Real-Time Digital Simulator (RTS). The Opal-RT RTS sends these waveforms as analog control signals to an Ametek RS540 grid simulator and measures the resulting complex current flows. The Opal-RT RTS also manages the (analog) voltage and current limits such that the Magna-Power PV simulator emulates changes to the PV current-voltage relation as a function of irradiance.

When fully implemented, Phase 2 will add a medium-voltage capacitor bank and its associated controller to the existing setup. Here, the physical PCC for the capacitor bank will also be generated using PHIL cosimulation, with the DOTS environment providing a second PCC voltage phasor corresponding to the capacitor location on the simulated feeder. This will be converted to analog waveform by the Opal-RT RTS to control a second Ametek RS540 grid simulator. Note that in the ESIF hardware, the PV inverter and capacitor bank PCCs consist of two separately derived systems located in two laboratories within the ESIF: the Power Systems Integration Laboratory and the Medium-Voltage Outdoor Test Area.

The ESIF power hardware used in the phase 1 testing effort included an Advanced Energy 500TX PV inverter as the advanced PV inverter—rated at 500 MW and including many advanced features; a 1.25-MW Magna PV simulator to provide the inverter DC input; a 540kVA Ametek RS540 grid simulator controlled by the Opal-RT RTS, and a combination of Python-based scripts and a DOTS client to generate the inverter PCC. Phase two will use second Ametek RS540 grid simulator controlled by the same Opal-RT, as well as a Beckwith M6280 capacitor bank controller and Cooper power systems 600-kVAR capacitor bank, both provided by Duke Energy. Images of the installed hardware for this work are shown in Figure 67. A functional diagram for Phase 1 (PV inverter only) and Phase 2 (PV inverter with capacitor bank controller and 600-kVAR capacitor bank) is included in Figure 68.

**Figure 67. Power hardware installed at NREL (500TX and capacitor bank)**

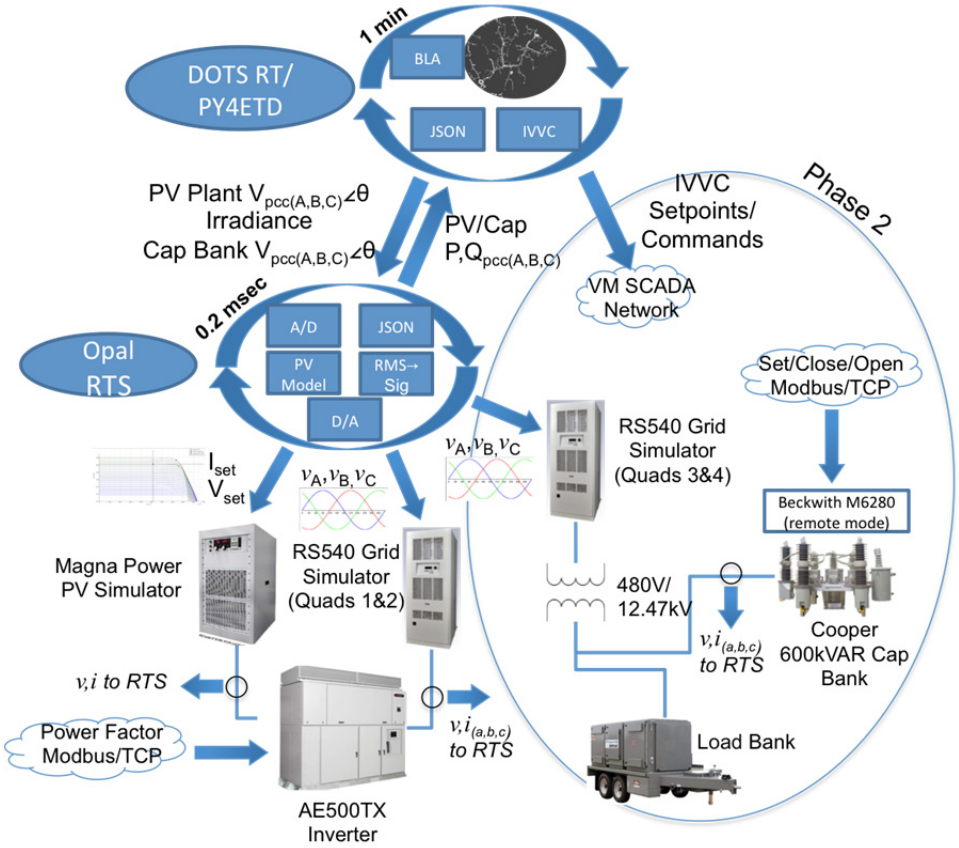


**Figure 68. Simplified diagram of PHIL cosimulation power and data flow**

## 7.2 PHIL Cosimulation

The PHIL configuration was built on the NREL-developed JSON-link cosimulation communications protocol to link the larger QSTS grid simulation in DOTS to hardware testing using the Opal-RT RTS. Additional descriptions of this protocol and cosimulation approach can be found in Palmintier et al. (2015). Detailed block diagrams of the setup can be found in Appendix B.

### 7.2.1 Cosimulation Sequence

As shown in Figure 68, the cosimulation proceeds as follows:

1. DOTS caches the previous time step's simulated state for all utility regulation equipment
2. DOTS allocates loads based on historic data.
3. DOTS manages the operating points for utility equipment by restoring the last simulated utility equipment operation state and managing the sequence of LVM commanded equipment operations when applicable.
4. DOTS solves the simulated power flow for the entire feeder.
5. At the start of the next time step, the three-phase unbalanced complex voltage phasor of the PCC is extracted from DOTS through py4etd and sent over JSON-link to the Opal-RT target. The solar irradiance and PV cell temperature (assumed equal to ambient) is also sent in this same packet.
6. The voltage phasors are used to update the continuously generated low-voltage analog AC waveforms from the Opal-RT.
7. These three low-voltage signals are amplified by the grid simulator to produce the corresponding nominal 277 V line-to-neutral (480 V line-to-line) AC signal to emulate the inverter's PCC with the grid.
8. At the same time, the irradiance and cell temperature are used to update the Opal-RT-based simulation of the current-voltage (IV) curve for the MagnaPower PV simulator to emulate the inverter's DC input.
9. After a small settling delay (1 second), the resulting complex three-phase AC currents and voltages are measured at the inverter AC outputs and fed into the analog-to-digital convertor on the Opal-RT target.
10. Opal-RT then computes the RMS real and reactive power and returns the result via JSON-link to DOTS.
11. DOTS Python then updates the inverter power for use in the next simulation time step, and the next simulation time step repeats steps 1–10.

### 7.2.2 Cosimulation Software Description

The cosimulation software design takes advantage of the modular architecture of both the Python-based DOTS simulation interface and the Python-based reference implementation of the JSON-link communications protocol. In this way, the identical functions used to drive the simulation are reused within the JSON-link protocol's state machine. The project also leverages

the existing C-based JSON-link code that runs on the Opal-RT target. In both cases, the JSON-link schema was updated as needed to manage the required data fields.

Timing for the exchange was controlled by the JSON-link state machine. Nominally this update happens once per minute because that is the fastest available data for irradiation and loads allocation; however, the flexibility of the JSON-link interface allowed varying the ratio of real time to simulation time. For some scenarios (e.g., constant power factor), the inverter response is so much faster (<< 1 second) than the 1-minute data rate that the hardware simulation could effectively be run two to three times faster than real time with no loss of fidelity. Running faster than this was not possible because of the time it takes on the DOTS side to read data, allocate loads, maintain utility equipment settings, and solve power flow.

## 7.3 PHIL Results

Phase 1 of the PHIL portion of the project focused on investigating the local control modes for DGPV. During Phase 2, we will also explore using IVVC through actual SCADA protocols to communicate with both the capacitor and the PV inverter. Between Phase 1 and Phase 2, all six of the simulated scenarios will be validated with PHIL. During IVVC operation (in Phase 2), the integrated DMS on the DOTS server can send real-time power and reactive power commands to the PV inverter and close/trip commands to the capacitor bank controller.

### *7.3.1 Baseline*

The baseline study was intended to demonstrate that the physical hardware in the PHIL cosimulation returns the same results as pure simulation. The advanced PV inverter power factor was set to the measured plant average of 0.99 absorbing (inductive), and a sample day— January 19 or Day-of-Year (DOY) number 19—was modeled for 1 hour (1 p.m.–1:59 p.m.). DOY19 1 p.m.–2 p.m. was chosen because it demonstrates significant variability from the PV plant—varying at times over 2.5 MW in less than 5 minutes throughout the hour.

Figure 69 shows the results of this PHIL run compared to the baseline pure simulation run for DOY19. The plot demonstrates that real power commanded to the advanced PV inverter was followed with a relatively small error compared to the simulation-only run. The observed differences in reactive power are largely due to the fact that while the actual PV plant operated slightly off unity power factor with an average power factor of 0.99, its power factor was not actually fixed. This results in small differences in absorbed VARs by the physical inverter set at a fixed power factor of 0.99.

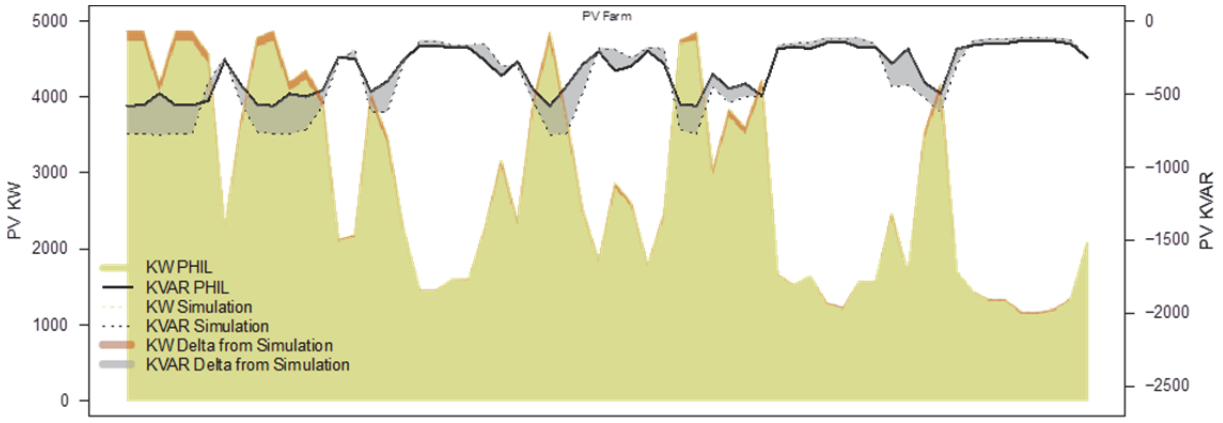


**Figure 69. Baseline PHIL DOY19 1-hour simulation with measured PV power factor of 0.99**

### 7.3.2 Local Advanced Inverter Control (Constant Power Factor, Volt/VAR)

#### 7.3.2.1 Constant Power Factor

Figure 70 shows the results of this PHIL run compared to the simulation run for DOY19 with the advanced PV inverter supplying power with a fixed power factor of 0.95 absorbing (inductive). The difference plot demonstrates that real power was again following commanded power with relatively small error for the entire hour. The reactive power plot shows that the advanced PV inverter absorbed VAR at a power factor of 0.95—nearly identical to the simulated run with the modeled inverter set to a power factor of 0.95.

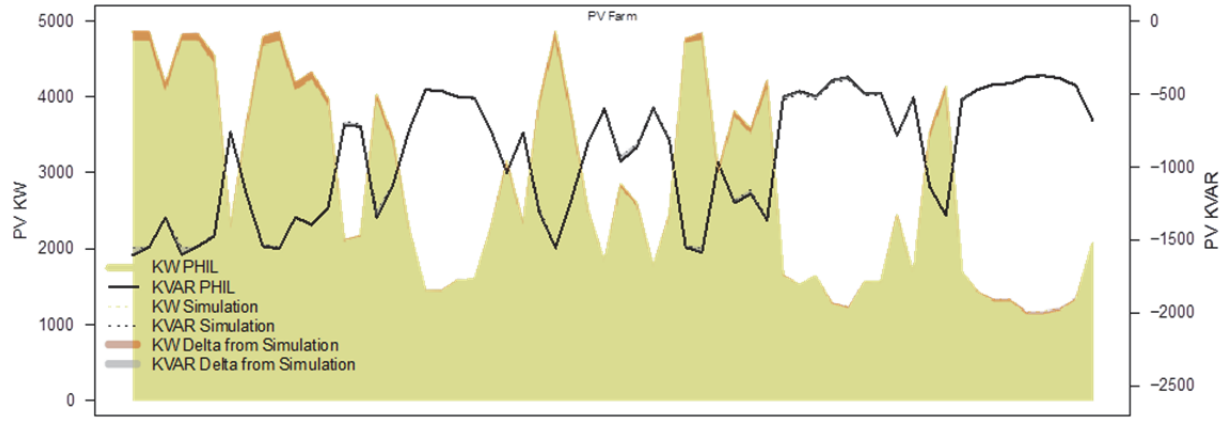


**Figure 70. PHIL DOY19 1-hour simulation (power factor of 0.95)**

#### 7.3.2.2 Autonomous Volt/VAR

Figure 71 shows the results of the PHIL run compared to the simulation run for DOY19 with the advanced PV inverter programmed with the volt/VAR curve used in corresponding DOTS simulations. The difference plot demonstrates that real power was again following commanded power, but the absorbed VARs oscillated significantly throughout the period. This oscillation was caused by delays introduced by the DOTS to the hardware connection, similar to the challenges found in Palmintier et al. (2015). A path forward in future developments would be to build a simplified dynamic phasor or transient differential-equation representation of the distribution feeder directly in the real-time Opal-RT RTS such that the inverter can correctly

interact with the changes in PCC voltage caused by its changes in reactive power without having to wait for the much slower DOTS update.

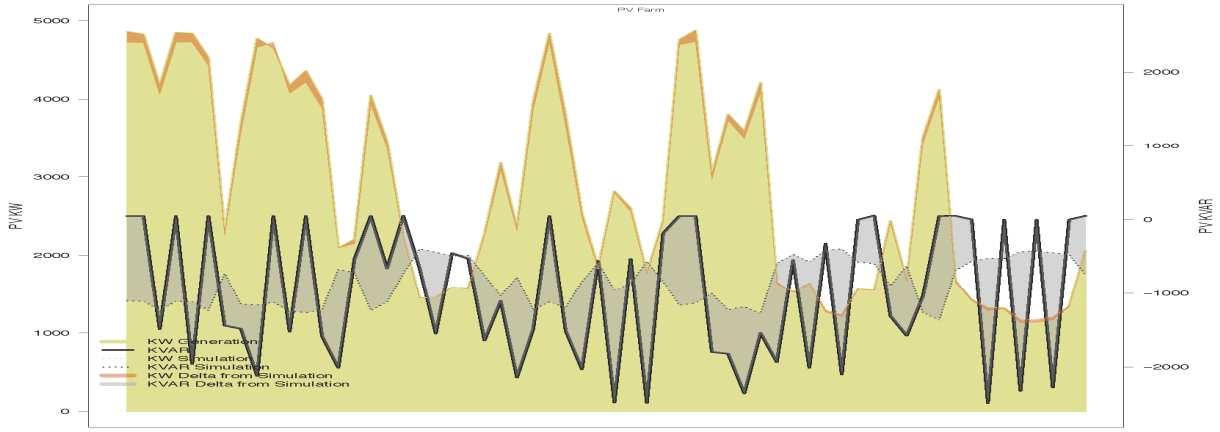


**Figure 71. PHIL DOY19 1-hour simulation (volt/VAR) showing the oscillations induced by the large time delays from one set point to another**

### *7.3.3 Toward PHIL with IVVC*

In preparation for Phase 2, the DOTS real-time interfaces via Modbus TCP/IP to both the capacitor bank controller and advanced PV inverter have been completed. In addition, manual SCADA control of both the advanced PV inverter and capacitor bank has been tested from within the DOTS/e-terra*distribution* platform. Both controls have been demonstrated at power. The next step will be to enable these control actions via py4etd. Full PHIL IVVC demonstration is expected to take place during the summer of 2016.

The development of these interfaces was not without challenges. Hardware and software complications arose when it was discovered that the Beckwith capacitor bank controller did not support DNP3 over serial due to a failed LAN port. There was a DNP3 driver for the Beckwith within the e-terra*distribution* communications architecture but no Modbus driver. Further, the 500TX early-development advanced-function board that provides user-configurable volt/VAR maps and external control was found to have unreliable Modbus communication. This resulted in the need to revert to the basic functions board for communications development.

# 8 Discussion and Conclusions

This report describes the methodology and results of using the native simulation environment built into GE Grid Solutions'/Alstom Grid's Advanced DMS software to perform time-series simulations via Python-based scripting and to explore the impacts of different PV advanced inverter control modes for voltage support in a real distribution feeder in Duke Energy's territory.

The existing 5-MW PV plant currently causes minimal voltage violations at load locations. The load voltage violations observed in the baseline scenario were not due to the adverse impact of the large PV plant because they occurred during nonproduction hours. A combination of careful control/set-point design in existing equipment—notably using cogeneration mode with substation LTC such that it disables line voltage drop when there is reverse power flow—and the fact that the PV plant is fairly close to the substation (2 miles) were sufficient to mitigate most adverse effects of PV to the voltage at load locations. Still, there is room for improvement in terms of fewer equipment operations and even fewer voltage challenges.

Two local PV control modes—a constant power factor of 0.95 absorbing (inductive) and volt/VAR—were simulated for the existing PV plant, but they resulted in no major changes in the operation of the voltage management equipment, and as such the local control modes had minimal effect on the number of voltage violations at load locations on the feeder. This was mainly because the PV plant is located close to the substation, and as such it is not able to impact the load voltage violations occurring downstream and during low- or no-PV production hours.

In the sensitivity case in which a second large PV plant (5 MW) was added at the end of the three-phase portion of the feeder, the local control modes became more effective because they were able to mitigate the adverse impacts to the voltages caused by the second large PV plant. In this case, volt/VAR provided the best performance because it reduced the total number of substation LTC and line regulator operations because it locally managed the voltage fluctuations caused by the large PV plant at the end of the feeder.

Using the DMS system's IVVC algorithm proved very effective at both minimizing equipment operations and better managing feeder voltage challenges. Interestingly, under IVVC (as configured in the study) the voltage management strategy in the study feeder changed drastically. The coordinated control of voltage regulation equipment reduced the daily number of operations of the substation LTC by more than half and drastically reduced the operation of the line regulators (in fact, for most of the days the line regulator was not used in the voltage regulation of the feeder). Instead, the voltage was largely performed by the capacitor. The load voltage violations still observed in the IVVC scenario occurred during highly variable PV days and because the IVVC algorithm solved every 10 minutes and the voltage management plan was locked in between solves. As such, the IVVC strategy was not able to fully compensate for large PV ramping events that happened in between solves.

Further work is needed in the area of integrating advanced inverters as controllable resources into IVVC optimization strategies. The increased load voltage violations (relative to IVVC without PV control) observed in the IVVC controlling the advanced inverter were mainly due to the effect of the PV variability in between solves. This situation could possibly be improved by

allowing the IVVC to set a power factor rather than a constant reactive power set point. In addition, including PV forecast data in the IVVC algorithm and/or using a faster solve rate with centralized algorithms could address some of the integration issues and enable advanced inverters to contribute more effectively to centralized voltage management methods. Interestingly, when IVVC was able to control the large PV inverter for reactive power support (Q set point), it opted to dispatch the inverter as a VAR source (opposite of what is expected to mitigate voltage rise), allowing the capacitor to switch less often.

Running IVVC and having the inverter provide local voltage support in the form of a constant power factor of 0.95 absorbing (inductive) showed the best performance of all of the strategies simulated for the feeder because the local control mode was able to compensate for the variability effects in between solves, whereas the IVVC solution solving every 10 minutes effectively managed the larger voltage regulation needs.

In summary, this project illustrates the potential for coordinated control of voltage management equipment, such as the central DMS-controlled IVVC algorithm evaluated here, to provide substantial improvement in distribution operations with large-scale PV systems by reducing regulator operations and decreasing the number of voltage challenges. It also shows how the effectiveness of local control modes—such as constant absorbing (inductive) power factor or reactive power adjustment as a function of voltage—is strongly dependent on the location of the PV system. These local PV controls were more effective on the study feeder with a larger solar power plant located far from the substation. These local PV control modes also offer an opportunity to manage the variability in between solves in solar production that otherwise represents a shortcoming of solving and implementing the IVVC algorithm every 10 minutes or longer. Faster solves and/or including PV forecasting in IVVC are enhancements that could be further explored to address such issues.

Overall, DMS-controlled IVVC shows promise for easing the integration of very high penetration PV in the distribution system and providing an additional way for advanced PV inverters to support grid operations. System-wide, this can accelerate the integration of very high penetration solar PV and lower costs to utilities and consumers alike.

# References


Braun, Martin, Thomas Stetz, Roland Bründlinger, Christoph Mayr, Kazuhiko Ogimoto, Hiroyuki Hatta, Hiromu Kobayashi, et al. 2011. "Is the Distribution Grid Ready to Accept Large-Scale Photovoltaic Deployment? State of the Art, Progress, and Future Prospects." *Progress in Photovoltaics: Research and Applications*, November. doi:10.1002/pip.1204.

Coddington, Michael, Barry Mather, Benjamin Kroposki, Kevin Lynn, Alvin Razon, Abraham Ellis, Roger Hill, Tom Key, Kristen Nicole, and Jeff Smith. 2012. *Updating Interconnection Screens for PV System Integration* (Technical Report NREL/TP-5500-54063). Golden, CO: National Renewable Energy Laboratory.

Electric Power Research Institute. 2014. *Common Functions for Smart Inverters, Version 3* (EPRI Report 3002002233). Palo Alto, CA.

GTM Research and SEIA. 2016. *U.S. Solar Market Insight Report: 2015 Year in Review* (Technical Report). Washington, DC: Solar Energy Industries Association. https://www.seia.org/research-resources/solar-market-insight-2015-q4.

IEEE 1547. 2003. "IEEE Standard for Interconnecting Distributed Resources with Electric Power Systems." *IEEE Std 1547-2003*, July, 1–28. doi:10.1109/IEEESTD.2003.94285.

IEEE 1547a. 2014. "IEEE Standard for Interconnecting Distributed Resources with Electric Power Systems - Amendment 1." *IEEE Std 1547a-2014 (Amendment to IEEE Std 1547-2003)*, May, 1–16. doi:10.1109/IEEESTD.2014.6818982.

Keller, J., and B. Kroposki. 2010. *Understanding Fault Characteristics of Inverter-Based Distributed Energy Resources* (Technical Report NREL/TP-550-46698). Golden, CO: National Renewable Energy Laboratory. http://www.osti.gov/servlets/purl/971441-jJGkWx/.

Nagarajan, Adarsh, Bryan Palmintier, and Murali Baggu. 2016. "Advanced Inverter Functions and Communication Protocols for Distribution Management." In *2016 IEEE PES T&D Conference and Exposition*. Dallas, TX.

NIST. 2016. "Smart Grid Interoperability Panel (SGIP)." https://www.nist.gov/programs-projects/smart-grid-national-coordination/smart-grid-interoperability-panel-sgip.

Palmintier, Bryan, Robert Broderick, Barry Mather, Michael Coddington, Kyri Baker, Fei Ding, Matthew Reno, Matthew Lave, and Ashwini Bharatkumar. 2016. *On the Path to SunShot: Emerging Issues and Challenges in Integrating Solar with the Distribution System* (Technical Report NREL/TP-5D00-65331). Golden, CO: National Renewable Energy Laboratory. http://www.nrel.gov/docs/fy16osti/65331.pdf.

Palmintier, Bryan, Blake Lundstrom, Sudipta Chakraborty, Tess Williams, Kevin Schneider, and David Chassin. 2015. "A Power Hardware-in-the-Loop Platform With Remote Distribution Circuit Cosimulation." *IEEE Transactions on Industrial Electronics* 62 (4): 2236–45. doi:10.1109/TIE.2014.2367462.

SEIA. 2016. "Top Ten Solar States." Solar Energy Industries Association. https://www.seia.org/research-resources/top-10-solar-states.

Seuss, J., M. J. Reno, R. J. Broderick, and S. Grijalva. 2015. "Improving Distribution Network PV Hosting Capacity via Smart Inverter Reactive Power Support." In *2015 IEEE Power Energy Society General Meeting*, 1–5. doi:10.1109/PESGM.2015.7286523.

Smith, J.W., W. Sunderman, R. Dugan, and B. Seal. 2011. "Smart Inverter Volt/Var Control Functions for High Penetration of PV on Distribution Systems." In *Power Systems*

*Conference and Exposition (PSCE), 2011 IEEE/PES*, 1–6. doi:10.1109/PSCE.2011.5772598.

Underwriters Laboratory. 2010. "Standard 1741 - Standard for Inverters, Converters, Controllers and Interconnection System Equipment for Use With Distributed Energy Resources." http://ulstandards.ul.com/standard/?id=1741_2.

# Appendix A Additional Description of the Cost-Benefit Analysis Tool

CBAAT has as its core a structural framework and data store for the cost, performance, classification, and configuration information on which the alternatives analyses depend. The data stores consist of the following databases:

- Company, jurisdiction, fuel type, plant type, and Federal Energy Regulatory Commission Uniform System of Accounts data with approved cost of capital information per company and jurisdiction, asset book life (for normalization) per company and Federal Energy Regulatory Commission account, historic operation-and-maintenance expenditure as percent of plant per company and Federal Energy Regulatory Commission account (for estimating operation and maintenance when not configured in temporal unit cost per scenario [user-selectable]), other historical expense categories as percent of capital expenditure by fuel and plant type, and tax rate information per company per service territory
- Energy and ancillary services cost/value data by price node, ancillary service region, market (day ahead, residual unit commitment, hour ahead, real-time economic dispatch, etc.), type (non-spinning reserve; spinning reserve; regulation up; regulation down; regulation mileage up; regulation mileage down; locational marginal price; and marginal cost of congestion, energy, and losses), time interval, and tools for converting time-of-use/time-of-production rates into full interval form
- Escalation/inflation rates by market and year for annually varying inflation treatment and application of market-appropriate inflation by cost or benefit type
- Multilevel unit cost database accommodating component costs (e.g., equipment, labor, transportation), unit costs (bills of materials), and "work package" costs (bills of materials of component and unit costs). The bills of materials also accommodate temporal assignment of costs (e.g., for anticipated operation and maintenance, repair, and replacement costs), and special operation and maintenance and replacement policies on equipment subject to wear and tear (such as switching equipment requiring maintenance or replacement at intervals depending on number of operations)
- Analysis characterizations database in which each alternative is configured and stored analyzing high-level information characterizing each scenario to be compared (unit costs, energy and ancillary services interval data, association of [potentially multiple] energy and ancillary services market vector(s) to the interval data, and state interval data on equipment subject to wear and tear).

The tool generates results in the form of tabulated and categorized annual cash flows, annual discounted cash flows, and cumulative annual discounted cash flows. The tool facilitates inspection of tagged individual data elements for insight into the way results were generated, and it facilitates cross-tabulation (pivot) for summarization of what is usually a large result data set.

After configuration and data import and processing, the tool generates results in the following steps:

1. Energy and ancillary services cost-benefit interval data are generated, classified, and aggregated by analysis, scenario, calendar year, price node, escalation element, energy source or sync, other applicable financial parameters, and reporting classifiers.
2. Last-simulated-year energy and ancillary services cost-benefit aggregates are extrapolated to years beyond the simulated years.
3. Component costs of unit and work package costs are broken out, calculated according to quantity, and assigned to analysis years as cash flows, and component and custom costs are calculated according to quantity and assigned to analysis years as cash flows.
4. Operation-and-maintenance cash flows to be estimated for capital expenditures based on historical percentages of plant based on fuel type, plant type, and Federal Energy Regulatory Commission account are calculated and assigned to analysis years.
5. Inflation rates for all year-assigned cash flows are queried and applied according to annual market-specific inflation rates.
6. Overhead rates are calculated and applied according to category of cost or expense.
7. Capital expenditure cash flows can be normalized, if configured, according to the method appropriate to the utility; capital expenditure and expense cash flows can have tax effects (such as for income and property tax) applied.
8. Discounted cash flows are calculated from all categorized intermediate cash flow results.
9. Cumulative discounted cash flows are calculated from all discounted cash flows.
10. Results are cross-tabulated and can be exported to other tools both in tabulated and pivot tabulated results formats for further inspection, exploration, and reporting.

At the highest summary level, results are presented by scenario for each analysis as cumulative discounted cash flow aggregates (essentially cumulative NPVs) at planning horizons of interest, e.g., 5, 10, 20, 40, 50 years. Table 10 shows an example these tabular results.

**Table 10. Cumulative NPVs at 5-, 10-, 20-, 40-, and 50-Year Planning Horizons**

| Scenario \ Year | 2014 | 2019 | 2024 | 2034 | 2054 | 2064 |
|---|---|---|---|---|---|---|
| **Baseline** | ($85,631) | ($81,932) | ($76,108) | ($65,674) | ($47,544) | ($34,310) |
| **Local PV Control (PF=0.95)** | ($87,690) | ($83,901) | ($77,938) | ($67,253) | ($44,493) | ($35,135) |
| **Local PV Control (Volt/VAR)** | ($86,362) | ($82,631) | ($76,758) | ($66,235) | ($43,819) | ($34,603) |
| **Legacy IVVC (Exclude PV)** | ($63,291) | ($60,556) | ($56,252) | ($48,540) | ($32,113) | ($25,359) |
| **IVVC with PV @ PF=0.95** | ($64,143) | ($61,372) | ($57,010) | ($49,194) | ($44,833) | ($25,700) |
| **IVVC (Central PV Control)** | ($66,920) | ($64,028) | ($59,478) | ($51,323) | ($33,954) | ($26,813) |

Tabulated scenario results can be expanded and collapsed to reveal category (e.g., loads, losses, PV production) and subcategory (specific system and expenditure or revenue stream annual items) detail and summary for deeper understanding of results. In addition, the tool generates summary charts for rapid visual comparisons. Charts of this type are presented in the figures included in the results section of this report.

# Appendix B Detailed PHIL Block Diagrams

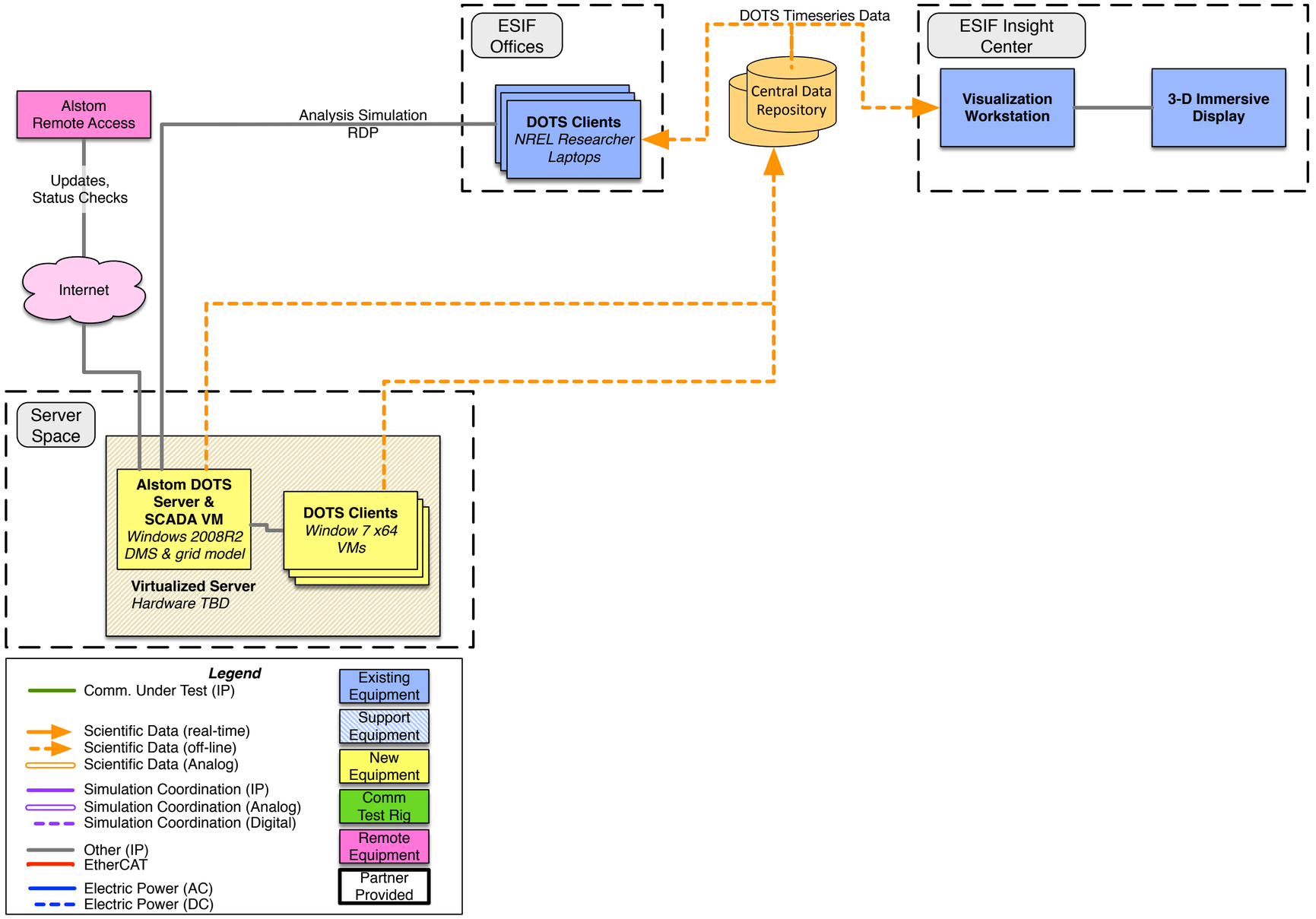


**Duke/Alstom Functional Block Diagram - Simulation Only (p 1/4)**

| *Ver* | *Date* | *Drawn by* | *Changes* |
|---|---|---|---|
| *1* | 02-Oct-2014 | Bryan Palmintier | Initial Version |
| *2* | 09-Dec-2014 | Bryan Palmintier | Refine DOTS representation |
| *3* | 18-Mar-2015 | Bryan Palmintier | Split into phases |
| *4* | 24-Mar-2015 | Bryan Palmintier | Clarify DOTS Scenario Control |
| *5* | 22-Apr-2015 | Bryan Palmintier | Equip. Specifics, Laptops, REDB path |
| *6* | 18-Aug-2015 | Bryan Palmintier | MVOTA and eterraControl updates |
| *7* | 03-Dec-2015 | Bryan Palmintier | MV sensing and controls |
| *8* | 08-Sep-2016 | Bryan Palmintier | Final Report Clean-up |

| Duke/Alstom Functional Block Diagram - PHIL Phase 1A (p 2/4) | | | |
|---|---|---|---|
| *Ver* | *Date* | *Drawn by* | *Changes* |
| *1* | 02-Oct-2014 | Bryan Palmintier | Initial Version |
| *2* | 09-Dec-2014 | Bryan Palmintier | Refine DOTS representation |
| *3* | 18-Mar-2015 | Bryan Palmintier | Split into phases |
| *4* | 24-Mar-2015 | Bryan Palmintier | Clarify DOTS Scenario Control |
| *5* | 22-Apr-2015 | Bryan Palmintier | Equip. Specifics, Laptops, REDB path |
| *6* | 18-Aug-2015 | Bryan Palmintier | MVOTA and eterraControl updates |
| *7* | 03-Dec-2015 | Bryan Palmintier | MV sensing and controls |
| *8* | 08-Sep-2016 | Bryan Palmintier | Final Report Clean-up |

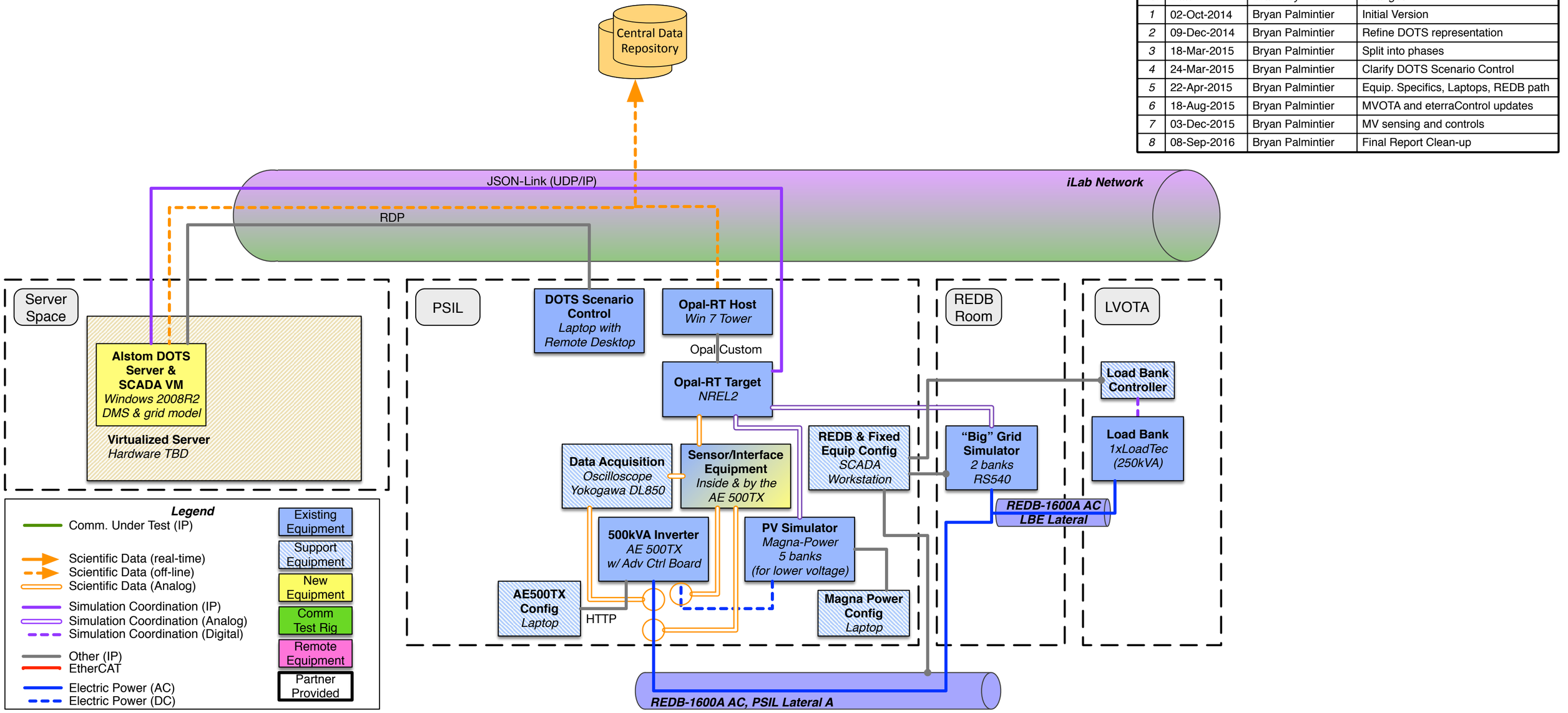

| Duke/Alstom Functional Block Diagram - PHIL Phase 1B (p 3/4) | | | |
|---|---|---|---|
| *Ver* | *Date* | *Drawn by* | *Changes* |
| *1* | 02-Oct-2014 | Bryan Palmintier | Initial Version |
| *2* | 09-Dec-2014 | Bryan Palmintier | Refine DOTS representation |
| *3* | 18-Mar-2015 | Bryan Palmintier | Split into phases |
| *4* | 24-Mar-2015 | Bryan Palmintier | Clarify DOTS Scenario Control |
| *5* | 22-Apr-2015 | Bryan Palmintier | Equip. Specifics, Laptops, REDB path |
| *6* | 18-Aug-2015 | Bryan Palmintier | MVOTA and eterraControl updates |
| *7* | 03-Dec-2015 | Bryan Palmintier | MV sensing and controls |
| *8* | 08-Sep-2016 | Bryan Palmintier | Final Report Clean-up |

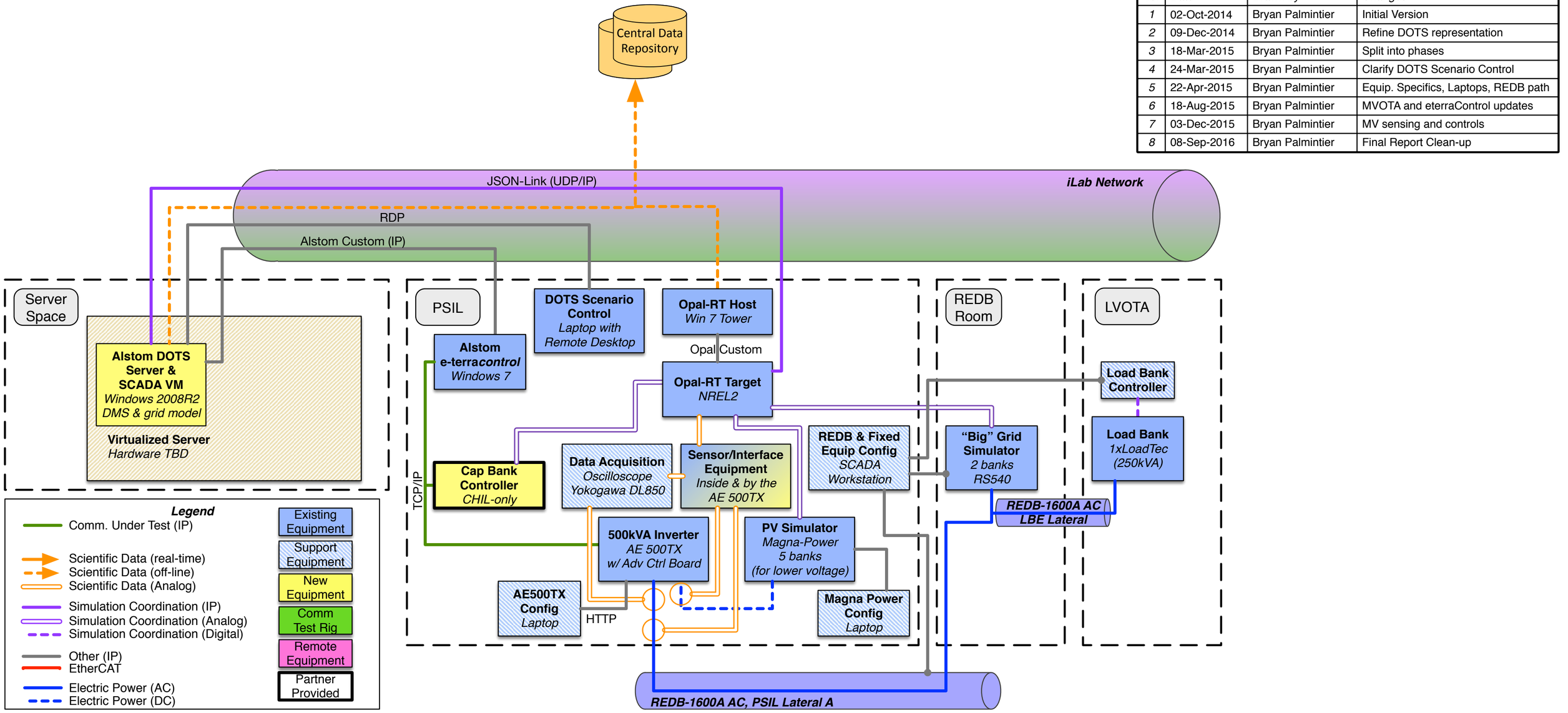

| Duke/Alstom Functional Block Diagram - PHIL Phase 2 (p 4/4) | | | |
|---|---|---|---|
| *Ver* | *Date* | *Drawn by* | *Changes* |
| *1* | 02-Oct-2014 | Bryan Palmintier | Initial Version |
| *2* | 09-Dec-2014 | Bryan Palmintier | Refine DOTS representation |
| *3* | 18-Mar-2015 | Bryan Palmintier | Split into phases |
| *4* | 24-Mar-2015 | Bryan Palmintier | Clarify DOTS Scenario Control |
| *5* | 22-Apr-2015 | Bryan Palmintier | Equip. Specifics, Laptops, REDB path |
| *6* | 18-Aug-2015 | Bryan Palmintier | MVOTA and eterraControl updates |
| *7* | 03-Dec-2015 | Bryan Palmintier | MV sensing and controls |
| *8* | 08-Sep-2016 | Bryan Palmintier | Final Report Clean-up |

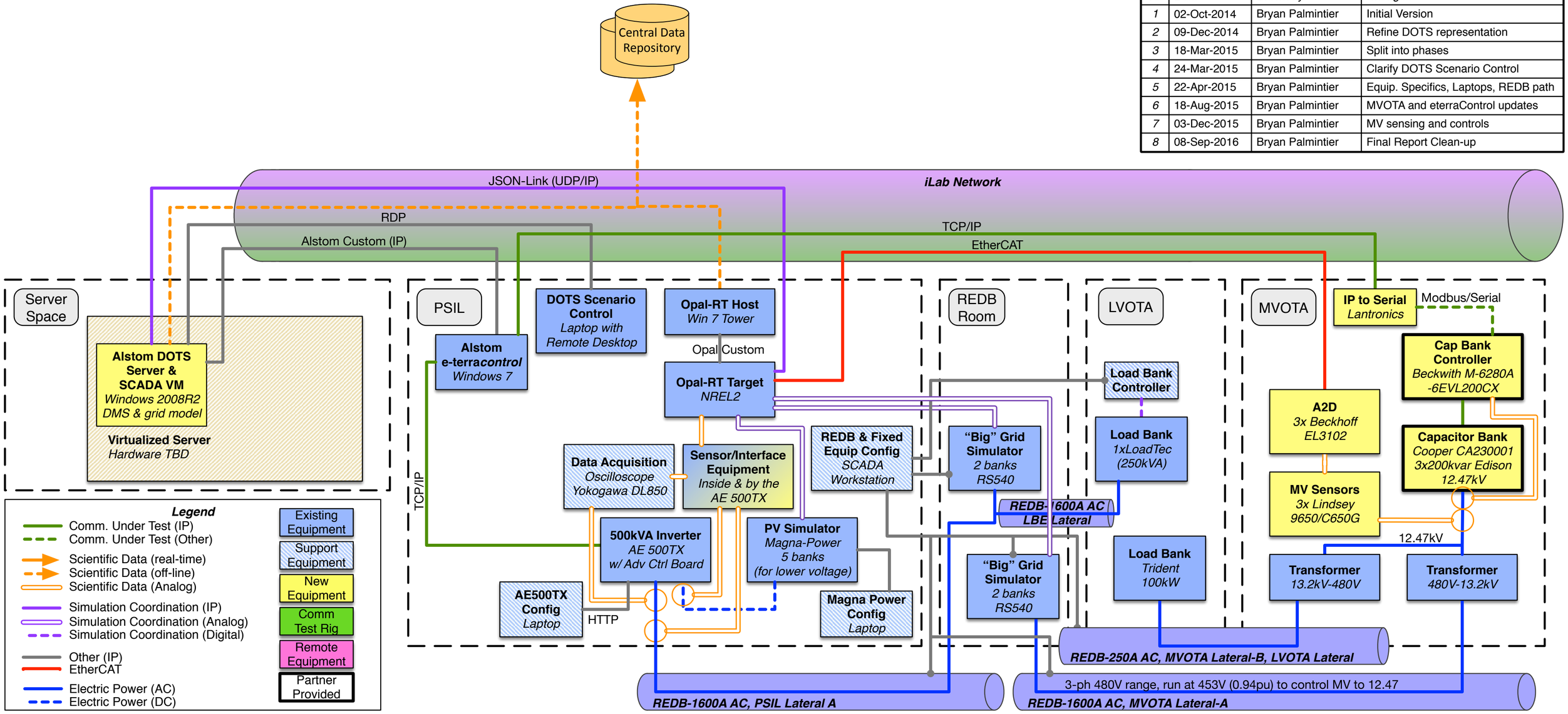

# Appendix C Additional Simulation Results

## C.1 40-Day Summaries

Figures begin on next page.

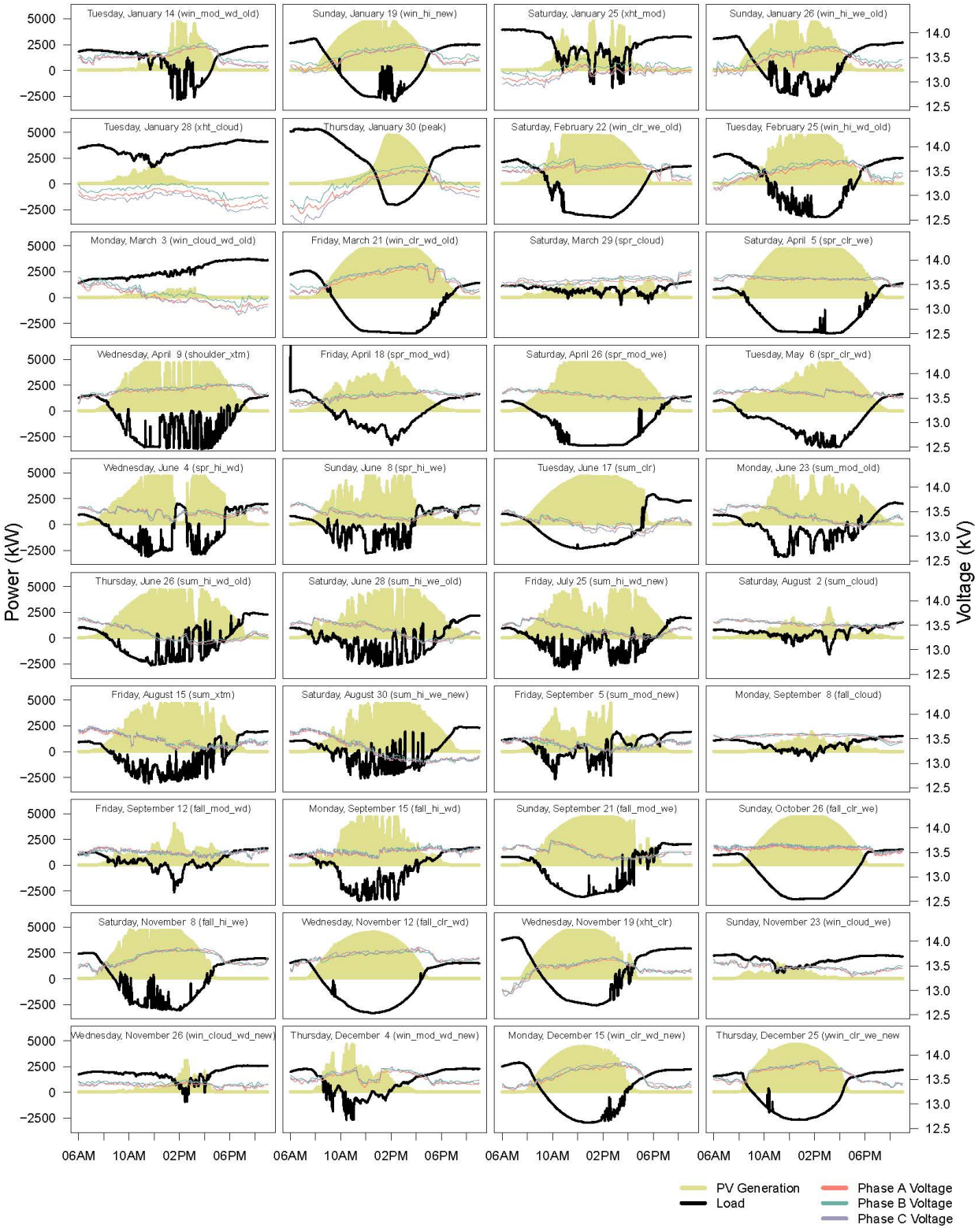


**Figure 72. Feeder-head summary for baseline**

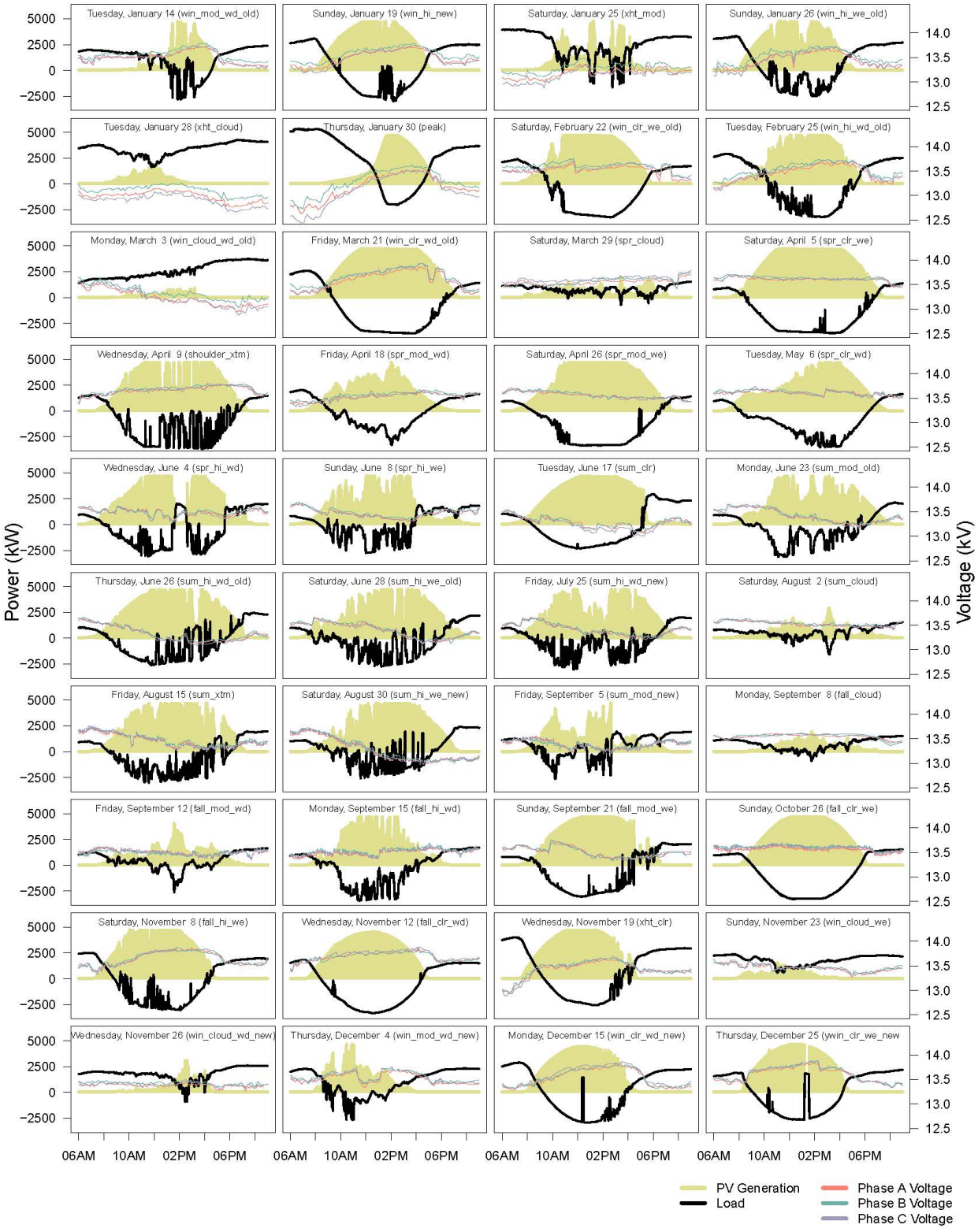


**Figure 73. Feeder-head summary for Local PV Control (PF=0.95)**

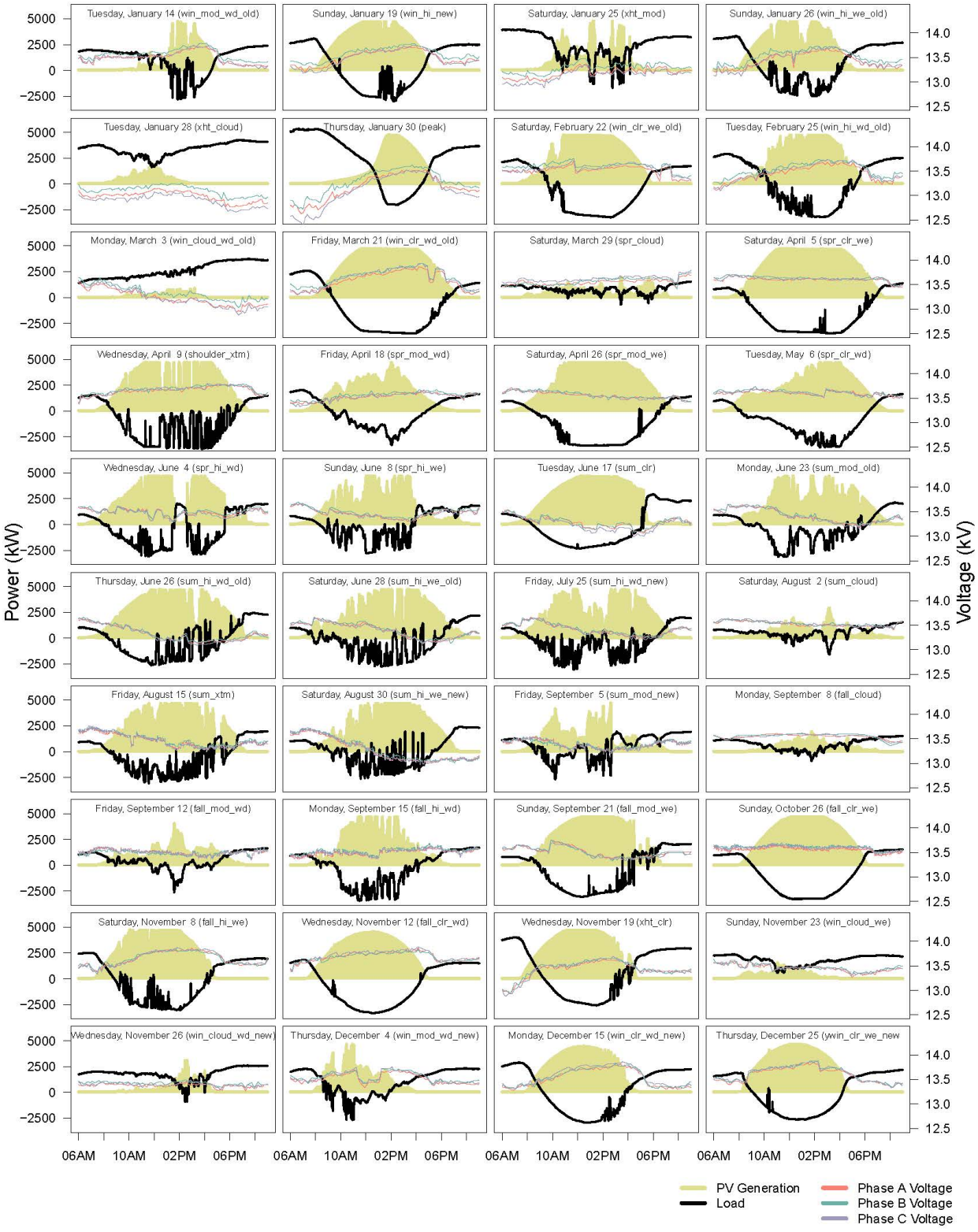


**Figure 74. Feeder-head summary for Local PV Control (Volt/VAR)**

## C.2 Voltage-Distance Plots for Sensitivity Analysis

The figures in this section plot a set of 3-phase traces for each 1-minute power flow across a 30-minute period. For each day, there are two times

Figures begin on next page.

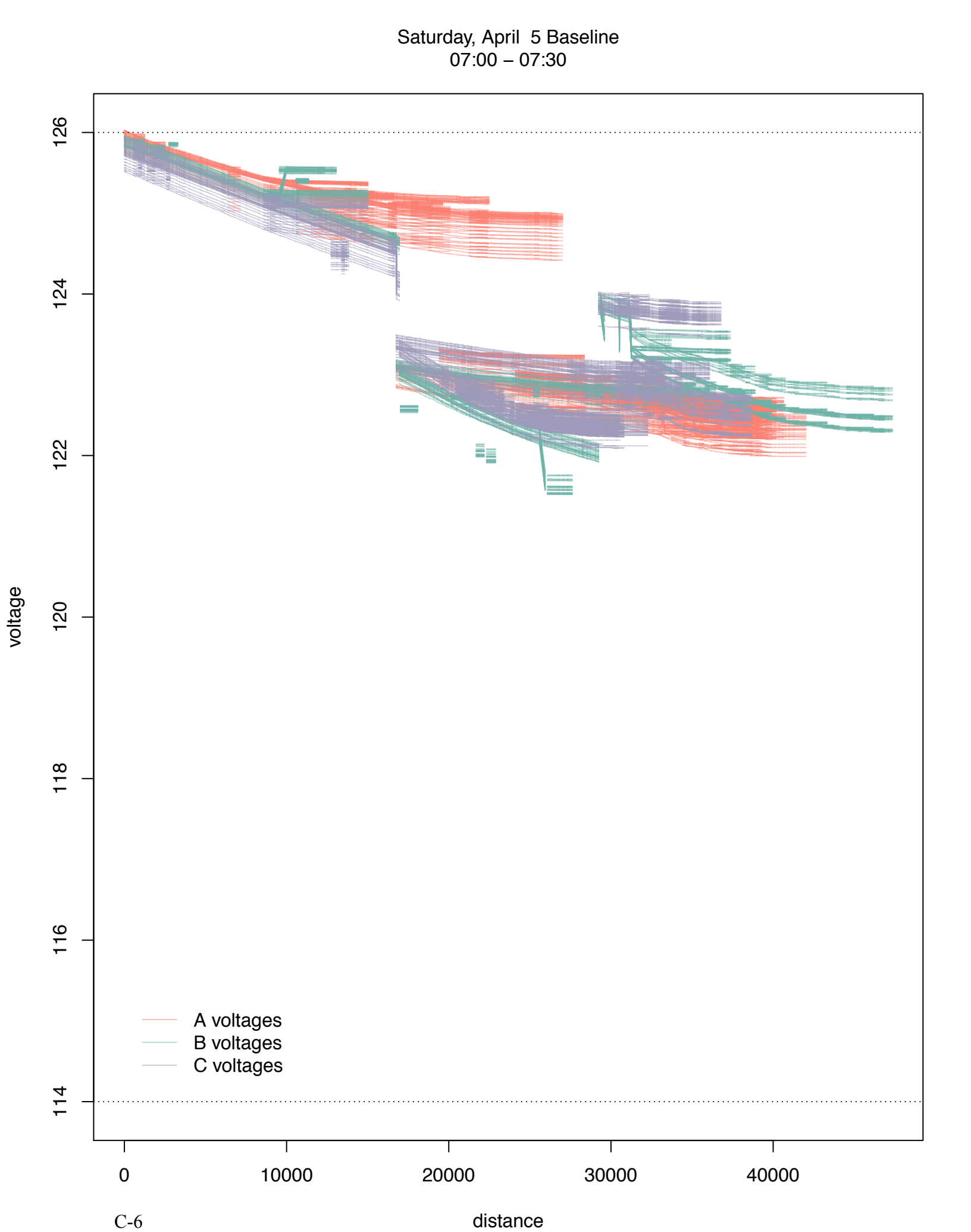

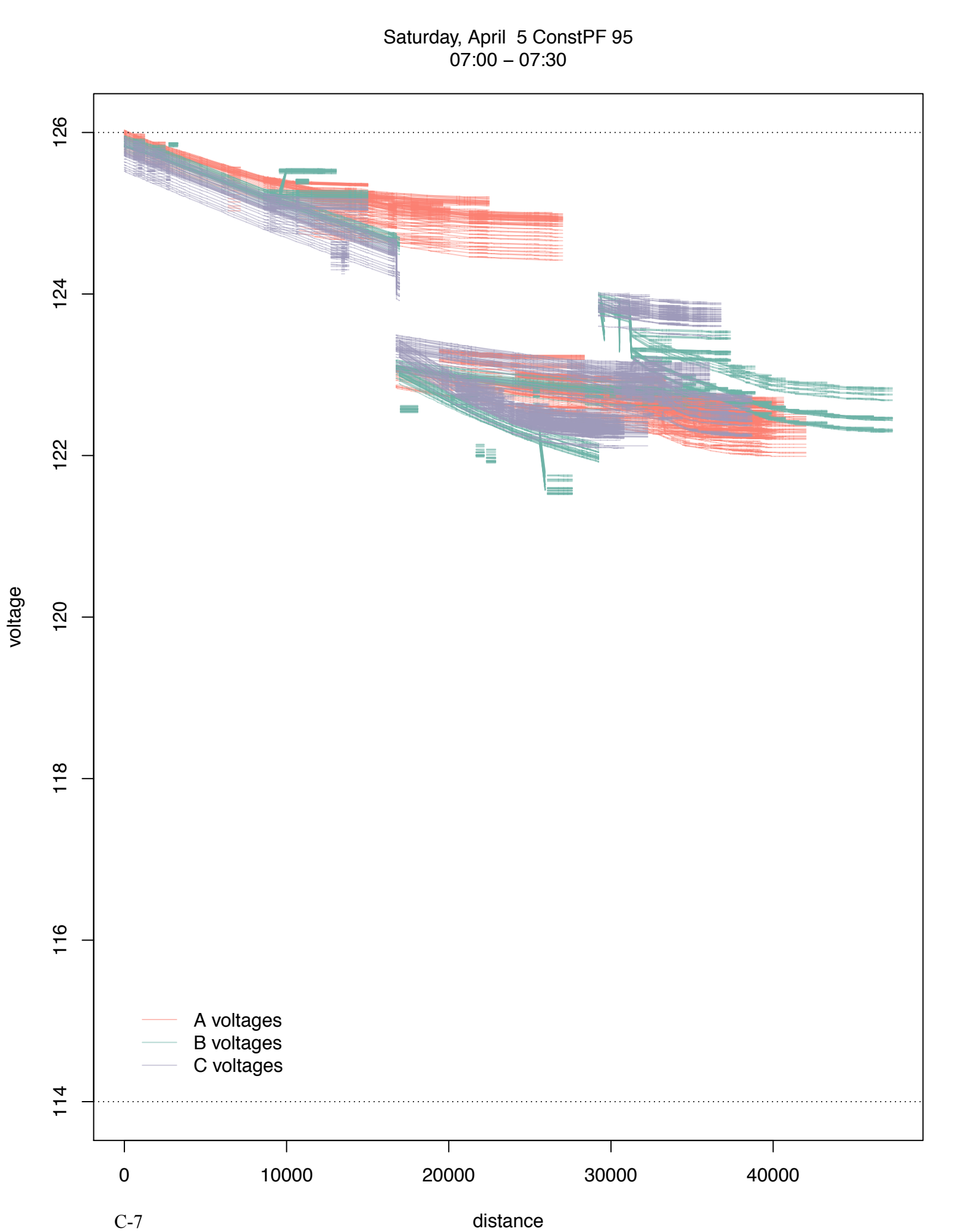

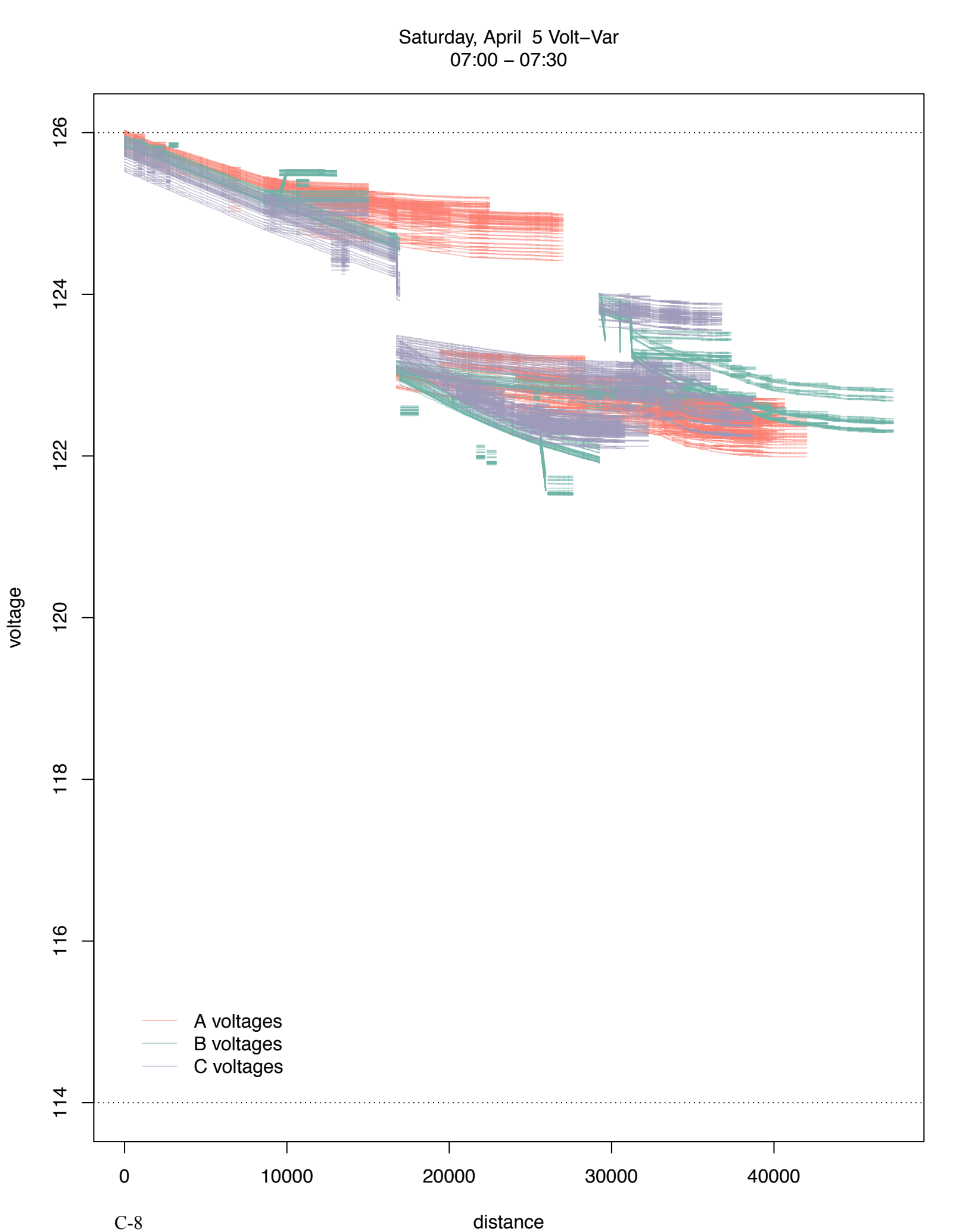

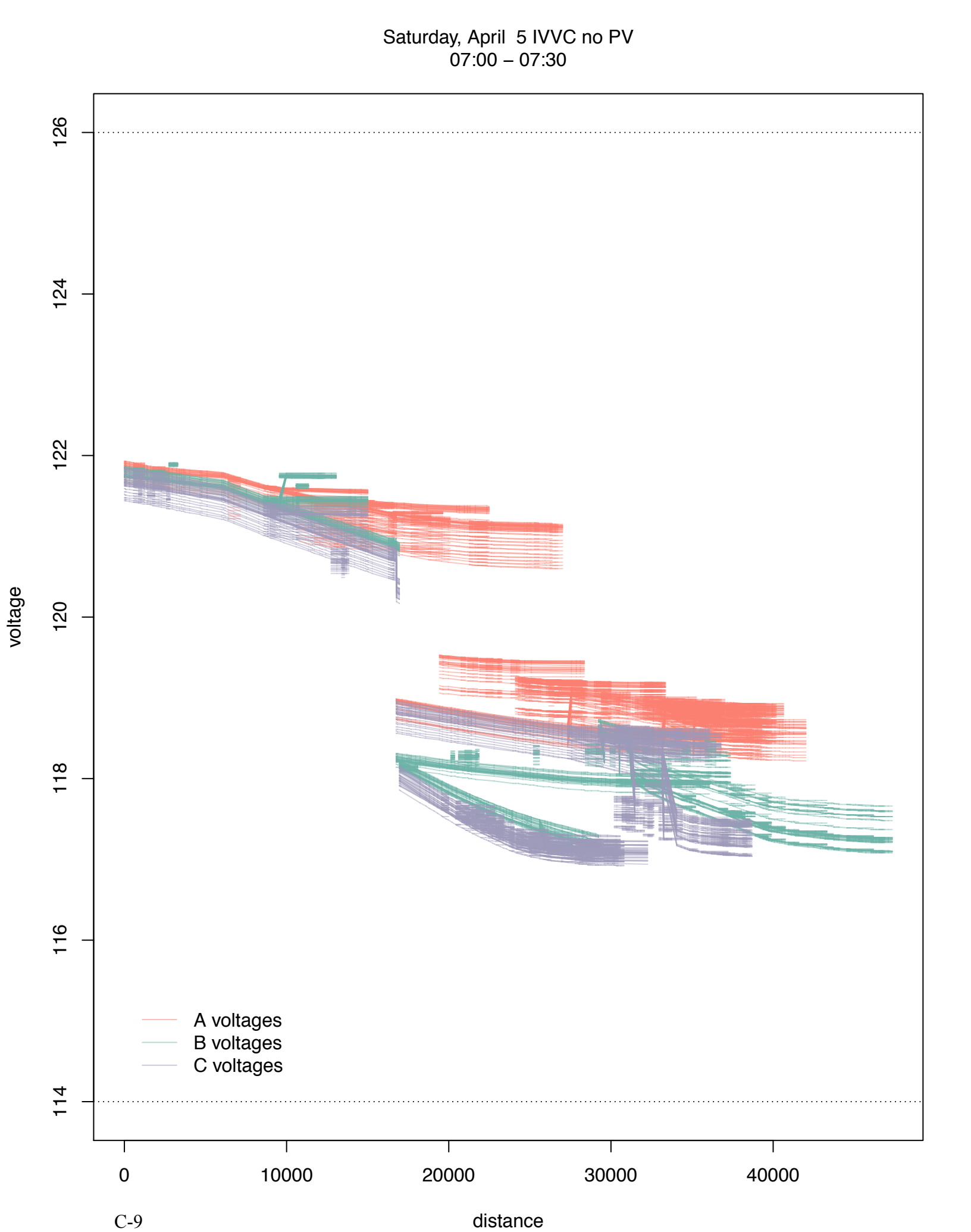

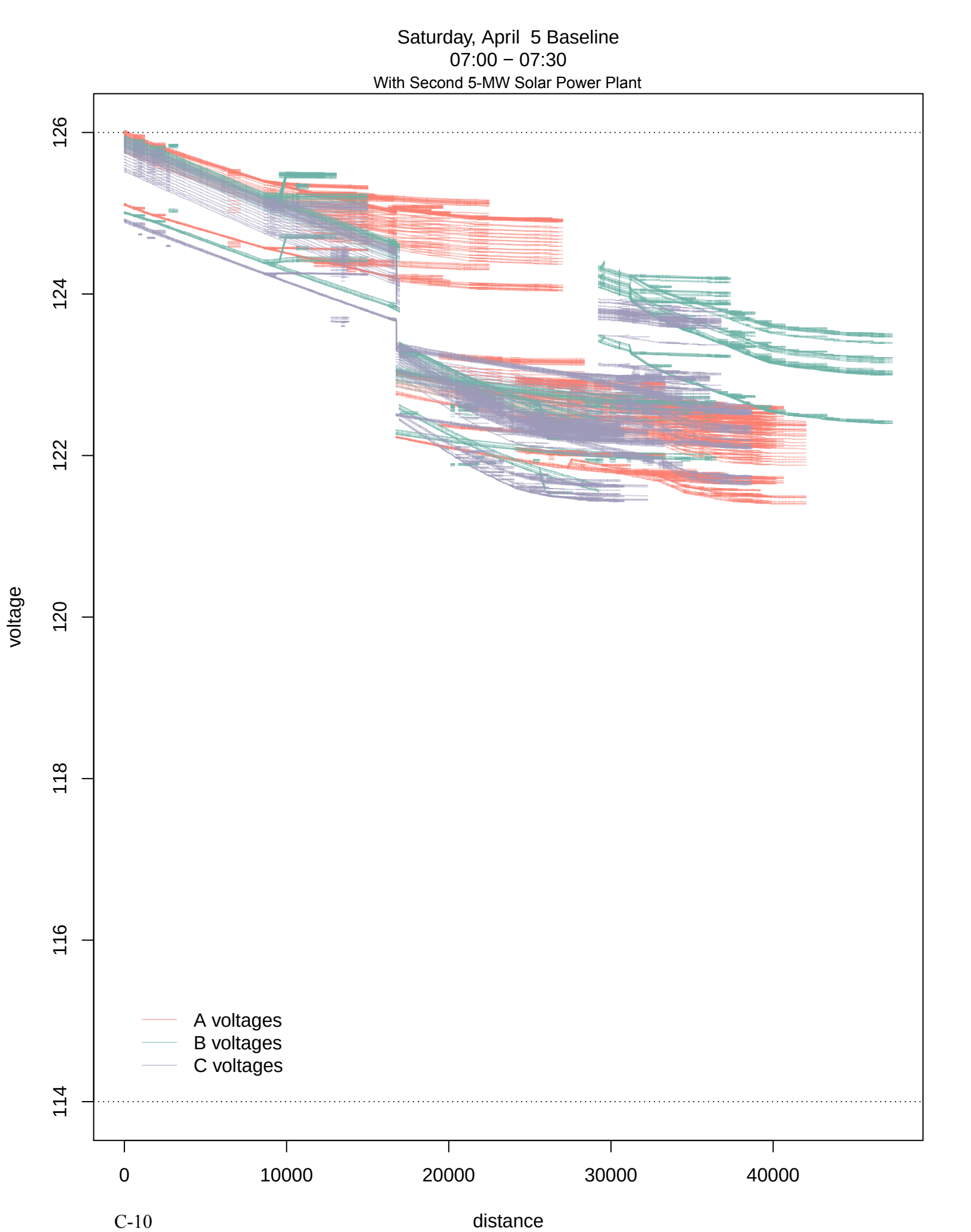

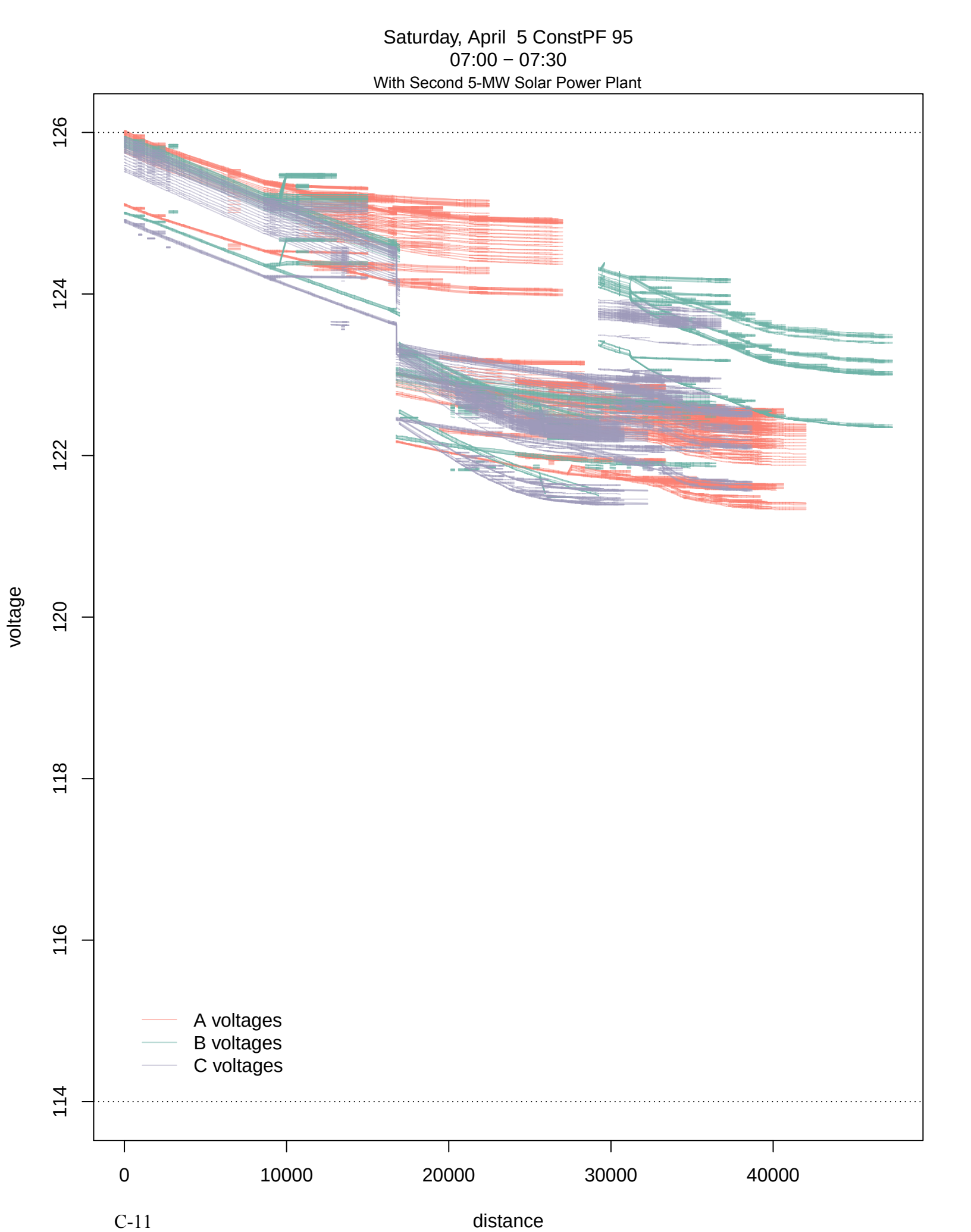

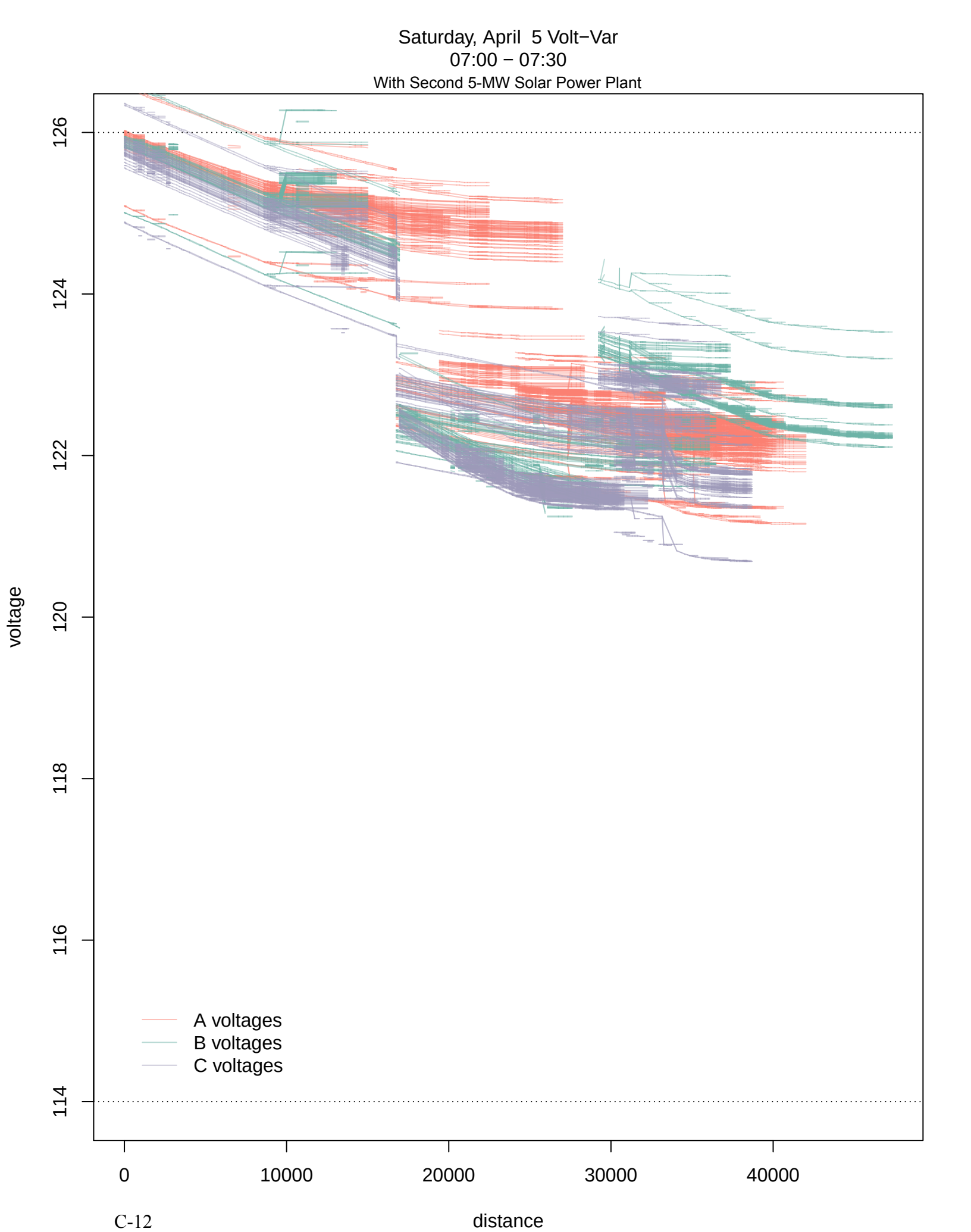

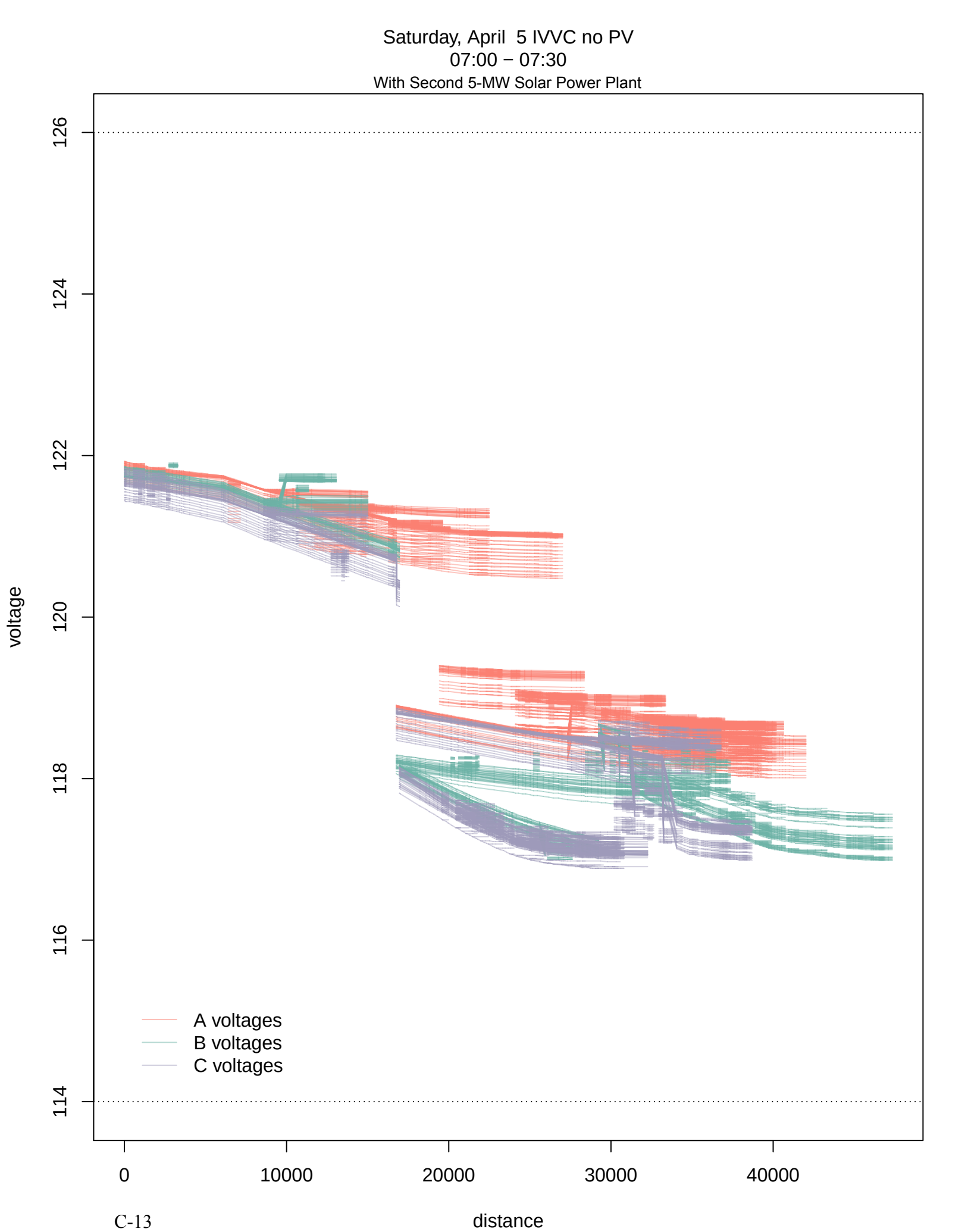

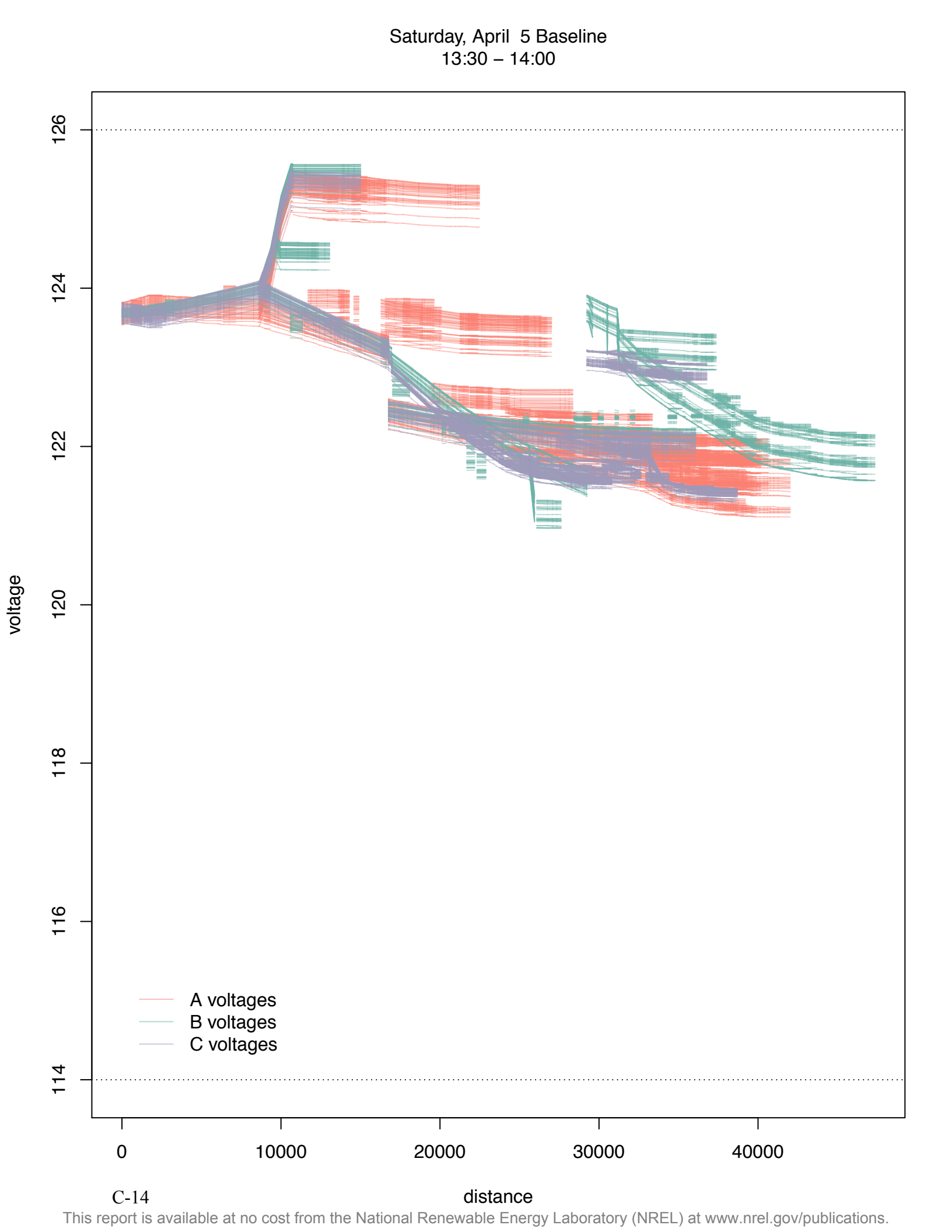

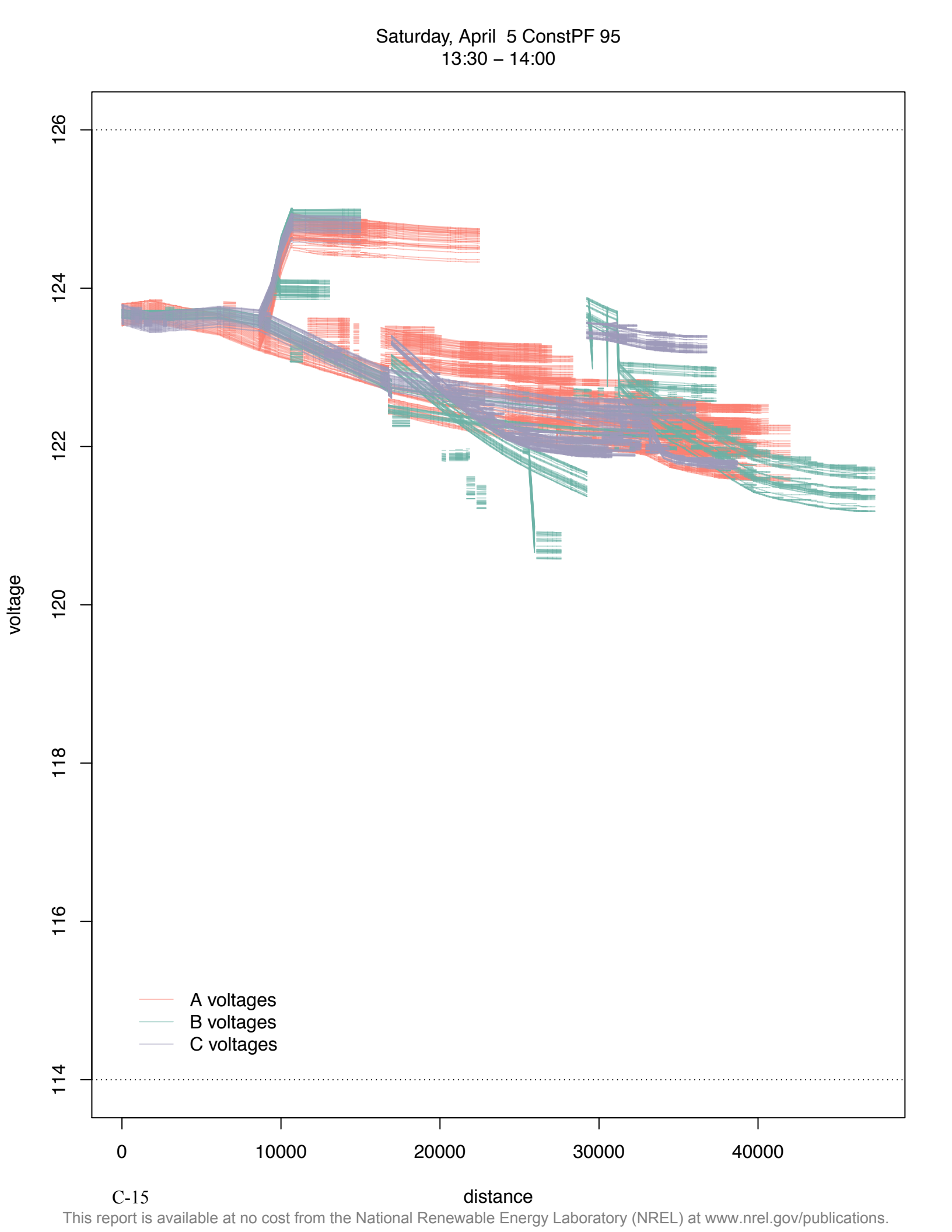

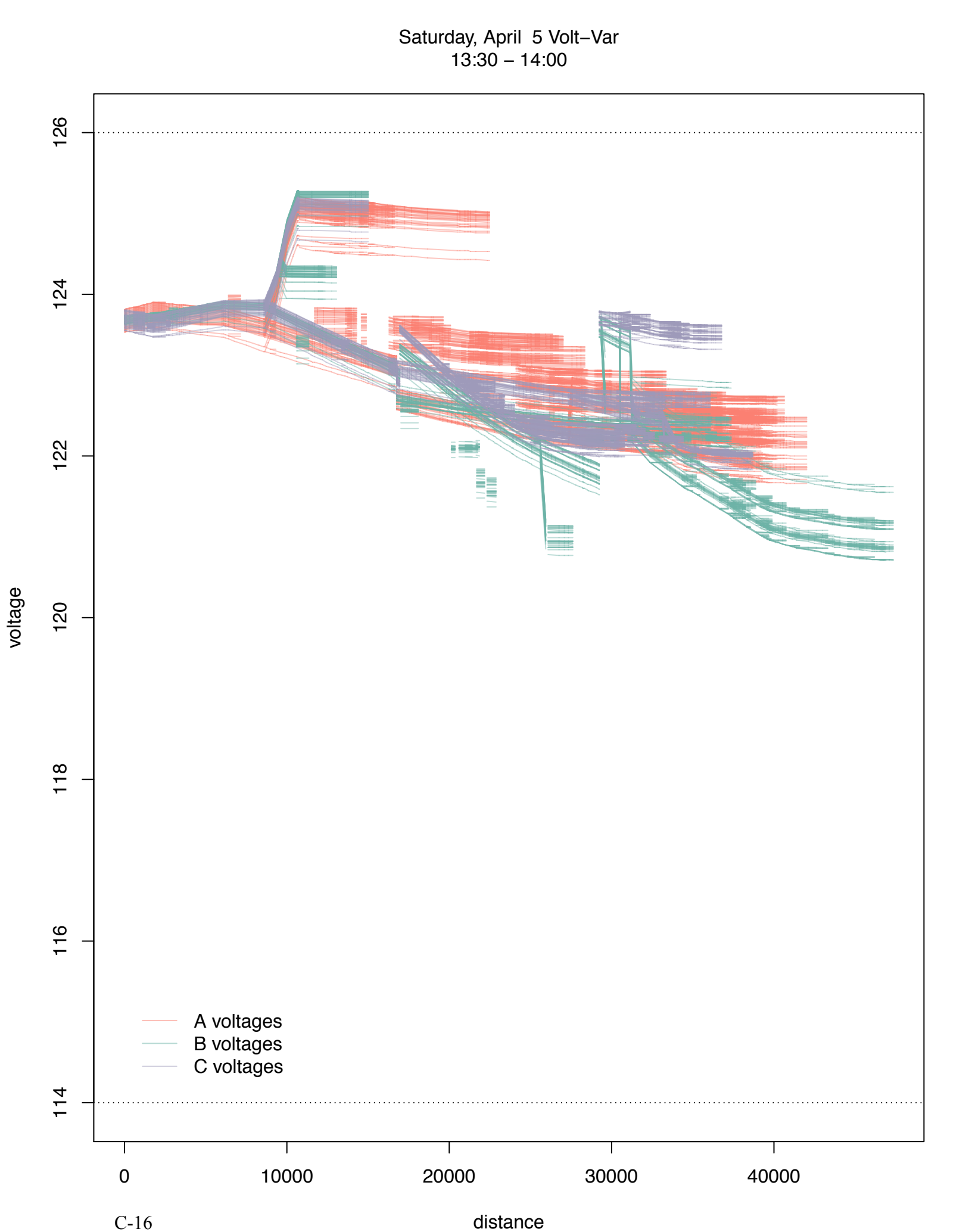

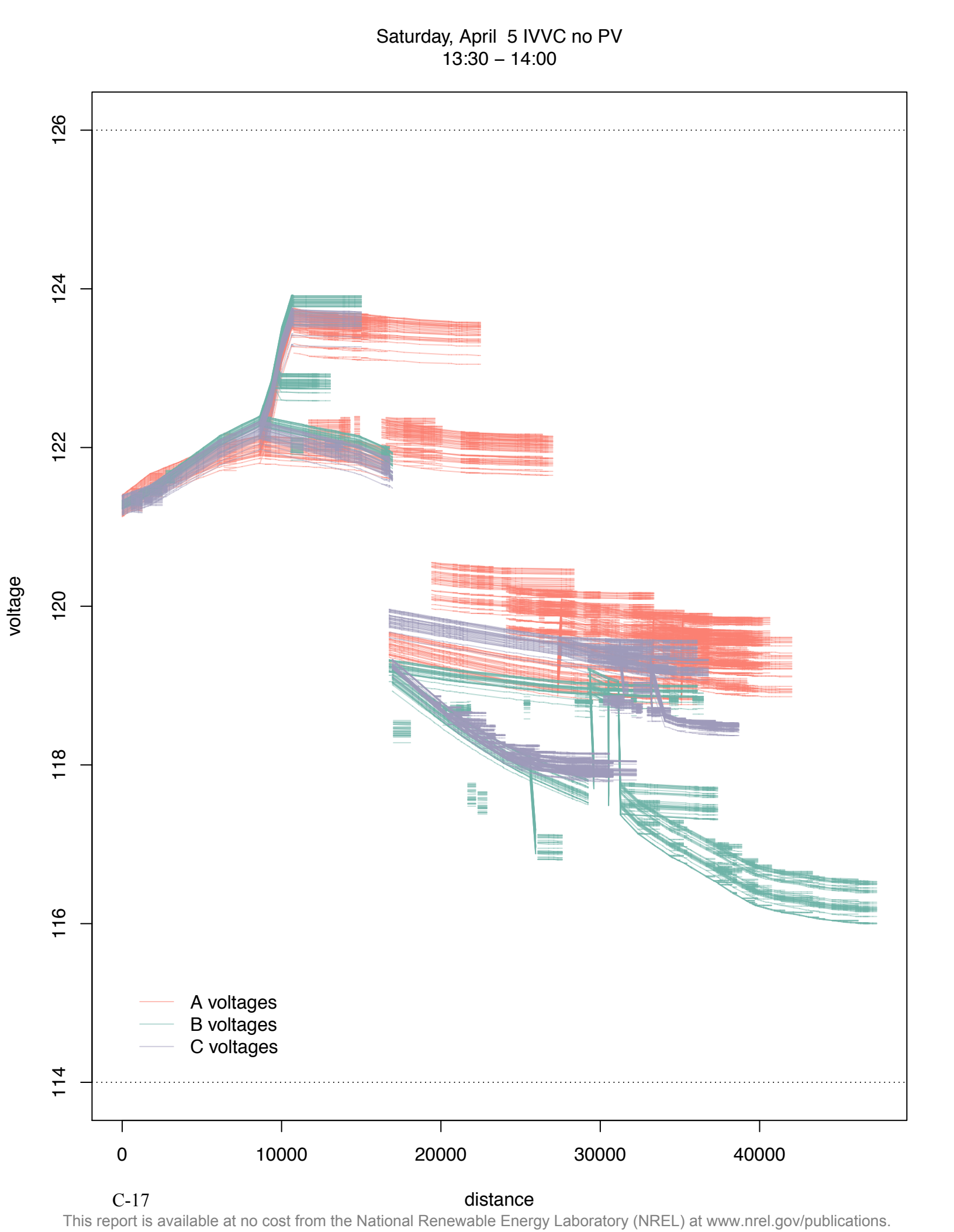

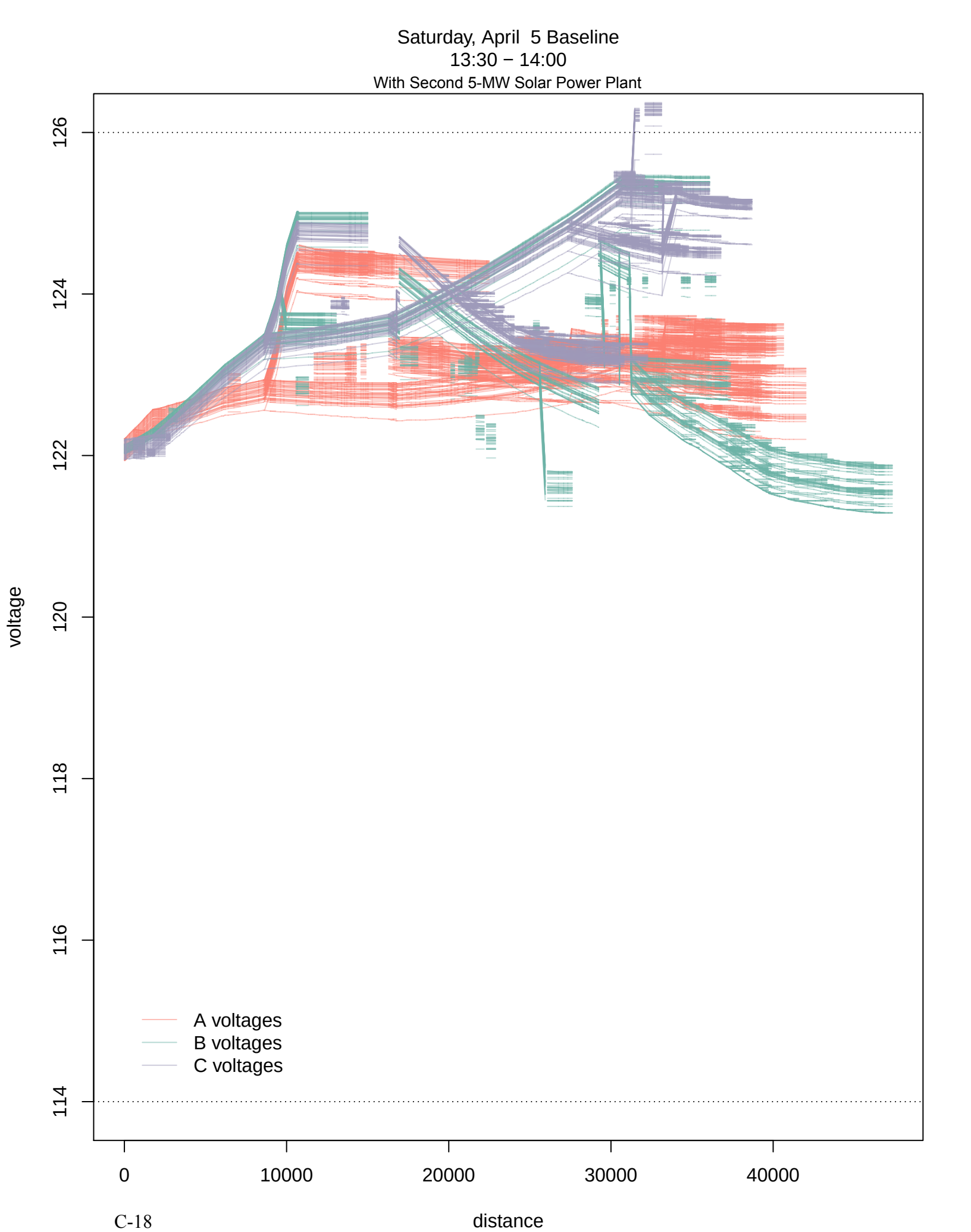

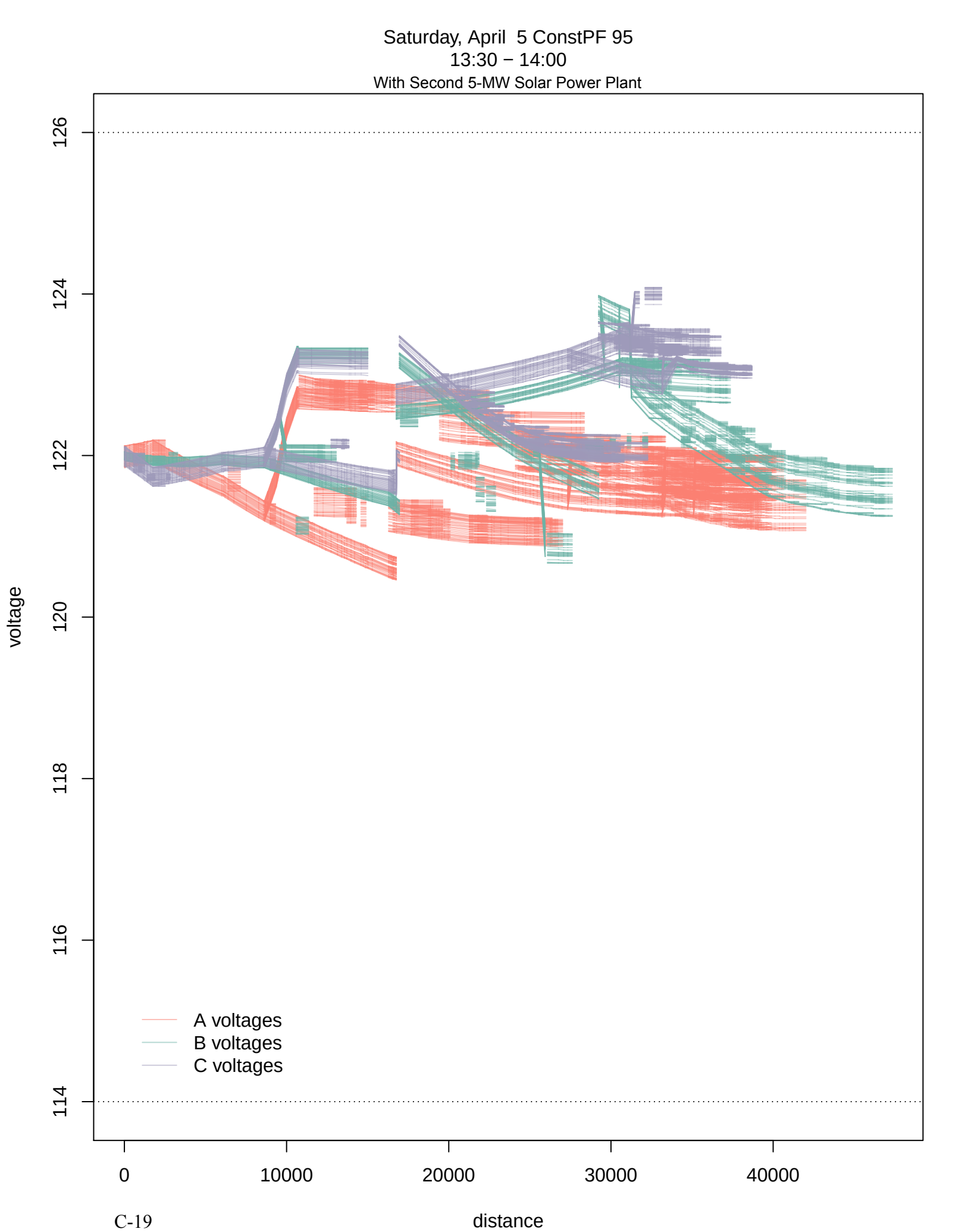

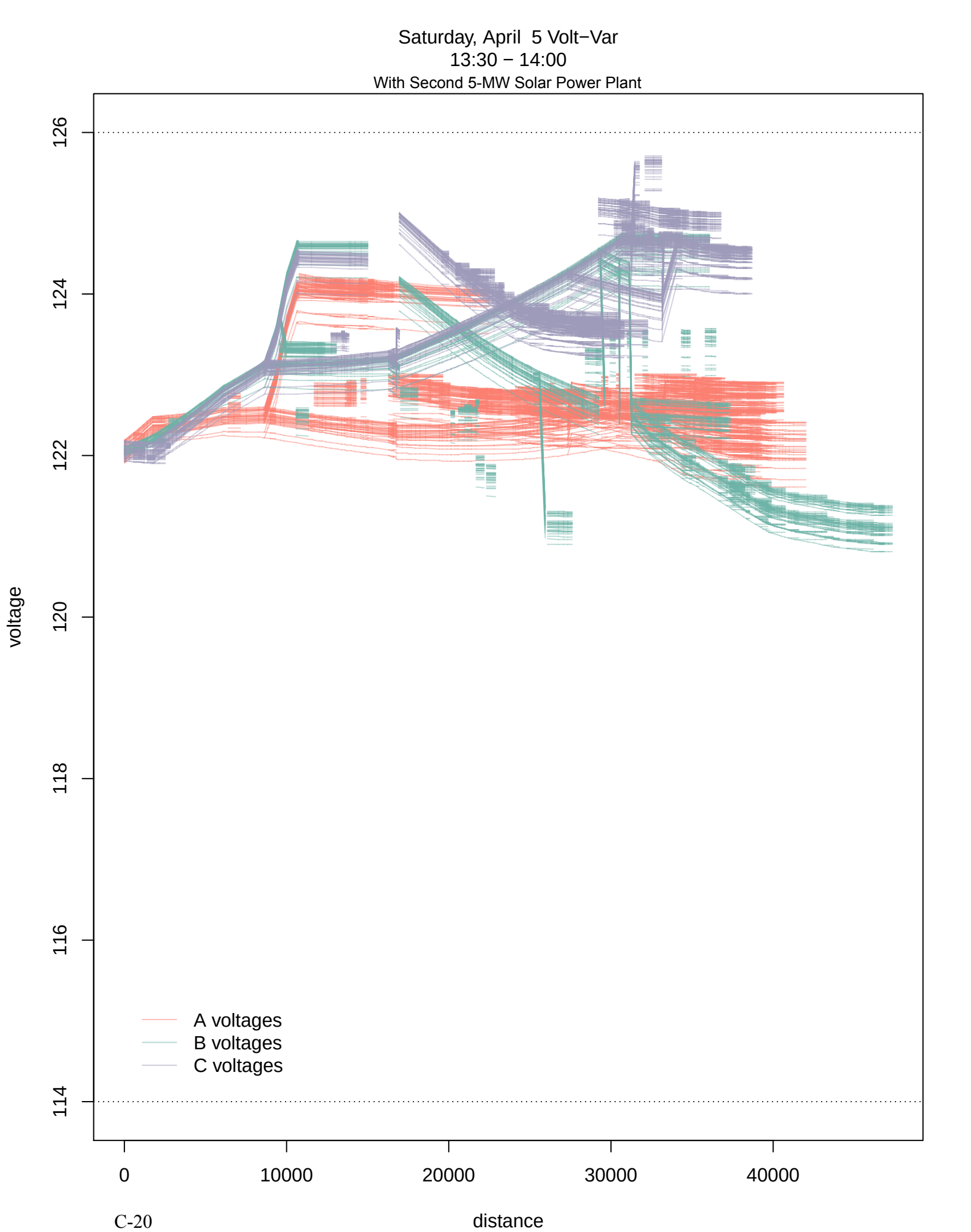

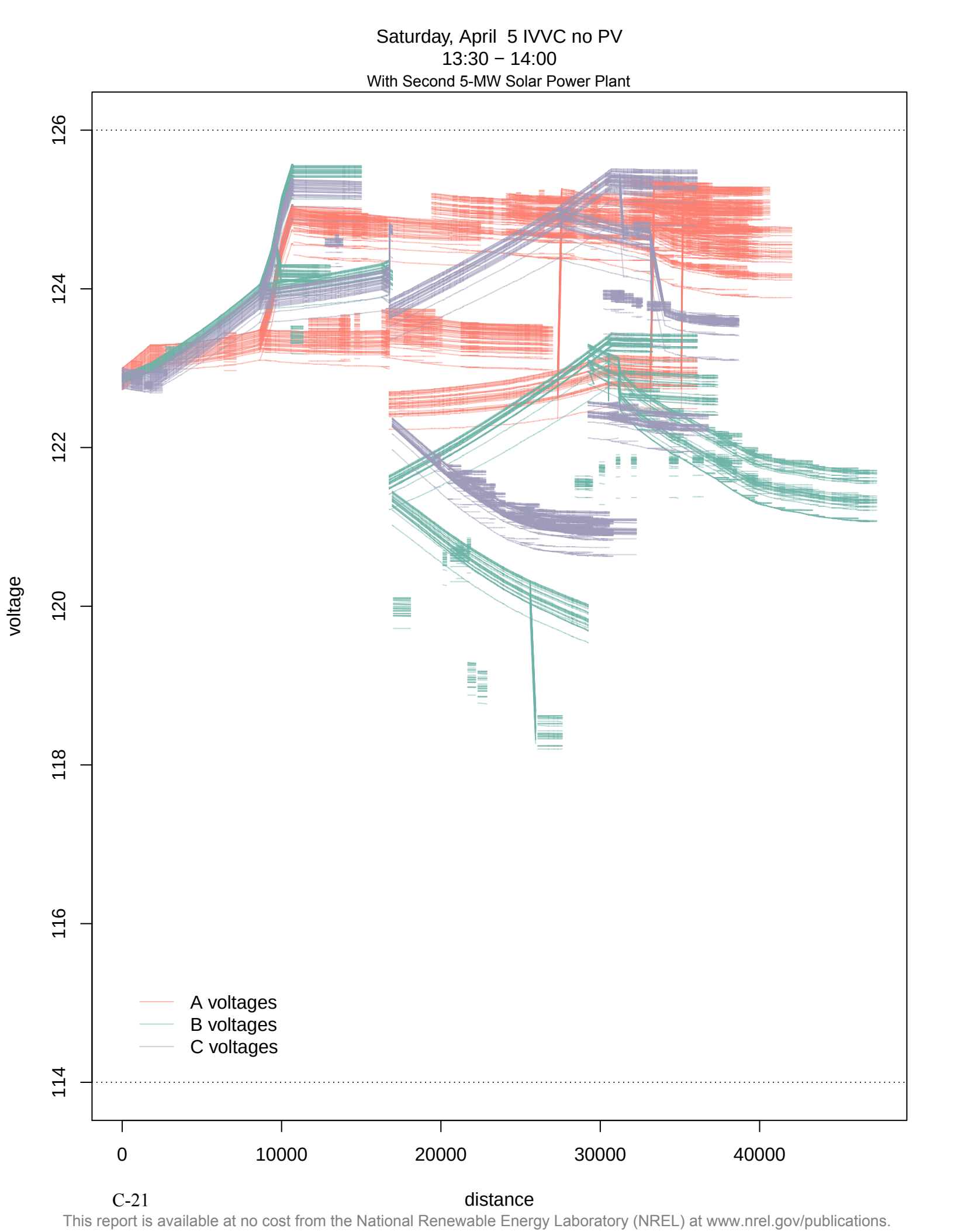

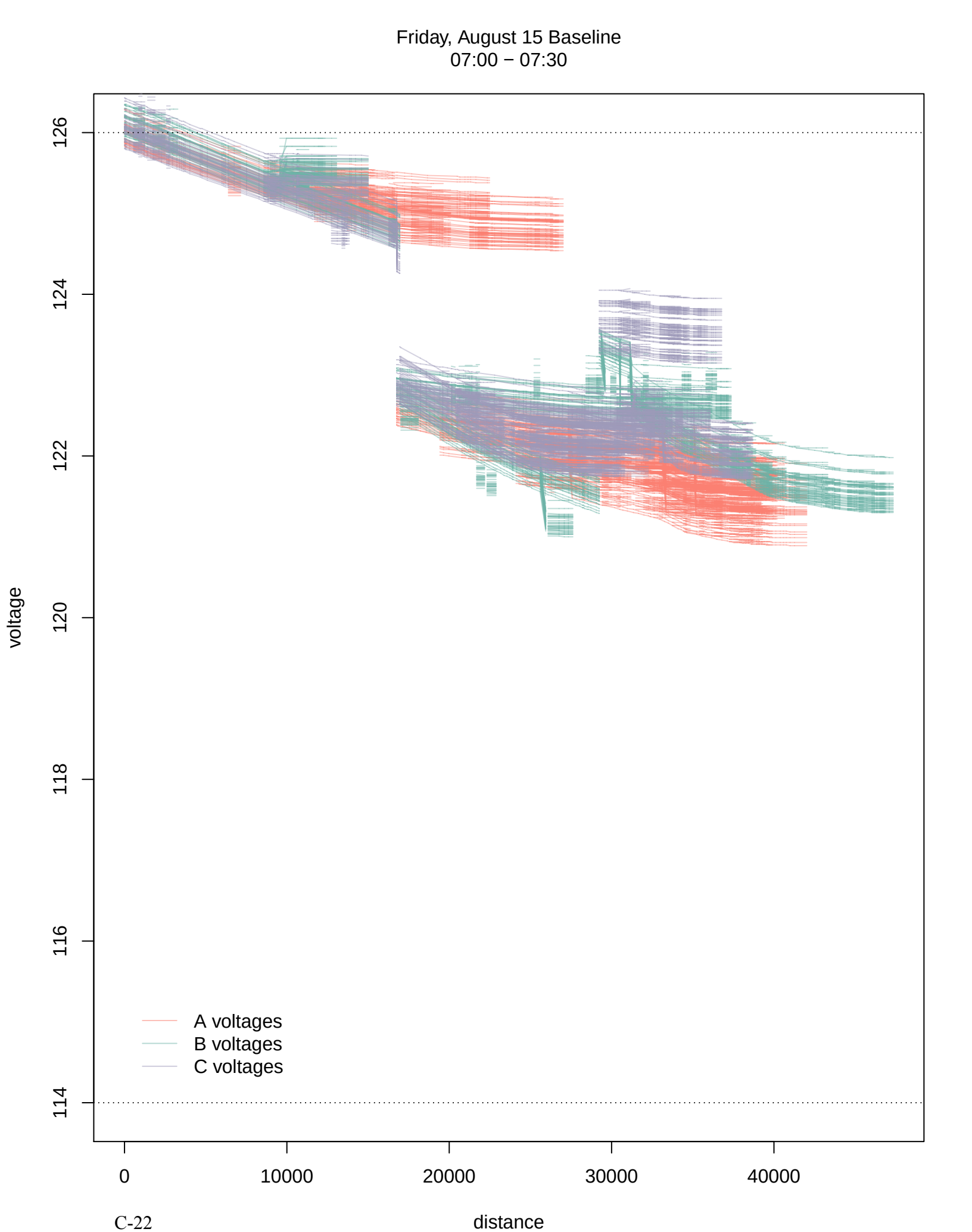

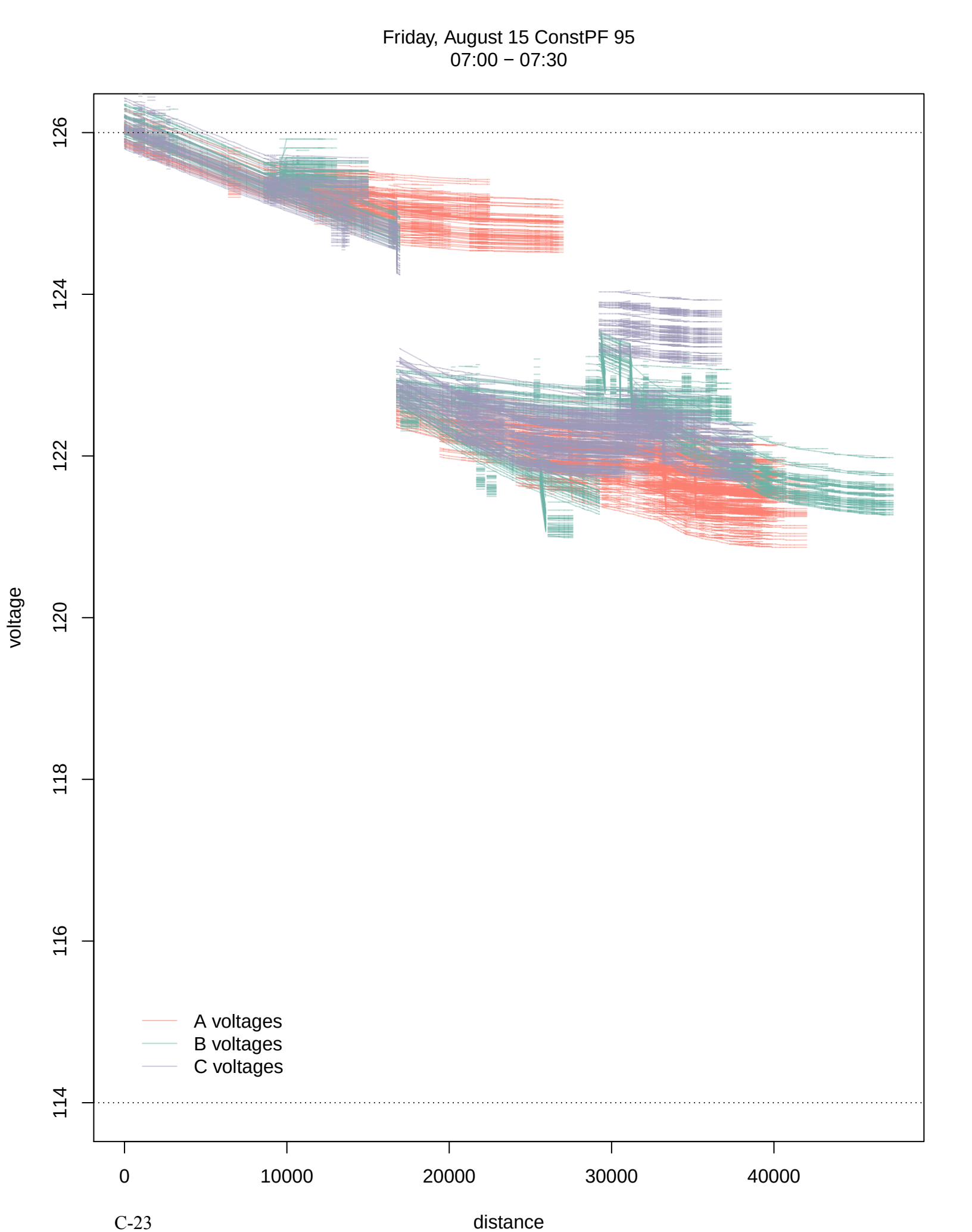

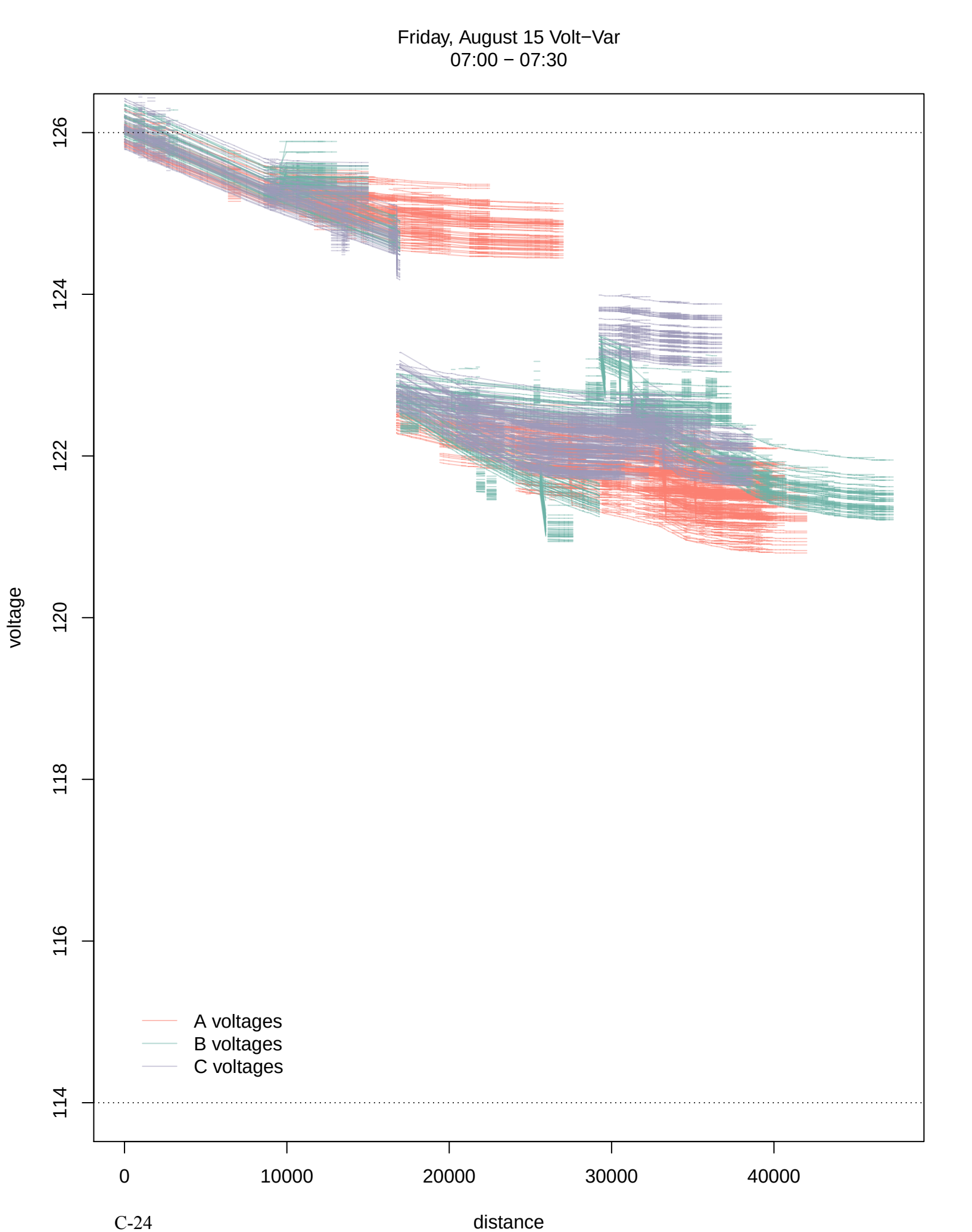

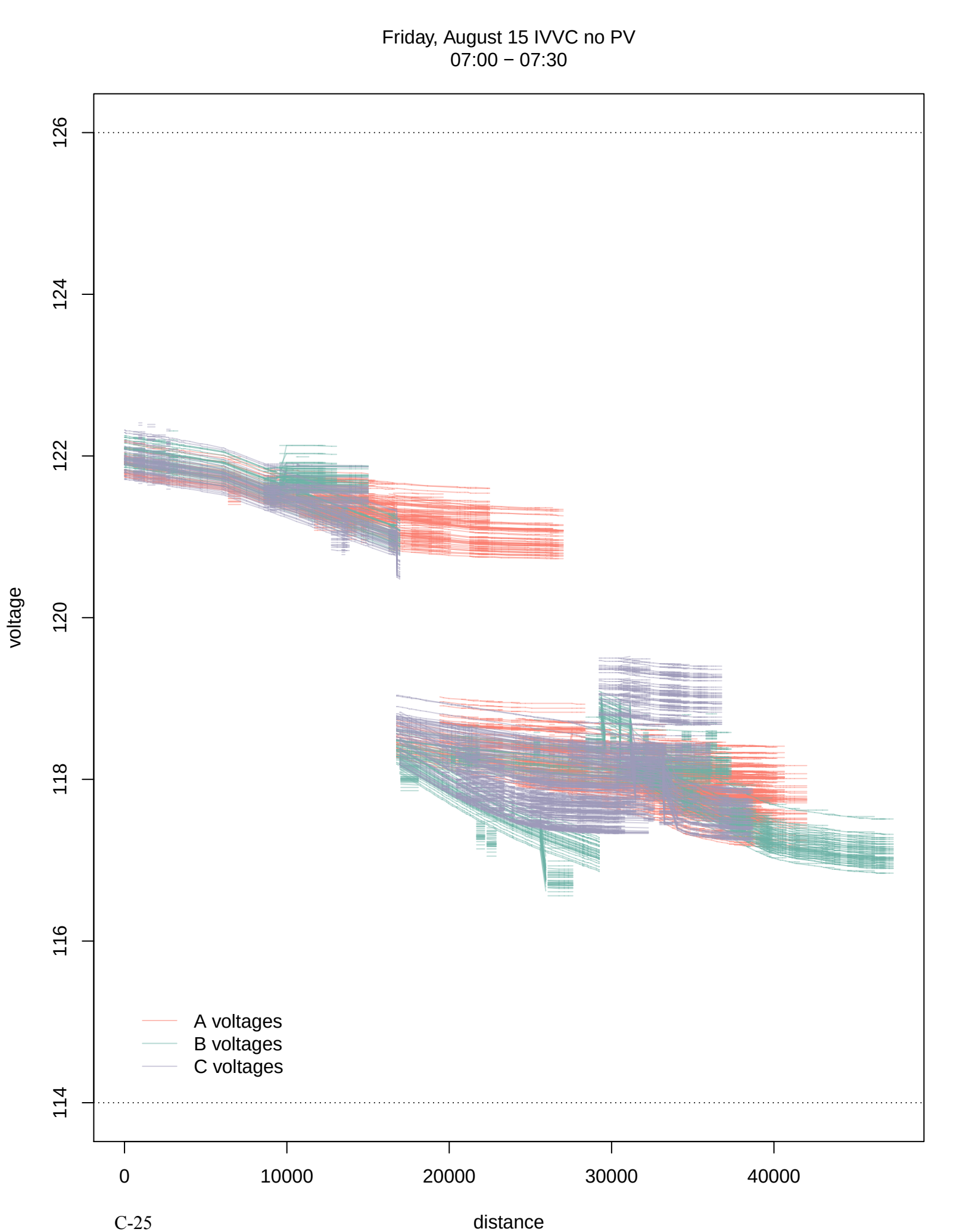

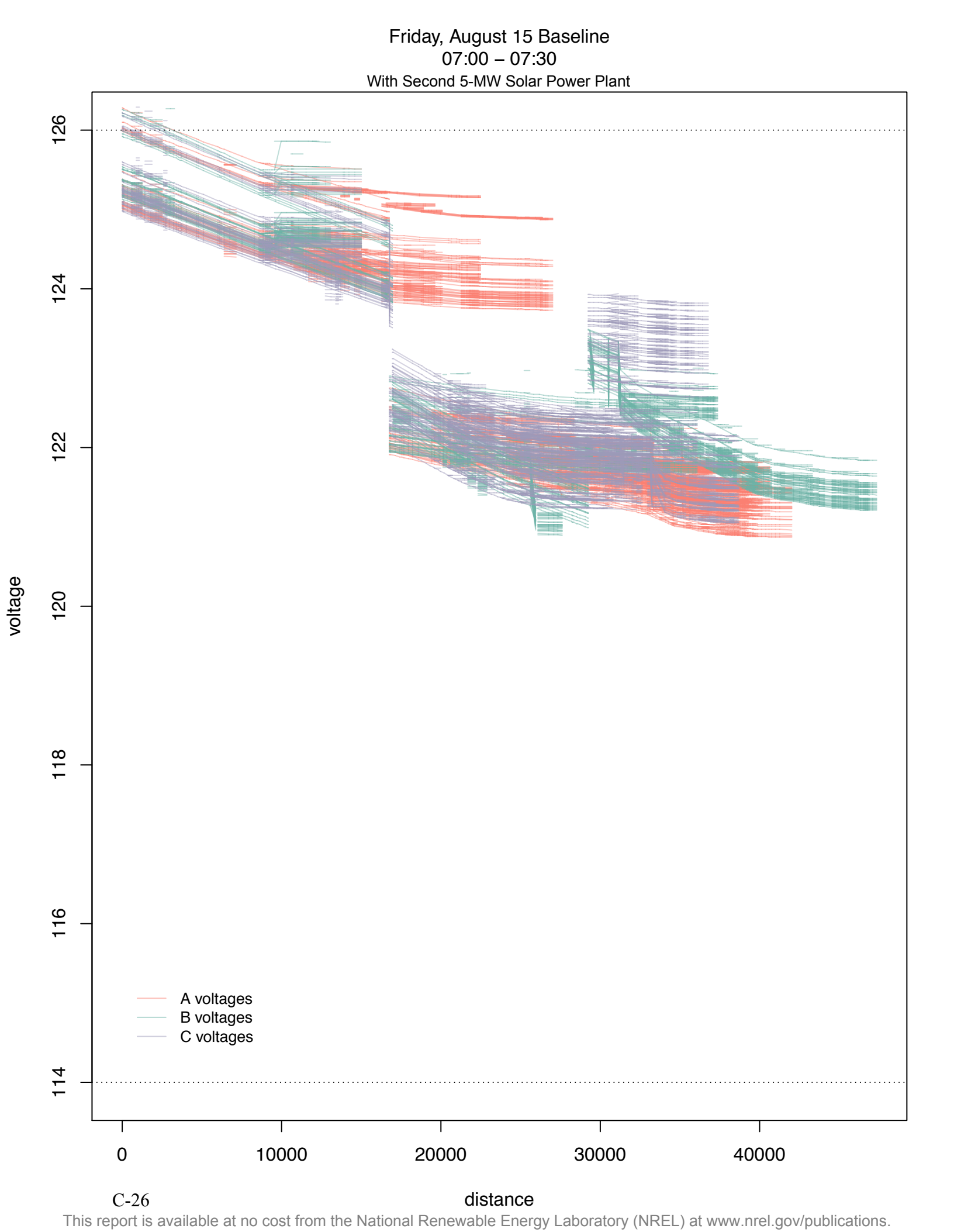

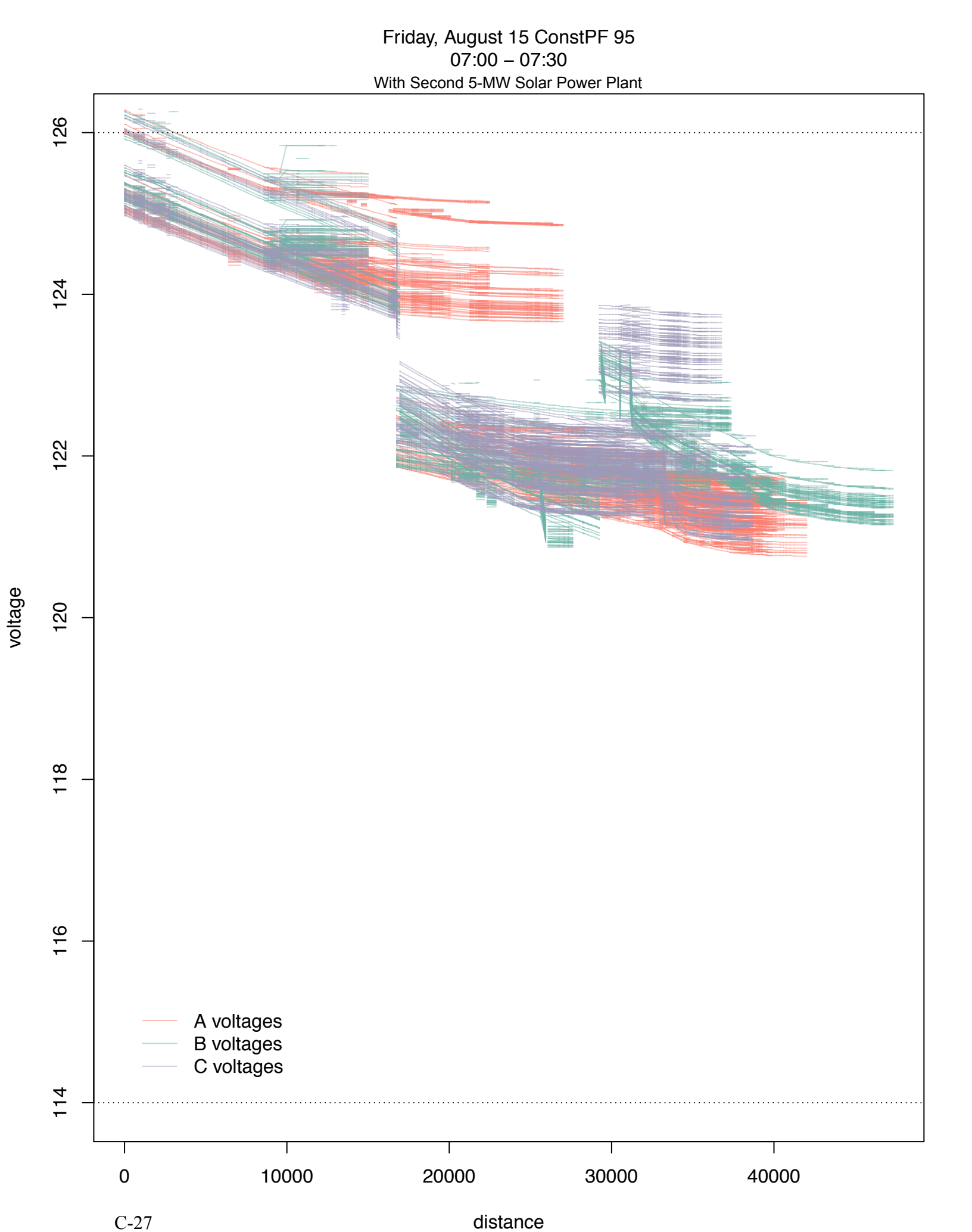

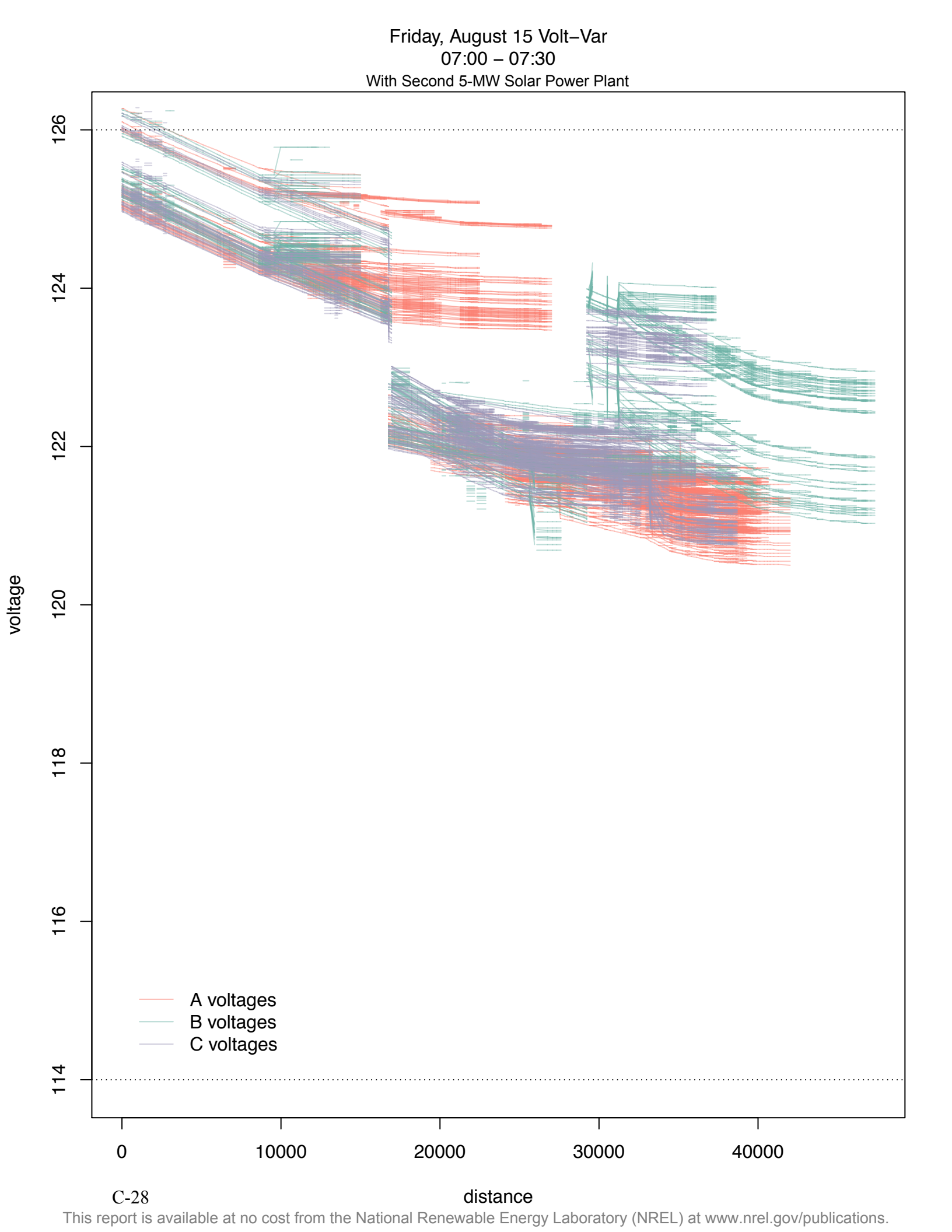

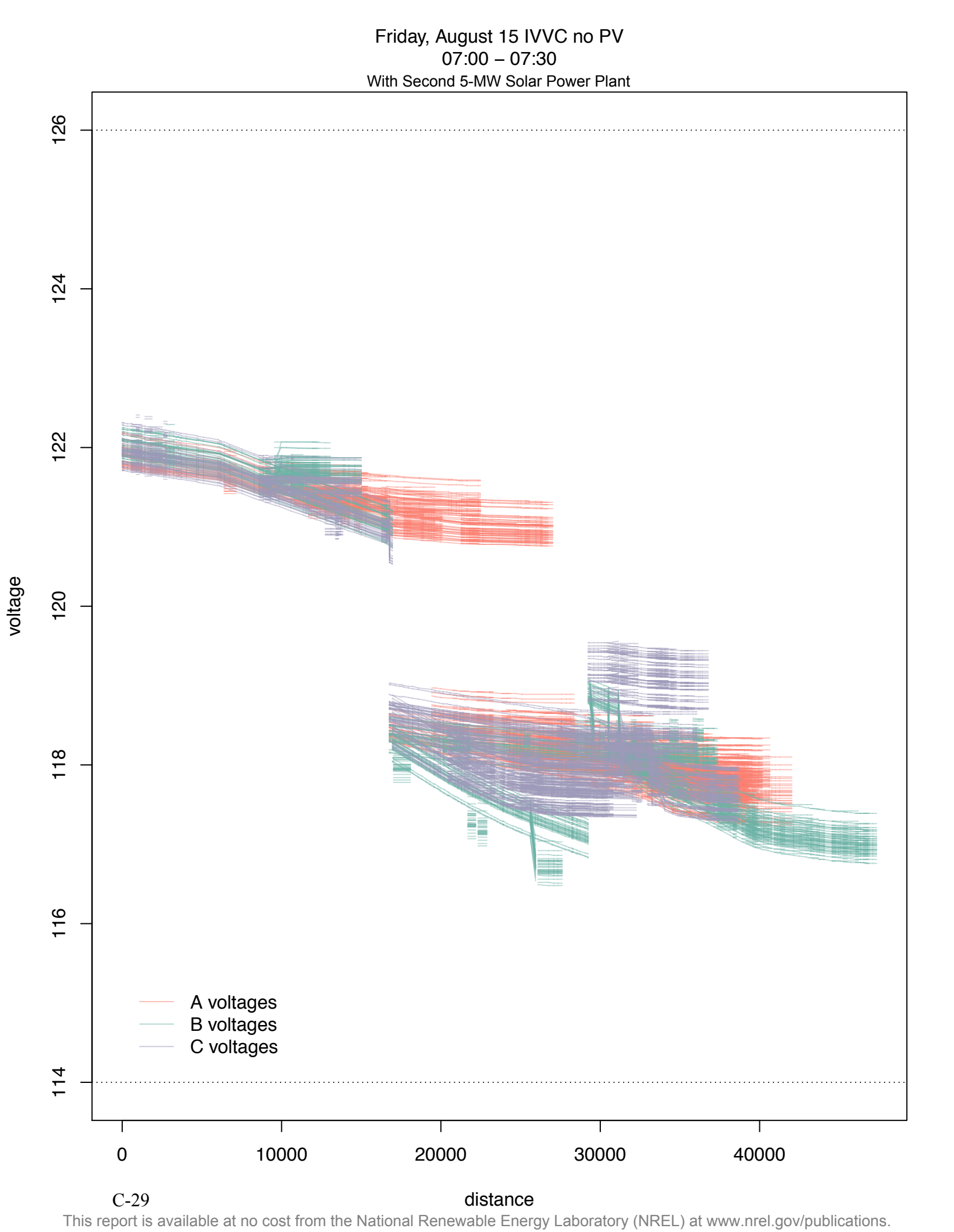

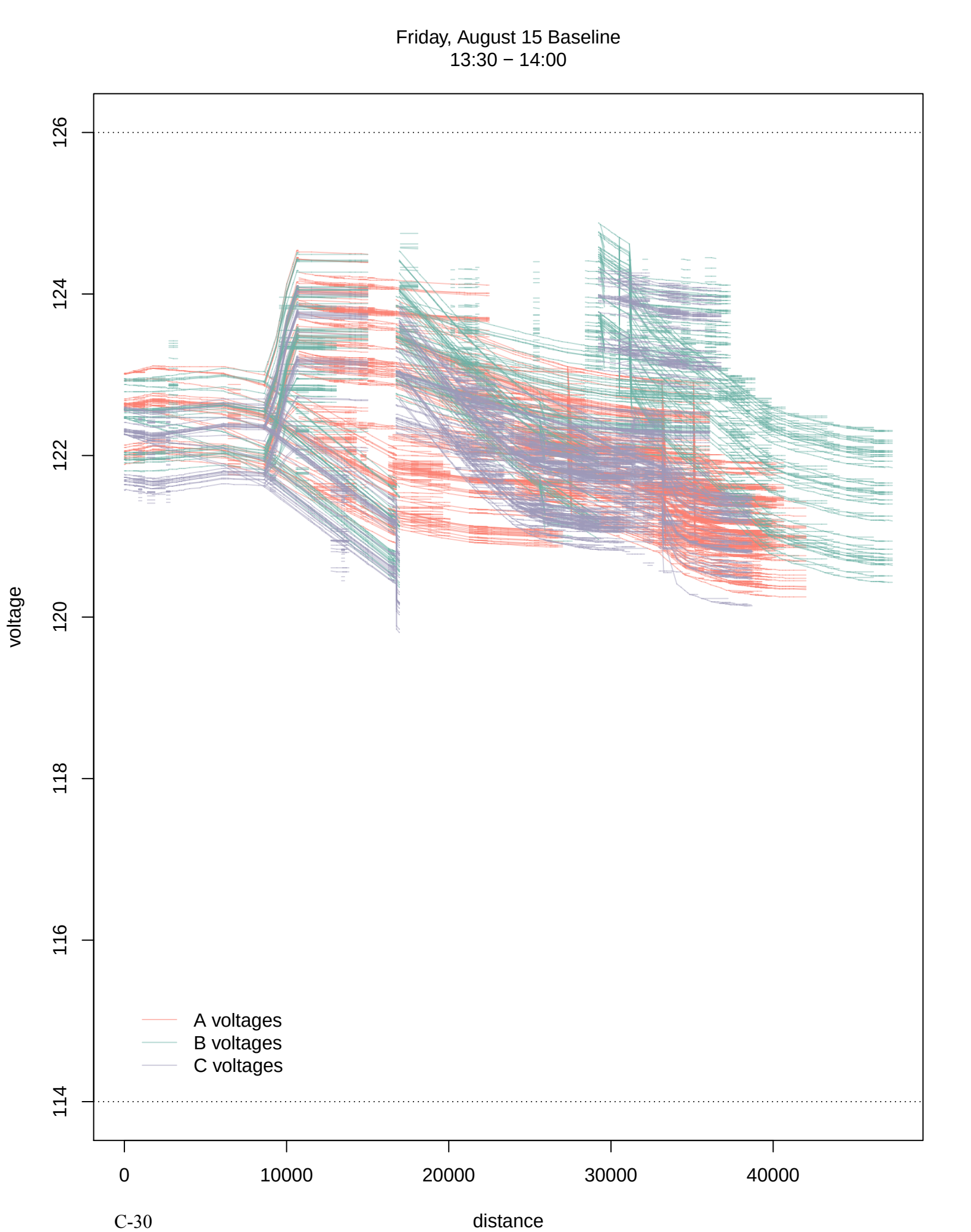

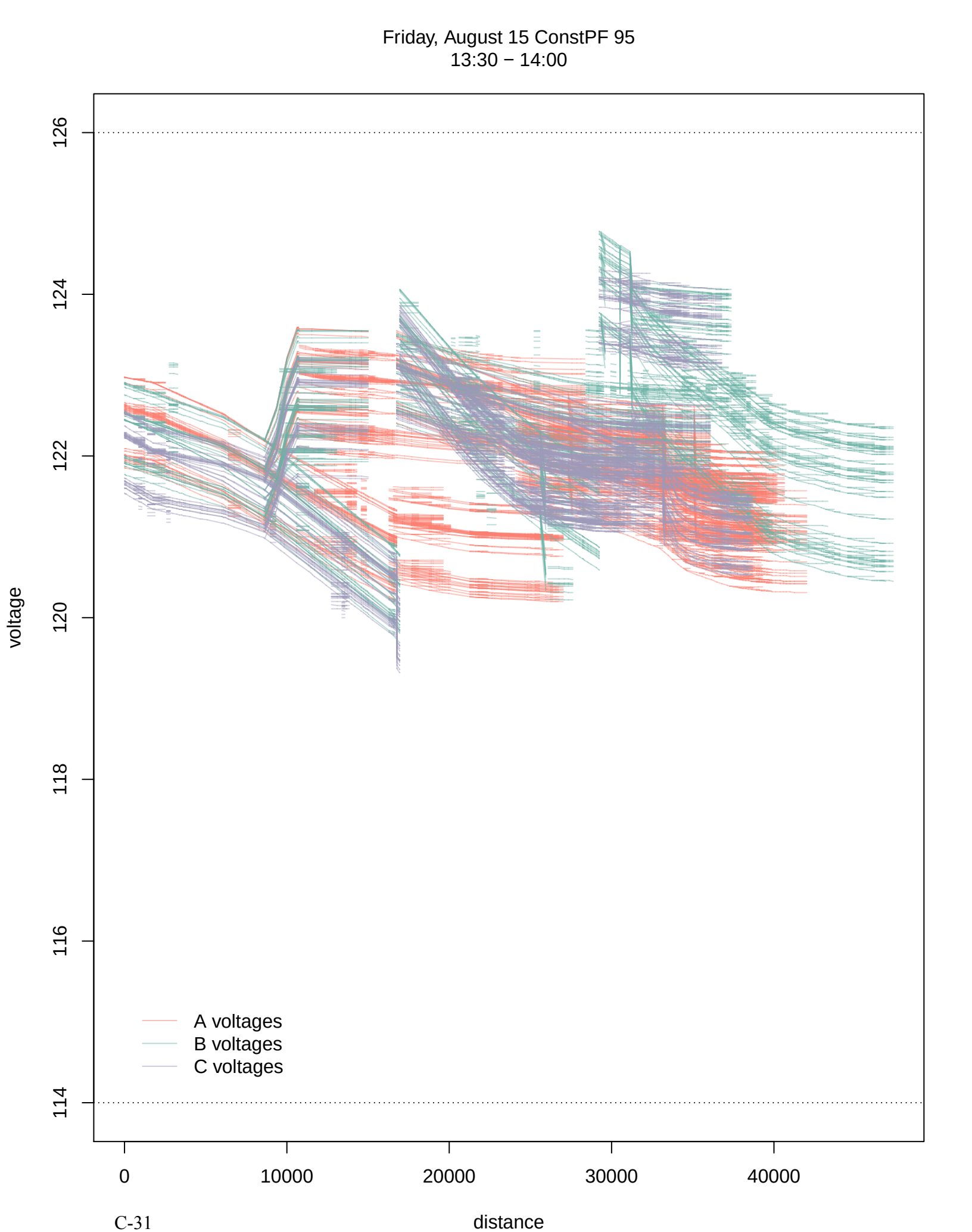

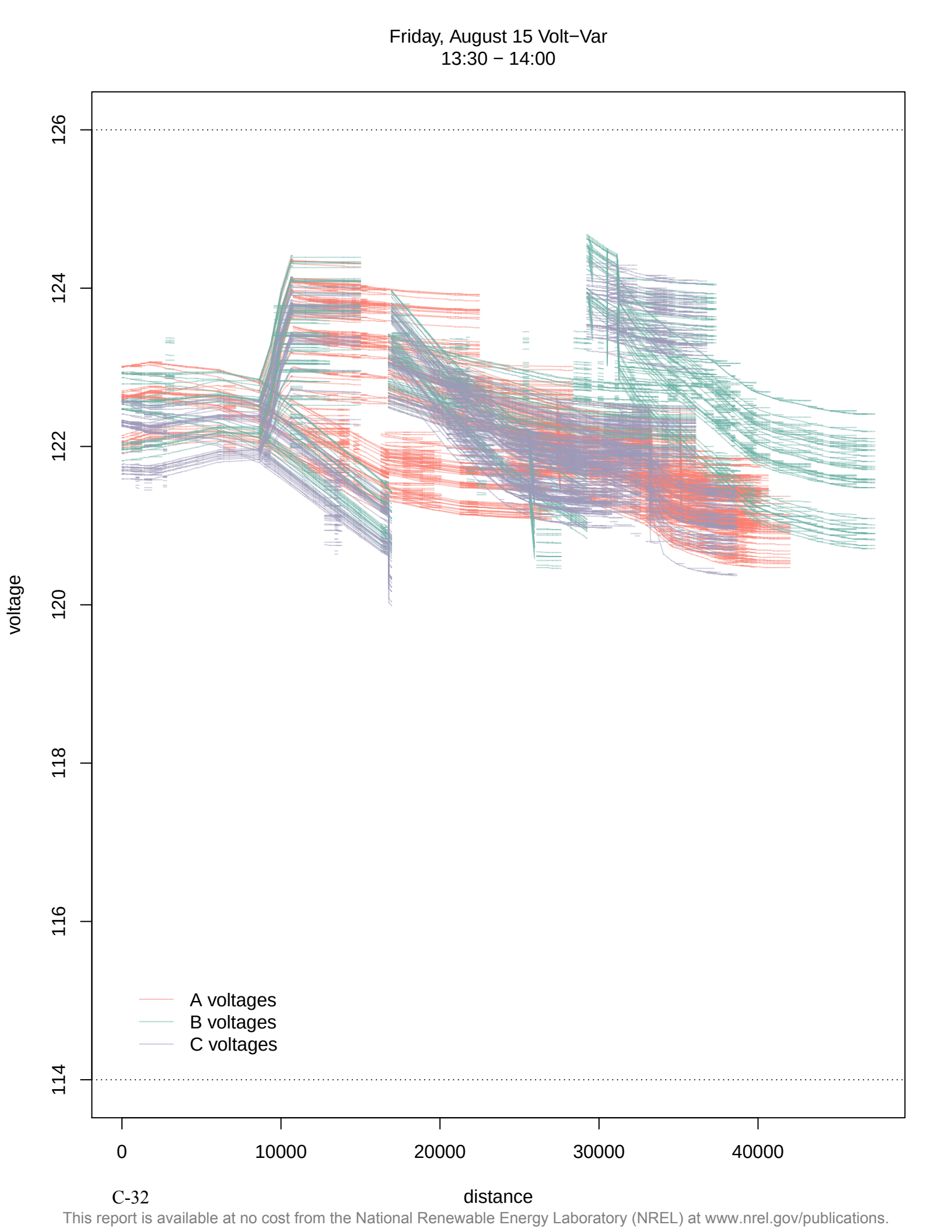

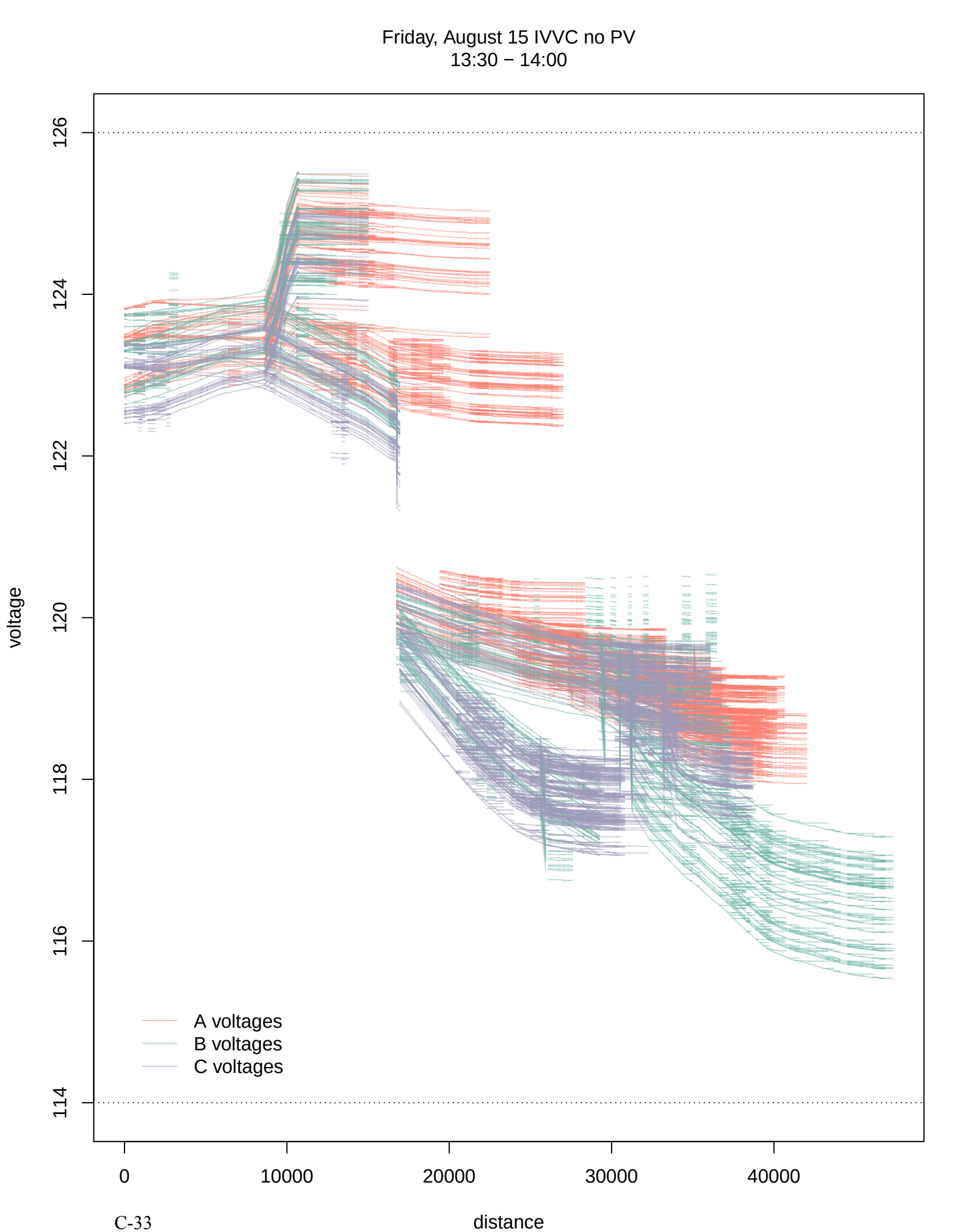

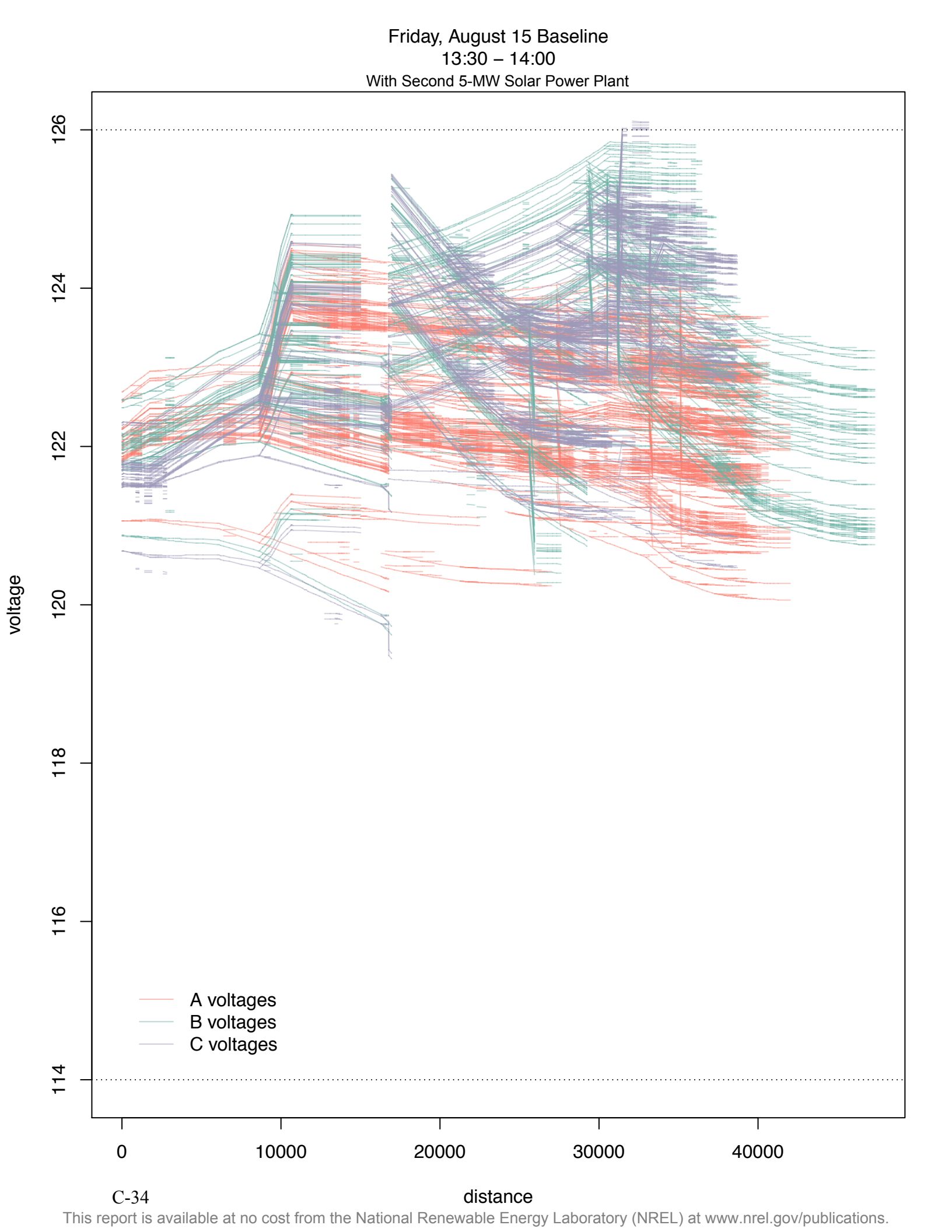

Friday, August 15 ConstPF 95
13:30 – 14:00
With Second 5-MW Solar Power Plant

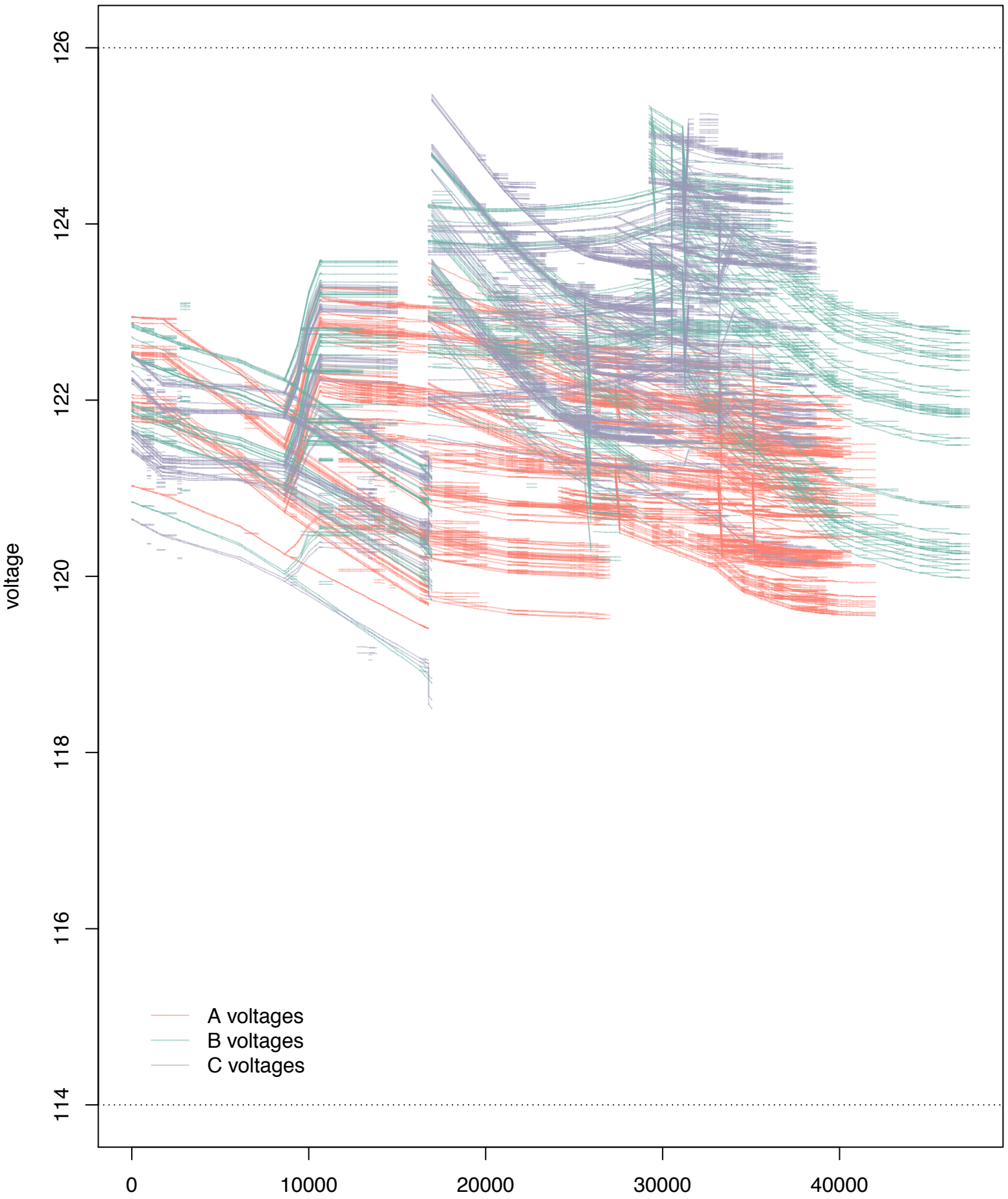

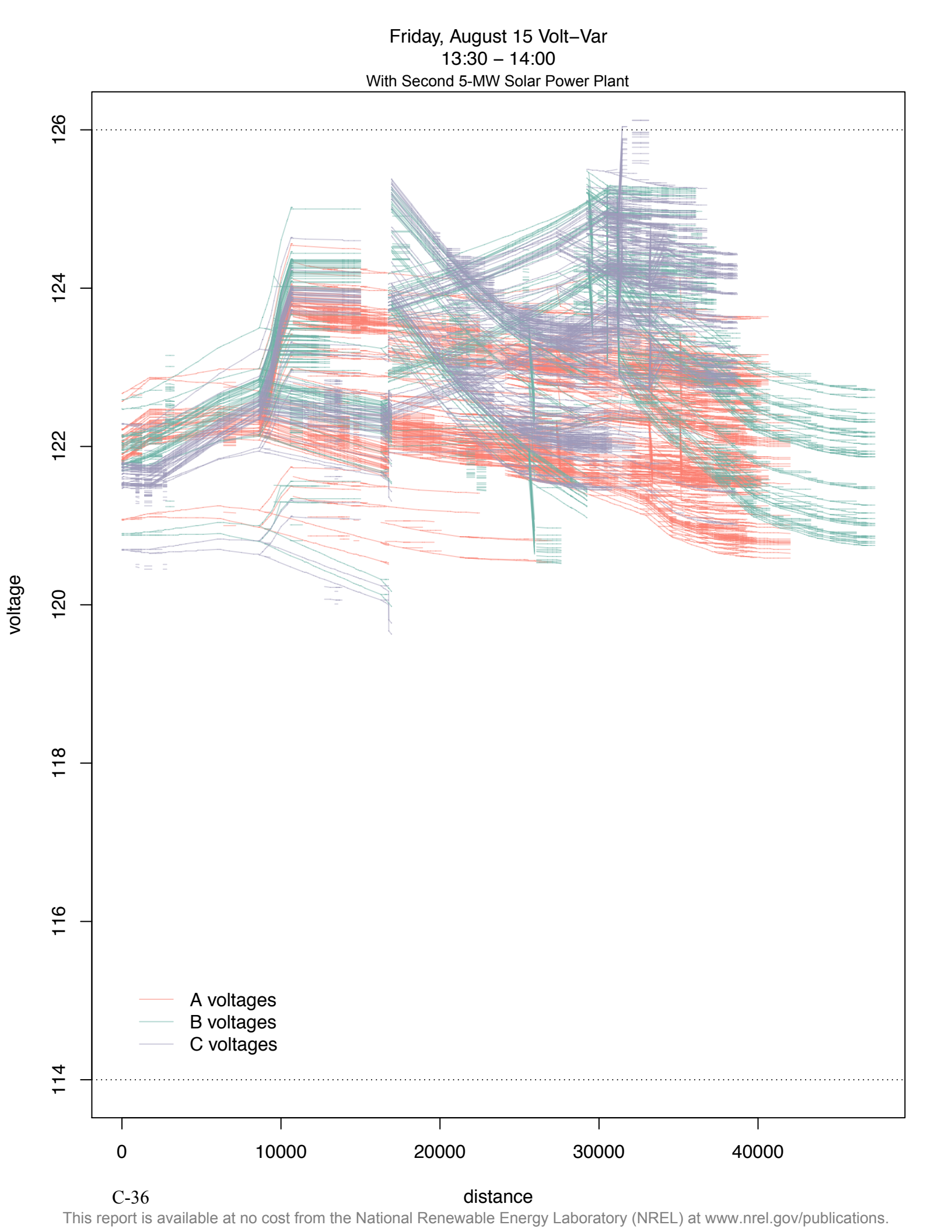

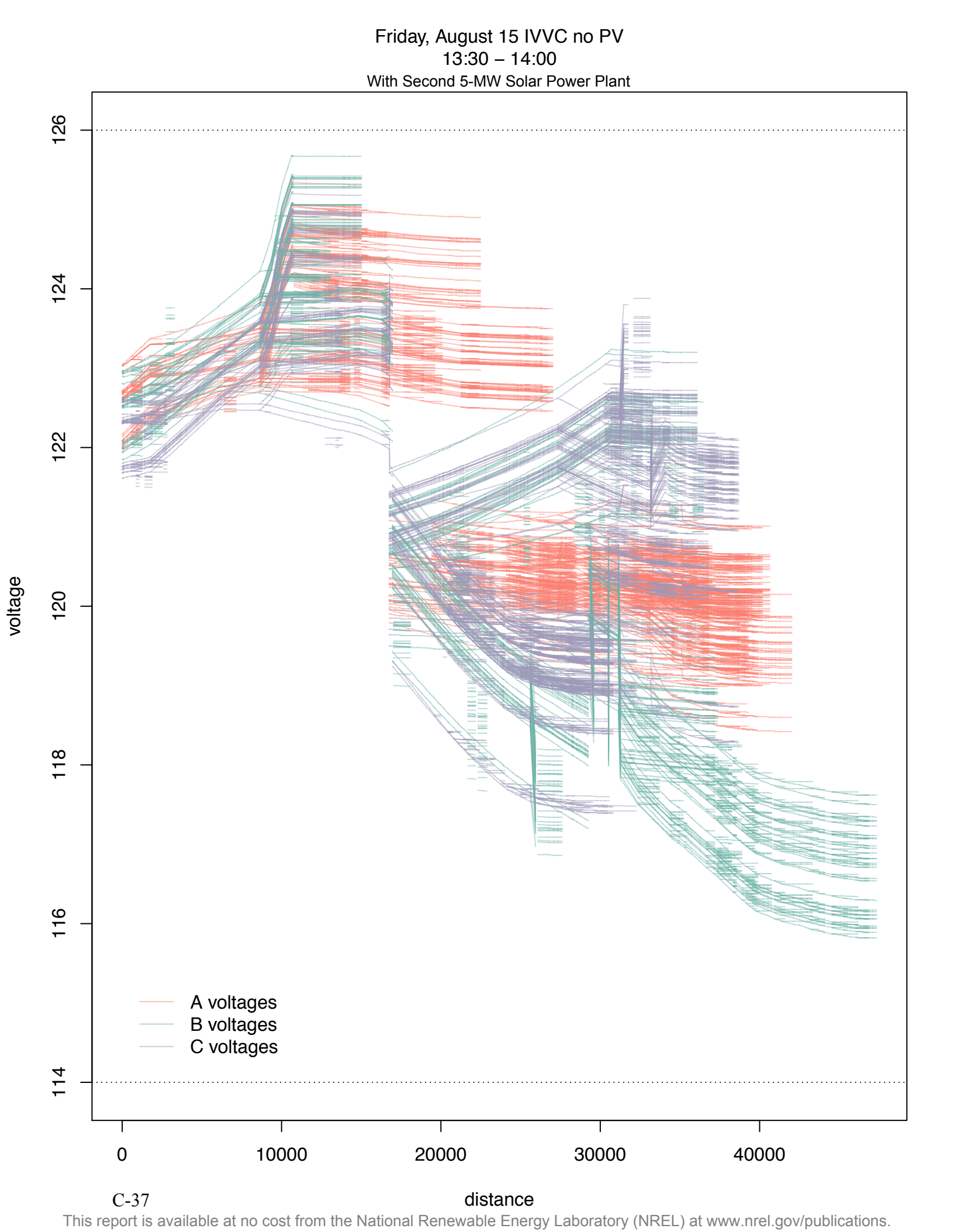

## C.3 Complete 40-Day Results

Figures begin on next page.

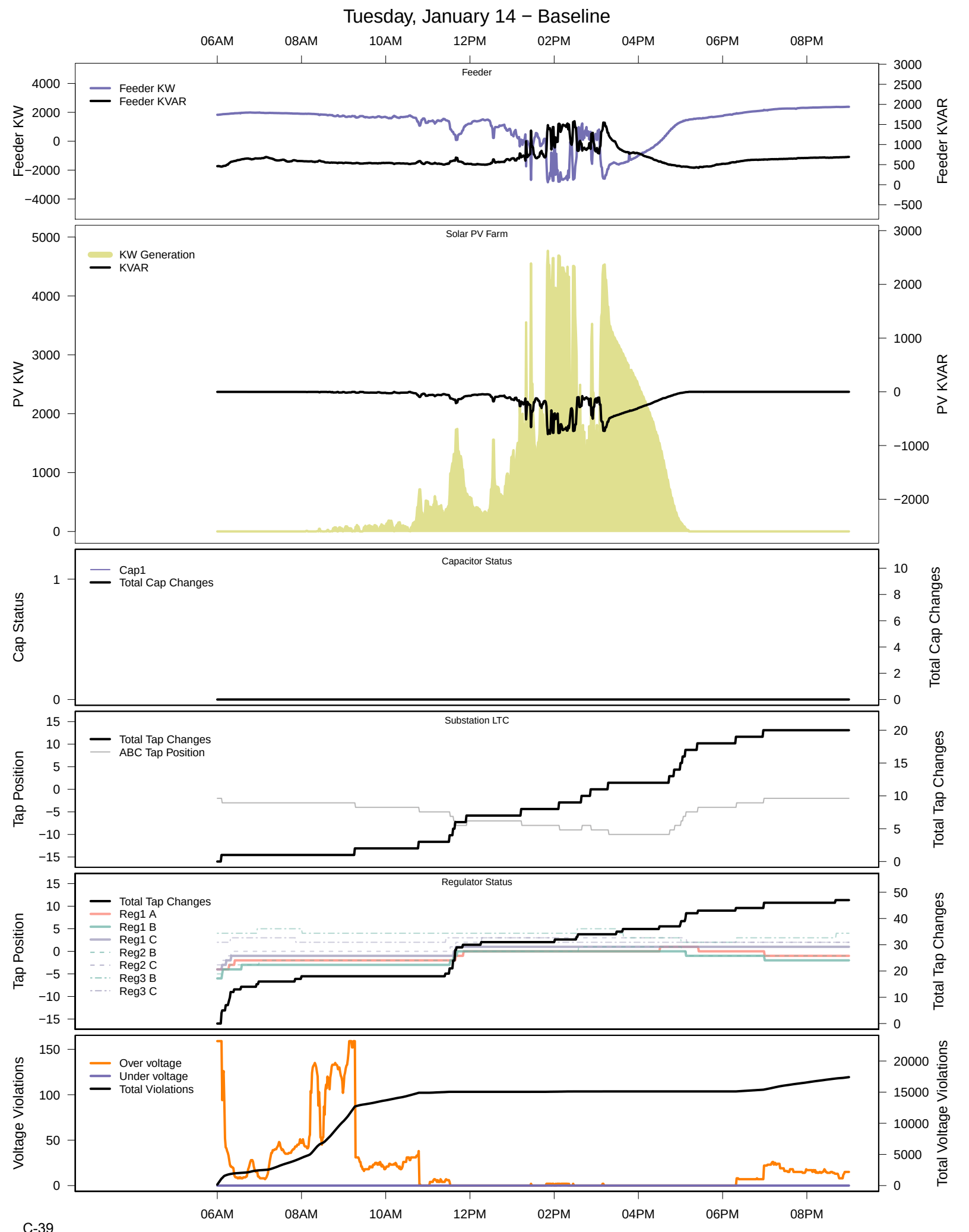

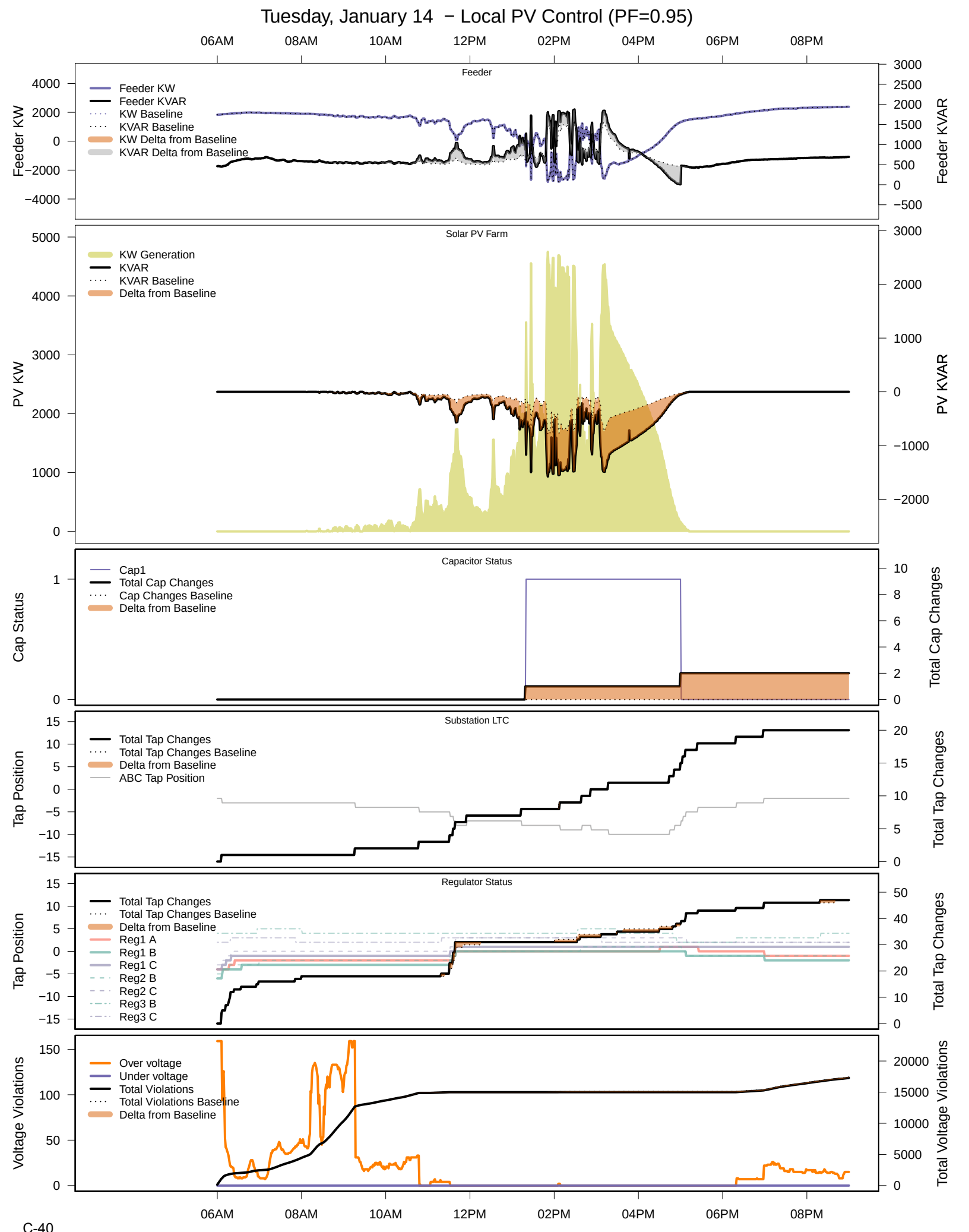

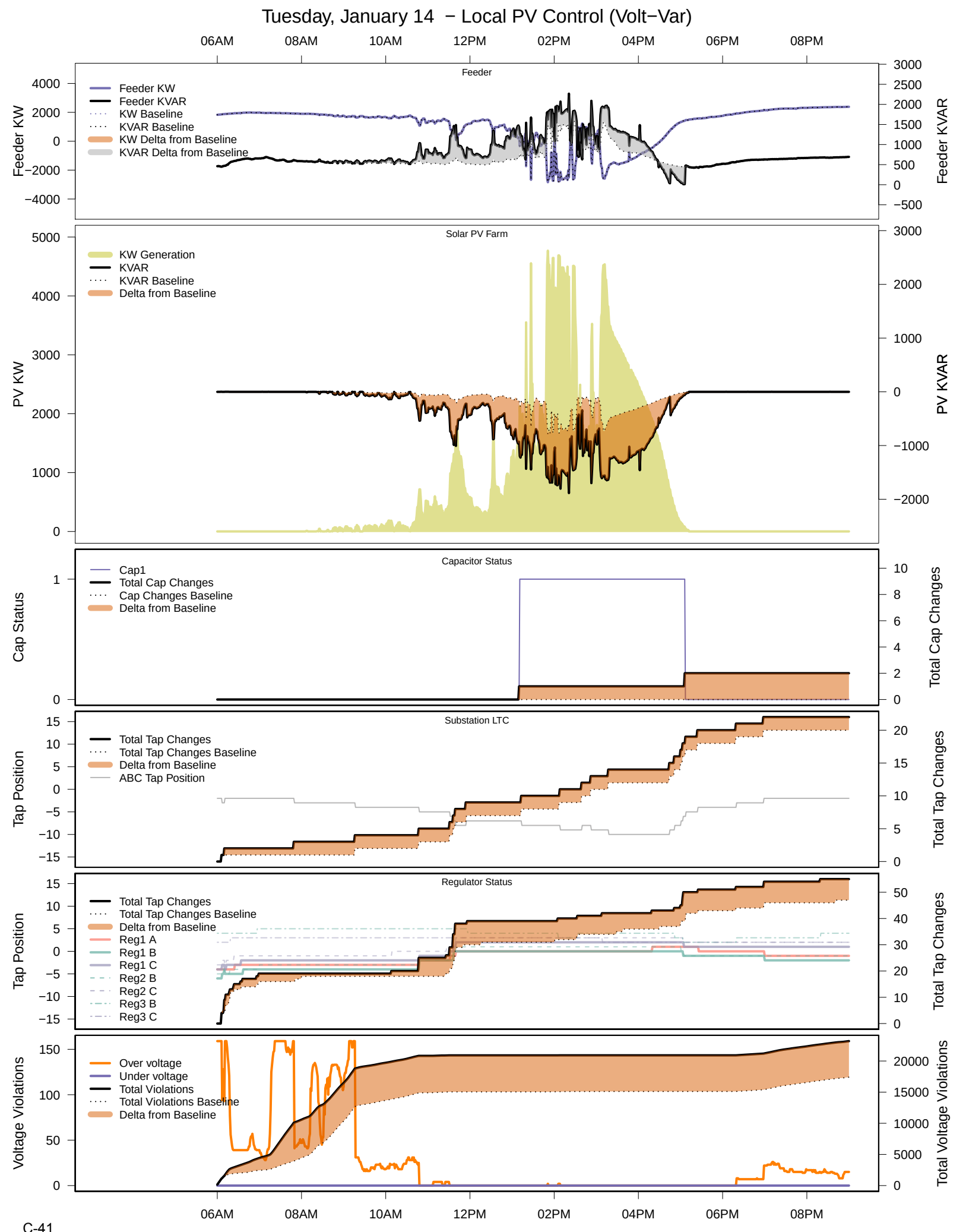

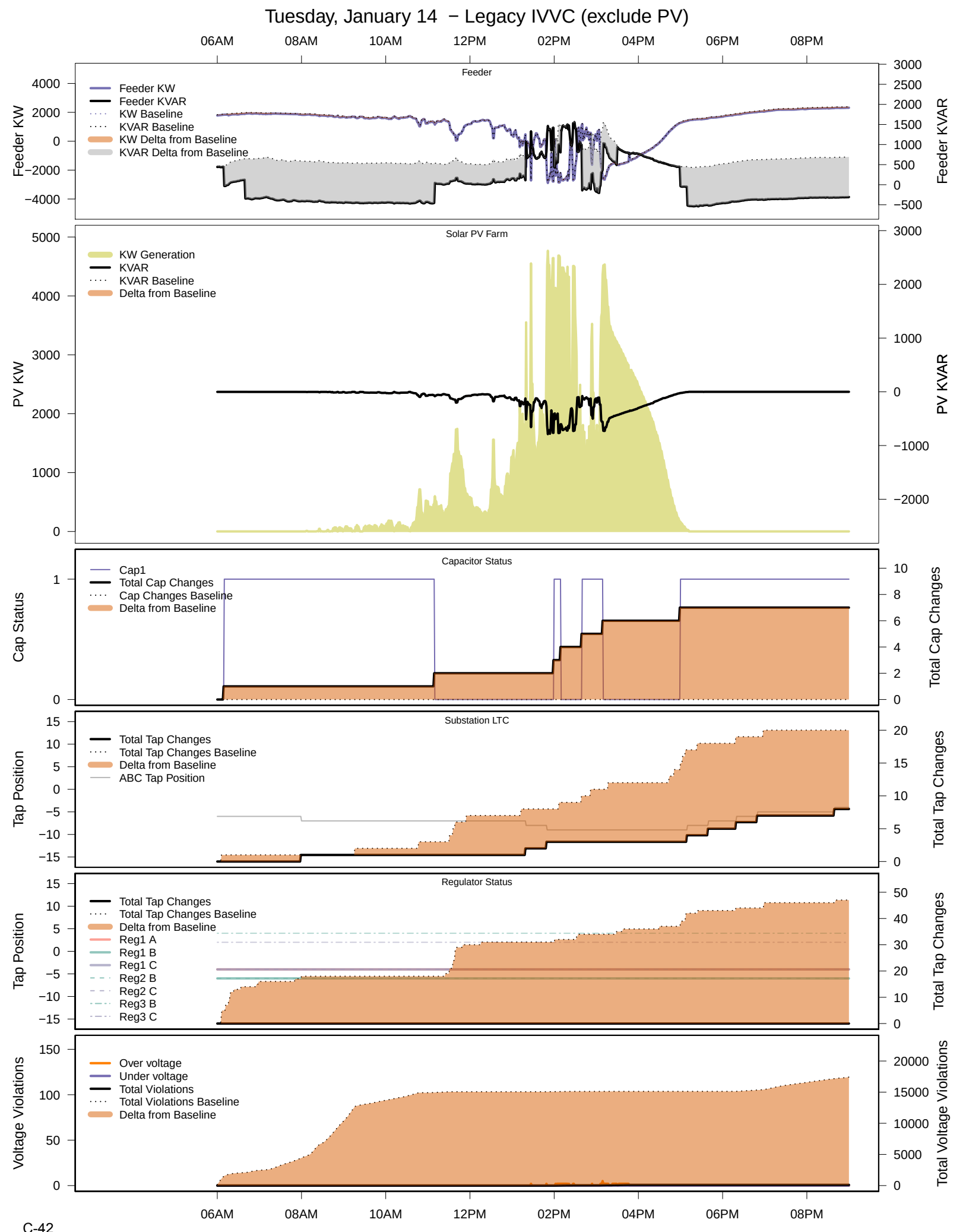

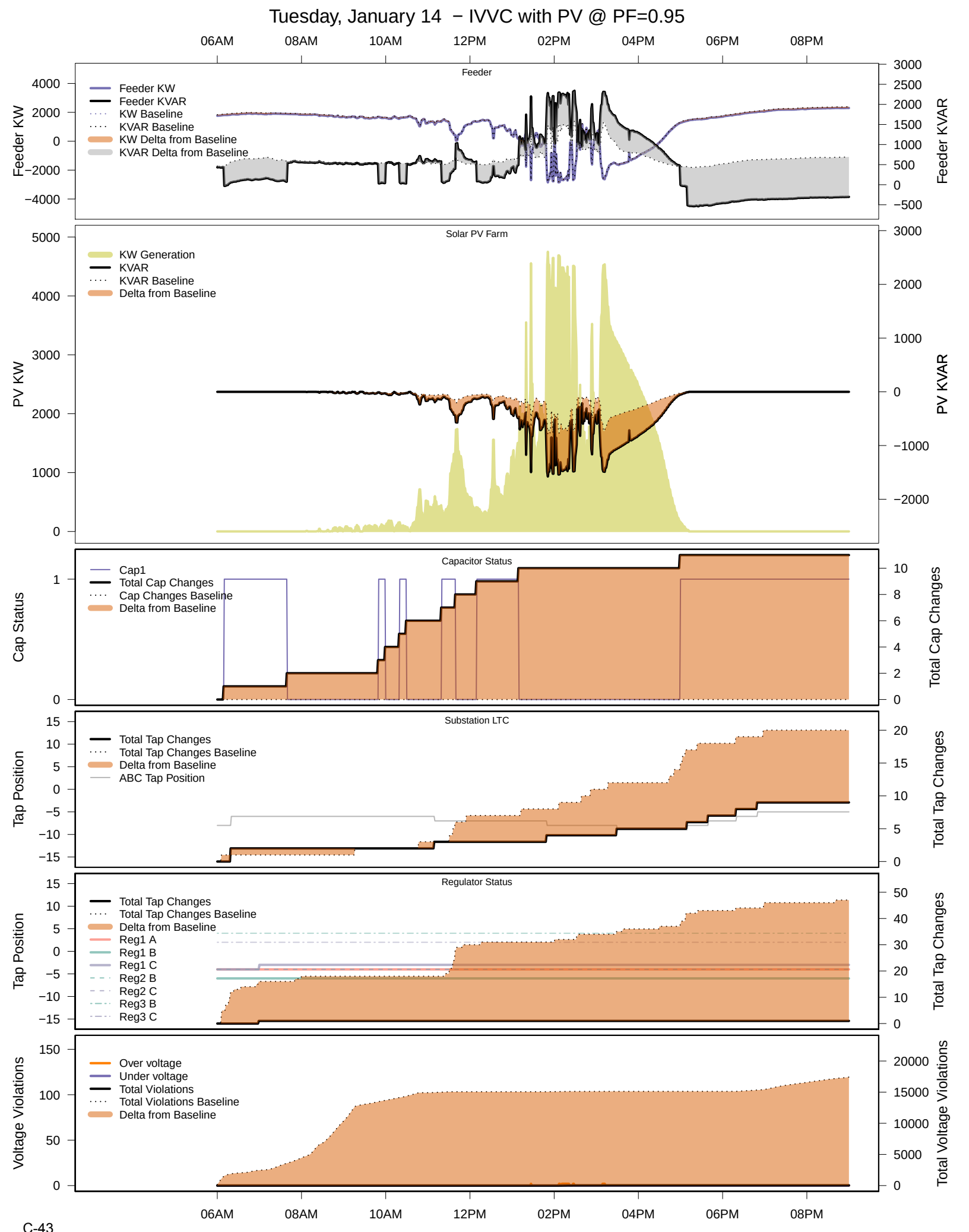

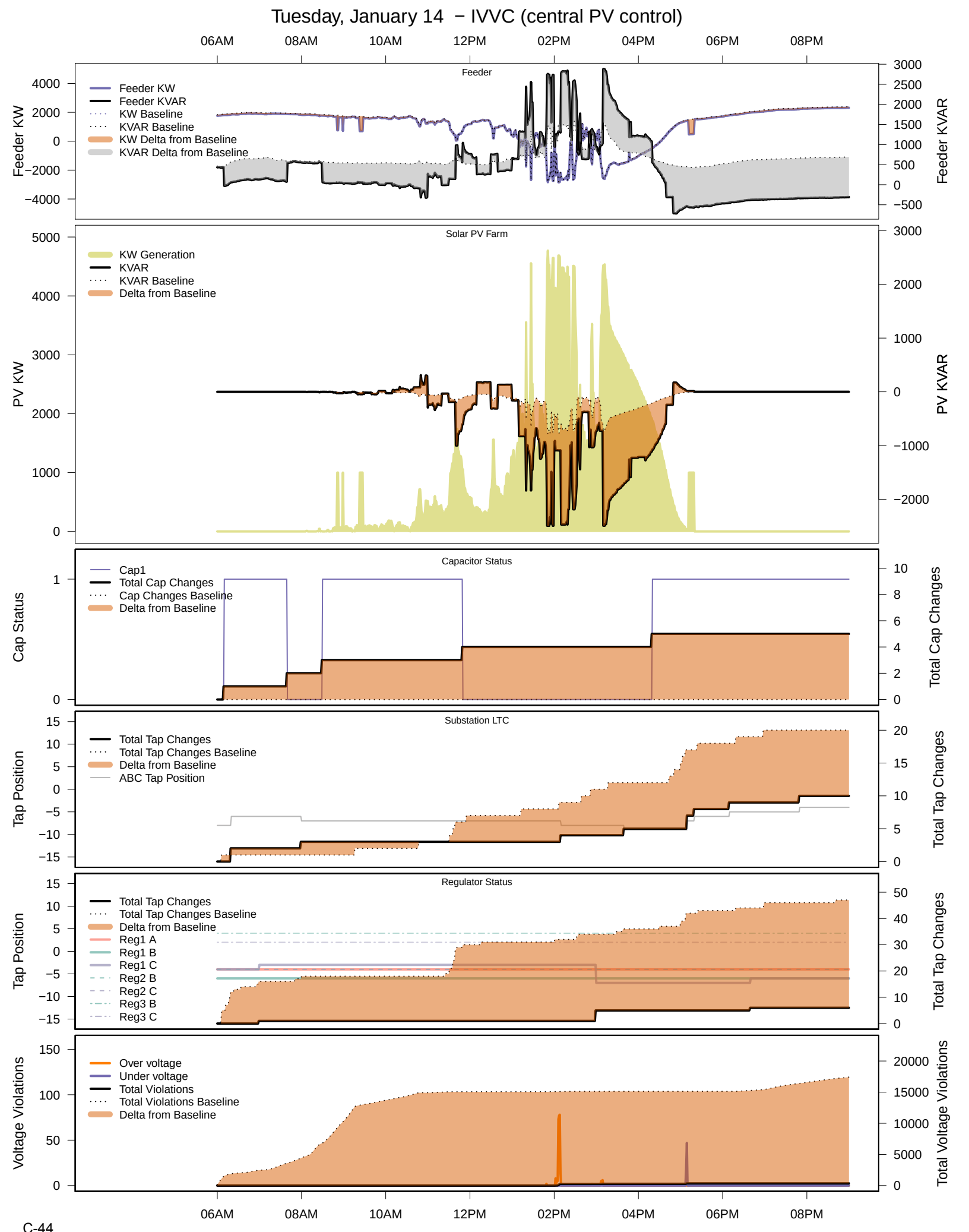

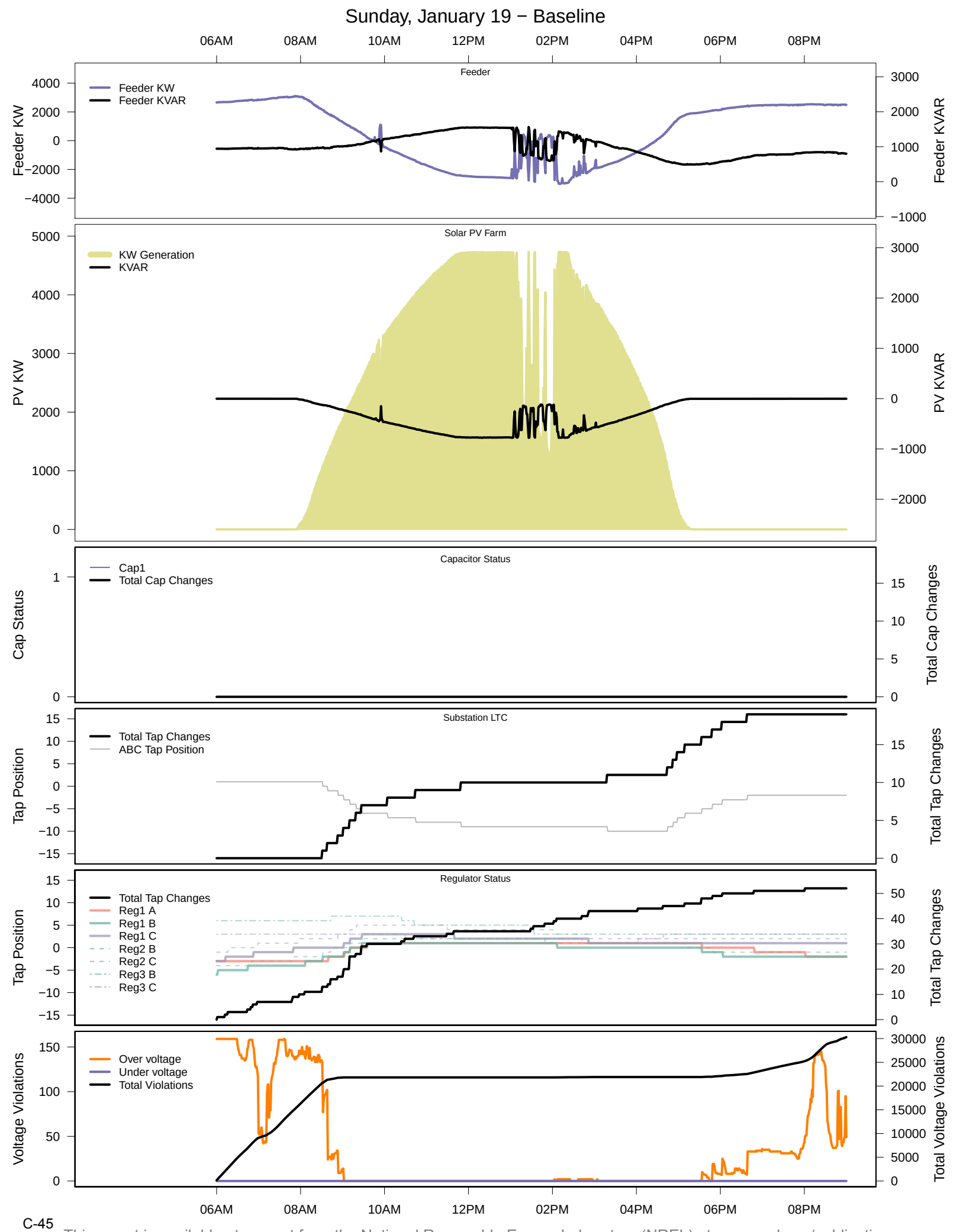

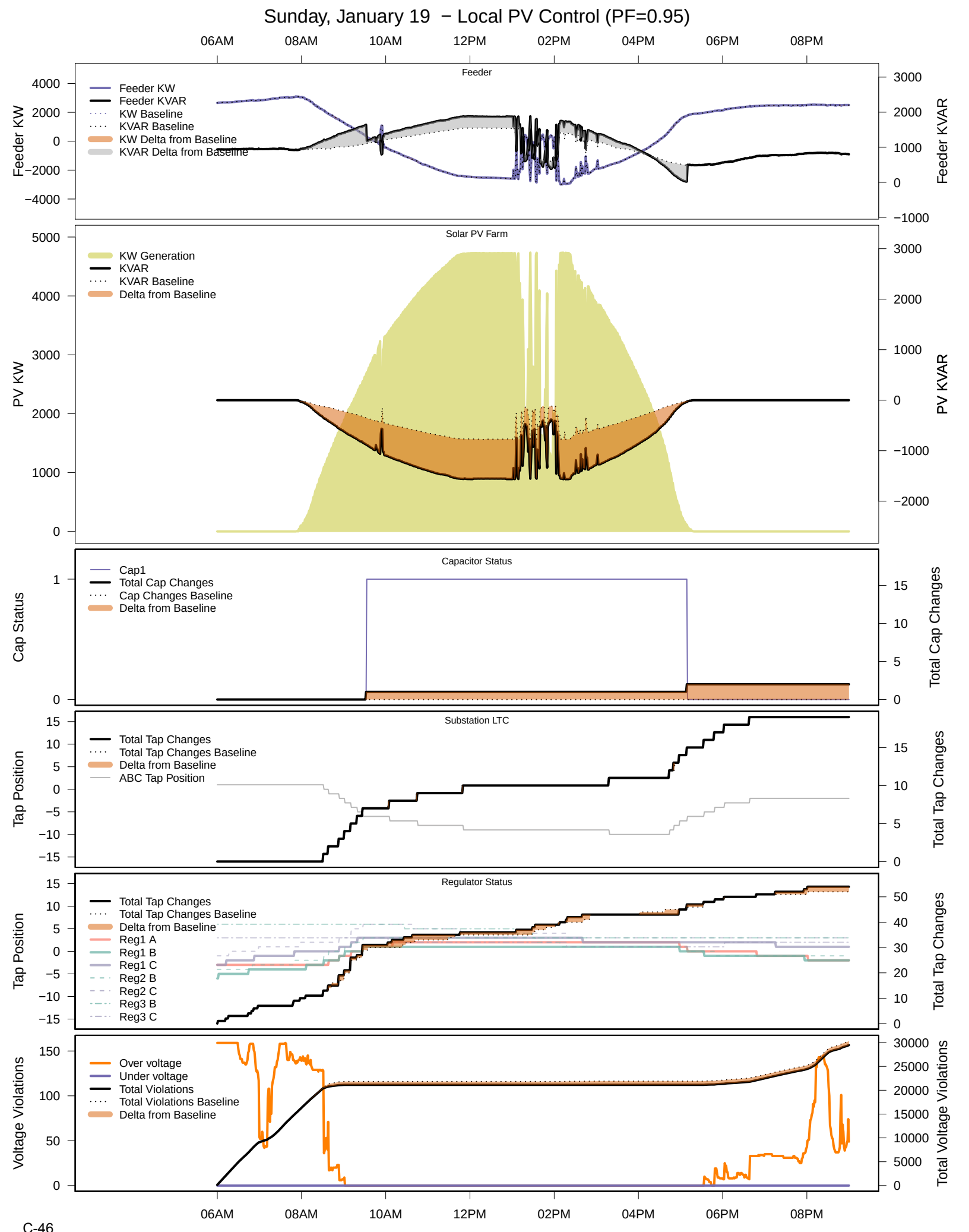

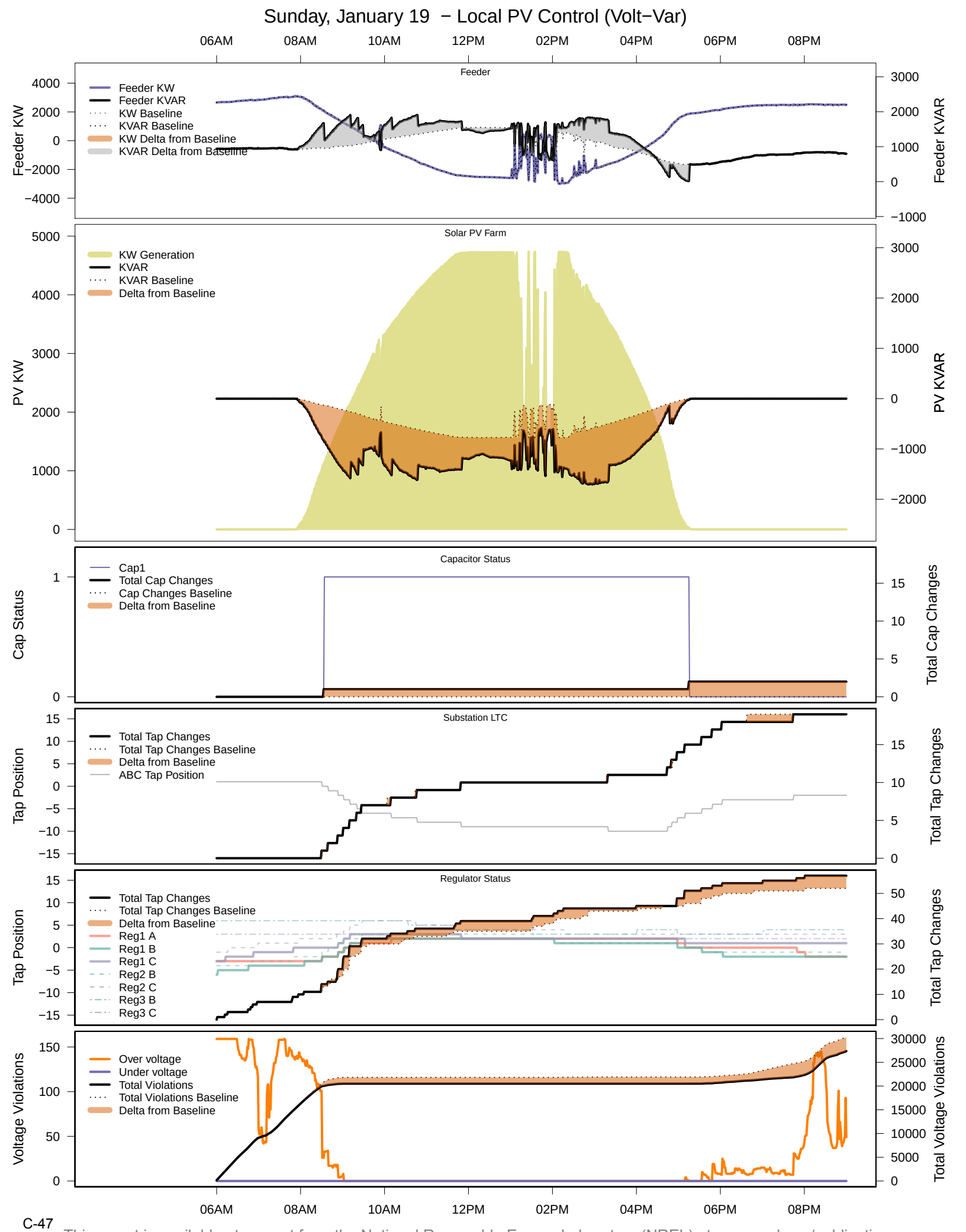

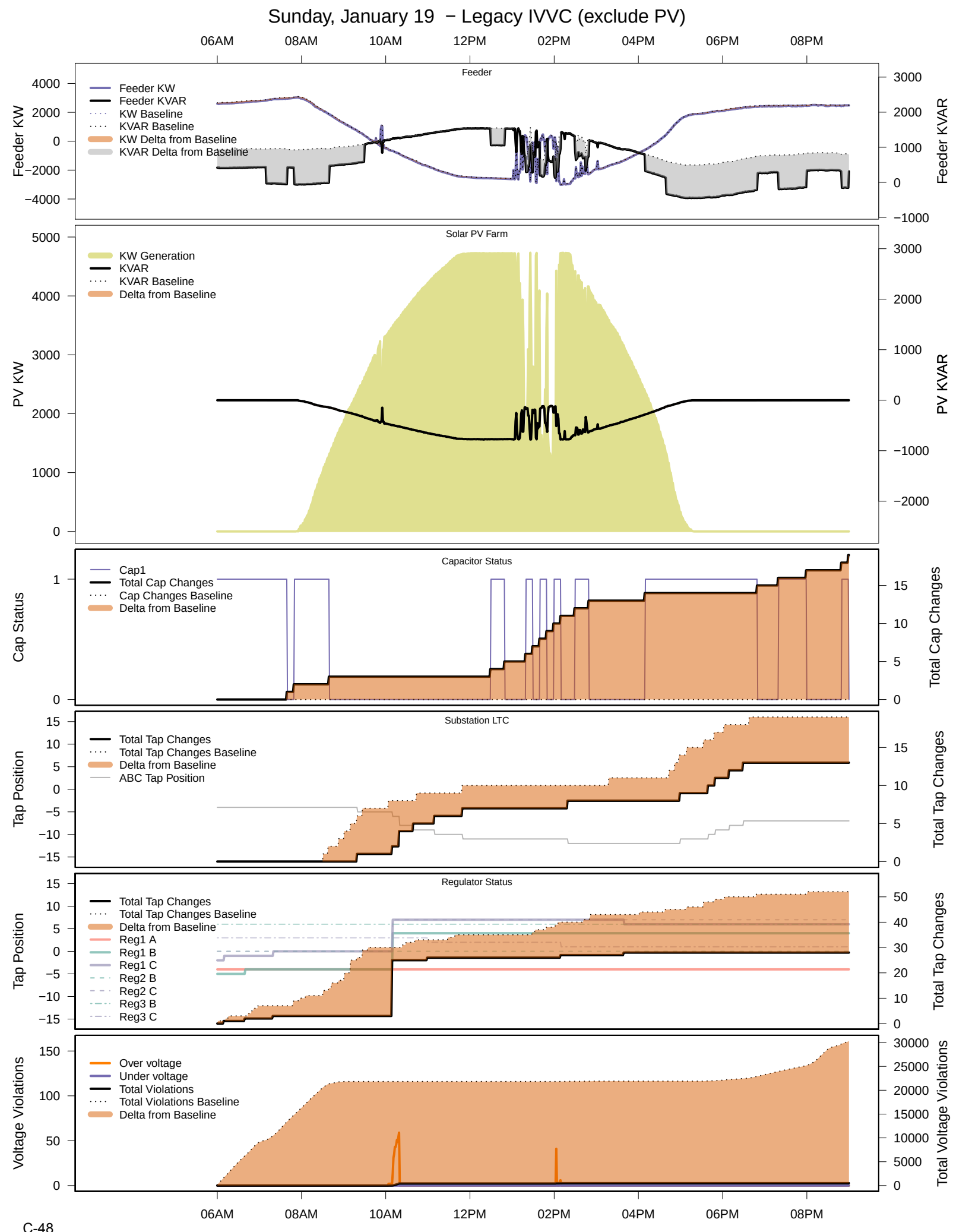

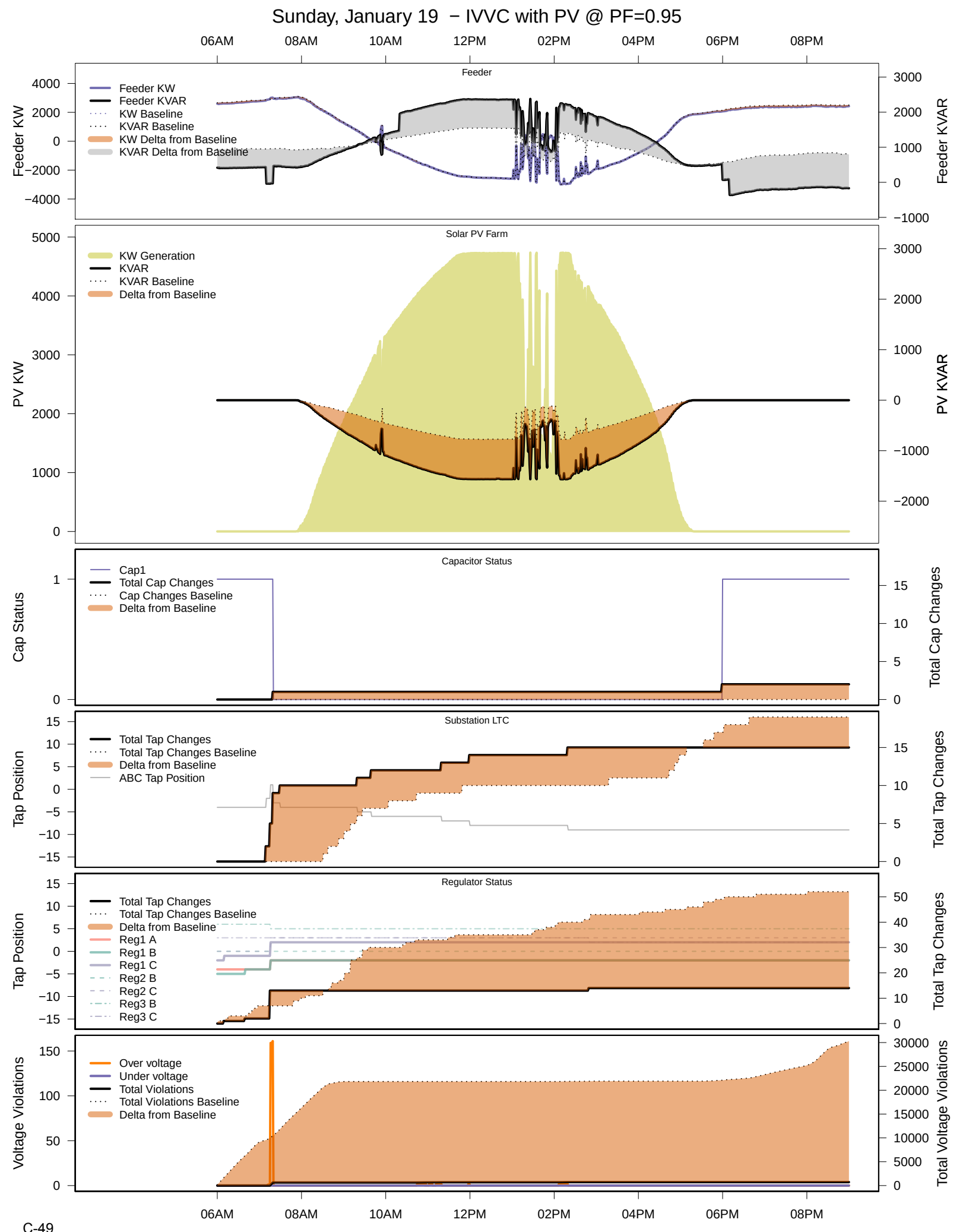

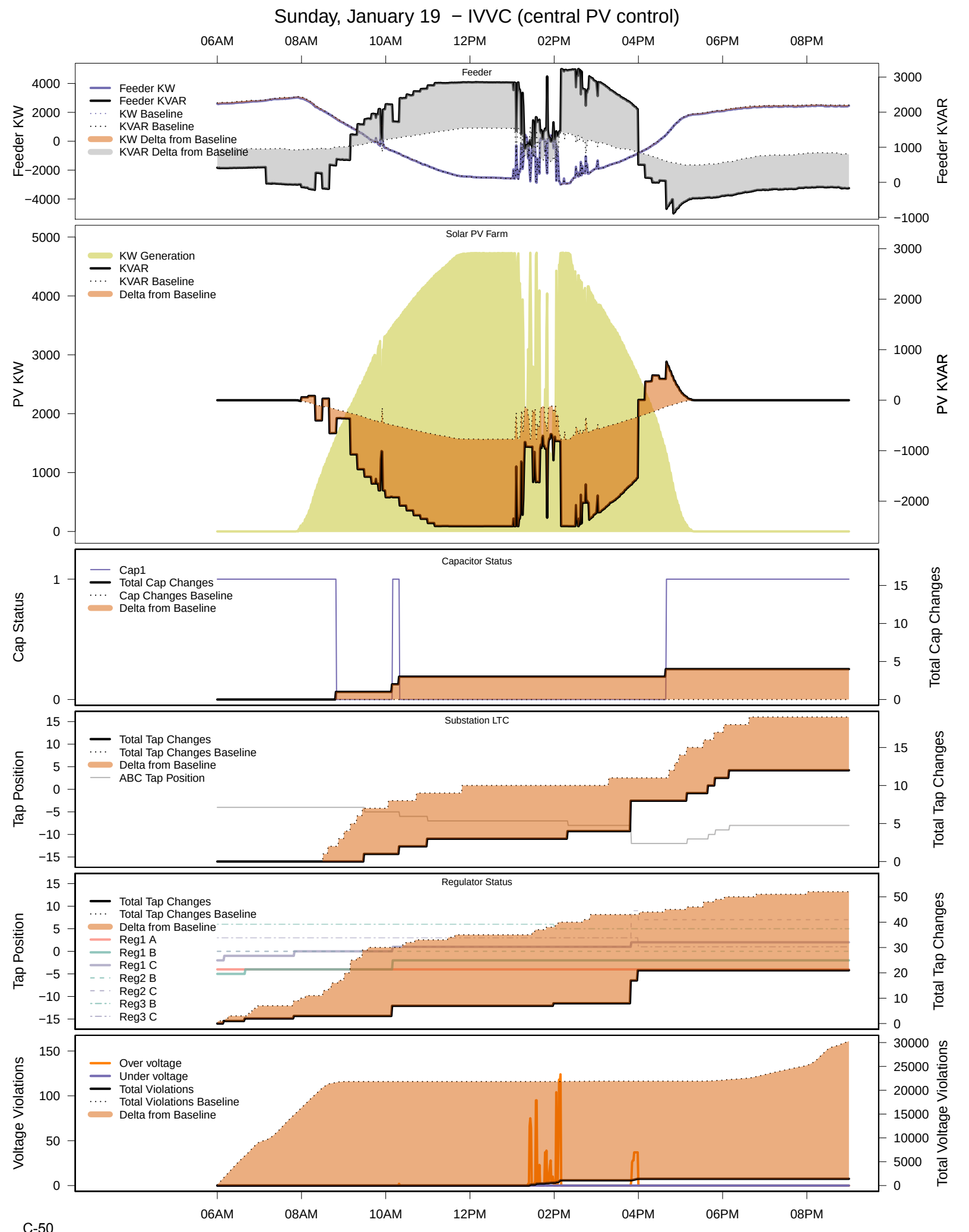

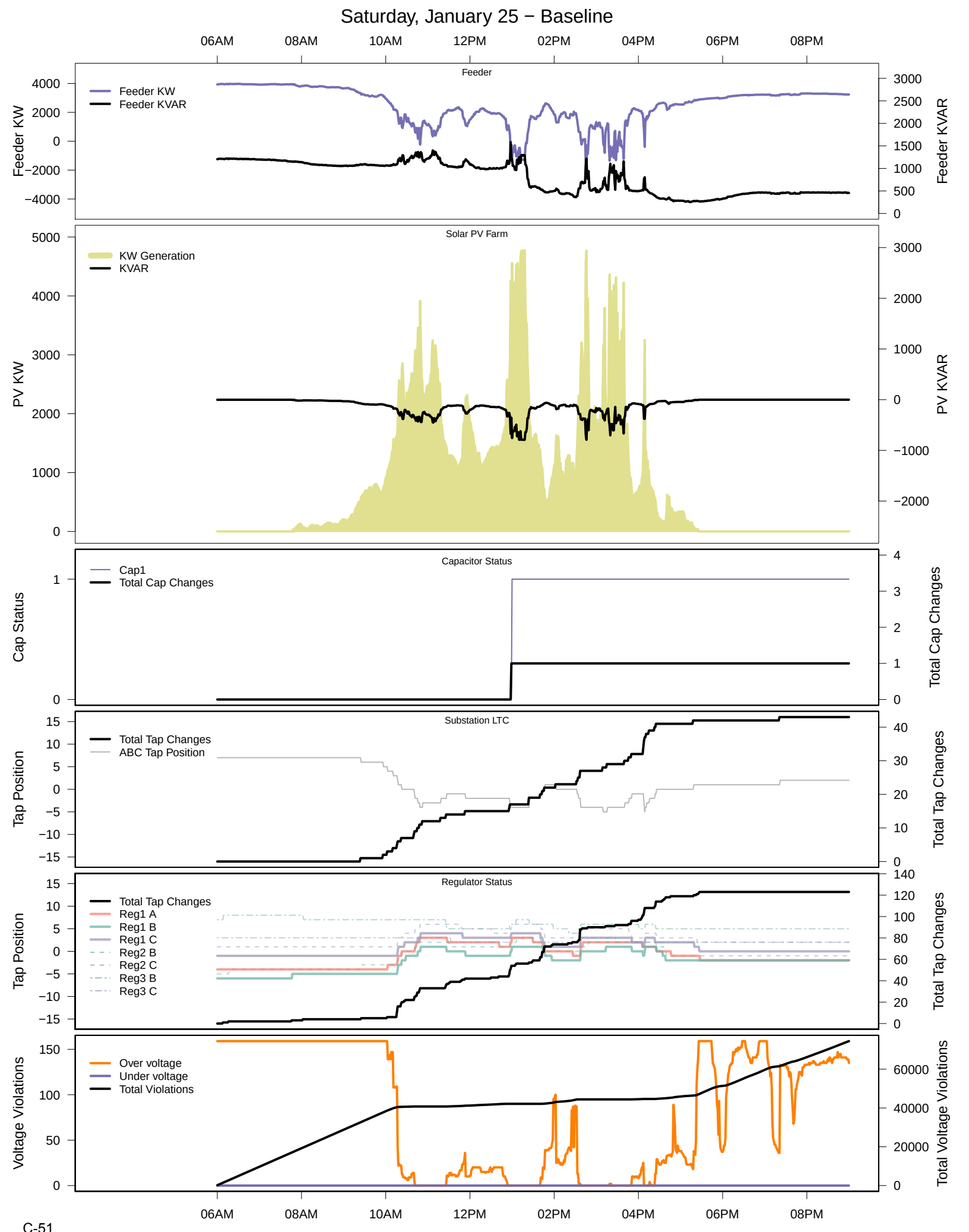

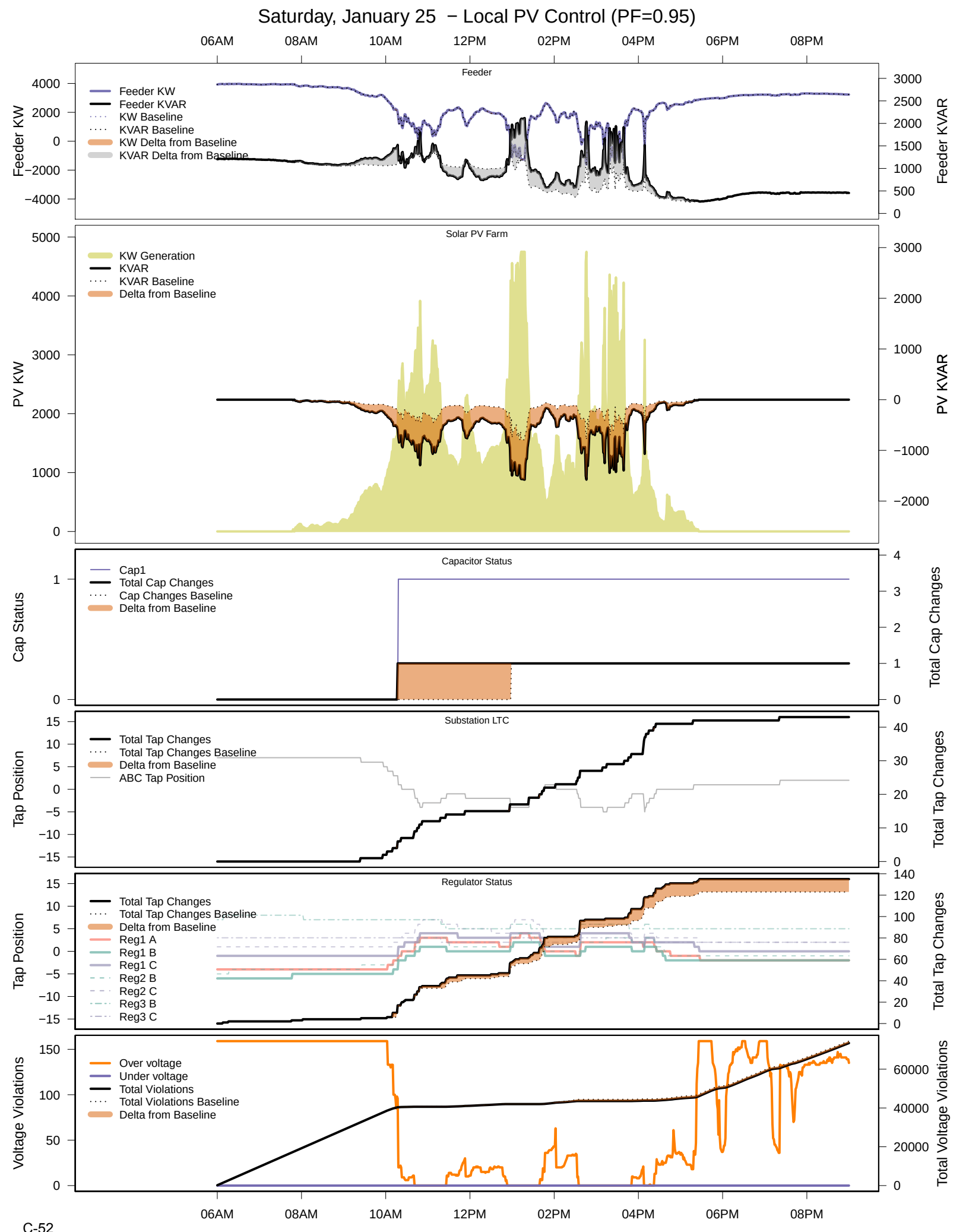

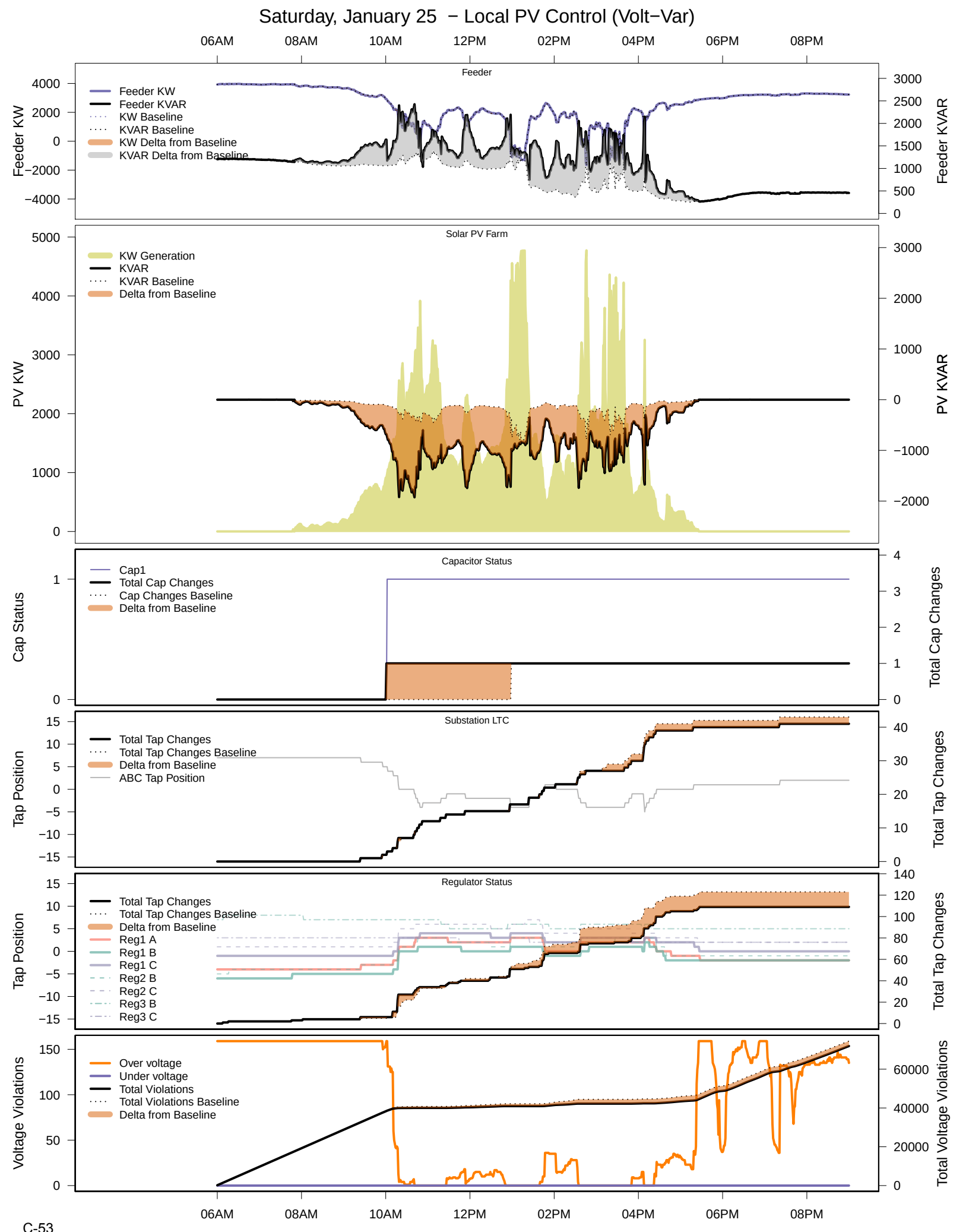

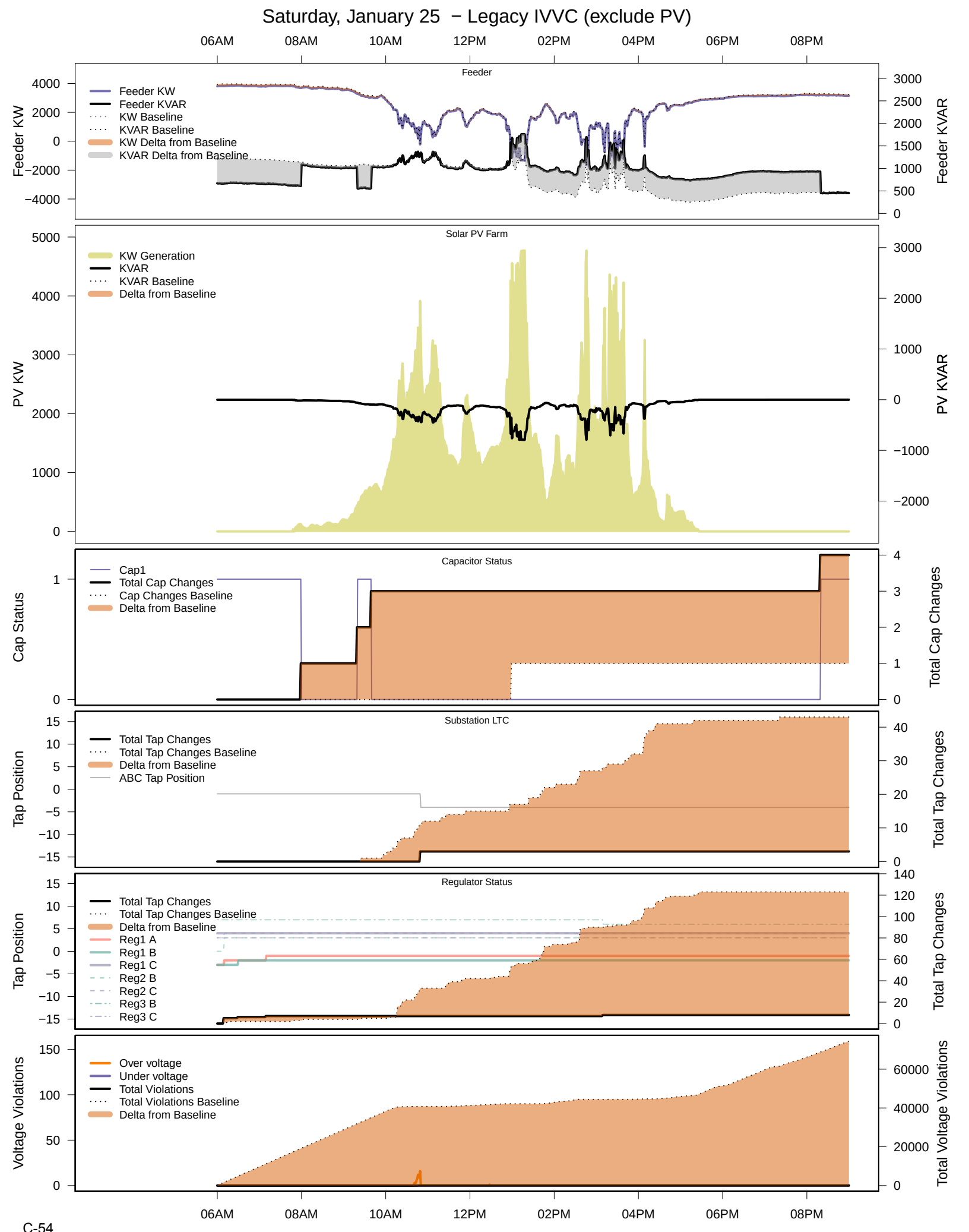

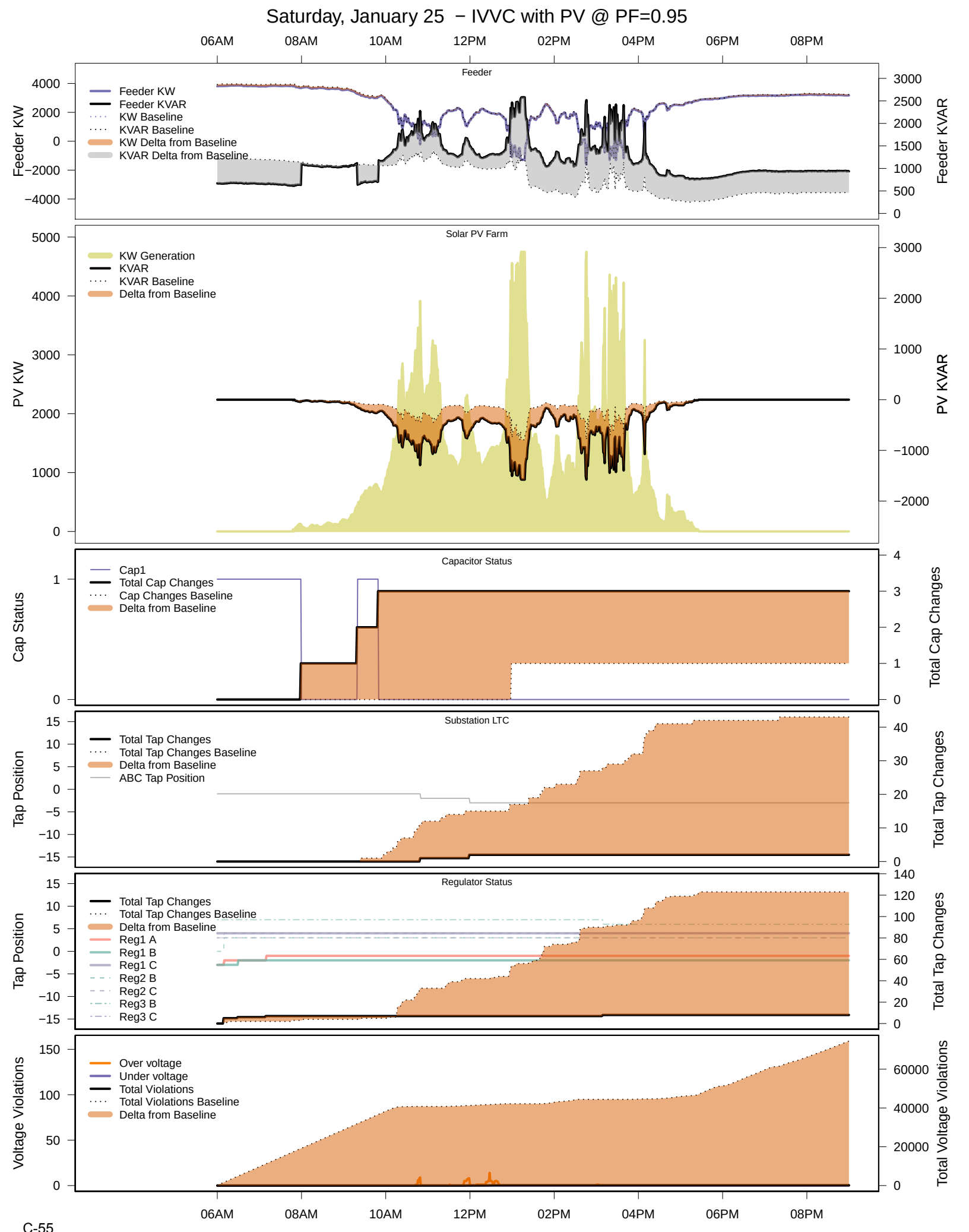

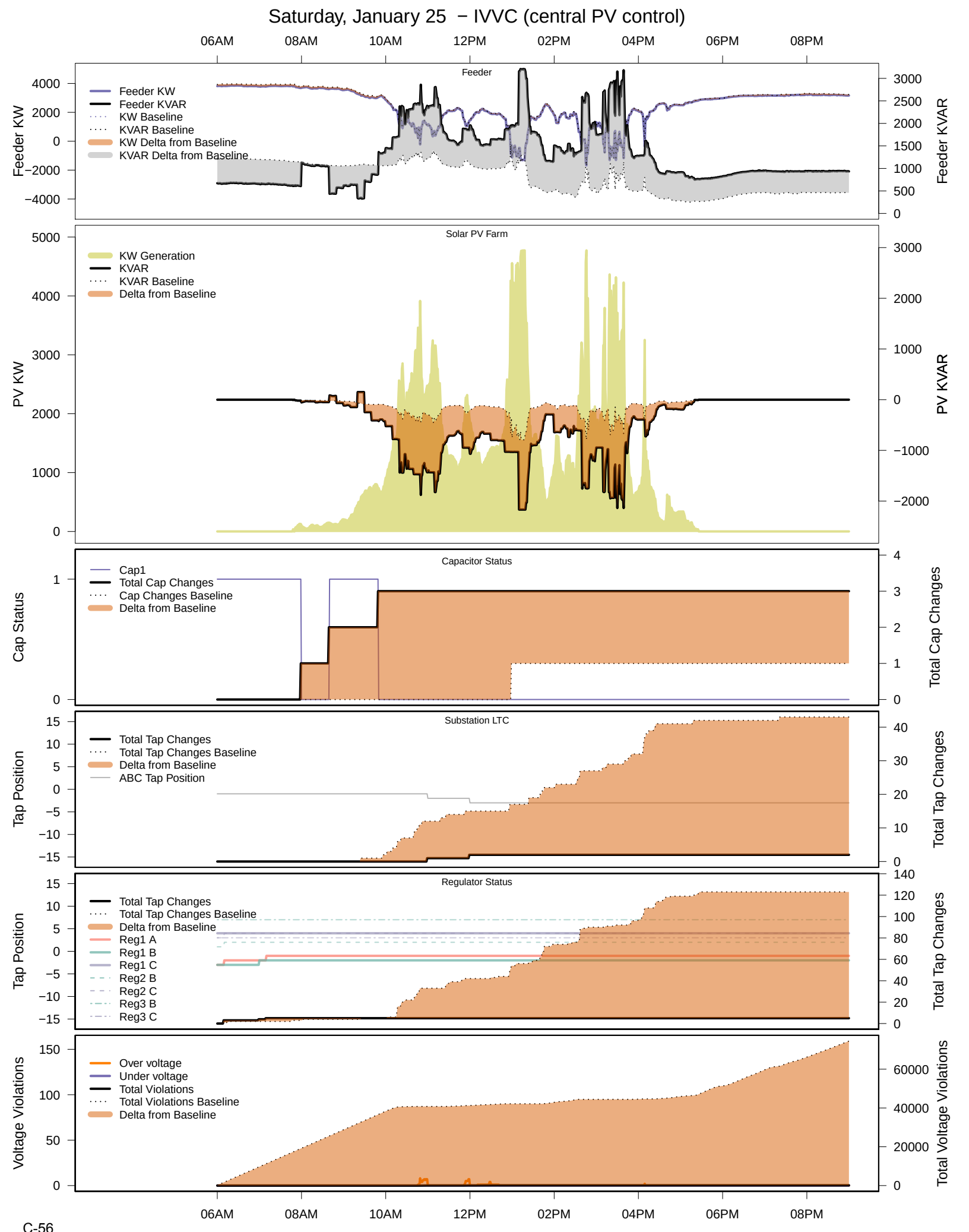

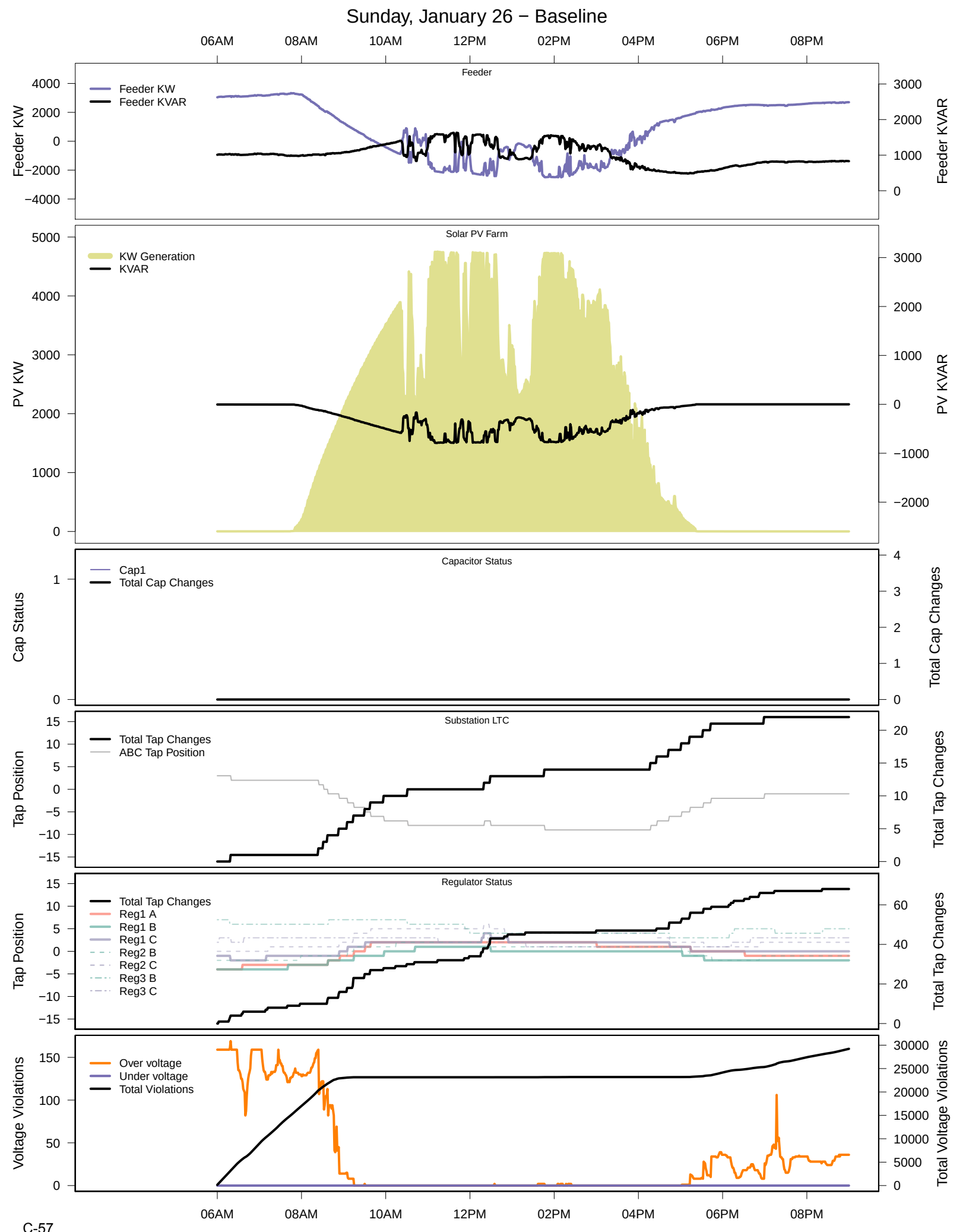

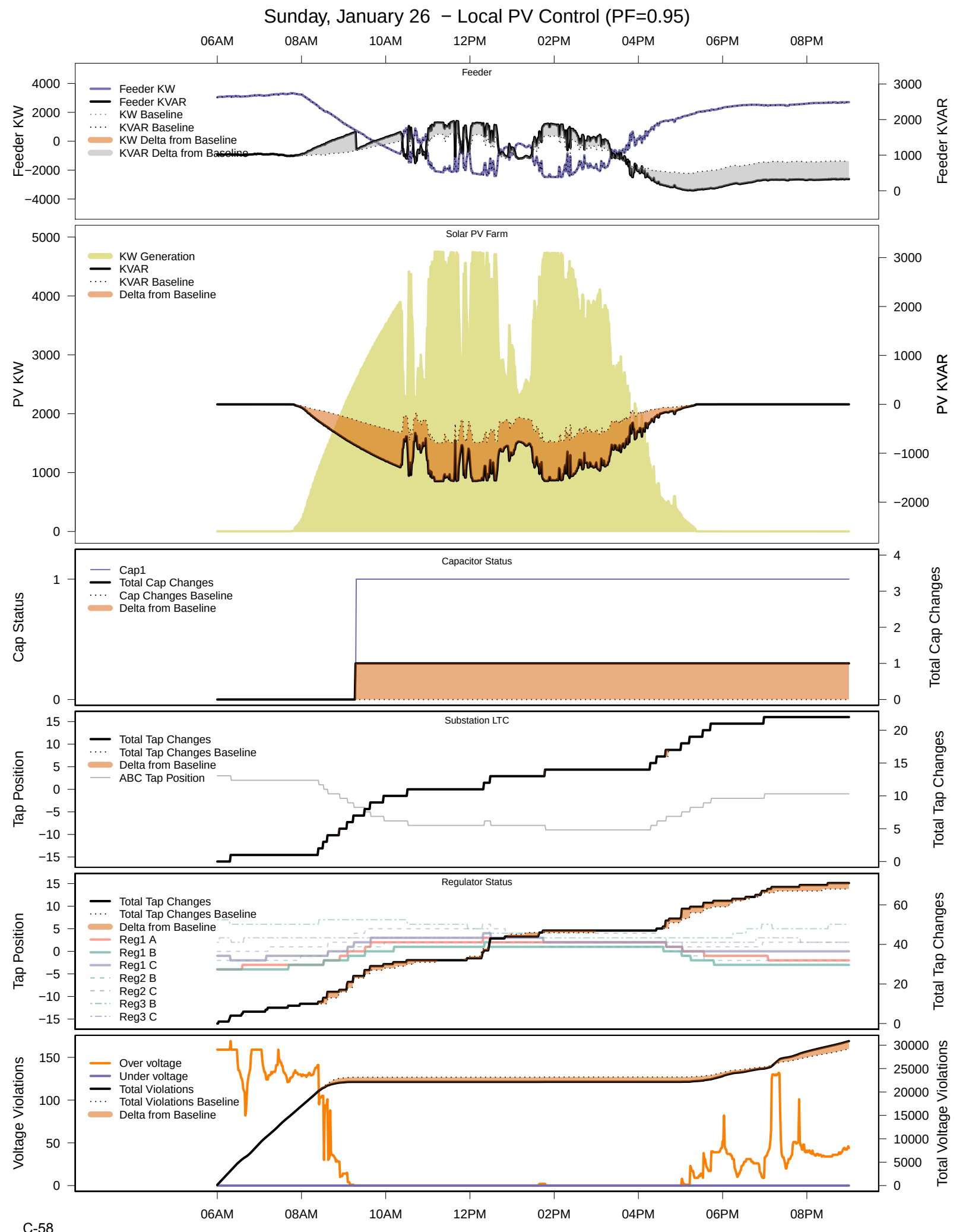

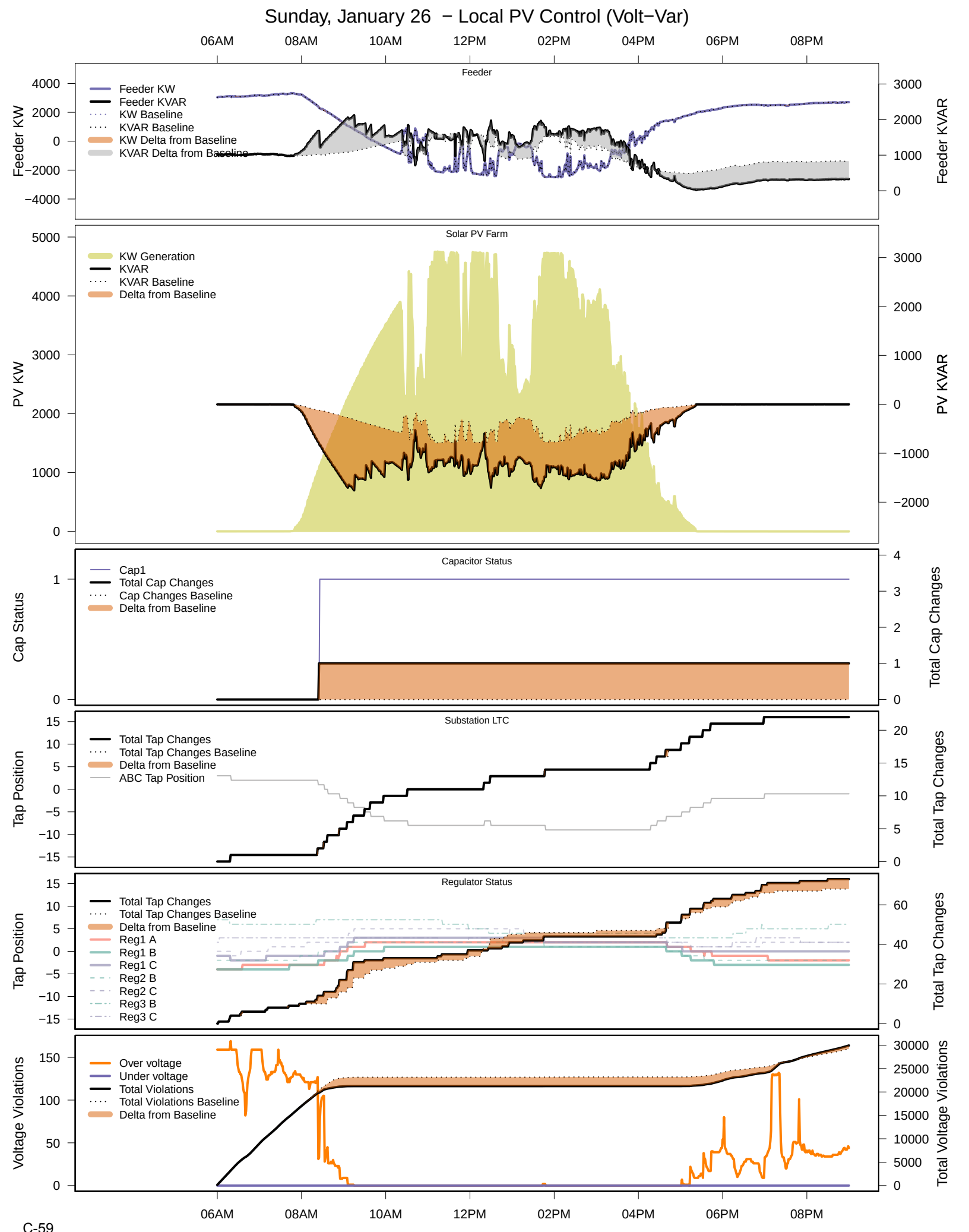

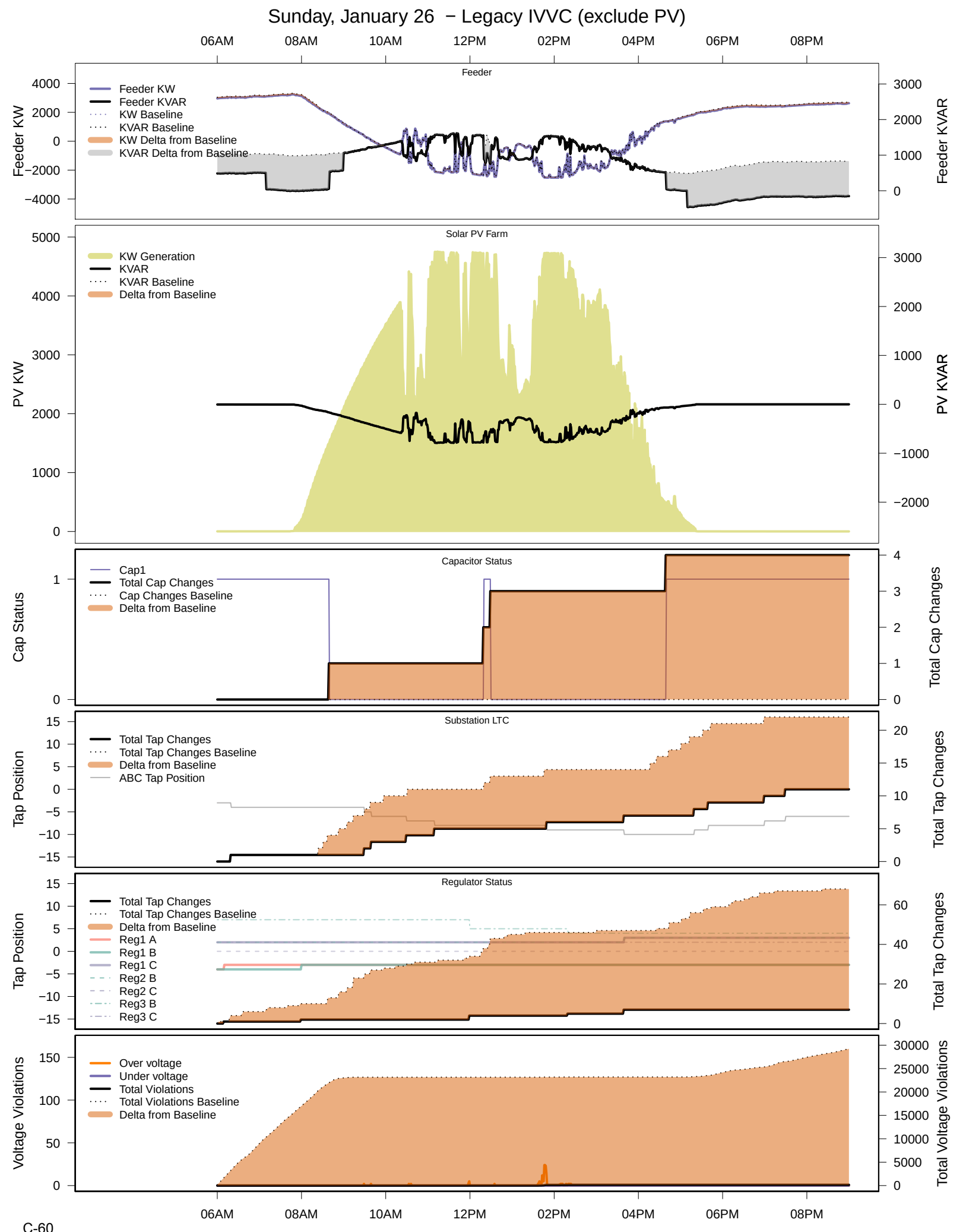

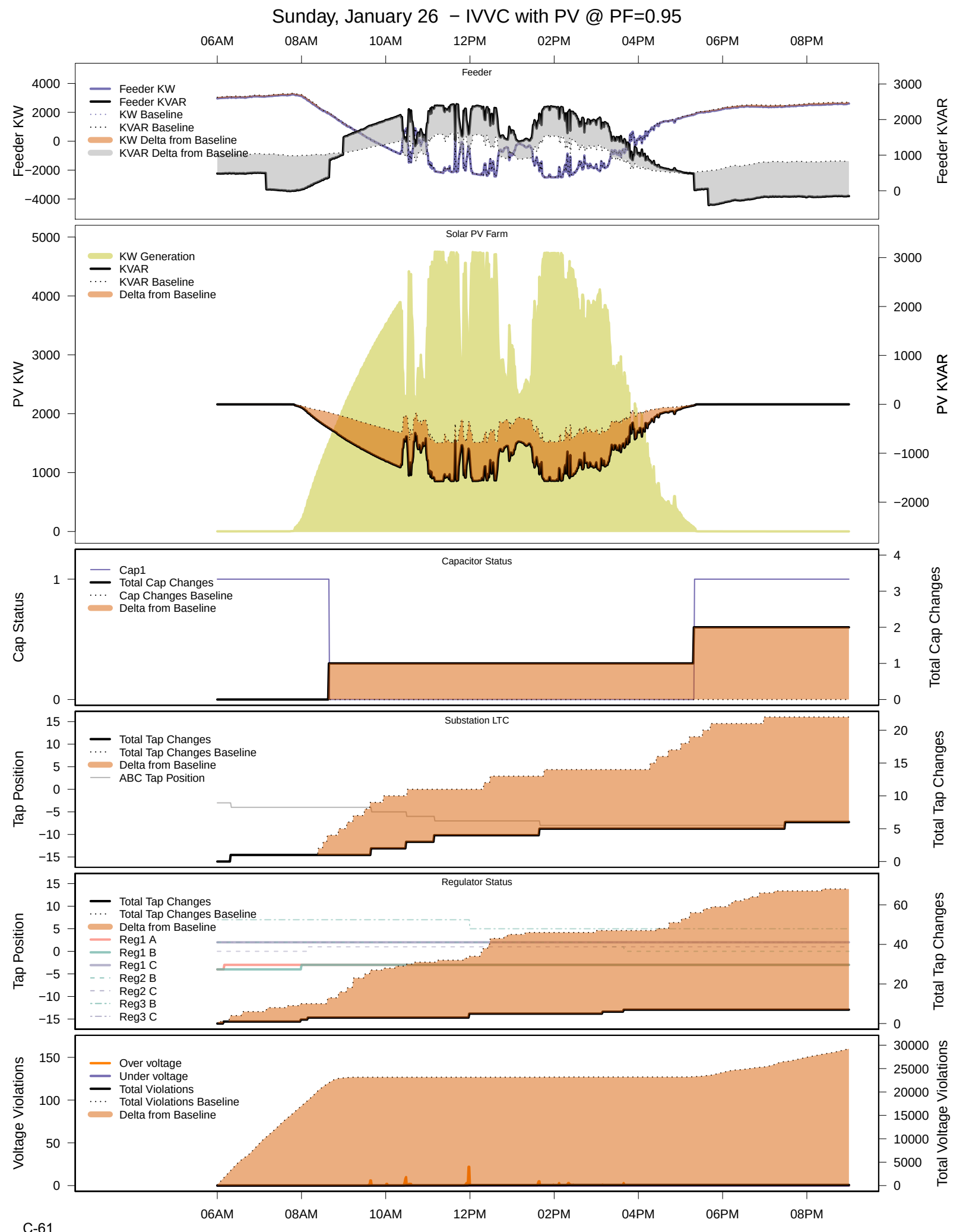

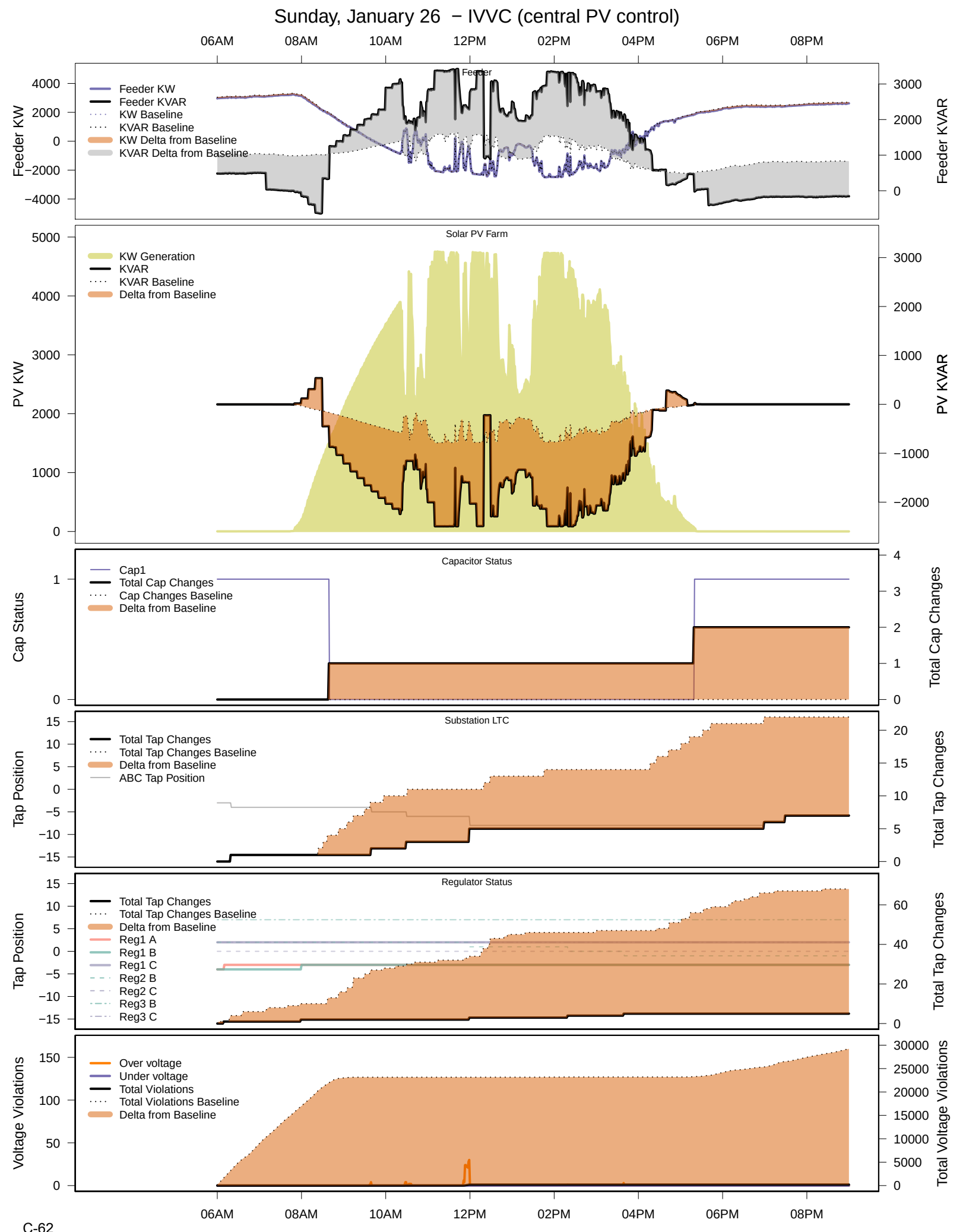

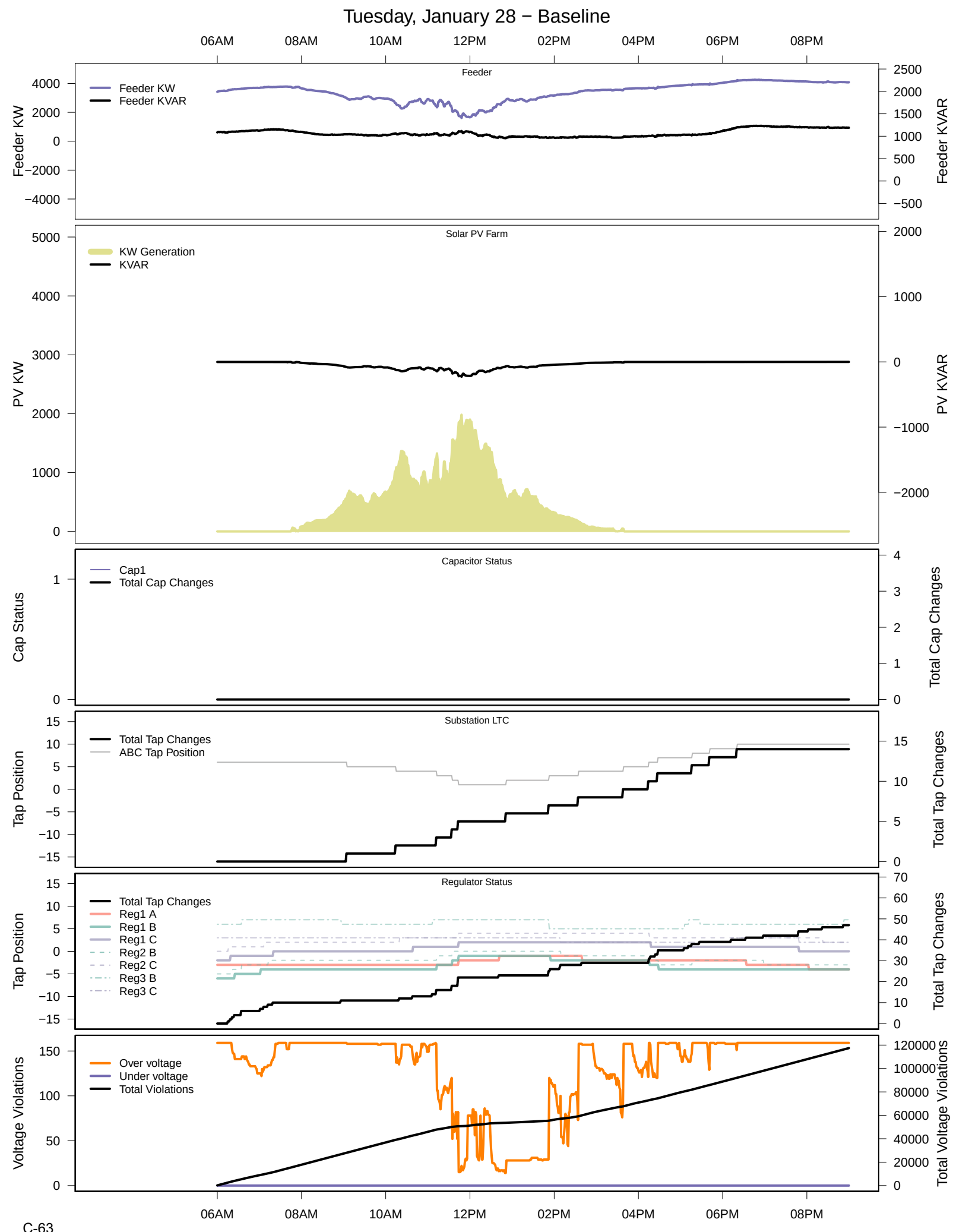

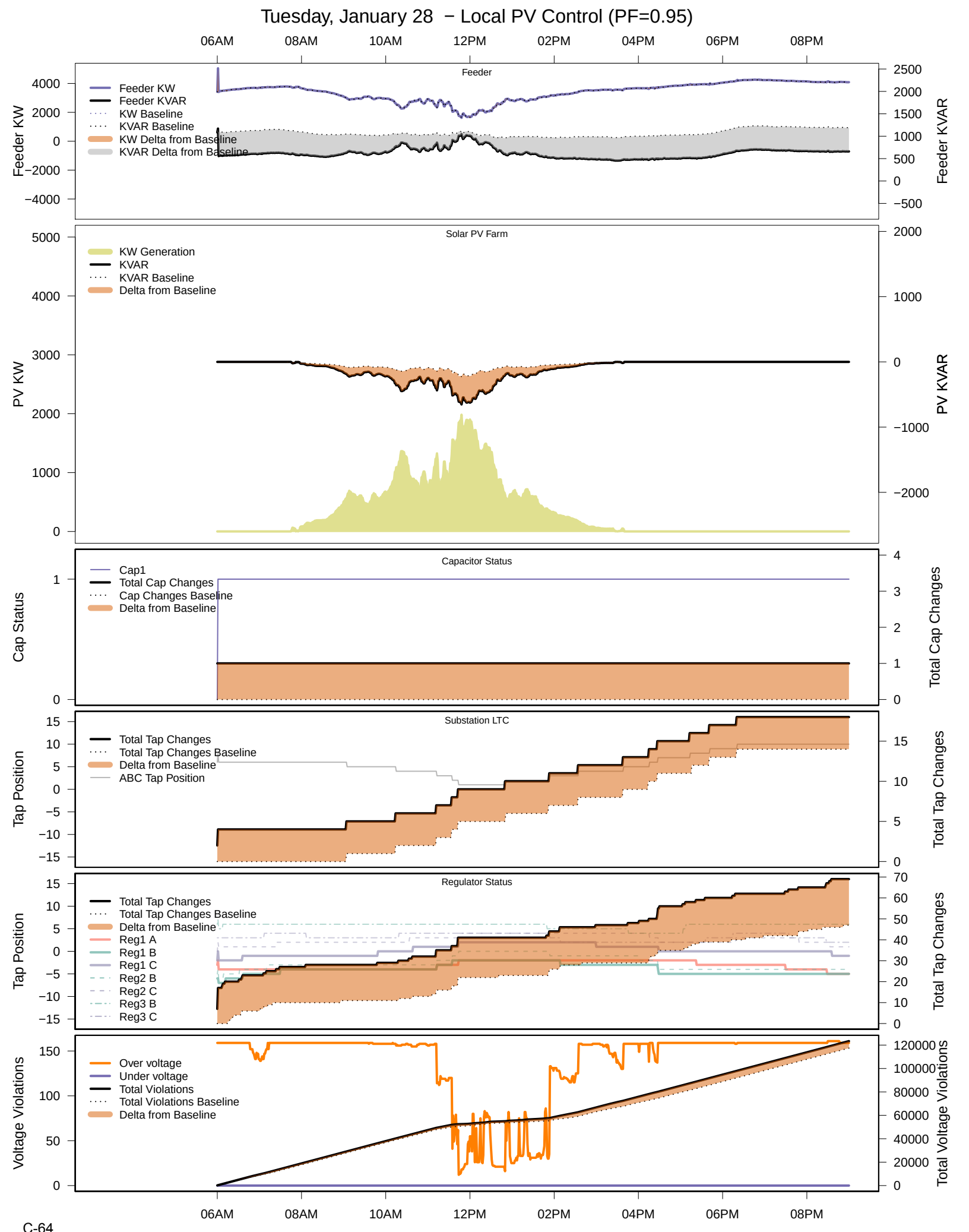

# Tuesday, January 28 − Local PV Control (Volt−Var)